PLASTICITY IN THE VERTEBRATE CENTRAL AUDITORY SYSTEM: CHANGES DURING DEVELOPMENT AND AFTER INJURY IN THE ADULT

BY

JUDITH ANNE CHAPMAN

B.S., CALIFORNIA STATE UNIVERSITY, LONG BEACH 1997

M.Sc., BROWN UNIVERSITY, 2003

SUBMITTED IN PARTIAL FULFILLMENT OF THE REQUIREMENTS FOR THE DEGREE OF DOCTOR OF PHILOSOPHY AT BROWN UNIVERSITY

PROVIDENCE, RHODE ISLAND

MAY 2008

This dissertation by Judith Anne Chapman is accepted in its present form

by the Department of Psychology as satisfying the

dissertation requirement for the degree of Doctor of Philosophy.

Date _____ _____

Professor Andrea Megela Simmons, Advisor

Recommended to the Graduate Council

Date _____ _____

Professor Anna Dunaevsky, Reader

Date _____ _____

Professor Justin R. Fallon, Reader

Approved by the Graduate Council

Date _____ _____

Dean Sheila Bonde, Dean of the Graduate School

CURRICULUM VITAE

Judith A. Chapman

Personal Information:

Brown University
89 Waterman Street
Box 1853
Rhode Island
02912

Telephone: (401) 863-3012
Email: Judith_Chapman@BROWN.EDU

Date and Place of Birth:

November 1st, 1974; Hollywood, California. U.S.A.

Education:

2008 (exp'd) PhD Brown University, Department of Psychology, Providence, Rhode Island.
Dissertation: Plasticity in the Vertebrate Central Auditory System: Changes During Development and After Injury in the Adult (expected 5/2008)
Advisor: Andrea Megela Simmons PhD.

2001-present Doctoral student, Department of Psychology, Brown University, Providence, Rhode Island.
Advisor: Andrea Megela Simmons PhD.

2003 MSc Brown University, Department of Psychology, Providence, Rhode Island.
Thesis: Gene Expression and Behavioral Recovery in the Adult Vertebrate After n.VIII Lesion. (Received 5/2003).
Advisor: Andrea Megela Simmons PhD.

1998- 2000 Graduate Student, Microbiology, CSULB, Long Beach, California.
Research: Differentially expressed mRNAs in the tumoricidal macrophage.
Advisors: Roger A. Acey PhD and Martin Jadus PhD.

1994- 1997 BSc, Microbiology, CSULB, Long Beach, California.
Minor, Chemistry, CSULB, Long Beach, California.

1992-1994 AA (6/1994), Chaffey College, Alta Loma, California.

1992-1994 AS (6/1994), Chaffey College, Alta Loma, California.

Honors and Awards:

2004-2007 Ruth L. Kirschstein National Research Service Award (NRSA) for Individual Predoctoral Fellows (F31).

2002 Rhode Island Space Grant Travel Award.

2001-2002 Rhode Island Space Grant Graduate Fellowship Award.

2001 Allan Schrier Fund Travel Award.

Professional and Academic Associations:

Sigma Xi, Scientific Research Society
International Society for Neuroethology (ISN)
Women in Technology International (WITI)
New York Academy of Science (NYAS)
Association for Women in Science, National (AWIS)

Publications:

Simmons, A.M., Tanyu, L.H., Horowitz, S.S. Chapman, J.A., and Brown, R.A. (2008). Developmental and Regional Patterns of GAP-43 Immunoreactivity in a Metamorphosing Brain. Brain Behav Evol *in press*.

Horowitz, S.S., Chapman, J.A., and Simmons, A.M. (2007). Plasticity of auditory medullary –midbrain connectivity across metamorphic development in the bullfrog, *Rana catesbeiana*. Brain Behav Evol 69: 1-19.

Simmons, A.M., Chapman, J.A., and Brown, R.A. (2006). Developmental changes in cell proliferation in the auditory midbrain of the bullfrog, *Rana catesbeiana*. Journal of Neurobiology. 66: 1212-1224.

Chapman, J.A., Weinstein, J.L., and Simmons, A.M. (2006). Cell proliferation in the *Rana catesbeiana* auditory medulla over metamorphic development. Journal of Neurobiology. 66: 115-133.

Simmons A.M., Chapman J.A. (2002). Metamorphic changes in GABA immunoreactivity in the brainstem of the bullfrog, *Rana catesbeiana*. Brain Behav Evol 60:4 189-206.

Horowitz, S.S., Chapman, J.A., Kaya, U., & Simmons, A.M. (2001). Metamorphic development of the bronchial columella of the larval bullfrog (*Rana catesbeiana*). Hearing Research. 154: 12-25.

Posters/Spoken Presentations:

Chapman, J.A., and Simmons, A.M. (2007). "Plasticity in the vertebrate central auditory system: Changes after injury in the adult." Society for Neuroscience Conference. San Diego, Ca.

Chapman, J.A., Barnstable A.J. and Simmons, A.M. (2003). "Cell proliferation in vertebrate development.." Society for Neuroscience Conference. St. Louis, LA.

Chapman, J.A., Barnstable A.J. and Simmons, A.M. (2002). "Behavioral and genetic responses during n.VIII regeneration in an adult vertebrate." Gordon Research Conference: Neuroethology, Oxford, England.

Chapman, J.A., Barnstable A.J. and Simmons, A.M. (2002). "Regeneration in the adult vertebrate nVIII: Behavioral and genetic responses." Association for Acoustical Research in Otolaryngology in St. Petersburg, Fl.

Chapman, J.A., Barnstable A.J. and Simmons, A.M. (2001). "Regeneration in the adult vertebrate n.VIII: Behavioral and genetic response." Boston Area Neuroscience Group, Boston, MA.

Chapman, J.A., Barnstable, A.J., Horowitz, S.S. & Simmons, A.M. (2001). "Regeneration in the adult vertebrate n.VIII: Behavioral and genetic responses." Brown University Neurosciences Graduate Program Research Presentation.

Chapman, J.A., Horowitz, S.S. & Simmons, A.M. (2000). "Developmental changes in GABA expression across metamorphic development." Brown University Neurosciences Graduate Program Research Presentation.

Chapman, J.A. (1999) "Differential mRNA expression in the tumoricidal macrophage". Thirteenth annual B.L.U.R.B.S., Cal. State Long Beach.

Chapman, J.A. (1999) *Differential mRNA expression in the tumoricidal macrophage*. Thirteenth annual B.L.U.R.B.S., Cal. State Long Beach.

Research Experience:

2001- Characterization of gene expression in normal and regenerating CNS and cranial nerve tissue in the American bullfrog (*Rana catesbeiana*) and African clawed frog (*Xenopus laevis*).

P.I.: Andrea Megela Simmons, PhD

2000- Immunohistochemical study of distribution of gamma-amino-butyric acid (GABA) across development in metamorphosing amphibians.
P.I.: Andrea Megela Simmons, PhD

2000- Neuroanatomical tract tracing and anatomical image analysis using lipophilic carbocyanine dyes in adult and developing anuran brain.
PI: Seth Horowitz, PhD

2000- Immunohistochemical study of expression of growth associated protein (GAP-43) and microtubule associated protein (MAP-2) in regenerating, normal and developing cranial nerve and central nervous system structures of ranid amphibians.
P.I.: Andrea Megela Simmons, PhD

1998-2000 Differential mRNA expression in the sM-CSF and mM-CSF macrophage.
P.I.: Martin Jadus, PhD

1997-1998 Presence of connexin-43 in rat intermedullary collecting duct.
P.I.: Mario Barajas, MD

1995-1998 SAPK induction in the myocardial infarcted rat.
Supervisor: Bruce Prins PhD

1995-1998 Research in various aspects of *Helicobacter pylori* toxin, including role in cancer of the digestive tract, induction of KATOIII cell death, and susceptibility to various antibiotic treatments.
Supervisor: Matthew Domek PhD.

Certifications, licensures, special skills:

Phlebotomy Certified (1992), trained and certified for vehicular transport of limited quanitities of radioative materials, trained and certified according to CAL/OSHA and Brown University hazardous material use in a research setting, laboratory safety and radioactive materials safety certified, research techniques, including: Differential Display, RT-PCR, bacterial transformation, GCG, PhosphorImaging System, immunocytochemistry, immunohistochemistry, animal surgery, radiolabelling, hybridoma production, ELISA, EagleEye transilluminator system, computer proficient, antibody production /purification (ascites/hybridoma and total antibody), chemiluminescence, UV Spectroscopy, DNA/RNA/protein electrophoresis, western/northern/Southern blot, fluorescent microscopy, digital image acquisition and analysis.

PREFACE AND ACKNOWLEDGEMENTS

I wish to express my deepest gratitude to my advisor, Dr. Andrea Simmons, to whom, I am forever indebted. She introduced me to a new body of research and gave me the support, trust and leeway to put my own spin on the research. She is a truly great role model, as a researcher and as a person, something I have never been able to tell her personally.

Professor Anna Dunaevsky and Professor Justin Fallon, thank you for taking the time out of your hectic schedule to support and advise on my dissertation as members of my committee.

I wish to thank my family for being my backbone and supporting me in all that I do. Mom, Dad David, my brother, and my husband Gary. I love you all more than I can express.

Thank you to the Rhode Island Space Grant Graduate Student Fellowship for funding my education and the Rhode Island Space Grant for funding this research. Thank you, Dorcas Metcalf and Dr. Peter Schultz for believing in me. Thank you to the Ruth Kirschensen NRSA F31 fellowship program for funding my studies and this work.

I am grateful to Dr. Seth S. Horowitz for believing in me and being a true friend and colleague. Thank you for making it alright to “think outside of the box” and giving creativity a place in science.

Table of Contents

LIST OF FIGURES

CHAPTER 1: GENERAL INTRODUCTION

CHAPTER 1: BACKGROUND

The ranid central nervous system (CNS) is highly plastic in development and in adulthood. The high degree of plasticity is seen in the developing organism as it undergoes dramatic metamorphic changes in order to transition from a wholly aquatic to semi terrestrial environment (Shi, 2000), and in the adult by its capacity to regenerate cranial nerves after damage (Sperry, 1944, 1945; Zakon & Capranica, 1981; Zakon, 1983). The purpose of the experiments reported here is to understand plastic events in the developing and adult anuran CNS. I will investigate developmental and adult plasticity in two series of experiments. In the first series of experiments, I quantify changes in mitosis in the developing auditory brainstem of the larval bullfrog, *Rana catesbeiana*. In the second series of experiments, I examine anatomical, behavioral and genetic changes subsequent to cranial nerve damage in adults of two species, the bullfrog *Rana catesbeiana*, and the African clawed frog, *Xenopus laevis.*

Plasticity during development: Metamorphosis

Metamorphosis in anurans, in all except permanently aquatic species, involves a change in habitat, from a wholly aquatic to an amphibious environment. Morphological effects of metamorphosis are dramatic as the animal prepares for life in a semi-terrestrial environment (McDiarmid & Altig, 1999). All sensory systems undergo reorganization during larval development (Spaeti, 1978). Hormonal changes are also prominent (Shi, 2000). The animal's body morphology in early stages of larval development is optimized for the aquatic, sexually immature, mute, and herbivorous tadpole, including a

streamlined body, gills, a long and laterally compressed tail complete with fins, lateral line system, a "beak-like" mouth, long intestine and laterally placed eyes (McDiarmid & Altig, 1999). These structures allow the tadpole to be a highly effective swimmer able to breathe and detect movement underwater. In addition, the tadpole's visual system has a large predator detection angle (Lannoo, 1999), and the mouth and digestive structures allow scraping and digestion of plant material. Post-metamorphosis, the animal, now characterized as a froglet or a frog, retains few of its tadpole structures or tadpole-like behaviors. This animal, a once aquatic prey, is now a semi-terrestrial and highly effective predator. The frog is still an adept swimmer, although it has lost its tail and now uses long, muscular legs, webbed feet, and a calcified skeleton to propel itself through the water while placing the new forelimbs tightly to its sides to reduce drag. In amphibious species, and the lateral line is lost (Fritzsch et al., 1984). Anatomical structures typical of herbivorous tadpoles have been replaced with tissues optimized for the carnivorous predator. The long intestine is no longer required in a carnivorous diet and has been shortened. The "beak like" oral structures are replaced by a wide mouth which retains a large tongue that the frog uses to catch prey. Target prey are now easily located using its 3-dimensional vision, allowed by the more rostrally placed eyes, but at the expense of the tadpole's wide view angle. Gills have been replaced with large capacity lungs (Burggen & Infantino, 1994) which, upon sexual maturity, males will use to vocalize in an attempt to establish territoriality and entice females to mate. Audition is of extreme importance in the social behavior of adult anurans, as dominance and territory for many species are established nocturnally. Males hear and respond to vocalizations

from other males, and gravid females locate and migrate toward calling males based on hearing these vocalizations as well (Gerhardt & Bee, 2006).

The peripheral and central auditory systems both undergo considerable reorganization across metamorphosis **(**Witschi, 1949; Li & Lewis, 1974; Spaeti, 1978; Hertwig, 1987; Jacoby & Rubinson, 1983; Smirnov, 1993; Kumaresan et al., 1998; Boatright-Horowitz & Simmons, 1995, 1997; Boatright- Horowitz et al., 1999; Horowitz et al., 2001; Simmons & Chapman, 2002; Simmons & Horowitz, 2006; Horowitz et al., 2007a,b). The auditory organs of the inner ear [saccule, amphibian papilla (AP), basilar papilla (BP)] begin to develop early in the postembryonic period, before development of the middle ear systems (Li & Lewis, 1974; Spaeti, 1978; Hertwig, 1987). In the youngest post-embryonic tadpoles, auditory information is transduced via saccular input, as the saccule is the earliest inner ear organ to develop (Witschi, 1949; Hertwig, 1987; Smirnov, 1993). During the earliest postembryonic stages in *Rana sp.* (hatchlings through stage 38 larval animals), sound is likely transmitted from the external environment by passing through the oval window and stimulating the otolith organs directly (Hetherington, 1987). It is not until the period directly before the onset of metamorphic climax, temporally coincident with the final differentiation of the hind limbs, that one component of the adult bullfrog's middle ear system, the opercularis system, forms. The opercularis system consists of the operculum cartilage overlying the oval window, and attached via the opercularis muscle to the shoulder girdle (Mason & Narins, 2006). In adult frogs, the opercularis pathway is believed to transduce seismic signals (Narins et al., 1993), but it appears to function in audition in tadpoles (Boatright-Horowitz & Simmons, 1997). During metamorphic climax, the stapes and extrastapes (columella and extracolumella)

begin to form, but the tympanic-columellar pathway is not fully functional until after climax, when the external tympanum first appears on the side of the animal's head (Boatright-Horowitz & Simmons, 1995, 1997; Hetherington, 1987).

The progressive development of these two external transduction pathways suggests that hearing sensitivity in *Rana catesbeiana* tadpoles will vary across the larval period. This variability has been shown in several electrophysiological studies examining auditory response properties of the torus semicircularis (TS) in the midbrain and in vestibular regions in the medulla (Boatright-Horowitz & Simmons, 1997; Horowitz et al., 2007b). Neural responses to sounds can be recorded from the TS of bullfrog tadpoles at all stages of postembryonic development, but the spectral and temporal sensitivity of these responses changes in a manner paralleling the sequential maturation of the opercularis and tympanic-columellar transduction pathways (Boatright- Horowitz & Simmons, 1997; Boatright-Horowitz et al., 1999). In larval *Rana catesbeiana*, robust auditory activity can be recorded from the torus until a specific period immediately preceding the onset of metamorphic climax, termed the "deaf period".

During the "deaf period" in *Rana catesbeiana* development, toral neural responses to sound diminishes or disappears, but recovers during metamorphic climax (Boatright-Horowitz & Simmons, 1997). This functional change occurs coincident with anatomical changes. In the middle ear, the opercularis transduction pathway begins to emerge, but connections with the opercularis muscle are not mature, and the operculum partially or totally blocks the oval window (Hetherington, 1987). This serves to diminish sensory input to the inner ear and subsequently the medullary auditory nuclei. Centrally, connectivity between the superior olivary nucleus (SON) and the torus is disrupted

(Boatright-Horowitz & Simmons, 1997; Horowitz et al., 2007a). This anatomical disconnection may involve retraction of processes and subsequent cell death in the SON due to absence of neural activity, followed by a spurt of cell proliferation as metamorphic climax proceeds and neural activity recovers. The role of cell proliferation in this process of anatomical disconnection will be evaluated in this thesis.

Plasticity in the adult: Cranial nerve regeneration

CNS damage in mammals is often irreversible and progressive, and can result from multiple factors including, trauma, ischemia, or disease. The inability of the mammalian CNS to recover from damage results from abortive attempts at neurite elongation, inability to enter and path find in the CNS, and/or failure of synaptogenesis with appropriate target tissues. Further, axonal damage can result in retrograde fiber degeneration and ganglionic cell death (Russell & Moore, 1995; Hafidi et al., 1999; Lohmann et al., 1999; reviewed in Schwab & Bartholdi, 1996).

The inability of the mature mammalian CNS to effectively and spontaneously regenerate after injury is likely due, not only to the absence of chemical signals that could promote survival and appropriate regrowth, but also to the presence of multiple growth-inhibitory factors (reviews: Carbonetto, 1991; Fawcett, 1992; Golding & Barres, 2000). Glial-derived inhibitory factors and certain inflammatory factors can inhibit neurite outgrowth and affect intracellular signal transduction pathways, producing growth cone collapse, apoptosis, or neurite degeneration (Fournier & Strittmatter, 2001). Current experimental protocols for overcoming limitations of CNS regeneration and recovery of function include peripheral and fetal-derived nerve grafts, antibody-based neutralization

of inhibitory molecules and neurotrophic factor supplementation (reviews: Grill & Tuszynski, 1999; Goldberg & Barres, 2000). In some cases, these strategies have yielded an increase in neurite sprouting and post-lesion viability; however, results have been limited by the small numbers of responding neurons, limited distance of neurite extension, low graft survivability, and unsuccessful neurite path finding. Neutralization strategies may be unrealistic due to the large number of inhibitory factors present in the CNS, and their different actions in various cell populations.. In order to develop therapeutic protocols to promote regeneration and recovery in the adult CNS after injury, it is critical to understand the molecular mechanisms involved in a system that is more permissive of such processes.

Growth Permissive and nonpermissive molecules

Axotomy of CNS neurons has been shown to result in apoptosis (Berkelaar, 1994) or necrosis (Yip & So, 2000). Multiple inhibitory factors have been elucidated which are shown to block axonal elongation, collapse growth cone or cause apoptotic cell death. Myelin associated glycoprotein (MAG), NOGO, Tenascin C, chondroitin sulphate proteoglycans (CSPGs), CD44, and many others are known to inhibit axonal growth, while neurotrophic factors such as NT-3, NT-4, NGF, CNTF, FGF, and BDNF have been shown to stimulate survival and/or outgrowth of CNS axons (Fawcett & Asher, 1999). The injured CNS neuron that is bombarded by these positive and negative growth signals, in the non regenerative (or apoptotic/necrotic/degenerative) condition is overwhelmed by negative growth signals. The signals can be shifted to favor positive growth signals by neutralizing antibody (Buffo et al., 2000). Further, addition of evolutionarily conserved

molecules such as, EGF, bFGF, TGFα, BDNF, IGF, FGF can stimulate mitosis, cell survival, differentiation (*e.g.* neural or glial phenotype) and/or recruitment of new cells *in vitro* or *in vivo* and has been replicated in a wide variety of species (Craig et al., 1996; Holzenberger et al., 1997; Kuhn et al., 1997; Tropepe et al., 1997; Jiang et al., 1998; Aberg et al., 2000; Fallon et al., 2000; Benraiss et al., 2001; Pencea et al., 2001). However, the downstream signaling mechanism is complex and not fully understood. What is known regarding the positive and negative effectors is that they are typically a complex web of signaling cascades in equilibrium that act on intracellular (and often intercellular) pathways leading to signaling cascades that can greatly amplify/reduce/combine/change or even reverse flux through cellular pathways.

These signaling cascades can be affected through kinase, phosphatase, transcription, translation, repression receptor activation/repression/ internalization/etc. Often these pathways are dynamic and depend on a multitude of factors not limited to: cell type, cell/tissue state, receptor population/modifications and bound proteins, second messenger systems including up- and down-stream pathways, which can lead to feed-forward or feed-back accessory pathways. The net result can propagate, abate, or have a seemingly unrelated link to the original input signal(s). The culmination of which can vary anywhere from cell death to mitosis, growth cone collapse and fiber degeneration to axonal elongation, neurite path finding and synaptogenesis.

Plasticity in frogs versus mammals

My research focuses on central nervous system (CNS) plasticity and functional recovery following nerve lesion in the frog model; an adult vertebrate well-documented

for the ability to functionally regenerate injured cranial nerves in the absence of experimenter assistance. Following cranial nerve lesion of either the optic (n.II) or the vestibuloauditory (n.VIII) nerves, blindness, and vestibular and/or auditory deficits, respectively, are noted in frogs followed by functional regeneration and behavioral recovery (Sperry, 1945; Zakon and Capranica, 1981; Zakon 1983)

In mammals, if n.VIII is damaged or transected, there is no regeneration into the CNS, and little or no recovery of auditory function (Wever & Neff, 1947; Schuknecht & Woellner, 1955; Spoendlin, 1971, 1975). Sensorineural deafness is commonly associated with cochlear damage; however, damage to inner ear hair cells can lead to subsequent degeneration in n.VIII (Spoendlin, 1975). Although hair cells themselves can regenerate in some species (frogs, birds; reviews: Cotanche & Lee, 1994; Stone et al., 1998), there is limited regenerative ability of n.VIII fibers. In addition, other types of pathology (such as acoustic neuroma, vestibular schwannoma, neurofibromatosis Type II, advanced Meniere's disease, aging) are associated with n.VIII damage or disease (Matthies et al., 1996; Pulec & Patterson, 1997; Ludemann et al., 2000; McGill, 2000).

In humans, vestibular compensation after damage to the vestibular nerve or organs does occur, but persistent deficits are still visible (Hamalgyi et al., 1990). The limited vestibular compensation that does occur has been interpreted in terms of changes in vestibular nucleus (VN) excitability and sensory substitution (reviews: Dieringer, 1995, Darlington & Smith, 2000).

As in mammals, the CNS of the adult frog expresses non-permissive inhibitory factors (Becker et al., 1995) which can prevent complete repenetration of all regrowing axons into the brain. In anurans, however, damaged cranial (optic, vestibuloauditory)

nerves can survive and regenerate into the CNS, and damaged spinal nerves can repenetrate through the dorsal root entry zone, in spite of these inhibitory factors (Sperry, 1944, 1945; Gaze 1959; Gaze & Jacobson, 1963; Zakon & Capranica, 1981; Zakon, 1983; Liuzzi & Lasek, 1985, 1986; Frank & Sah, 1986; Peng & Frank, 1988; Newman & Honrubia, 1992; Kunkel & Dieringer, 1994; Mears & Frank, 1994; Becker et al., 1995; Hernandez et al., 1998; Beaver et al., 2001; Goto et al., 2002; Dunlop, 2003). In addition, regenerated nerve fibers are functional, showing behavioral and physiological response properties similar to that of conrols (Sperry, 1945; Zakon & Capranica, 1981; Dieringer & Precht, 1982; Caston, 1995; Dieringer, 1995). Additionally, there is recovery of both static (head tilt) and dynamic (response to acceleration) vestibular function (Caston, 1995). The extent to which this behavioral recovery is correlated with n.VIII regeneration is unknown (Caston, 1995). It may, as in mammals, be linked to functional substitution by other sensory systems (vestibular compensation; Dieringer 1995).

Research to discover methods allowing effective CNS regeneration and functional recovery in the mammalian adult is of clear clinical relevance. However, many favorite animal models are incapable of CNS regeneration in adulthood. In order to discover and understand how effective CNS regeneration with functional recovery occurs, research must be undertaken utilizing animal models which are capable of functional CNS regeneration following injury. Discovery of regeneration-promoting factors and pathways employed by these animal models might allow further understanding of the discrepancies that exist in animals that are incapable of CNS recovery in the hope that effective clinical targets may be discovered and therapeutically utilized in humans.

SECTION I: PLASTICITY IN DEVELOPMENT

CHAPTER 2: CELL PROLIFERATION IN THE DEVELOPING RANA CATESBEIANA AUDITORY NUCLEI

CHAPTER 2: INTRODUCTION

Metamorphosis in ranids requires vast reorganization in anatomy, physiology, molecular and behavioral systems over a time span of only a few weeks or months (McDiarmid & Altig, 1999; Shi, 2000). Animals that do not remain wholly aquatic post-metamorphosis require additional modification of auditory and vestibular systems in order to adapt to hearing and ambulation in an in-air environment.

Central auditory nuclei are plastic in developing Rana catesbeiana

Anatomical plasticity

Results of a recent cell quantification study using stereological estimation techniques shows a decrease in the number of mature-looking neurons and an increase in numbers of undifferentiated cells, in the SON during metamorphic climax, These findings are further evidence that the SON undergoes considerable reorganization during and after the deaf period (Boatright-Horowitz & Simmons 1997; Templin & Simmons, 2005). Other central nuclei also undergo considerable anatomical rearrangements during larval development. In amphibian species, cells of the medullary lateral line nuclei die (Fritzsch et al., 1984), the dorsolateral nucleus (DLN; presumed anuran homolog of the mammalian cochlear nucleus) migrates from a more lateral to a more dorsomedial position in the medulla (Jacoby & Rubinson, 1983; Kumaresan et al., 1998). The torus differentiates into distinct subnuclei with its medial part (the developing principal nucleus) forming laminations (Simmons & Chapman, 2002).

Functional plasticity

Along with these anatomical changes, the TS also shows considerable variability in its functional sensitivity to auditory stimulation over metamorphic development. In particular, neural responses from the TS indicate the presence of a functional, transient "deaf period" occurring immediately prior to the onset of metamorphic climax, during which sensitivity to sound sources is markedly decreased from that observed both in earlier larval stages and in climax itself (Boatright-Horowitz & Simmons, 1997). The anatomical reorganization of the auditory system across development involves changes in volume and density of medullary auditory nuclei (Templin & Simmons, 2005). Aside from an earlier qualitative report focusing on the DLN during a limited period of development (Jacoby & Rubinson, 1983), the extent to which any of these processes involve birth of new cells is unknown.

Developmental assessment of mitotic cells central auditory nuclei

In these experiments, I examine central auditory nuclei across metamorphic development in *Rana catesbeiana* to determine if numbers of mitotic cells are correlated with known stage dependent plastic events in the medulla (DLN and SON) and midbrain (TS).

Chapter 2 Hypotheses: Mitotic events in the developing Rana catesbeiana auditory nuclei.

Hypothesis 1: I expect that mitotic cells will be present in DLN, SON and TS and mitotic cell counts will increase and decrease with total numbers of cells in each nucleus rather than change in volume of nuclei.

Hypothesis 2: I expect there will be a dramatic reduction in mitotic cell counts during the "Deaf Period" stages in the SON and TS concurrent with reduced function and retraction of anatomical fibers and decreased auditory responses seen in functional reports.

Hypothesis 3: During metamorphic climax, I predict the numbers of mitotic cells to peak due to reestablished fiber connectivity following the "Deaf Period" and in response to the new ear structures in preparation for atmospheric-based hearing. I further expect numbers of mitotic cells to peak due to increased levels of circulating thyroid hormone.

Peaks in cell birth should also occur in the DLN during metamorphic climax, reflecting the final transformation of the middle ear system as it prepares for semi-terrestrial life. The TS receives input from both the DLN and the SON, but the specific pathways and strength of this input vary across larval development (Horowitz et al., 2007a). The TS also reorganizes over development, changing in volume and cell density and becoming progressively more differentiated into distinct subnuclei by the end of metamorphic climax (Kumaresan et al., 1998; Simmons & Chapman, 2002).

Hypothesis 4: I hypothesize that the reorganization of the auditory brainstem that occurs over development will be accompanied by stage-specific patterns of cell proliferation. I also expect newly born cells to differentiate and express either neural or glial phenotypic markers.

Peaks in cell birth should also occur in the DLN during metamorphic climax, reflecting the final transformation of the middle ear system as it prepares for semi-terrestrial life.

Cellular "Birth-Dating" with BrdU

Mitotic cells are quantified using the pulse-chase method of cellular "birth-dating" followed by immunohistochemical localization of the "pulsed" antigen. Tadpoles of various stage groups ranging from hatchlings through postmetamorphosis are injected intraperitoneally (i.p.) with (50 mg/kg) of the thymidine analog, 5 -bromo -2' – deoxyuridine (BrdU). The "pulsed" BrdU is rapidly distributed systemically due in part to the small size of the BrdU molecule, its diffusibility, and injection site. Although BrdU is a foreign antigen, it is analogous to thymidine, and may be incorporated into the DNA of cycling cells [during the S-phase (the DNA synthesis phase)]. Animals are allowed to recover to a post-injection defined time-point. Animals are then euthanized and the brain is removed. BrdU, within cellular DNA is localized using antigen-directed immunohistochemistry.

A BrdU-positive cell may undergo many different scenarios during the post-injection "chase" period. These scenarios include: 1) the cell may enter a stationary/quiescent state; or 2) the cell may migrate to other tissues; or 3) the cell may be a member of a rapidly proliferating population, and unless free BrdU is present, BrdU within the DNA is diluted with each mitotic event; or 4) the cell may undergo necrosis or apoptosis before tissue is analyzed; or 5) may be allowed to differentiate prior to BrdU-antigen localization with antibodies. Although post-mitotic cells can differentiate into a

number of cell types, the ability to follow a post-mitotic cell for extended post-injection time-points is especially important for locating BrdU positive neurons. The ability to "chase" following BrdU injection is imperative for locating BrdU positive neurons since neural precursors are typically generated in the periventricular zone and do not begin to differentiate until the final mitotic event and after migrating to the final tissue destination (Hatten, 1999).

BrdU "birth-dating" can indicate when even a mature neuron (labeled with BrdU) entered the S-phase of the cell cycle (prior to differentiation) at least once during the short period of time free BrdU was present after the "pulse". The BrdU method of cellular "birth-dating" is widely used in many animal models. Free BrdU is generally excreted relatively rapidly in all species and will only be incorporated into DNA strands in cycling cells that are actively replicating DNA while free BrdU is present. The availability of free BrdU may be even shorter in tadpoles and frogs than in other species due to frogs' ability to readily pass water and small molecules through their skin. Pilot studies were employed to optimize the number of injections which gave an acceptable signal-to-noise ratio while minimizing the number of BrdU injections.

This study investigates mitotic events as indexed by incorporation of the thymidine analog, BrdU, over the entire range of postembryonic larval development. I predict that cell proliferation will be found in these three brainstem nuclei concurrent with overall growth of the brain. I further predict, on the basis of the anatomical and functional data described above, that a selective decrease in the numbers of mitotic cells will be seen in the SON and TS during the deaf period. This should be followed by an increase during metamorphic climax. Peaks in cell birth should also occur in the DLN

during metamorphic climax, reflecting the final transformation of the middle ear system as it prepares for semi-terrestrial life. The TS receives input from both the DLN and the SON, but the specific pathways and strength of this input vary across larval development (Horowitz et al., 2007a). The TS also reorganizes over development, changing in volume and cell density and becoming progressively more differentiated into distinct subnuclei by the end of metamorphic climax (Kumaresan et al., 1998; Simmons & Chapman, 2002). I hypothesize that the reorganization of the auditory brainstem that occurs over development will be accompanied by stage-specific patterns of cell proliferation. I also expect newly born cells to differentiate and express either neural or glial phenotypic markers.

CHAPTER 2: MATERIALS AND METHODS

Subjects:

Animal procedures were authorized and overseen by the Brown University Institutional Animal Care and Use Committee (IACUC) and conform to NIH guidelines. *Rana catesbeiana* larvae were obtained from a commercial supplier (Dozier Lester, Duson, LA), staged according to Gosner (1960), and separated into major developmental groups as described by McDiarmid & Altig (1999). Data were obtained from animals in the following stage groupings (Table 2.1): hatchlings (stages 21–25; DLN and SON, n = 11; TS n = 10); early larval stages (stages 26–30, undifferentiated hind limb buds but no external limbs; DLN and SON, n = 14; TS, n = 9); late larval stages [(stages 31–41, showing a range of hind limb development, from initial differentiation to full development of toes; DLN and SON, n = 37; TS, n = 78; (late larval animals were further separated into two groups, late larval, stages 31-37, DLN and SON, n= 20, TS n = 58; and deaf, stages 38-41, DLN and SON, n= 17, TS, n = 20 (Boatright-Horowitz & Simmons, 1997)]; and metamorphic climax (stages 42–46, showing fully-developed hind limbs and forelimb emergence, and a range of head structure development, DLN and SON, n = 10; TS, n = 34). Post metamorphic froglets (snout-vent lengths 5.5- 7.0 cm, 1–90 days after completion of climax; DLN and SON, n = 10; TS, n= 9) were also used.

Animals that did not survive the injection procedure or died prior to euthanasia were not included in the sample size. These animals either did not wake from the anesthesia given prior to the BrdU injection or died due to possible BrdU toxicity. BrdU-based fatality is more likely in animals surviving for a period of time following BrdU

administration. Tadpoles were group housed in plastic aquaria containing dechlorinated, aerated water and fed cooked, unsalted spinach *ad libitum*. Froglets were housed individually in plastic terraria containing soil and water and were fed crickets *ad libitum*. The colony room was maintained at 25-28°C on a 12:12 light: dark cycle.

Table 2.1. Quantitative index of mitotic cells in central auditory nuclei. Sample size of *Rana catesbeiana* in each stage group.

	Stage Group	DLN and SON	TS
Hatchlings	21-25	11	10
Early Larval	26-30	14	9
Late Larval	31-37	20	58
Deaf	38-41	17	20
Climax	42-46	10	34
Froglet	< 5.5cm	10	9

BrdU Injections:

Animals were anesthetized by submersion in 0.15% (weight per volume, w/v) tricaine methanesulfonate (MS-222; pH 8; Sigma, St Louis, MO) for 2-5 minutes or until all reflexes disappeared, then injected intraperitoneally (i.p.) with 5-bromo -2'-deoxyuridine (BrdU; 50 mg/kg; pH 9; Sigma) in 0.9% (w/v) sterile saline. Number of injections and survival period were varied in separate groups of animals.

One group of animals (for DLN and SON, n = 19; for TS, n = 53) received one BrdU injection and survived 24 hour post injection. A second group of animals (n = 29) received two injections, 24 hour apart, and survived 48 hour after the initial injection. A third group of animals (n = 8) received two injections 24 hour apart, and survived 72 hour after the initial injection. These short survival periods were chosen to minimize the possibility of animals changing stage groups (e.g., from late larval to deaf period) during the period between BrdU injection and euthanasia. This is a particular issue when studying animals in metamorphic climax stages, because once entering climax, animals typically transform into froglets within 72–96 hour. In contrast, late larval animals and froglets can remain in these stage groups for multiple weeks. Under the housing conditions of this study, animals in the remaining developmental groups would enter a new stage group after approximately 7–21 days.

In a separate experiment, 12 additional animals, all in metamorphic climax, were given one injection of BrdU and allowed to survive for either 2 (n = 6) or 12 (n = 6) hours. Eight late larval animals were given one injection of BrdU and allowed for survive for 2 (n = 4) or 12 (n = 4) hours. Six animals (one hatchling, four late larval, one froglet) received two BrdU injections and survived 4, 7, 14, or 30 days.

Histology:

Animals were euthanized by submersion in 0.6% MS-222 for 5 minutes or until all reflexes disappeared and transcardially perfused with heparinized 0.9% (w/v) saline, followed by ice cold 4% (w/v) paraformaldehyde (pH 7.4). Brains were immediately removed and post fixed in 4% paraformaldehyde for 12 hours at 4°C. The brain was

removed of overlying membranes and embedded in 5% (w/v) agarose (ISC Bioexpress, Kaysville, UT). Brains were sliced coronally by vibratome at a thickness of 50 µm. Sections were placed on gelatin-subbed glass slides and allowed to dry at room temperature.

Some brains underwent immunohistochemistry for BrdU only. For a majority of brains, consecutive sections were placed on different gelatin-subbed glass slides, creating different slide sets so that each individual brain could undergo multiple histological treatments . Individual slide sets were histologically treated using one of the following: cresyl violet acetate, α-BrdU antibody, double label immunohistochemistry, or control.

Cresyl Violet:

For visualization of cell bodies, slide sets were placed in 0.5% (w/v) cresyl violet acetate staining solution (pH 3.7) and dehydrated using a graded ethanol series.

Brdu immunochemistry:

For all sections in which BrdU was to be localized, DNA strands were denatured with room temperature 2 N hydrochloric acid (HCl; Fisher Scientific, Pittsburgh, PA) for 2-5 minutes. Sections were incubated in murine monoclonal anti-BrdU (1:1000; Sigma B2531), or rat monoclonal anti-BrdU (1:1000; ab6326 AbCam), then in secondary antibodies conjugated either to biotin (1:1500; Sigma B7151) and developed with 3,3'-diaminobenzidine tetrahydrochloride (DAB Substrate Kit with nickel enhancement; Vector Laboratories, Burlingame, CA), or to fluorescent antibodies (goat anti-mouse

Alexa Fluor 594; 1:750; A11005; or donkey anti-rat Alexa Fluor 488; 1:750; A21208; both from Invitrogen, Eugene, OR).

Double label immunochemistry:

In brains undergoing multiple histological procedures, every third slide set (or second for early hatchlings) was processed using double label immunohistochemistry for BrdU in combination with the glial cell marker, glial fibrillary acidic protein (GFAP; 1:100; Sigma G9269), or the early neural marker, Turned-On-After-Division (TOAD-64; 1:5000; BD PharMingen, San Diego, CA). These antibodies were both generated in rabbit and visualized using fluorescence (secondary antibody Alexa Fluor 488; 1:750; A11008; Invitrogen).

Controls:

As controls, antibody treatments were performed in the absence of BrdU injection (sections from two brains), or with either the primary (sections from three brains) or secondary antibodies (sections from five brains) omitted. In these cases, label above the expected background was not observed.

Western Blot:

Prior to this study, antibodies generated against GFAP and TOAD-64 mammalian antigens had not been tested for specificity and selectivity towards anuran tissue. I tested the applicability of these antibodies for use in *Rana catesbeiana* using Western blot

assay. Late larval tadpoles (n = 2) were terminally anesthetized in 0.6% MS-222, and whole brains were quickly removed and immediately frozen on dry ice. Tissue was crushed using glass mortar and pestle and resuspended in Laemmli Lysis Buffer under denaturing conditions (Sigma cat# C8738). Fifty micro liters of sample was loaded onto polyacrylamide precast gels (10% and 4-20%; ISC Bioexpress) alongside prestained molecular weight marker (Sigma, Colorburst; cat# C8738) and separated by SDS-PAGE according to a previously published protocol (Ausubel, 1997).

Proteins were then transferred onto nitrocellulose membranes using the Bio-Rad Semi-Dry Transblotting system according to published protocols (Semi-Dry TransBlotter System product sheet; Bio-Rad) and thoroughly dried. Membranes were then incubated with antibodies specific for GFAP or TOAD-64 overnight in blocking buffer (phosphate buffered saline1XPBS supplemented with 1% horse serum and 0.1% Bovine Serum Albumin (BSA); 4°C, shaking). Membranes were then washed in three changes of blocking fresh buffer followed by incubation in fresh blocking buffer containing peroxidase-conjugated secondary antibody (1:1000; goat anti-rabbit peroxidase conjugate #A0545; 2 hours, R/T, while shaking). Membranes were then washed in three changes of saline containing 3´3 diaminobenzene DAB (Vector Laboratories). Upon identification of the chromagenic signal-to-noise ratio, membranes were rinsed briefly in water and allowed to air dry. Membranes were digitally scanned and imported into Corel Photo Paint (v.11, 13; Corel Corporation) for figure production and analysis.

Microscopy:

Slides were viewed through an Olympus (Melville, NY) BX-60 fluorescence microscope with custom filters attached to a MagnaFire digital camera (Optronics, Goleta, CA). Cresyl violet and DAB-labeled BrdU-positive cells were visualized at 10x and 40x using transmitted white light. Cresyl violet staining was dark purple-blue against a white background and DAB-labeled cells were purple-black against a brown background, respectively. Alexa Fluor 594 and 488 labels were viewed by fluorescence through custom made filters. BrdU-positive cells fluoresced red, and GFAP-, TOAD-64-positive cells fluoresced green, both against a yellow-orange background.

Images were captured using an IEEE-1394 PCI frame grabber (Texas Instruments, Dallas, TX) and saved to a Dell Pentium 4 2.4 GHz computer running image acquisition (MagnaFire, Optronics) software and stored as 24-bit RGB TIFF files. Brightness and contrast corrections if necessary were performed using Corel Draw (v.11) software. For preparation of black and white images from fluorescent label, the full color image was split into 8-bit grayscale for each of the red, green, and blue channels, using Corel Draw (v.11) software. The red channel (AlexaFluor 594) or green channel (AlexaFluor 488) was used to identify BrdU label.

Confocal Microscopy

A subset of cells were remounted in AntiFade Gold (Molecular Probes) and imaged using using a Leica TCS SP2 confocal microscope system (sequential scan mode, Leica Microsystems, Bannockburn, IL) for confirmation. Z-stacks were taken through each section at 0.5 μm steps. Images were viewed in orthogonal planes (X,Y,Z). If needed, brightness and contrast were adjusted using Leica Lite confocal software (Leica

Microsystems). Snapshot images were imported into Corel Draw (v.11) software for figure production.

Determination of Mitotic Index:

Nuclear boundaries for the DLN, SON and TS were determined by reference to stage-specific cresyl violet stained sections and published criteria (Jacoby & Rubinson, 1984; Boatright-Horowitz & Simmons, 1997; Kumaresan et al., 1998; Horowitz et al., 2007a). I performed cell counts for the DLN, SON and TS. All cell counts performed in the TS included pooled counts from the TLTD and magnocellular nucleus but did not include the ventricular zone. DLN and SON are easily located in cresyl violet stained sections. The internal organization of the TS changes across larval development (Kumaresan et al., 1998), and for many larval stages the developing principal and magnocellular nuclei cannot be differentiated. The laminar nucleus, directly ventral to the ventricular zone, can be determined for all stage groups investigated. However, the quantified numbers of BrdU-labeled cells in each nucleus of interest is a function of total numbers of cells available for labeling. Since developing *Rana catesbeiana* show a general increase in cell number within brain nuclei across development and because nuclear volume and cell packing density varies with development, I employed a correction factor to adjust for these developmental changes.

Determination of equation for T

I counted the total number of cells within a 50µm slice through each nucleus for animals at sample stages. I graphed the number of cells per 50µm slice versus animal stage and then fit a regression line which allowed calculation of the total number of cells in a 50µm brain slice for any developmental stage (T). This allows the number of BrdU labeled cells to be reported as a fraction of the total number of cells available for labeling of MI.

Cells located within in the ventricular zone (identified as the four cell-thick layer directly abutting the ventricular border) were visualized but not counted. Parenchymal cells were counted in every other section to avoid double counting split cells. Different cell types (neurons, glia, small cells; Templin & Simmons, 2005) were not differentiated in the cresyl violet counts. Cell counts were performed by the author and also by two independent observers who were blind to both the animal's developmental stage and the hypothesis of this experiment. Data from the three counters were averaged to obtain the final counts for that developmental group (variance between observers less than 2%). The total numbers of cells (T) available for labeling were derived from direct counts of cresyl-violet-stained cells in 12 animals (57 sections). These counts were then used to estimate total cell number. For tadpoles (hatchling through metamorphic climax stages), the best-fitting regression between cell count and Gosner stage was calculated (Microsoft Excel 2003). The trend line from this regression was used to estimate values of T in all tadpole brains. Data from froglets were not included in calculation of the trend line, because froglets cannot be assigned a Gosner stage number. Instead, the mean count of cresyl-

violet-labeled cells from the two froglets directly counted was used to estimate T. The resulting trend line for all stages is plotted for each nucleus.

Calculation of M.I.

The number of sections through the each nucleus and cell density varies with developmental stage. In order to normalize for these stage differences, the numbers of BrdU-labeled cells are expressed as counts per 50 μm section. The percentage of BrdU-labeled cells is expressed by the mitotic index (MI; Pizarro et al., 2004), as determined by the equation:

$$\textit{Equation 1:}\ \text{Mitotic Index} = \frac{[B]}{[T]} = \frac{[\ \text{BrdU Labeled Cells}\ ]}{[\ \text{Total Number of Cells}\ ]} \times 100$$

where B represents the number of BrdU-labeled cells (normalized over survival time) and T is the total number of cells available for labeling (calculated).

Analyses of change in normalized MI over development were performed using SPSS (v. 11.5; Jandel Scientific). A significance level of $p < 0.05$ was adopted.

CHAPTER 2: RESULTS

Quantification of Total Number of Cells in Central Auditory Nuclei

DLN and SON boundaries.

During development, the number of cells in each of the DLN, SON, and TS increase in overall number. However, the size of each nucleus and density of the cells vary over development as well. Figure 2.1 shows every second 50µm thick coronal brain slice (rostral to caudal) through the medulla of a stage 36/37 tadpole. Brain slices have been stained using cresyl violet acetate. Cell nuclei stain purple-blue, and were used to count the total number of cells in each 50µm section for each stage group and from which T is calculated. The relative volume and cell number in the DLN and SON vary from minimum to maximum to minimum with each advancing brain slice. DLN and SON boundary examples are indicated in Fig 2.1F and Fig 2.1E, repectively. Cell number and volume occupied by the DLN is in the slice pictured in Fig 2.1B but increases gradually with subsequent slices until they reach a maximum in Fig 2.1F (40x magnification) and decreases to a minimal volume and cell count in Fig 2.1L. A similar trend occurs in the SON. Cell number and volume occupied by the SON are at a minimum in Fig 2.1A and gradually increase with each 50µm brain slice until reaching a maximum in Fig 2.1E [(SON in Fig 2.1E is shown under high power magnification]. SON size is minimal in Fig 2.1H, and disappears in Figure 2.1I.

T was calculated by counting cells in each nucleus from every second (or every third) 50µm coronal brain slice. A correction factor was applied to estimate how many

cells were in the entire rostro-caudal extent of the nucleus which was then divided by the number of 50μm sections that could be sliced through each nucleus. The data were plotted with the total number of cells counted on the Y axis and the animal stage on the X axis and a best fit trend line was plotted. This trend line allowed calculation of T for any stage, even stages that T was not counted. For metamorphic frogs, T was not calculated by the trend line, Instead it was calculated using the means from two animals.

INSERT FIG 2.1 ABOUT HERE

Mitotic Cells are Present in Ventricular Zones

Mitotic cells, indicated by positive BrdU label, were found in the ependymal, subependymal and ventricular zones throughout the caudorostral extent of the brain, including the cerebellum, optic tectum, tegmentum and the hypothalamus in all developmental stages. Since these areas consistently exhibited high rates of cell proliferation, they were used as positive controls for both the fluorescent [Fig. 2.2(A)] and DAB [Fig. 2.2(B)] labeling techniques. In controls, no labeling of cells above background autofluorescence was found [Fig. 2.2(C)].

INSERT FIG 2.2 ABOUT HERE

Qualitative analysis indicates that proliferating cells are present, to varying degrees, in the DLN and SON of all stages. Although there were some 50 μm brain sections that had no BrdU-labeled cells, particularly in hatchlings and deaf period

animals, all animals had some BrdU-labeled cells in at least some sections. BrdU-labeled cells were often found immediately outside of the boundaries of the DLN and SON, and the number of proliferating cells was often qualitatively greater in non-medullary areas, including the TS.

Number of Mitotic Cells in the DLN Varies with Developmental Stage

Figure 2.3 shows representative sections from individual animals (early larval through froglets) showing the number of BrdU labeled cells in the DLN (arrowheads) 48 hours post-BrdU injection. Cresyl violet staining [Fig. 2.3(A), left panel] shows the dorsolateral placement of the DLN (circled in middle and right panels) in early larval animals. Hatchlings averaged 0.9 BrdU positive cells per 50 μm section (range 0-6) and it was common for the youngest hatchlings in the group to have sections with zero BrdU positive cells (data not shown). There was on average 2.8 BrdU labeled cells per 50 μm section in early larval animals (range, 0-11). Example images show 2 BrdU positive cells in the DLN of two different animals in this stage group [Fig. 2.3(A), center and right panels, respectively]. Sections from late larval animals averaged 3.2 BrdU positive cells per section (range 0-11). Representative images show one and 2 labeled cells, respectively [Fig. 2.3(B), center and right panels]. During the deaf period, an average of 2.2 BrdU positive cells per section is seen (range 0-11). Representative images from a stage 41 DLN show 2 and 0 BrdU positive cells [Fig. 2.3(C), center and right panels]. During metamorphic climax, the mean number of BrdU positive cells per section is 8.5 (range 1-19). Figure 2.3D shows 13 and 8 BrdU positive cells in a stage 43 DLN [Fig. 2.3(D), middle and right panels]. Often, these cells appear as "doublets," suggesting that

cells are produced as the result of a local mitotic event (Kornack & Rakic, 2001). Doublet cells appear in earlier stage groups as well, although they were most common in climax stages. In froglets, mean BrdU positive cell counts per 50 μm section decrease to 4.6 (range 0-34). A low and high power shot of a froglet DLN show one BrdU positive cell in each case [Fig. 2.3(E), middle and right panels].

INSERT FIG 2.3 ABOUT HERE

Mitotic Indices in the DLN

Figure 2.4 summarizes the mean M.I. per stage group co-plotted with the trend line showing the change in T across stage category for the DLN data. The best fitting trend line was calculated using data from early stage larval, late stage larval, deaf period, and metamorphic climax animals. No cresyl violet counts were obtained from hatchlings. Inclusion of the froglet data considerably lowered the fit. For this reason, data from froglets were excluded from the trend line analysis. T was determined based on the mean counts per 50μm slices from the two froglets. The best fitting trend line, $T_{larval} = 0.016x^3 - 0.847x^2 + 18.56x$, $R^2 = 0.99$, $p < 0.001$ where x = stage), was used to generate T for calculations of MI in tadpoles. One way between-groups analysis of variance indicates the presence of a significant difference in the MI [F (5, 47) = 2.4, p = 0.05] across developmental stages. Post-hoc tests (LSD test) showed a significant decrease in MI between the late larval and deaf period groups, between late larval and froglet groups, and between metamorphic climax and froglet groups. There was a significant increase in MI between the deaf period and metamorphic climax stages. There was no significant

change in MI between hatchling and late larval stages, even though T increases over this time period (Fig. 2.4).

INSERT FIG 2.4 ABOUT HERE

Number of Mitotic Cells in the SON Varies with Developmental Stage

Figure 2.5 shows representative images of BrdU labeled cells in the SON 48 hours post-BrdU injection. Boundaries of the SON are circled and BrdU positive cells within these boundaries are marked with arrowheads. In hatchlings (data not shown), a mean of 1.4 labeled cells per section is seen, with a range of 0-7. Sections from early larval animals show a mean number of BrdU positive cells of 2.9 (range of 0-9) per 50 μm section. Example images from a stage 26 SON shows BrdU labeled cells are often located on the border [Fig 2.5(A), middle panel; 1 cell] as well as within central areas of the nucleus [Fig. 2.5(A), right panel; 2 cells]. In sections from animals in late larval stages, there is an average of 1.8 BrdU labeled cells per section (range 0-9). Although there is little label in the central portion of the SON itself, some labeled cells are located ventrally and laterally immediately adjacent to the nucleus boundaries [Fig. 2.5(B), middle panel]. During the end of this stage category (stages 36 and 37), there is a slight increase in numbers of BrdU positive cells. These cells are often located in the ventral-most portion of the SON [Fig. 2.5(B), right panel]. The mean number of BrdU positive cell counts per 50 μm section is 2.2 (range 0-12) during the deaf period. Most sections show 0 or 1 labeled cells [Fig. 2.5(C), middle and right panels]. Cell proliferation in the

SON increases to the highest mean counts of all stage groups at the onset of metamorphic climax, at 9.5 (range 3-19), and is maintained at this high level throughout the remainder of the climax period. Shown are 19 BrdU positive cells in a stage 43 SON [Fig. 2.5(D), middle panel]. During climax, labeled cells appear mainly as doublets [Fig. 2.5(D), right panel]. Doublets were present in the SON of earlier stage groups as well, but they were not as numerous as in climax stages. In froglets, the mean number of BrdU positive cells per 50 μm section decreases to 3.8 (range 0-8). Shown in this example are 6 BrdU positive cells (center panel), and 2 BrdU positive cells on the right [Fig. 2.5(E)]. Areas surrounding the SON, however, have cell proliferation rates that remain high [Fig. 2.5(E), middle panel].

INSERT FIG 2.5 ABOUT HERE

Mitotic Index in SON

Figure 2.6 summarizes the SON quantitative data. The best-fitting trend line through the larval data was $T_{larval} = 0.127x^2 + 8.72x$, $R^2 = 0.87$, $p < 0.01$. Including froglets in the trend line calculation decreased the fit considerably, so to be consistent with the DLN data, the T for the 2 froglets counted was used to calculate MI for this group. There was a significant difference in MI between groups [F (5,37) = 4.4; $p <$ 0.01]. There was a significant peak in numbers of proliferating cells during metamorphic climax compared to all other stages (LSD test). In addition, number of proliferating cells in the deaf period was significantly lower than that seen in early larval stages. These changes in MI do not follow the changes in T over this developmental time span.

INSERT FIG 2.6 ABOUT HERE

Summary of Proliferating Cells

The distribution of proliferating cells in the DLN and SON is summarized by representative images from animals in all developmental groups (Fig. 2.7). Figure 2.7(A) shows a representative 50 μm section from an early larval tadpole (stage 26). BrdU positive cells are heavily clustered around the ventricle, while there are few cells in the DLN and SON (group data are shown in Figs. 2.4, 2.6). Heavy clustering of labeled cells around the ventricle is also seen in hatchlings (data not shown). At stage 31 [Fig. 2.7(B)], the beginning of the late larval period, numbers of labeled cells around the ventricle decrease. There are slightly fewer labeled cells in the DLN but more in the SON. In the middle of the late larval period [Fig. 2.7C, a stage 36 tadpole], numbers of labeled cells around the ventricle have declined from those seen in earlier stages. The number of positive cells in the SON is at a level similar to that seen in stage 31 animals; however, the number of labeled cells in the DLN increases. The number of proliferating cells drops off at stage 41, in the deaf period [Fig. 2.7(D)]. Numbers of proliferating cells in the ventricular region have increased from those seen in late larval stages. The highest numbers of proliferating cells in both the DLN and SON are found in metamorphic climax animals [Fig. 2.7(E)]. Proliferating cells are not seen around the ventricle itself, but large numbers are apparent in the medulla as a whole. In froglets [Fig. 2.7(F)], numbers of labeled cells decreases in both the DLN and SON [Fig. 2.7(F)]. Proliferating cells are again found in the ventricular areas.

For both the DLN and SON nuclei, data were subdivided into those collected during the summer months (April-September) and those collected in the winter months (October-March). Analysis of variance showed no difference in the MI as a function of season; the trends observed in Figures 2.4 and 2.6 were consistent in both summer and winter.

INSERT FIG 2.7 ABOUT HERE

Distribution of Proliferating Cells at Extended Survival Periods

The distribution of proliferating cells at three different time points in late larval tadpoles and froglets is summarized in representative images (Fig. 2.8). Figure 2.8 (top, left) shows BrdU positive cells in the medulla of a late larval tadpole 48 hours after the initial BrdU injection [stage 31 is shown in Fig. 2.8 (top, left), also shown in Fig. 2.7(B)]. As described in Figure 2.7, BrdU-positive cells are present adjacent to the ventricle [Fig 2.8 (top, left); ventricle is marked with an asterisk], or clustered in non-auditory areas of the brainstem. Few cells in the DLN are labeled after 48 hours, while more are labeled in the SON. Late larval animals that were allowed to survive two weeks after the initial BrdU injection [stage 34 is shown in Fig. 2.7 (top, center)] show a similar number of positive cells in the DLN (1 cell is shown) and SON (4 cells are shown), as seen in the 48 hour survival point. However, the pattern of labeled cells appears more evenly distributed throughout the brainstem than at the 48 hour survival period, and there are qualitatively fewer labeled cells adjacent to the ventricle [Fig. 2.8 (top, center)]. Late larval animals that were allowed to survive post injection for one month [stage 34 is

shown in Fig 2.8(top, right); the animal was initially injected with BrdU at stage 33] have overall qualitatively fewer numbers of labeled cells throughout the brainstem and adjacent to the ventricle [Fig. 2.8 (top, right)]. The number of labeled cells increases slightly in the DLN but decreases in the SON [2 and 0 cells are shown, respectively; Fig. 2.8 (top, right)].

In froglets, 48 hours after the initial BrdU injection, there are many BrdU-positive cells throughout the brainstem and adjacent to the ventricle [Fig. 2.8 (bottom, left)]. Labeled cells are seen within the DLN [Fig. 2.8 (bottom, left) and Fig. 2.7(F)] and SON [Fig. 2.8 (bottom, left) and 2.7(F)]. After one month of survival, there are fewer BrdU-labeled cells overall in the medulla, including the ventricular zone, but numbers are higher than seen in late larval animals at the same survival period. Numbers of labeled cells in the DLN and SON are similar to those at 48 hours [3 and 5 cells, respectively; Fig. 2.8 (bottom, right)].

INSERT FIG 2.8 ABOUT HERE

Specificity of GFAP and TOAD-64 antibodies in to Rana antigens

Figure 2.9 shows that GFAP and TOAD-64 directed antibodies are specific in *Rana* tissue. Figure 2.9A shows western blot results of GFAP antibody specificity when probing protein from rodent and *Rana catesbeiana* tissues. The absence of protein sample in Lane 1 shows there is no nonspecific binding of antibody. Lane 2 contains concentrated rodent brain homogenate, to which GFAP is expected to bind and is used as

a positive control. A positive DAB reaction product is seen as two bands [(Fig 2.9(A) Lane 2: white arrows)]. Lanes 3 and 4 contain tadpole brain homogenate, and show a positive DAB reaction product shown as two (or three) bands (Lanes 3, 4; black arrows). Bands in Lane 2 and the bottom two bands between Lanes 3 and 4 appear similar in pattern, although bands in Lanes 3 and 4 appear slightly lower in molecular weight.

Figure 2.9b shows western blot results of TOAD-64 antibody specificity when probing protein from rodent and bullfrog tissues. Lane 1 contains no protein sample and is used as a control. There is no DAB signal in this lane. Lane 2 contains concentrated rodent brain homogenate, to which TOAD-64 binds and is used as a positive control. A positive DAB reaction product is seen as one band [(Fig 2.9B Lane 2: white arrow)]. Lanes 3 and 4 contain the tadpole brain homogenate, and shows a positive DAB [reaction product shown as one band (Lanes 3, 4; black arrow)]. Bands in Lane 2 and between Lanes 3 and 4 appear similar in pattern, although bands in Lanes 3 and 4 appear slightly lower in molecular weight.

INSERT FIG 2.9 ABOUT HERE

Phenotype of Newly Proliferating Cells

At the 48 hour survival point, BrdU/GFAP, and BrdU/TOAD-64 were all expressed in medullary tissue, but the only co-localization seen was with BrdU and in medullary tissue outside of the DLN and SON (data not shown). The vast majority of BrdU-positive cells were located in ventricular and subventricular zones. Cells directly

abutting the ventricle were often labeled with BrdU but never co-localized with BrdU and TOAD-64 or GFAP at any survival period or any developmental stage. After 2 weeks of survival, there were overall fewer BrdU-positive cells than at the 48 hour time point, but BrdU-positive cells were still observed in the ependymal layer adjacent to the ventricle, and there were more BrdU-positive cells in the parenchyma. The proportion of BrdU/GFAP double labeled cells were observed at 2 weeks post-BrdU injection (2 BrdU/GFAP double labeled cells are shown in this example froglet DLN, Fig. 2.10A); however, TOAD-64/BrdU positive cells were only found in animals surviving at least one month post BrdU injection (1 BrdU/TOAD-64 double labeled cell is shown in a stage 36 DLN, Fig. 2.10B).

INSERT FIG 2.10 ABOUT HERE

Number of BrdU Positive Cells and MI in TS Vary across Developmental Stage Groups

At all survival times and at all developmental stages, some BrdU-labeled cells were observed around the optic ventricle. Figure 2.11 shows representative images through the TS, at approximately the midpoint, from one animal in each of the six stage groups (data are from the 48 hour survival period). Labeled cells are observed around the optic ventricle (figures show its ventral edge, immediately dorsal to the area of the developing laminar nucleus) at all stages, but the concentration of labeled ventricular cells appears greater in hatchling, deaf period, and froglet stages than in early or late larval stages. When ventricular label is present, labeled cells appear to be spread out

across the entire medial-to-lateral extent of the ventricular zone, rather than being concentrated in any particular area. Labeled cells were also found around the fourth ventricle in the region of the tegmentum (Fig. 2.13). Labeled cells were also found more ventrally in the TS itself.

INSERT FIG 2.11 ABOUT HERE

Mitotic Index in TS

The total number of TS cells per 50 µm section available for label (T) increased with Gosner stage according to a cubic function ($T = 0.4681x^3 - 32.836x^2 + 643.62x$, where x = stage, $r^2 = 0.70$, $p > 0.05$). Values of T for tadpoles as calculated from this regression are plotted in Figure 2.12 (y axis, top right). The trend line shows that T is high in hatchlings, declines up to late larval stages, and then increases during the deaf period and metamorphic climax. T calculated from froglets was similar to that estimated from the regression line for climax animals. MI averaged and normalized over the 24, 48, and 72 hour survival times is plotted on the same figure (y axis, bottom left). MI was low in hatchlings and increased slightly in early and late larval stages. This was followed by large increases in MI in deaf period and metamorphic climax with a subsequent decline in froglets. Differences in MI were statistically significant across developmental stage groups SD, [one-way analysis of variance (ANOVA), $F(5, 55) = 10.5$; $p < 0.001$]. Post hoc testing (least significant difference test) revealed that MI is significantly lower in hatchlings through late larval animals than in deaf period through froglet animals. MI

does not vary significantly between the hatchling, early larval, and late larval groups. MI in deaf period animals is significantly higher than in hatchling, early larval, and late larval animals, but significantly lower than in metamorphic climax animals. There is no significant difference in MI between tadpoles in metamorphic climax tadpoles and froglets, or between deaf period tadpoles and froglets.

INSERT FIG 2.12 ABOUT HERE

Cell Proliferation at Different Survival Times in TS

The number and distribution of BrdU-labeled cells at different survival time points are shown in representative schematics in Figure 2.13 (left column, late larval animals; right column, metamorphic climax animals). Late larval animals were allowed to survive for times of 2 (n = 4), 12 (n = 4), 24 (n = 4), and 48 (n = 8) hours, and 14 (n = 1) and 30 (n = 2) days. Animals in metamorphic climax were allowed to survive for times of 2 (n = 6), 12 (n = 6), 24 (n = 5), and 48 (n = 3) hours. For both groups, BrdU-labeled cells, if present, were congregated in proliferative zones around the third and fourth ventricles. Particularly in the metamorphic climax animals, labeled cells were concentrated around the midline of the TS, but also extended more laterally around the entire extent of the optic ventricle. For the late larval group compared to the metamorphic climax group, fewer labeled cells were found in the ventricular zones at any time point. Some label was still present in late larval animals at 14 and 30 days post injection, however. In both developmental groups, more labeled cells were seen at 24 and 48 hour

than at 2 or 12 hour. The numbers of BrdU-labeled cells in the ventricular zone at the 24 and 48 hour time points were considerably higher in metamorphic climax than in late larval stages. In both stage groups, BrdU-labeled cells were also seen outside the ventricular zone, and the numbers increased with survival time, particularly in the metamorphic climax group. Few BrdU- labeled cells were seen in the TS at the 2 hour survival time in either group, and those that were visible were preferentially located laterally and around the boundaries of the TS. At the 12 hour time point, labeled cells were also observed within the TS itself, both near the ventricular zone and also more ventrally. Considerable numbers of BrdU-labeled cells [Fig. 2.13A] were found in the TS of metamorphic climax animals at both the 24 and 48 hour time points.

INSERT FIG 2.13 ABOUT HERE

BrdU-Positive Cells Expressing Neural or Glial Markers Are Present at Long Survival Times

Results of western blot analyses (Fig. 2.9) show that these antibodies recognize both GFAP and TOAD-64 are in larval *Rana* tissue. Neither GFAP nor TOAD-64 were expressed in the ventricular zone at any developmental stage, but both proteins were found in the TS parenchyma in all stage groups investigated. Cells double labeled with BrdU and either GFAP or TOAD-64 were observed only at survival times of 14–30 days (GFAP) or 30 days (TOAD-64). Examples of orthogonally rotated confocal z-stack images show the presence of cells double-labeled with BrdU/GFAP [Fig. 2.14(A)] and with BrdU/TOAD-64 [Fig. 2.14(B)] in the TS (area of the laminar nucleus) of a froglet

surviving 30 days post- BrdU injection. At the 30 day survival time point, approximately 20% of BrdU-labeled cells were also labeled with GFAP, while approximately 10% of BrdU-labeled cells were labeled with TOAD-64.

INSERT FIG 2.14 ABOUT HERE

CHAPTER 2: DISCUSSION

Summary of results

These experiments show that cell proliferation in the auditory brainstem of *Rana catesbeiana* varies in a stage-dependent manner across metamorphic development. A peak in cell proliferation occurs at metamorphic climax in the DLN, SON and TS. In the TS, proliferation is significantly higher in later stages of development (deaf period through froglet stages) than in earlier stages (hatchling through late larval stages). This trend differs from those observed in both the DLN and the SON, where proliferation was low during the deaf period and relatively higher in early/late larval stages. These differences in the pattern of proliferation in the TS on the one hand and in the DLN and SON on the other suggest that the mechanisms underlying cell proliferation differ in these different nuclei in the auditory pathway.

Methodological Considerations

Methodological issues resulting from the use of BrdU include its toxicity (Stockdale et al., 1964; Kolb et al., 1999), the possibility that BrdU could label cells undergoing DNA repair as well as those undergoing mitosis (Cooper-Kuhn & Kuhn, 2002), and the influence of environmental factors such as temperature, photoperiod and housing conditions (Gould & Gross, 2002; Radmilovich et al., 2003; Pizarro et al., 2004). Observations made during the conduct of the present study indicated that the doses used (50 mg/kg) did not produce any visible side effects (nausea, abnormalities in swimming behavior) or death. This dosage has also been identified in the literature as not producing

appreciable toxic effects in other developing tissues (Miller and Nowakowski, 1988; Takahashi et al., 1992). Because all cell populations undergo DNA repair, we would expected to see much higher counts of BrdU labeled cells than we observed, and we would expected to see these labeled cells at high numbers throughout the brainstem at all developmental stages. The observations that M.I. was typically less than 2% and that it varied across developmental stage groups suggest that cells undergoing DNA repair were not labeled. Temperature, photoperiod and housing conditions were standardized for all animals used in our study, and thus could not measurably affect the data. Most of our data were collected from April through September, when animals were readily available. Close inspection of the data revealed no clear differences in MI between brains prepared during the spring/summer months versus the winter months, but the small sample size in the winter months precluded statistical analyses of any differences

The majority of my data are based on survival periods of 24 and 48 hours, which were identified as being long enough to allow cells to take up BrdU and undergo mitosis, but short enough to prevent animals from changing stage groups (e.g., from deaf period to metamorphic climax) before euthanasia. Short survival times also have the advantage of minimizing the loss of label due to dilution of BrdU through successive cell divisions. Survival periods of 24-48 hours were long enough to visualize labeled cells within the TS itself; these cells may be generated *in situ* or migrate from the ventricular zone. Survival periods of 72 hours or longer were only used for late larval animals and froglets, who can remain within these respective stages for 30 days or longer without transforming into the next stage group.

I could not determine sex in the animals used in this study because tadpoles have undifferentiated or ambiguous gonads (Swingle, 1926). In juvenile zebra finches, cell proliferation rates vary with the animal's sex (Dewulf & Bottjer, 2002). Males, who sing as adults, exhibit more newly-born cells in the telencephalic ventricular zone (close to the forebrain song control nuclei) than females, who do not sing. Because adult male bullfrogs emit advertisement calls while females do not, it is possible that a similar sex difference would be found in this species, perhaps visible at later stage groups. I found no sex differences in cell proliferation in the vocalization pathway of larval *Xenopus laevis*, another anuran species with sexually dimorphic calling behavior as adults. Gorlick and Kelley (1987) attributed sex differences in cell numbers in this pathway in adults to differential patterns of cell death/survival or cell differentiation, rather than to cell proliferation.

Cell Number and Cell Proliferation Vary with Developmental Stage

From hatchling to metamorphic climax stages, the TS increases in volume by about 800%. The change in numbers of TS cells over larval development follows a cubic trend. The relatively large value of T in hatchling stages may reflect the outcome of a large amount of cell proliferation or a small amount of cell death in preceding embryonic stages or may be a function of the higher density of cells in the TS in these early stages (because T is calculated per 50 µm section). T declines in the early and late larval stages. Because cell proliferation, as indexed by MI, increases in these stage groups over what is observed in hatchlings, the decline in T may reflect increased brain volume and/or increased cell death during these particular periods of development. Both T and MI

increase during the deaf period and metamorphic climax. MI declines during the froglet period, to the level observed during the deaf period, while T appears to plateau. The overall pattern of change in both T and MI suggest that cell proliferation is not simply occurring in parallel with the overall increase in the volume of the TS. In the DLN, the change in T across larval development also follows a cubic trend, while in the SON, the change in T best follows a quadratic trend. Also between MI comparisons show that the changes in cell number in different parts of the auditory pathway do not necessarily follow parallel developmental time courses. Changes in volume of brain nuclei during development reflect not only changes in cell number but also changes in packing density, which are probably more related to increases in fiber outgrowth and extent of dendritic arbors rather than to birth of new cells.

In all three nuclei of the auditory pathway so far studied, MI peaks during metamorphic climax, and decreases during the froglet stage from the level observed in climax. At earlier developmental stages, there are clear differences in rates of cell proliferation between these nuclei. In both the DLN and SON, MI declines during the deaf period from its level in late larval stages, while in the TS, MI increases during the deaf period from its level in late larval stages. Moreover, in the TS, MI during the hatchling, early larval and late larval stages is approximately constant, and lower than observed in either the DMN or SON, where there are significant differences in MI between these developmental stages. These two findings – cyclical changes in cell proliferation and differences in peaks of cell proliferation between different nuclei in the same neural system – are consistent with what has been observed in the vocalization pathway (Gorlick & Kelley, 1987) and in the olfactory bulb (Fritz et al., 1996) of larval

Xenopus. Our finding of a peak in cell proliferation at metamorphic climax in all three nuclei of the auditory pathway has not been reported previously in larval *Rana.* In the spinal cord, for example, peaks of mitotic activity occur early in the larval period, in both *Rana* (Pollack 1976; Clorfene& Pollack 1994) and *Xenopus* (Schlosser et al., 2002). Numbers of PCNA-labeled cells in ventricular proliferative zones of larval *Xenopus* brain decrease over the larval period (Wulliman et al., 2005). These investigators did not quantify numbers of labeled cells in the brain parenchyma itself, and we did not quantify numbers of labeled cells in the ventricular zone. Pizarro et al. (2004) in lamprey, another metamorphosing species, found little change in cell proliferation in the rhombencephalon and spinal cord between larval and adult animals.

Proliferating Cells Are Found in Parenchyma

At short survival times, more BrdU-labeled cells are found in the ventricular zone than in the brain parenchyma (Figs. 2.3, 2.5, and 2.11), consistent with previous studies of the spatial distribution of proliferating cells in developing animals (DeWulf & Bottjer, 2002; Pizarro et al., 2004; Wulliman et al., 2005). As survival time increases up to 24–48 hours, increasingly more BrdU-labeled cells are found in the TS itself. One explanation is that newly proliferating cells are migrating from the ventricular zone (Hatten, 1999). The differences between the late larval and the metamorphic climax groups in the numbers of labeled cells in the TS at any survival period (Fig. 2.13) suggest that the time course and mechanisms underlying cell migration differ across developmental stages. The few cells seen in the TS itself at the 2 hour survival time point indicate that the cell cycle may be longer than 2 hours, or that a small proportion of cells may be born *in situ.*

Particularly in metamorphic climax stages, BrdU-labeled cells in the TS at 12–48 hour time points often occur as doublets, also suggesting that some cells are dividing *in situ*. Consistent with previous results in the DLN and SON, double labeling experiments with GFAP and TOAD-64 suggest that a subset of new cells differentiate into glia or neurons. Because most of our tissue was processed with fluorescent-conjugated antibodies, we were unable to determine cell identity by structural features, as can be performed by [^{3}H]-thymidine counter stained with cresyl violet (Gorlick & Kelley, 1987; DeWulf & Bottjer, 2002). GFAP and TOAD-64 were each expressed in the DLN, SON, and TS in animals of all stage groups investigated in this study and would sometimes co-label with BrdU at long survival time periods. No cells labeled with either GFAP or TOAD-64 were ever observed in the ventricular zone, consistent with the view that these ventricular cells are pluripotent precursors (Minturn et al., 1995; Rao & Mayer-Proschel, 2000). In both late larval and froglet animals, double label of either GFAP or TOAD-64 with BrdU was seen only at relatively long survival times (14– 30 days). Because we studied only a limited number of developmental groups at these long survival periods, and because our sample size was small, we cannot determine if similar patterns of double label would be observed in other developmental stage groups. It is likely that cells born in situ at shorter survival times are glia and not neurons because glia can proliferate in parenchyma. New neurons are born in ventricular zones and must migrate to their destination before expressing TOAD64.

Mechanisms Underlying Proliferative Activity

The mechanisms underlying these changes in cell proliferation, both across developmental stages and between different nuclei in the auditory pathway, are unknown. Possibilities include (1) changes in sensory input driving changes in cell birth rates as the peripheral auditory pathways develop and mature and (2) changes in thyroid hormone levels concurrent with metamorphosis drive increased cell proliferation.

Larval development features significant changes in afferent and efferent connectivity in the auditory pathways (Jacoby & Rubinson, 1984; Boatright-Horowitz & Simmons, 1997; Horowitz et al., 2007a). These neuroanatomical changes may require cell turnover and may reflect the sequential development of the adult frog's two middle ear transduction systems. As early as the hatchling stage, many features of afferent and efferent connectivity between the auditory medulla and midbrain can be observed in much the same pattern as seen in adult frogs. These connectivity patterns provide a central basis for the responsiveness of the TS in tadpoles younger than the deaf period to auditory stimulation (Boatright-Horowitz & Simmons, 1997). During the deaf period, both afferent and efferent connectivity between the SON and the ipsilateral TS is disrupted (Horowitz et al., 2007a), and neural responsiveness of the TS declines (Boatright-Horowitz & Simmons, 1997). These central effects are correlated in time with changes in the otic capsule during these stages (Simmons & Horowitz, 2006). Before the deaf period, the oval window is covered only by connective and epithetial tissue, and input to the inner ear organs is likely mediated by direct stimulation of the hair cells through the body wall and the oval window (the "fenestral pathway;" Hetherington,

1987). Between stages 38-41, the operculum cartilage begins to grow around and over the area of the oval window producing a partial or total blockade of the input to the inner ear organs (Hetherington, 1987). The disruption of sensory input during these stages (the deaf period) may be responsible not only for the decline in neural responsiveness of the TS to auditory stimuli during these stages, but also to the decline in number of mitotic cells in both the DLN and SON. However, this does not explain the increased numbers of Brdu labeled cells in the TS during the deaf period. Fig. 2.12 shows MI is low in hatchlings through late larval stage groups and increases in deaf through froglet stges. The increase in MI in TS may instead result from the decrease in cell packing density in TS between hatchling through late larval stages (see Fig 2.12). T decreases with advancing stage groups. The decrease in T is not due to an overall cell loss in the stages. T actually increases in the TS as a whole but the volume of the nucleus increases dramatically lowering the number of cells in each SON slice. This may be due to contact inhibition. During metamorphic climax, the operculum begins to partially retract from the oval window as the footplate of the stapes develops. Anatomical connectivity between the SON and the TS is restored and the TS again responds to auditory stimulation, but in a broader frequency range (Boatright-Horowitz & Simmons, 1997). The peak in cell proliferation in the DLN and SON during metamorphic climax may reflect the resumption of peripheral sensory input and the need to generate or replace cells required for development and maintenance of input from the newly emerging tympanic/columellar pathway. The completion of the tympanic/columellar pathway at the end of metamorphic climax and beginning of the froglet period could signal a decreased need for new cell proliferation, although some amount may still be present to accommodate continued

changes in neural responsiveness in the postmetamorphic period (Boatright-Horowitz & Simmons, 1995). The progressive growth of the *Xenopus* eighth cranial nerve across development (Lopez-Anaya et al., 1997) is consistent with these effects, but comparable data have not been reported in *Rana*.

Changes in sensory input during larval development may also be correlated with growth and turnover of inner ear hair cells themselves. The formation of the inner ear organs has been described in both larval *Rana* and larval *Xenopus* (Lewis & Li, 1973; Hertwig, 1987; Diaz et al., 1995; Quick & Serrano, 2005). By the early larval stages, the morphology of the inner ear organs resembles that seen in adult animals; however, it is not yet known when hair cells in the different organs become functionally active. The large amounts of cell proliferation in the DLN and SON during early and late larval stages suggest that inner ear hair cells might become functionally active during these stages.

Changes in peripheral input may provide some basis for the developmental patterns of cell proliferation in the DLN and SON, particularly the decline during the deaf period and the subsequent peak in metamorphic climax. On the other hand, changes in peripheral input from the inner ear do not easily explain the increase in cell proliferation in the TS during the deaf period. Other anatomical changes in the ascending auditory pathways may play a role. During the deaf period, afferent connectivity between the SON and ipsilateral DLN first emerges (Horowitz et al., 2007a), and this new pathway may affect the patterns of neural input from these medullary nuclei to the TS. Increased cell proliferation during the deaf period might reflect the need to maintain these functions in the face of the disruption of input from the SON. The peak in cell proliferation during

climax might reflect, not only the renewed input from the ipsilateral SON, but the emergence of input from the contralateral SON (Horowitz et al., 2007a).

In other vertebrate species (mammals: Cant, 1998; avians, Kubke & Carr, 2005), cell birth in embryonic auditory pathways occurs in a sequential, although partially overlapping order, with medullary nuclei developing prior to midbrain nuclei. This general sequence of development is consistent with my results in larval *Rana*, where the early peaks of cell proliferation in the auditory medulla occur prior to that in the TS. My data also show that peaks of cell proliferation in all three auditory nuclei so far examined occur at metamorphic climax, in final preparation for the transition from a fully aquatic to an amphibious life. In other metamorphosing systems (*Xenopus* spinal cord and retina), increased cell proliferation during certain developmental times has been attributed to changes in the levels of thyroid hormone and changes in the expression of thyroid hormone receptors (Schrieber et al., 2001; Schlosser et al., 2002; Marsh-Armstrong et al., 1999, 2004). Changes in levels of thyroid hormone and its receptors drive metamorphic change, with the time course of change in different sensory and motor systems being correlated with times of peak expression (Denver, 1998). It is possible that changes in levels of thyroid hormone and expression of thyroid hormone receptors are correlated with the changes of cell proliferation described here.

SECTION II: PLASTICITY IN THE ADULT

SECTION II: INTRODUCTION

The ability of an organism to regenerate tissue has been suggested to vary inversely with species complexity. For example, the planarian has the capacity to fully regenerate and can not only regenerate an amputated part, but can also regenerate a second full planarian from the amputated stump (Agata, 2007). Most vertebrate animals are only fully regenerative in the earliest embryonic stages and lose this ability as development proceeds (Russell & Moore, 1995; Hafidi et al., 1999; Lohmann et al., 1999; review: Schwab & Bartholdi, 1996). Fish and amphibians remain highly regenerative at maturity and are widely studied for their ability to regrow many but not all tissues. In contrast, mammals have extremely limited regenerative ability and most damage is permanent, especially in adults.

It is of clear clinical relevance to develop novel treatments to stimulate recovery of function in models incapable of adult CNS regeneration. The CNS of adult anurans has many similarities to that of mammals, including multiple factors that are expressed in CNS substrate as “nonpermissive” or “repulsive” molecules. These substances effectively abate any attempted neurite entry and/or extension within the CNS substrate. Although adult ranids also express many of these these nonpermissive molecules (Becker et al., 1995), these animals have long been known for highly robust regenerative abilities (Sperry, 1945). Anatomical and physiological studies have demonstrated that the damaged n.VIII of ranids can regenerate and functionally reform proper anatomical connectivity in the auditory brainstem (Zakon & Capranica, 1981; Zakon, 1983; Newman et al., 1987, 1989; Newman & Honrubia, 1992). Furthermore, in frogs, not only do

n.VIII ganglion cells not degenerate after injury, but lesioned n.VIII fibers undergo active regeneration and reconnection into the "nonpermissive" CNS substrate, reestablishing appropriate organization and synaptic target density similar to that of the non-lesioned nerve (Zakon & Capranica 1981; Zakon 1983; Newman et al. 1987, 1989; Newman & Honrubia 1992). This regenerative capacity makes the anuran auditory system a useful model for exploring recovery of function following cranial nerve trauma.

How do adult ranids show such a robust regenerative response into nonpermissive CNS substrates, even in the absence of any biological treatment? Adult ranids offer an ideal model to investigate how regeneration and functional recovery occurs in a vertebrate known to express molecules nonpermissive to regeneration. It is possible that regenerating neurites in adult ranids can "override" nonpermissive signals which may induce growth cone collapse, abortive neurite extension, inappropriate neurite path finding, chemorepulsive signaling, etc. If such "override" signals are characterized in this animal model capable of CNS regeneration, they may be further investigated for clinical relevance in mammalian models incapable of effective CNS regeneration, including humans.

This study investigates effects of cranial nerve lesion on behavior, anatomy, and gene expression in two species of adult ranids: the American bullfrog, *Rana catesbeiana*, and the African clawed frog, *Xenopus laevis*.

1). Behavioral assessment (Chapter 3)

Changes in posture is examined after unilateral crush of the n.VIII. Unilateral crush lesion is expected to result in a behavioral head tilt toward the side of the lesion.

Head tilt angles in animals subjected to unilateral n.VIII crush are expected to be large and significantly different from that of nonsurgical control animals or of animals subjected to sham surgery at short time periods after damage. Head tilt angles are expected to decrease at longer post-operative survival times. In *Rana*, head tilt appears to normalize by 4-12 weeks after lesion (Zakon, 1983; Zakon & Capranica, 1981; Dieringer, 1995). I expect to replicate these findings in *Rana*, and to observe a similar time course of recovery in *Xenopus*.

2). Anatomical experiments (Chapter 4)

These experiments investigate the time course of re-innervation of the medulla following damage to the n.VIII. First, fluorescent lipophilic tracers are placed into n.VIII nerve branches of control animals and animals subjected to n.VIII crush (distal to the lesion site). I expect to find that neurite density and projection extent in the lesioned animals will be significantly less than that of controls at short time points, but will approach that of control animals at longer time points. The recovery of projection density is expected to mirror behavioral normalization. Second, differences in numbers of mitotic cells in auditory and vestibular nuclei of the medulla will be quantified in the different experimental groups. Animals are injected with the thymidine analog, 5-bromo-2'-deoxyuridine (BrdU), which is incorporated into cells undergoing mitosis. Following euthanasia, immunohistochemical analysis of brain tissue slices for BrdU will indicate which cells underwent division immediately following the BrdU injection. In addition, the phenotype of BrdU-positive cells will be explored using double label

immunohistochemistry for BrdU in combination with proteins implicated in glial (GFAP), or neural (TOAD-64) phenotype or neurite extension (GAP-43).

Glial-fibrillary acidic protein (GFAP), specific to glia, has been shown to be upregulated in CNS tissue following injury, particularly at CNS/PNS transitional zones (Malloch et al., 1987).

Turned On After Division-64kDa (TOAD-64), is one of the earliest neural-specific markers expressed post mitosis (Minturn et al., 1995a,b). TOAD-64 ndicates positive neural phenotype earlier than protocols which require fully mature cell populations such as those investigating neural phenotype based on neural-specific morphology or immunolocalization of mature neural antigens (i.e. NeuN).

Growth-Associated Protein-43kDa (GAP-43) has been associated with neural plasticity, neurite outgrowth, retraction, and synaptogenesis in both development and during regeneration (Skene et al., 1986; Reh and Kliavin, 1989; Illing et al., 1999). GAP-43 antigen will be localized in different n.VIII lesion groups to determine if localization of this protein differs over the time course of behavioral and anatomical regeneration.

3). Genetics (Chapter 5)

In these experiments, differences in gene expression between n.VIII surgical groups will be examined using the gene discovery technique of differential display, DD-PCR (Greeve et al., 2000). This technique is a non-hypothesis-driven, pattern recognition approach which attempts to find genes differentially regulated between animal treatment groups, or within an animal whose tissues are subjected to different conditions. Although this technique does not involve hypothesis-based techniques, the nature of these

experiments allows for discovery of novel genes that can be subsequently analyzed using more stringent, and hypothesis-driven techniques.

CHAPTER 3: BEHAVIORAL EFFECTS OF N.VIII LESION AND PLASTICITY IN TWO ADULT VERTEBRATE MODELS: *RANA CATESBEIANA* AND *XENOPUS LAEVIS*

CHAPTER 3: INTRODUCTION

Anatomy of the anuran auditory and vestibular systems

The anuran vestibuloauditory nerve (n.VIII) projects from auditory and vestibular endorgans located in the periphery to distinct auditory and vestibular nuclei in the ipsilateral medulla (Altman and Dawes, 1983; Nikundiwe and Nieuwenhuys, 1983). In postmetamorphic animals, endorgans are located in the bony periphery of each ear. Auditory and vestibular endorgans are generally distinct, although there is some overlap in organs most sensitive to long wavelength vibratory stimuli. The amphibian and basilar papillae are sensitive to low/mid- or mid/high-frequency vibrations, respectively, and are generally categorized as auditory endorgan structures. Auditory endorgans send afferents ipsilaterally via n.VIII fibers to the dorsolateral nucleus (DLN) of the medulla, thought to be homologous to the mammalian cochlear nucleus. The DLN projects to the ipsilateral and contralateral superior olivary nucleus (SON), the first nucleus to receive auditory input from both ears and has been implicated in localization of sound (Jacoby and Rubinson 1983; Goto et al., 2001; reviewed in Dieringer 1995).

The vestibular endorgans include three orthogonally oriented semicircular canals that measure angular acceleration of the head. There are also three maculae, the utricle, lagena and saccule that measure linear acceleration and gravity. In addition, the saccule is particularly sensitive to low frequency vibratory stimuli propagated through substrate (Table 3.1; reviewed in Dieringer 1995).

n. VIII deafferentation effects

Interruption of n.VIII input to the auditory and/or vestibular nuclei of the medulla by labyrinthectomy or n.VIII lesion results in deafness and/or vestibular deficit, respectively, on the operated side. A unilateral n.VIII lesion that abates input to auditory nuclei behaviorally affects sound localization ability since the source is generally determined by measured differences in input between the two ears.

Table 3.1. Labyrinthine organs in the frog and their function.

Labyrinthine Organs in Frog						
Semicircular Canals			Maculae		Papillae	
Anatomy	Function		Anatomy	Function	Anatomy	Function
Lateral	Angular Acceleration		Utricular	Gravity, Linear Acceleration	Amphiborum	Vibration (Substrate,Air)
Anterior	Angular Acceleration		Saccular	Vibration (Substrate)	Basilaris	Vibration (Air)
Posterior Vertical	Angular Acceleration		Lagenar	Gravity, Linear Acceleration	*Reviewed in Dieringer, 1995	

A unilateral n.VIII lesion which affects vestibular projections has immediate behavioral effects which resemble excitation of the contralesional vestibular nuclear complex (VNC). This is due to asymmetrical interruption of the "labyrinthine tonus", a bilateral background resting excitation in vestibular nuclei (VN) which exerts inhibitory effects on the contralateral vestibular nuclei through commissural projections (reviewed in Dieringer 1995). The resultant vestibular behavioral effects largely depend on the

location and extent of n.VIII lesion (Table 3.2) and are common across many species (Dieringer 1995). Vestibular deficits are broadly categorized as static/postural effects, seen when the animal is resting, or dynamic effects, when the animal is in motion (Hamalgyi et al., 1990; Dieringer 1995; Darlington & Smith 2000).

Table 3.2. Behavioral effect of lesion to selected labyrinthine organs in frog.

Static Behavioral Effect of Unilateral Lesion in Frog Labyrinthine Organs					
Semicircular Canals			Lesion Effect		
Anatomy	Function		Left	Right	Behavioral Effects
Lateral/Horizontal	Angular Acceleration	RA		X	
Anterior Vertical	Angular Acceleration	RA		X	Ipsi Head Tilt Downward (Minor contribution)
Posterior Vertical	Angular Acceleration	RP		X	Ipsi Head Tilt Downward (Minor contribution)
Maculae			Lesion Effect		
Anatomy	Function		Left	Right	Behavioral Effects
Utricular **	Gravity, Linear Acceleration	RA		X	Ipsi Head Tilt Downward (Heavy contribution)
Saccular	Vibration (Substrate)	RA		X	
Lagenar	Gravity, Linear Acceleration	RP		X	Ipsi Head Tilt Upward (Opposite of Utricular Lesion)
Papillae			Lesion Effect		
Anatomy	Function		Left	Right	Behavioral Effects
				X	
Amphiborum	Vibration (Substrate,Air)	RP		X	Deaf in ipsilateral ear. Auditory localization impaired.
Basilaris	Vibration (Air)	RP		X	Deaf in ipsilateral ear. Auditory localization impaired.

Vestibular behavior effects

The postural effects seen immediately following unilateral n.VIII lesion or labyrinthectomy in the "static" condition are largely due to a perceived rotation of the head toward the intact side. This perceived rotation is caused by the loss of n.VIII excitatory input and thus "quieting" of the ipsilesional vestibular nuclei (iVN). The decrease in iVN activity disinhibits the contralateral (intact) vestibular nuclei (cVN). This results in an increase in responsiveness of the cVN to input which further inhibits the iVN through increased activity in inhibitory commissural fibers. The perceived head angle rotation is opposite of the lesion due to this abnormal excitatory responsiveness of the cVN. As a result, the animal will tilt the head toward the lesioned side in a behavioral attempt to correct perceived head rotation. In addition, the ipsilesional limbs are flexed and may be tucked under the body with the contralesional limbs extended. A highly variable ocular counter roll is also common in most species and depends on the flexibility of the eye within the orbit. Spontaneous nystagmus is typical in species but does not occur in frogs.

Vestibular compensation

The postural effects following unilateral VN deafferentation either by n.VIII lesion or labyrinthectomy is highly variable between species and differs on the type and magnitude of deficit in addition to the timeline and extent of recovery. The partial

normalization of static vestibular behavior in the acute post-operative period is described by the process of "vestibular compensation." A vestibular compensatory response occurs to some extent in most species, even in animals that are not capable of n.VIII regeneration following lesion (i.e. adult mammals) and in animals subjected to hemilabyrinthectomy from which regeneration does not occur.

Vestibular compensation following n. VIII injury occurs due to the plasticity within the central vestibular nuclei and targets and is not due to regeneration of the lesioned n.VIII. Compensation in the absence of regeneration has been evidenced by the fast onset of marked behavioral recovery and can occur on the order of hours to days, and is much faster than the timeline for regeneration.

Vestibular compensation in non-regenerating species

The ability of an animal to undergo vestibular compensation is highly variable and some of the most pronounced compensatory responses occur in nonregenerative mammals. For example, within six hours following unilateral labyrinthectomy, rats exhibit one of the most pronounced postural responses of any species investigated. Their head tilt angle immediately following labyrinthectomy is so large the animal will often lie on its side. A significant reduction in head tilt is present twenty four hours after lesion due to behavioral compensation (Cirelli 1997). The extent to which recovery will occur has been the topic of much debate. Reports of normal postural recovery at 3 days post-operatively to a maintained 30^{o} head tilt have appeared (Vidal 1998). Rabbits, however, seem to have a limited ability to elicit a compensatory response as they never recover a normalized static posture . Humans display one of the most effective compensatory

responses following VN deafferentation. In contrast to most other species, humans exhibit minimal head tilt following lesion which may be due to the unique head-body axis (Basel 1998). Sensory substitution may also affect compensation effectiveness as indicated by an increase in observed head tilt angle in humans under low light conditions (deWeale et al. 1997). Humans also display spontaneous nystagmus and an approximately 9-10 degree ocular roll tilt after lesion which causes a visual perceptual deficit and may be responsible for head tilt. Spontaneous nystagmus is dramatically reduced after a few days following lesion and the magnitude of ocular tilt decreases slowly although it never completely recovers (Curthoys 1991).

Vestibular compensation in regenerative species

Goldfish are able to regenerate damaged cranial nerves (n.II and n. VIII) and following unilateral deafferentation of the VN will exhibit tilt behavior and spontaneous nystagmus immediately after lesion. Spontaneous nystagmus in goldfish is similar to that seen in animals incapable of regeneration but compensates more quickly, in about an hour (Ott and Platt 1988). The ability of an animal to regenerate does not appear to affect the time course or extent of regeneration, however. Frogs, following unilateral VN deafferentation, exhibit immediate head tilt and postural behaviors typical of most species. However, unlike in goldfish, the frog's behavioral compensation is gradual and generally occurs over a matter of weeks, (although frogs are similarly capable of regenerating damaged cranial nerves). The magnitude of head tilt and the time course of postural normalization in frogs following unilateral VN deafferentation vary in the literature. Some reports indicate that frogs fully recover normal postural behavior while

others show frogs do not fully normalize and always display chronic residual tilt (Dieringer 1995).

Vestibular behavioral recovery may follow regeneration

Behavioral recovery seen in n.VIII lesioned frogs after long post-operative recovery periods may be the result of regeneration instead of compensation. The lesioned n.VIII in anurans, unlike in mammals, can regenerate and functionally recover distal and proximal n.VIII fibers (Hernandez et al. 1998; Sperry 1945; Zakon and Capranica 1981; Zakon 1983).

Aims

The aim of these experiments is to measure postural effects in the frog following unilateral n.VIII crush lesion and during post-operative recovery time points of between one day and three months as a non invasive behavioral indicator of n.VIII regeneration extent. In Chapter 6, I will correlate these behavioral findings with my anatomical data in Chapter 4.

Post n. VIII lesion vestibular behavior

In this study I will measure head tilt angle and tilt direction in *Rana catesbeiana* and *Xenopus laevis* and limb sprawl in *Xenopus laevis* following unilateral n.VIII lesion. As an assessment of behavioral tilt or sprawl, the animals will be photographed either

head on or from directly overhead. I will analyze the data for trends in vestibular behavior versus recovery time.

The data were then analyzed for trends which may allow a non-invasive behavioral indicator of the extent of n.VIII regeneration following crush. The vast majority of past anatomical and physiological literature in anurans has focused on the genus *Rana,* while molecular biologists have concentrated on the genus *Xenopus.* There is an extreme paucity of literature which bridges the void between these two frog models, each heavily studied on their respective fields. Thus the rationale behind using two frog species was an attempt to link the disconnect between frog-model species of choice between anatomy/physiology-based studies, versus molecular-oriented reports.

In studies outlined in Chapter 4, animals were injected with 5- bromo- 2'-deoxyuridine (BrdU) for a quantitative assessment of CNS mitotic activity following unilataeral n.VIII lesion. The safety of BrdU on behavioral recovery following n.VIII lesion was evaluated in this study.

CHAPTER 3 Hypotheses: Vestibular behavioral effect of n.VIII lesion in Rana and Xenopus.

Hypothesis 1 : I hypothesize there will be no significant effect in postural tilt or sprawl between nonsurgical and sham surgical treatment groups or between pre-operative (Days = 0) and post-operative (Days > 0) recovery time-points.

Hypothesis 2 : I do not expect a significant effect of BrdU injection on vestibular behavior in control or lesioned animals.

Hypothesis 3 : I do, however, expect there will be a significant difference in tilt and sprawl posture between pre-operative and post-operative recovery time-points for the unilateral n.VIII lesion condition.

Hypothesis 4 : Furthermore, similar to previous reports showing behavioral recovery following unilateral n.VIII lesion/hemilabyrinthectomy in other anuran species, I expect the magnitude of behavioral deficit following unilateral n.VIII lesion in both species to be greatest immediately following lesion and decrease exponentially with recovery time-point becoming indistinguishable from controls after one month post-operatively.

Hypothesis 5 : I expect the head tilt magnitude and recovery trends following n.VIII lesion to be similar between *Rana catesbeiana* and *Xenopus laevis,* but that *Xenopus,* the smaller frog, will display a normalized head tilt earlier than *Rana catesbeiana* due to the shorter distance n.VIII must travel to reach medullary targets .

CHAPTER 3: MATERIALS AND METHODS

Animals:

Animal procedures were authorized and overseen by the Brown University Institutional Animal Care and Use Committee (IACUC) and conform to NIH guidelines. All surgical procedures were performed using aseptic techniques. Adult male *Rana catesbeiana* (n=13; Sullivan, TN) and adult male *Xenopus laevis* (captive bred animals n=39; Xenopus Express, Plant City, FL) were used in these experiments. Only adult male animals were used, to avoid female hormonal cycle confounds. Naive animals were fed *ad libitum* (adult crickets, *Rana catesbeiana*; 3/16" floating frog food pellets, cat# FFF2/ 45% protein, Xenopus Express, *Xenopus laevis*) and group housed in plastic terraria (separated by species) containing damp soil and access to water (*Rana catesbeiana*) or water (supplemented with Start-Right, Jungle Laboratories Corporation, *Xenopus laevis*). Animals were housed in our facility maintained at 23-25°C on a 12:12 light: dark cycle.

Surgical Procedures

Rana catesbeiana

The animals were separated into three groups: nonsurgical control, sham surgical control and unilateral n.VIII surgical lesion. Adult male animals (n=13; Sullivan, TN) were anesthetized by immersion in 0.6% (w/v) 3-aminobenzoic acid ethyl ester methanesulfonate (MS-222, pH 8; Sigma) for 5-7 minutes or until all reflexes

disappeared. Animals were placed in a supine position and skin was kept moist by placement of wet gauze over the ventral surface (Johnson & Johnson). Both n.VIIIs were exposed via a ventral approach through the roof of the mouth and one of three surgical procedures was performed: bilateral sham, unilateral left n.VIII crush lesion with contralateral sham, or right n.VIII crush lesion with contralateral sham. Briefly, skin overlying the ear was carefully removed while paying special attention to preserve the overlying optic blood vessels. The bone ventral to n.VIII was drilled out using diamond tipped burrs (Dremel, Racine, WI). For animals in which n.VIII lesion was to be performed, the n.VIII was lesioned by crush using Dumont #5 forceps (Fine Science Tools, Canada) at the medullary insertion point. n. VII crush was repeated three to five times until the lesion was visualized. There is extensive vasculature around the n.VIII that is spared using the crush versus the cut technique.

For sham surgical conditions, the overlying bone was drilled out and no crush was performed. In all surgical conditions, the bony socket was gently packed with antiseptic Gelfoam [(Pharmacia & Upjohn Company, Kalamazoo, MI) presoaked in 0.9% (w/v) sterile sodium chloride solution; Johnson & Johnson] and the skin was closed using 4/0 Vicryl sutures (Ethicon, NJ). The margins of the wound were swabbed with a topical triple antibiotic gel containing lidocaine (Neosporin). Frogs were allowed to recover between 1 hour and 3 months in order to observe temporal changes in behavioral recovery. These time points were chosen based on previous studies showing n.VIII regeneration in adult frogs (Zakon 1983; Newman & Honrubia 1992). Upon assignment to a post-surgical treatment group all animals were individually housed. Animals were maintained on damp blue diapers (instead of soil substrate) and food restricted for the

first seven days following surgical procedures to allow wound healing. Our pilot studies have shown surgical animals will not attempt to eat for approximately the first 5-10 post-operative days (double sham animals will eat earlier than lesioned animals; personal observations). Live crickets, when introduced into the post-surgical animal's cage prior to one week post-operatively were not eaten and appeared to cause stress to the subject (personal observations). Beginning seven days post operatively, and every second day thereafter, live crickets were offered. If no food catching attempt was made after five minutes, crickets were removed. If food catching behavior was attempted and failed following 3-5 repeated attempts, the live cricket was held immediately in front of the animal with a hemostat. Most post-operative animals were eventually able to successfully hunt without assistance.

Xenopus laevis

Adult male *Xenopus laevis* (n=39; Xenopus Express) were assigned to one of four surgical group categories: 1). Left n.VIII Lesion with contralateral sham; 2). Right n.VIII Lesion with contralateral sham, 3) Bilateral n.VIII Sham; or, 4). Nonsurgical Control. Upon assignment to a surgical group, animals were individually housed in plastic aquaria containing 10-15 cm deep of Start-Right conditioned water until surgery. Animals were anesthetized by immersion in 0.6% (w/v) 3-aminobenzoic acid ethyl ester methanesulfonate (MS-222, pH 8; Sigma) for 5-7 minutes or until all reflexes disappeared. Animals were placed lying ventrally, and skin was kept moist by placement of wet gauze over the animal's back (Johnson & Johnson). Both n.VIIIs were exposed via a dorsal approach through the top of the head. Although this approach requires the

researcher to traverse through more tissue than one using a ventral approach (as in *Rana catesbeiana* surgery), the n.VIII is inaccessible through the roof of the mouth in *Xenopus* due to the much smaller mouth size.

Briefly, the anesthetized animal was packed in ice to minimize bleeding, as the musculature, n.VIII and surrounding areas are highly vascular and bleeding could easily obscure the field. A skin flap was then created, so a large area of tissue could be removed from the surgical area while all of the vasculature on one side of the flap was retained. This allowed for post-surgical closure of the flap (in contrast to surgical removal of the skin) which minimized tension on both the healing skin flap and sutures holding the flap in place, and expedited the healing process (personal observations). The musculature overlying the bony ear capsule was pushed aside using blunt dissection in order to preserve all head, neck, and shoulder girdle musculature necessary for food catching and swimming behaviors. Upon visualization of the bony ear capsule, the bone overlying the n.VIII was removed using a rotary drill and diamond tip engraving bit (Dremel, Racine, WI). For animals in which n.VIII lesion was to be performed, the n.VIII was lesioned by crush using Dumont #5 forceps (Fine Science Tools, Canada) medial to the saccule (n=4) or at the medullary insertion point (n=20). Crush was repeated approximately five to seven times, and each crush was held for approximately five seconds until the lesion was visualized. n.VIII lesion by crush was chosen to spare vasculature and membranes of the n.VIII (as in *Rana catesbeiana* subjects). For sham surgical conditions, the overlying bone was drilled out and no crush was performed. In all surgical conditions, the bony socket was gently packed with antiseptic Gelfoam (Pharmacia & Upjohn Company, Kalamazoo, MI) presoaked in 0.9% (w/v) sterile

sodium chloride solution (Johnson & Johnson), musculature was gently moved back to the original pre-surgical location, and the skin was closed using 6/0 Vicryl absorbable sutures or 5/0 Ethicon sutures (Ethicon, NJ). The margins of the wound were swabbed with a topical triple antibiotic gel containing lidocaine (Neosporin). Frogs were then placed in aerated water tanks (with the head held in air) until the animal began to wake from the anesthesia. Animals were then placed in aquaria containing an under pad dampened (less than ½" deep) with Start-Right supplemented water. Tanks, including under pads, were changed every 24 hours post-operatively. Beginning 24 hours post-operatively, and every second day thereafter, animals were placed in water tanks for photography (under constant supervision, water was between 7.5 - 15 cm deep). Animals were assisted to the surface by the researcher (to breathe) if the animal was having difficulty on his own. Animals were immediately placed back in the home tank with a damp under pad following photography. Post-surgical animals were placed in deep water tanks with enough water allowing them to swim after seven days if the animal could regularly swim unassisted to the water surface to breathe. Although sham surgical animals recovered the ability to surface in deep water tanks quicker than the lesioned animals, they were not returned to deep water tanks earlier than seven days in order to approximate the conditions of the n.VIII lesioned surgical animals. Food (2-3 pellets) was offered immediately on being placed in the deep water tank and every second day thereafter. Between seven and fifteen days post operatively, most animals would eat, or attempt to eat (many n.VIII-lesioned animals made unsuccessful food catching attempts). Animals that attempted to catch food but were unable to do so after 3 – 5 trials were assisted by the researcher. Any food uneaten after 15-20 minutes was removed.

Euthanasia

Rana and *Xenopus* were allowed to recover for variable periods postoperatively. Animals were then were terminally euthanized by immersion in 0.6% (w/v) tricaine methanesulfonate (MS-222, pH 8; Sigma) for 15 minutes, followed by transcardial perfusion with 60 mLs of heparin-containing 0.9% saline and 60 mLs of cold, 4% (w/v) paraformaldehyde (in saline, pH 7.4; Sigma, St. Louis, MO).

Photographic procedures

Documentation of Behavioral Head Tilt

Photographic documentation of head tilt angles were compiled for both, *Rana catesbeiana* and *Xenopus laevis*. The photographs were taken head on with the camera at the approximate height of the animal, as indicated in the schematic (Fig. 3.1A). Photographs were taken at randomly spaced intervals for *Rana catesbeiana*, as these animals were studied earlier than *Xenopus* during the initial optimization of the behavioral protocol. Photographs of *Xenopus* were taken every second day. For those animals that underwent surgical procedures, the photographic sequence began 24 hours postoperatively. As a control, a subset of *Xenopus* was also photographed preoperatively. Photographs of *Rana catesbeiana* were taken as the animal rested on a flat, terrestrial surface while photographs of *Xenopus laevis* were taken with the animal completely

submerged in aquaria filled with water in order to reduce effects of the air-water interface on head tilt behavior.

Documentation of Limb Sprawl

Photographic documentation of limb sprawl behavior was recorded only for *Xenopus laevis* animals. *Rana catesbeiana* were not analyzed for limb sprawl because this experiment was added was added after *Rana catesbeiana* had been studied. Photographs documenting limb sprawl in *Xenopus laevis* were shot while the animal was maintained in plastic aquaria containing water. Limb sprawl photographs were taken for the same animals and during the same postoperative time points that they were photographed for head tilt. Photographs analyzed for limb sprawl were shot from directly overhead (Fig. 3.1B).

*** INSERT FIGURE 3.1 ABOUT HERE ***

Behavioral analysis

Measurement of Head Tilt

Photos of head tilt were imported into CorelDraw (v.11,13) software and the direction and extent in degrees were determined using the "Angular Dimension Tool." This tool reports the angle between two experimenter-generated rays. In *Rana catesbeiana*, one ray was generated through the line of the animal's mouth to establish a head axis while the second ray, which represents the horizontal reference, was generated

from the edge of a level bench top surface on which the frog was resting (Fig 3.2). Head tilt angles for *Xenopus laevis* photos was reported between one ray generated through the center of both animal's eyes, and the second ray, representing the reference (horizontal) ray, was generated from the edge of the air-water interface (Fig 3.3). Tilt measurements were analyzed by the experimenter and at least one additional measurer blind to the premise of the experiment and to the animal's treatment.

*** INSERT FIG 3.2 ABOUT HERE***

*** INSERT FIG 3.3 ABOUT HERE***

Measurement of Limb Sprawl

Limb sprawl data were analyzed from individual photos of *Xenopus laevis* shot from directly overhead. Photos were imported into CorelDraw software (v.11,13) and limb sprawl angles were measured in degrees using the "Angular Dimension Tool". Four appendage angle measurements were recorded for each image defined as: left arm, right arm, left leg and right leg. Sprawl measurements were analyzed by the experimenter and at least one additional measurer blind to the premise of the experiment and to the animal's treatment.

The measurer was directed to find the angle from rays generated from the metatarsal-phalanges, or metacarpal-phalanges junction, to ensure measurements between animals/photographs were consistent. For each limb, the angle for the appendage of

interest was determined according to the metatarsal-phalanges or metacarpal-phalanges point on the angle vertex. Each ray was generated through each of the adjacent appendages. To standardize limb sprawl data between animals and photographs, each limb angle was normalized to the proportion it contributed to the total angle for all limbs. Normalization was performed by dividing each limb angle by the sum of all 4 limb angles per photograph, and multiplied by 100. Although every attempt was taken to photograph animals from directly overhead, an internal control paper square (3x3 Post-It ®) was placed in each photograph and each of the four corner angles also measured. Each of the four angles on the control paper should measure 90 degrees. If a deviation in angle measurement of greater than 2% was measured, the photograph was not used.

*** INSERT FIG 3.4 ABOUT HERE***

CHAPTER 3: RESULTS

n.VIII-Lesion Results in Abnormal Posture

Rana catesbeiana exhibit head tilt following unilateral n.VIII crush

Post-surgical head tilt measurements of *Rana catesbeiana* were analyzed from photographs taken at randomly spaced post-operative time points in three groups of animals: unilateral right n.VIII lesion with contralateral sham, unilateral left n.VIII lesion with contralateral sham, and bilateral sham. Post operative photographic analysis indicated that animals subjected to unilateral n.VIII crush exhibit a characteristic postural deficit which includes preferential behavioral head tilt toward the lesioned side (Fig.3.5, Left Panel, Right Panel). 100% of animals subjected to unilateral n.VIII-lesion preferentially displayed these head tilts. Head tilt angle is most pronounced immediately following n.VIII lesion but gradually decreases with post operative survival (Fig. 3.5; 3.6; 3.7) . Bilateral sham surgical animals exhibit no significant head tilt immediately post operatively (bilateral sham, Fig.3.5 center top) or with more advanced post operative survival time (Fig 3.5, center, bottom).

*** INSERT FIG 3.5 ABOUT HERE***

Analysis of Data

Two representative head tilt datasets plotted as degrees head tilt on the abscissa versus postoperative survival time point are shown in Figure 3.6. Head tilt data are

measured beginning at 2 days post operatively for the sham surgical control animal. At post operative day 2, the sham surgical animal exhibits a small head tilt angle of 3 degrees (Fig. 3.6, sham, Gray Square; Post-Operative Day =2, Head Tilt Angle = 3 Degrees). This angle is not significant as 3 degrees is less than the variability due to tilt measurement procedural limitations. Normal postural head tilt variability in pilot studies using naive animals exhibits a variety of head tilt angles. These pilot studies have resulted in an experimentally-derived threshold of 8 degrees (inclusive). Head tilt angles at or below the 8 degree threshold in these studies are categorized as non-tilted. The sham surgical control animal exhibits head tilt angles below the 8 degree threshold.

The variability in head tilt in an individual animal with left n. VIII lesion is shown in Fig 3.6. At day 4 the tilt measured 24 degrees, at day 8 – 30 degrees, day 11 – 21 degrees, day 12 - 26 degrees, day 14 – 16 degrees, day 19 – 24 degrees, day 22 – 14 degrees and day 26 – 15 degrees. The tilt a day 33 was 18 degrees and declined to 16 degrees at day 36 and 9 degrees at day 40. A similar pattern of variability is demonstrated when data from multiple lesioned animals is analyzed (Fig 3.7) when compared to the sham group. The plot of head tilt in an individual lesioned animal (Fig. 3.6) and in the pooled data (Fig. 3.7) show the decrease in head tilt with post-operative recovery.

INSERT FIG 3.6 ABOUT HERE

INSERT FIG 3.7 ABOUT HERE

Xenopus laevis: Analysis of Behavioral Head Tilt:

Post operative photographic analysis of unilateral n.VIII lesioned *Xenopus laevis* show they also exhibit head tilts toward the lesioned side (see Fig 3.3). The magnitude of head tilts were greater than shown in *Rana catesbeiana* unilateral lesion conditions (see Fig. 3.6 and Fig 3.8). *Xenopus* also show similar post-operative trends in that head tilt gradually decreases over time as shown in a representative animal in Fig. 3.8. Preoperatively, mean head tilt angles for the control and n.VIII-lesioned animals were 1.6 and 8.3 degrees, respectively (Fig. 3.8).

Head tilt means (<10.0 degees) for the control group were similar to preoperative tilts during the course of the study. (Fig 3.8, Control; Gray Triangle, Ordinate > 0). In contrast, head tilt angles were greater than 10.0 degrees for all survival points beginning 24 hours post-operatively for the unilateral n.VIII-lesioned animal [Fig 3.8; Post-Operative Head Tilts, n.VIII Lesion Condition (Left n.VIII Crush Lesion with Right n.VIII Surgical Sham), Blue Triangle, Ordinate > 0].

The degree of head tilt in the lesioned animal continues to increase reaching a peak at day 5 (Fig 3.8; Blue Triangle, Days Post-Operative = 5, Head Tilt = 48.8 Degrees, Left Direction). Following the peak in head tilt angle at 5 days, head tilt angle magnitude and variability trends gradually decrease. (Fig 3.8, n.VIII Lesion, Blue Triangles, Post-Operative = 1 Week through 2 Months, Head Tilt Range, 37.8-17.7 Degrees, Left Direction).

BrdU Injection does not Affect Head Tilt

Figure 3.9 shows mean head-tilt measurement data plotted from *Xenopus laevis* unlesioned animals either, uninjected (Fig 3.9A) or injected with BrdU (Fig3.9B). At timepoint=0 (Fig 3.9A, Black Square; Fig 3.9B, Gray Square), the mean head tilt angles for both groups are below 8 degrees indicating no tilt. From timepoint=1 Day forward, mean angle measurements are below 8 degrees for the non injected (Fig 3.9A) and BrdU injected (Fig 3.9B) conditions.

Figure 3.10 shows mean head-tilts from *Xenopus laevis* n.VIII lesioned animals either, uninjected (Fig 3.10A) or injected with BrdU (Fig.3.10B). At time = 0 (Fig 3.10A, Gray Square; Fig 3.10B, Blue Square), the mean tilt angle for both animal means is below 8 degrees indicating no tilt. From time =1 day forward, mean angle measurements for noninjected (Gray Triangles) and BrdU injected (Blue Triangles) animals are very tilted. The magnitude gradually decreases with recovery period in the noninjected animals (animals still exhibit significant tilt). The BrdU injected animals do not exhibit a similar tilt reduction but they have a shorter post operative recovery and trends are similar in the noninjected animals during post-operative time points through 30 days.

INSERT FIG 3.9 ABOUT HERE

INSERT FIG 3.10 ABOUT HERE

Xenopus laevis: Analysis of Limb Sprawl:

Animal limb sprawl is calculated from individual photos taken from a dorsal view of animals in a water tank. The four measurements taken from each image were defined as: left arm, right arm, left leg and right leg.

Figure 3.4 shows that normal limb sprawl in control *Xenopus laevis* is roughly equal between the animal's right and left appendages (control, Fig 3.4 A,B). n.VIII lesioned animal limb sprawl angles are highly discrepant (n.VIII, Fig 3.4 C,D). Quantitative limb sprawl data from two control *Xenopus laevis* representative remain roughly equal over the observation period.

The preoperative limb angle in the group subjected from to n.VIII crush lesion was similar to sham surgical animal data (see Fig 3.11B, Ordinate = 0). However, the data is highly variable post operatively (Fig 3.11B, Ordinate > 0). The angle data were dissimilar between the corresponding contralateral appendages beginning 24 hours post operatively. Arm angles generally show larger angles over leg angles in pre-operative and nonsurgical control conditions. Preoperative arm angle measurements did not overlap in contrast to leg measurements. However, ipsilateral and contralateral arm and leg angles were dramatically different post operatively (see Fig 3.11B, right limb angles, Post- Op Days = 1; Right Arm, Blue/Gray Circle, Angle = 29.9; Right Leg, Solid Blue Square, Angle = 18.1). Limb sprawl is evident 24 hours post operatively and continues across multiple

post-operative survival points. However, limb angle data are highly variable (Fig. 3.11B, Post- Op Survival = 3 Days – 2 Months; Left Arm, Red/Gray Circle Angle Range = 21.4 – 30.8; Right Arm, Blue/Gray Circle, Angle Range = 20.8 - 28.9; Left Leg, Solid Red Square, Angle Range = 21.8 - 31.9; Right Leg, Solid Blue Square, Angle Range = 16.8 – 26.3).

INSERT FIG 3.11 ABOUT HERE

Summary of Head Tilt Recovery Trends

Figure 3.12 shows mean control and unilateral n.VIII-lesioned head tilt data plotted from *Xenopus* and *Rana*. Figure 3.12A shows the mean degree head tilt for *Rana* (red triangles) and *Xenopus* (blue circles) subjected to unilateral n.VIII lesion between post operative day 1 through day 85. Head tilt data for both species are approximately within 5° at post-operative days 1 and 3, however after post-operative day 3 mean head tilts and trends between *Rana* and *Xenopus* differ dramatically.

Head tilt in *Rana catesbeiana,* (shown separately in Fig 3.12B) shows an overall initial decrease and then recovery such that at day 41 the tilt is reduced to 9°. These data are best described as following a cubic trend (Fig 3.12B; shown as red dotted line, $y = -0.0011x^3 + 0.0728x^2 - 1.6689x + 30.579$; $R^2 = 0.48$).

Xenopus laevis head tilt data are shown separately in Figure 3.12C for post operative recovery days 1 – 18. Fig. 3.12D plots head tilt from days 18 through 85 in order to describe two substantially different trends in the data. Beginning 1 day after

n.VIII lesion, *Xenopus* exhibits a substantial mean head tilt toward the lesioned side. The extent of the tilt decreases until approximately 7-9 days which is then followed by an increase in head tilt peaking at approximately 17 days. The mean head tilt data for days 1-18 are best described as following a cubic trend [see Fig 3.12C; blue trend line, $y = 0.0029x^3 + 0.0633x^2 - 1.5911x + 34.227$ ($R^2 = 0.52$)].

Figure 3.12D shows the mean post-operative head tilt for *Xenopus* subjected to unilateral n.VIII lesion from day 18 through day 85. After 18 days, the animal exhibits a head tilt towards the side of the lesion which is similar to the head tilt exhibited during post operative day 1 (see Fig 3.12A, and 3.12C), however, it is significantly less than the magnitude of head tilt at post operative day 17. Subsequent to day 18, mean head tilt shows a decrease with increasing survival period. The mean head tilt data for days 18-85 are best described as following a quadratic trend [(see Fig 3.12D; blue trend line, $y = 0.0038x^2 - 0.5345x + 45.182$ ($R^2 = 0.48$)].

CHAPTER 3: DISCUSSION

Summary of Results:

In this study I have investigated the postural effects following unilateral n.VIII lesion, and analyzed trends in behavioral recovery over postoperative survival in adult *Rana catesbeiana* and *Xenopus laevis*. I chose to study behavioral head tilt in both species in an effort to bridge the gap in frog studies. *Rana* has long been the favorite frog model for behavioral, anatomical, and physiological research. Molecular biological studies in frog uses *Xenopus* as the preferred model. Behavioral studies investigating the vestibular system in adult *Xenopus* are few and are most prevalent in *Rana*. Head tilt angles from control animals of both species (naive, sham surgical, and pre-surgical conditions) were consistently at or below the tilt threshold and control groups were indistinguishable within species. Immediately following unilateral n.VIII lesion, *Rana* and *Xenopus* exhibit a strong head tilt toward the lesioned side. When compared at similar postoperative recovery times, the magnitude of head tilt in was greater in *Xenopus* than *Rana* and decreased with post-operative recovery, *Xenopus* had a delayed and less pronounced recovery.

Limb sprawl was also analyzed in *Xenopus* (but not Rana). There was no significant limb sprawl in control animals but immediately following unilateral n.VIII lesion, *Xenopus* exhibited significant limb sprawl which decreases with post operative recovery time. Limb sprawl does not normalize even after long time points.

This study adds to previous studies investigating postural behavior and recovery following n.VIII crush in adult frogs. This is the first study measuring postural head tilt and sprawl trends following unilateral n.VIII crush lesion over postoperative recovery in adult *Xenopus.*

In studies described in Chapter 4, a marker was used to indentify cell proliferation in the brain. I determined that the marker, 5-bromo–2'–deoxyuridine (BrdU) was not toxic and did not affect the behavioral changes. This observation of the lack of a behavioral effect of BrdU allowed me to correlate the observed behavioral events with cellular brain changes.

Unilateral n.VIII Lesioned Animals Exhibit Abnormal Head Tilt Posture

Immediately following unilateral n.VIII crush, both species of frogs exhibit a strong head tilt toward the lesioned side. The degree of head tilt was quantified over the post operative recovery period in lesion and control animals. Control and sham operated animals did not exhibit any significant head tilt at any experimental time point. Since sham and experimental (lesioned) animals were identically treated head tilt associated with n.VIII lesion was not due to other surgical factors (i.e. anesthesia, bone drilling, drainage of otic fluid surrounding n.VIII, etc.). Postural changes in the lesioned animal were visualized at the first post-operative measurement, 24 hours. This time point was chosen to allow anesthesia clearance.

Head tilt data was geometrically generated from photographs of *Rana catesbeiana*. The process involved indentifying the angle between a longitudinal ray that was defined by the table top and a second ray drawn though the mouth. The mouth was

chosen since it provided two data points (corners of the mouth) through which a line could be drawn. This process allowed measurement reproducible between animal groups.

Head tilt data from *Xenopus laevis* photos was similarly obtained. The tilt angle was measure between a horizontal ray was the water line and a ray passing through the eyes . The pupils of the eye were chosen as they were more easily discerned in the photographs of the submerged frog.

The measured tilt angles were generally greater in lesioned *Xenopus* than in *Rana catesbeiana*. The greater magnitude in head tilt seen in *Xenopus* may be due to the animal being under water. The difference in the tilt angles may also be the result of measurement techniques. In *Rana* the mouth was used at a reference for one ray since it was easier with two defined points (the corners) to through which to draw the ray. The eyes were used in *Xenopus* as they were easier to identify under water. The difference in tilt might also be due to anatomical differences as *Rana* has greater cervical mobility than *Xenopus.*

Recovery in *Rana* was much faster than in *Xenopus* (Fig 3.6). This may be due to a real difference in regenerative ability. It may also be due to the differences in the surgical approaches used to lesion the n.VIII nerve. A ventral approach was used in *Rana* to achieve the lesion while a dorsal approach was necessary in *Xenopus*. In addition, there may be significant differences in the recovery processes in both animals due to their environments since *Rana* recovered essentially out of water while *Xenopus* was submerged during recovery. Recovery may also be enhanced in *Rana* due to a greater sensory input as *Rana* has proprioceptive input through surface contact with its

four limbs, while this input in *Xenopus* may be significantly diminished due to buoyancy in the aquatic environment. Studies by Basel show that removal of proprioceptive or somatosensory inputs or reduction of visual input by low light conditions or experimental blinding delay or prematurely terminate vestibular compensation (Basel 1998).

The early recovery of head tilt following n.VIII lesion in both *Rana* and *Xenopus* is probably due to compensatory mechanisms and not regeneration of the nerve. These fast times frames are not consistent with time sequence necessary for the growth of neurons.

Behavioral Recovery from n.VIII Xenopus laevis Limb Sprawl

As an additional behavioral measure for recovery from n.VIII lesion, limb sprawl was geometrically quantified over post surgical time for *Xenopus laevis*. Limb sprawl appears generally similar between left and right appendages in nonsurgical and sham animals (see Fig. 3.11A). Lesion of the n.VIII in *Xenopus* caused a marked change in limb sprawl angles. The animal flexes the limbs ipsilateral to the lesion and extends the contralateral limbs. The results are variable over the post surgical period (see Fig. 3.11B). Limb sprawl recovered to approximated 25^{o} at the longest recovery time points. The recovery of normal limb sprawl at the later time points may be due to regeneration of neural pathways rather that compensation.

Stereotyped Postural Response Following Unilateral Vestibular Deafferentation

Although the postural response described in this study differ in magnitude and recovery trend for *Rana catesbeiana* and *Xenopus laevis* following unilateral n.VIII

lesion, both species adopt a similar postural response, including head tilt toward the lesioned side and characteristic limb sprawl. Similarities in the stereotypical postural response and differences in magnitude of the postural deficit and recovery time course have been noted in other studies and may result from a general difference in species response, surgical methodology (n.VIII crush, n.VIII cut, or labyrinthectomy), or behavioral measurement protocol.

Recovery of Postural Deficit Occurs Despite Regenerative Ability

It is generally accepted that unilateral vestibular deafferentation in most adult vertebrates, especially in mammals, does not result in regeneration with functional recovery. However, the stereotyped postural deficit seen in most species immediately following unilateral vestibular deafferentation can exhibit behavioral recovery even in mammals. Furthermore, postural compensation can occur more quickly in mammals than in species capable of n.VIII regeneration due to greater sensory input.

The initial onset of vestibular compensation, and the extent to which vestibular upset is reduced depends largely on the type and conditions of lesion and the species involved. For example, static vestibular compensatory effects can be seen as early as 3 days in rats and guinea-pigs, cats prior to one week post operative exhibit dramatic vestibular impairment are effectively compensated at one month (Lacour et al., 1997). Rabbits have never exhibited normalization of static head tilt, even after post operative periods of six months. (Dieringer, 1995).

Postural Deficit

The postural deficit arising from unilateral n.VIII injury or labyrinthectomy in this study resulted in an imbalance in signaling to the affected central vestibular nucleus. This can result in a variety of detrimental vestibular effects depending on the nature of the injury.

The reduction in head tilt seen within the first post operative week is considered too early for n.VIII regeneration to occur. It is likely due to effects of central vestibular compensation which is not exclusive to frogs and has been studied in a wide variety of animal models.

Although many adult animals subjected to unilateral vestibular deafferentation or labyrinthectomy are able to compensate quickly for static vestibular effects, compensation for dynamic vestibular tests are less common and are largely dependent on the species involved, type and degree of vestibular injury, and type of dynamic vestibular compensation being investigated (Darlington & Smith 2000).

Vestibular Compensation

Vestibular compensation is known to occur after unilateral vestibular deafferentation (by nerve lesion or labyrinthectomy) and is known to occur in the absence of these vestibular inputs as follows: First, vestibular compensation is often studied in animal models incapable of regenerating vestibular inputs back to the centrally located vestibular nuclei. Second, euthanasia and dissection of lesioned vestibular inputs show

either no regeneration or ineffective neurite sprouting. And, third, many of the vestibular compensatory effects occur temporally much earlier than would be required for neurite regeneration, path finding, and appropriate synaptogenesis.

Since vestibular compensation does not result from regeneration of injured inputs that lie outside the CNS boundaries into centrally located vestibular nuclei, it has been suggested that responsible factors must be located within the CNS capable of plasticity. The full complement of factors responsible for vestibular compensation are complex and only a subset of factors are known, and some remain a matter of conjecture. However central factors allowing vestibular compensation is likely due to the species and the type of vestibular injury.

CHAPTER 4: ANATOMY OF THE RECOVERING ADULT N.VIII POST INJURY

CHAPTER 4: INTRODUCTION

Central nervous system injury in adult humans usually results in profound and often irreversible loss of function, due to the inability of the mammalian CNS to regenerate and reestablish appropriate connections with synaptic targets. Most species of adult vertebrates, including humans, are not efficient in stimulating neuronal survival and proper reestablishment of connectivity subsequent to injury. Although limited regenerative capacity is seen during early development, in most vertebrates, the potential for axonal growth and regeneration after damage decreases considerably as development proceeds (Russell and Moore 1995; Hafidi et al. 1999; Lohmann et al. 1999; Schwab and Bartholdi 1996). It is of clear clinical and social significance to develop scientifically-based treatments to stimulate recovery of function. The CNS of adult ranid frogs has many similarities to that of mammals, including factors in the CNS considered "nonpermissive" to axonal growth (Becker et al., 1995; Lohmann, et al 1999) yet shows more extensive regeneration abilities, including the ability to reform functional connections with appropriate targets, even in the absence of exogenous biological treatment. For example, frogs can regenerate lesioned cranial nerves (optic, vestibuloauditory) into the CNS resulting in synaptic density, behavioral, and physiological function that is similar to unlesioned animals (Newman et al., 1987, 1989; Newman and Honrubia 1992; Sperry 1944, 1945; Gaze 1959; Gaze & Jacobson 1963; Zakon and Capranica 1981; Zakon, 1983). This regenerative ability directly contrasts the retrograde degeneration often seen after injury to mammalian cranial nerves, often

causing death of the ganglion itself (Schuknecht and Woellner 1955; Spoendlin 1971, 1975).

The purpose of these experiments is to investigate effectiveness of n.VIII crush lesion surgery and the extent to which the crush lesioned n.VIII can regenerate. In addition we investigate glial, neural,, and neurite extension implicated protein ti see if concentrations are affected by CNS injury and /or regeneration. Finally, we investigate total umbers of cells and BrdU incorporation in n.VIII CNS targets in naive, sham operated, and lesioned animals to see if cranial nerve injury has cell proliferative effects.

Fiber Analysis

In order to verify effective surgical techniques including extent of n.VIII lesion resulting from crush, and to verify that n.VIII remained intact under sham surgical, and nonsurgical control conditions, and to examine the capacity of the crush-lesioned n.VIII to regenerate at different time points during the recovery process, some animals were utilized in a tract tracing study using fluorescent lipophilic dyes. Analysis of fiber reinnervation following n.VIII lesion in *Xenopus laevis* will allow comparisons with our behavioral, genetic and cell proliferative response following n.VIII lesion in addition to previous studies investigating n.VIII regeneration in other species of frog (Zakon and Capranica 1981; Zakon 1983; Newman et al., 1987; 1989; Newman and Honrubia 1992).

Neural pathways have been studied in many species using tracers such as horseradish peroxidase (HRP), Pha-L, Cholera toxin β subunit, biotin dextran amine,

radio labeled glucose (2-deoxyglucose; Paton, et al 1982), and fluorescent lipophilic tracers. Radiolabeled glucose can show effects of metabolism due to experimental stimulus although requires histological development of the radioactive signal resulting in a black precipitate. The fluorescent lipophilic tracers used in this study are advantageous because they are vital dyes, nontoxic to the cell, travel bidirectionally along the membrane's lipid bilayer, require no secondary histological development to visualize label, and can be purchased in a variety of photon excitation and emission maxima allowing tissue to be doubly labeled.

Cell Proliferation

Mitotic cells have been well-documented in the brains of many species of adult animals (lamprey, Pizarro et al, 2004; birds, Goldman and Nottebohm 1983, 1998; *Rana catesbeiana*, Simmons et al. 2008a ;human, Eriksson et.al., 1998) and studies investigating cell phenotype in nonmammalian species have shown that newly generated cells can differentiate into neurons and glia, but is variable depending on species and anatomical location within the brain.

Neurogenesis in the CNS of reptiles, fish and birds is widely accepted to occur. The adult reptilian brain undergoes continuous neurogenesis in many telencephalic areas including, anterior dorsal ventricular ridge (ADVR), accessory and main olfactory bulbs (AOB/MOB) rostral forebrain (RF), dorsal, medial, lateral and dorsomedial cortices (DC/MC/LC/DMC), septum (Sp) (*Podarcis hispanica, Tarentola mauritanica*, and

*Trachemys scrip*ta; Font, et.al. 2001) and the nucleus sphericus (NS; *Podarcis hispanica* and *Tarentola mauritanica*; Font, et.al. 2001) and striatum (St; *Podarcis hispanica, Tarentola mauritanica,* and *Trachemys scrip*ta; Font, et.al. 2001), and nucleus sphericus (NS; *Podarcis hispanica* and *Tarentola mauritanica*; Font, et.al. 2001). Beyond these telencephalic areas, only the cerebellum (Cb) exhibits neurogenesis in the adult *(Podarcis hispanica* and *Trachemys scrip*ta; Font, et.al. 2001). Adult teleost fish also undergo neurogenesis in many areas including the ventricular zone (VZ), optic tectum (OT), olfactory bulb (OB), cerebellum (Cb) and the central posterior/prepacemaker nucleus of the electric fish (CP/PPn; Zupanc 2001). Findings of neurogenesis in these animals is readily accepted and is likely more prevalent than neurogenesis in mammals possibly due to continual neural addition as the reptilian and teleost brains continue to increase in size in adulthood (Font, et.al. 2001; Zupanc and Horschke 1995). In many species of birds, new neurons are added seasonally to the adult high vocal center (HVC) and interestingly follows a wave of cell death (Scharff, 2000; Nottebohm 2002)

However, in adult mammals, neurogenesis is limited to few areas including the olfactory bulb (OB) and dentate gyrus (DG) of the hippocampus in all mammals studied including hamsters (Huang, DeVries and Bittman 1998) mice, rats, tree shrews, marmosets, macaques and humans (Fuchs and Gould 2000 Gage, 2000; Alvarez-Buylla and Lim, 2004). Neurogenesis has also been demonstrated in monkey prefrontal, temporal and parietal cortices (Gould and Gross 2002), although this is controversial (Rakic)

Prior to 1962, it was thought that neurogenesis did not occur in the adult mammalian brain and that all neurons were generated early in development because new

neurons are not generated *in situ*, and mature neurons actively undergoing cell division are not seen. Instead, neural precursors are generated in proliferative zones and migrate prior to differentiation and extension of processes upon reaching their final destination (Font et al. 2001). Neurogenesis in the adult mammalian brain was finally demonstrated using "pulse-chase" techniques to label proliferating cells (pulse) using a thymidine analog [(radioactive thymidine, adult rat and cat; Altman 1962) or (5- bromo -2'-deoxyuridine (BrdU), Gould 1999], followed by waiting (chase) for migration and neuronal maturation. Olfactory neuron precursors are produced in the SVZ and migrate via the rostral migratory stream into the OB (Taupin and Gage 2002) and granule cell neurons proliferate within the dentate sub granular zone (SGZ) and migrate along radial glia to the granule cell layer (GCL).

At different time points following generation, new neurons express neural markers (i.e. Hu, TOAD-64, NeuN) allowing them to be distinguished from other cell types using immunohistochemistry or *in situ* hybridization. After differentiation and synaptogenesis, neural phenotype may be distinguished using EM, or tract tracing may be used to trace the path of neural processes. Many new neurons, however, do not integrate into functional networks as they undergo apoptosis before leaving the proliferative zones (mice; Blaschke, Weiner and Chun 1998), during migration, or after reaching their destination.

Mitosis Increases Following CNS Injury

Mitosis can increase after CNS trauma and can differentiate into neurons or glia (birds, Peterson et al 2007; neurons and glia in telencephalon of lizards, Font et al., 1995; and mammals Darsalia 2005; Gould and Tanapat, 1997). Removal of certain cell populations by apoptosis, disease or injury can induce replacement of the lost cells and contribute to anatomical (Font et al., 1991, 1997; Molowny et al., 1995) and behavioral recovery of functional deficit. Selective removal of specific neuron populations in birds have shown neurogenesis and network integration in populations which normally undergo seasonal apoptosis and proliferation the following year (HVC – RA projecting neurons, Scharff, 2000) but no replacement of neurons that are only generated in development and do not undergo seasonal replacement (HVC – Area X projecting neurons, Scharff, 2000).

Similar to other animal models that are capable of a high degree of plasticity in adulthood, we expect to find a cell proliferative response to n.VIII lesion. Furthermore, we expect that some of these newly proliferating cells will express neural phenotype. Finally, we expect to find an interruption in fluorescent lipophilic tracer travel to the brainstem following n.VIII crush lesion (when tracer is applied distal to the lesion site) followed by a gradual regaining in n.VIII connectivity as shown by increased amounts of fluorescent tracer travel into the brainstem with increasing post operative recovery timepoint.

CHAPTER 4: MATERIALS AND METHODS

Verification of n.VIII Lesion: Lipophilic Dyes:

In order to verify medullary target sites of the n.VIII were interrupted following n.VIII crush surgery, and that these fibers remained intact under sham surgical conditions, an experiment was performed in which fluorescent lipophilic tracers were deposited in the n.VIII proximal to the saccular end organ and distal to the crush site for crush surgical conditions. For sham and nonsurgical control conditions, tracer was applied to the same region of the n.VIII as in those exposed to n.VIII crush. For each experimental condition, one of the following bidirectional tracers was used: 1,1′-dioctadecyl-3,3,3′,3′-tetramethylindocarbocyanine perchlorate (‘DiI′; DiIC18(3)) 4-(4-(dilinoleylamino)styryl)-*N* -methylpyridinium iodide (FAST DiA™ oil; Di□ 9,12-C18ASP, I) ; 1,1′-dioctadecyl-5,5′-diphenyl-3,3,3′,3′-tetramethylindocarbocyanine chloride (5,5′-Ph2-DiIC18(3)); 1,1′-dioctadecyl-3,3,3′,3′-tetramethylindodicarbocyanine, 4-chlorobenzenesulfonate salt (‘DiD′solid; DiIC18(5) solid) ; 4-(4-(dilinoleylamino)styryl)-N -methylpyridinium iodide (DiA; Ex Max 456nm, Em Max 590nm), 1,1′-dioctadecyl-3,3,3′,3′ tetramethylindocarbocyanine perchlorate (DiI; Ex Max 549nm, Em Max 565nm), or , 1,1'-dioctadecyl-5,5′-diphenyl-3,3,3′,3′-tetramethylindocarbocyanine chloride (DiI-Ph; Ex Max 576nm, Em Max 599nm), all from Invitrogen, Carlsbad, Ca) and were chosen for their excitation/emission characteristics (above), in addition to their abilities to travel in both, live or aldehyde-fixed tissues.

Determination of Lipophilic Dye Travel into Medullary Tissue

In order to determine whether n.VIII regeneration following lesion occurs, and its extent, fluorescent lipophilic tracers were placed bilaterally into the n.VIII of a subset of animals. Following n.VIII crush, animals were allowed to recover for one day, one week, or two months prior to euthanasia, paraformaldehyde fixation, and tracer deposition into both n.VIIIs. Tracer was allowed to travel at room temperature for a minimum of one week. After which, brains were sliced by vibratome in the horizontal plane at 50µm. Sections were placed on gelatin-subbed slides and mounted using Aquamount Mounting Media (Polysciences) and viewed by fluorescence microscopy. Color fluorescence images were taken using an Olympus BX60 fluorescence microscope and saved as RGB Tiff files. In order to determine the amount of tracer that traveled to the medulla between the lesioned and sham-operated sides, the relative amount of red fluorescence was measured between the ipsilateral and contralesional medulla of each animal.

Fluorescent microscope RGB Tiff files were separated into 8-bit grayscale red, green and blue channels. The mean levels of the 8-bit separated red channel and of the intact RGB Tiff were measured using Corel Photo Paint (v.13) for 3 images per animal on each, the ipsi- and contralesional medulla. The red channel level was corrected for overall image brightness and auto fluorescence by the RGB image measurement and corrected values were expressed as the proportion from measurements from both the ipsilateral and contralesional medulla for each animal. Measurements were also taken from an animal not injected with lipophilic tracer was measured as a control.

Specificity of Antibodies for use in Xenopus laevis: Western Blot:

Prior to this study, antibodies generated against GFAP and TOAD-64 mammalian antigens had not been tested in a side by side study for specificity and selectivity towards mammalian versus anuran tissue, although antibodies have been well documented for use in mammalian tissue or anuran tissue alone. We tested the applicability of these antibodies for use in adult *Xenopus* using Western blot assay. Adult *Xenopus laevis* (n = 1) was terminally anesthetized in 0.6% MS-222, and whole brain was quickly removed and immediately frozen on dry ice. Brain tissue (obex through forebrain) was dissected and crushed using glass mortar and pestle, and split in half. Negative and positive control samples consisting of 0.9% sterile saline (for negative control) and mouse brain lysate (1 microgram in saline, BD Pharmingen), and *Xenopus* brain homogenate samples were resuspended in Lysis Buffer plus glycerol under denaturing conditions (Sigma Aldrich). Fifty microliters of each sample were loaded onto two polyacrylamide precast gels (8% and 10% concentration for TOAD-64 and GFAP antibodies, respectively; ISC Bioexpress) alongside 1 microliter of prestained molecular weight marker (ColorBurst; Sigma) and separated by SDS-PAGE according to previously published protocols (Ausubel 1997).

Proteins were then transferred onto nitrocellulose using the Bio-Rad Semi-Dry Transblotting system according to company protocols (Semi-Dry TransBlotter System product sheet; Bio-Rad) and thoroughly air dried. Membranes were then incubated with antibodies specific for GFAP or TOAD-64 for 4 hours in blocking buffer (1XPBS supplemented with 1% horse serum and 0.1% BSA; R/T, shaking). Membranes were

then washed in three changes of PBS followed by incubation in fresh blocking buffer containing peroxidase-conjugated secondary antibody (1:1000; goat anti-rabbit peroxidase conjugate #A0545; or goat anti-mouse peroxidase conjugate #A4416; both from Sigma-Aldrich, 2 hours, R/T, while shaking). Membranes were then washed in three changes of saline and the signal was developed using DAB (Vector DAB dropper kit; or Vector VIP Dropper kit; both from Vector Laboratories, Burlingame, MA). Upon development of appropriate DAB signal: noise ratio, membranes were quickly rinsed in water and allowed to air dry. Membranes were digitally scanned (Umax Scanner) and imported into Corel Photo Paint (v.13; Corel Corporation) for figure production and analysis.

Mitosis in Xenopus laevis Following n.VIII Damage

In order to determine whether the number of mitotic cells varies following n.VIII damage in *Xenopus laevis*, a subset of animals are injected with the thymidine analog, 5-bromo-2'-deoxyuridine (BrdU), which is incorporated into cells undergoing the S-phase of mitosis. Following euthanasia, immunohistochemical analysis using BrdU-specific antibodies mark which cells underwent division during the BrdU pulse. A subset of BrdU positive cells will be doubly labeled with antibodies indicating glial or neural phenotype which may indicate n.VIII-lesion induced proliferative response of specific cell populations. Utilization of the BrdU pulse-chase methodology is advantageous over other immunohistochemical techniques targeting cyclins (i.e. PCNA, Ki-67), present in

actively cycling cells as new neurons do not express phenotypic markers until they have undergone their final division and migrated away from the proliferative zone.

Determination of Cell Phenotype

In order to determine whether mitotic cells differentiate into neurons or glia, some animals were processed for double-label immunohistochemistry using antibodies specific for BrdU and either, neural [Turned On After Division, 64kDa (TOAD-64)] or glial [Glial Fibrillary Acidic Protein (GFAP)] markers.

Glial Fibrillary Acidic Protein (GFAP)

Glial cells will be shown by immunohistochemistry for the glial specific marker, glial-fibrillary acidic protein (GFAP). Glia are present in the CNS under normal conditions but have been shown to increase after injury, and are associated with the "glial scar" implicated in the growth-cone collapse of mammalian neurites attempting to enter the CNS transition zone (Fournier & Strittmatter 2001).

Turned On After Division, 64kDa (TOAD-64)

The neural-specific marker, TOAD-64 (Turned On After Division, 64 kDa) is one of the earliest neural-specific phenotypic markers expressed post-mitosis and is

implicated in neurite outgrowth and path finding (Minturn et al., 1995a; Minturn et al., 1995b; Quinn et al., 1999). It is expressed in neural development and in adult mammals TOAD-64 is down regulated in neurons following neurite outgrowth becoming nearly undetectable in the adult nervous system (Minturn et al., 1995a). However, TOAD-64 expression is up regulated during regeneration of motor neurons toward peripheral targets (in adult rats following sciatic nerve lesion, Minturn 1995b).

TOAD-64 is advantageous over using more mature neural markers (i.e. NeuN) or morphological determination of neural cell type as TOAD-64 is expressed prior to full neural maturity allowing earlier detection of post mitotic neurons.

GAP-43

Tissue will also be processed for Growth-Associated Protein-43kDa (GAP-43) to investigate n.VIII lesion-induced changes in the adult frog. GAP-43 is localized in growth cones and is associated with neural plasticity (Skene et al. 1986; Skene 1989; Benowitz & Routtenberg 1997), including neurite elongation and synaptogenesis. Although GAP-43 is highly expressed in development (Reh and Kliavin 1989; Schrama et al., 1997; Simmons et al. 2008b), it is down regulated in most mature neurons (Skene 1989) but GAP-43 expression is increased in neurite sprouting, elongation and sprouting post-injury (Skene 1989; Skene and Willard 1981a,b; Bendotti et al., 1991, 1994; Doster et al.,1991; Schreyer and Skene 1991; Mearow et al., 1994; Schaden et al., 1994; Horvath et al., 1997; Illing et al., 1999).

Lipofuscin

Lipofuscin, or "age pigment" is found in many different types of post-mitotic cells, especially neurons, and accumulates as nondegradable protein/carbohydrate/lipid components in lysosomes (Terman and Brunk, 2004) which accumulates increasingly with advancing age (Darsalia et al. 2005; Dowson, 1985) and oxidative stress (Keller et al., 2004). Lipofuscin appears as yellow-brown 1-20 µm granular structures within the cell under standard microscopy and wide-band auto fluorescence using fluorescence microscopy techniques (Billinton and Knight, 2001). It represents a challenge to this study because of its wide emission spectrum of auto fluorescence (Brunk and Terman, 2002; Billinton and Knight, 2001) which overlaps and must be distinguished from emission spectra of most fluorescent tags.

Immunohistochemistry Post n.VIII Lesion in Xenopus laevis: BrdU Injections:

Animals (n = 19) were anesthetized by submersion in 0.6% (w/v) tricaine methanesulfonate (MS-222; pH 8; Sigma, St Louis, MO) for 2-5 minutes, until all reflexes disappeared, then injected intraperitoneally with BrdU (1.0 mg BrdU/g; pH 9; Sigma) in 0.9% (w/v) sterile saline. Number of injections [1 Injection, or 2 Injections (second BrdU injection 24 hours after injection #1)] and survival period were varied in separate groups of animals. Survival times were characterized as short (0-3 day; 2 injections, n=3; 1 injection, n=1), medium (7-10 days; 2 injections, n=5) or long (2 weeks-1 month; 2 injections, n=8; 1 injection, n=2).

Following survival periods, above, animals were euthanized by submersion in 0.6% (weight per volume, w/v) tricaine methanesulfonate (MS-222; pH 8; Sigma, St. Louis, MO) for 5 minutes, or until all reflexes disappeared and transcardially perfused with heparinized 0.9% (w/v) saline, followed by ice cold, 4% (w/v) paraformaldehyde (pH 7.4). Brains were immediately removed and post fixed in paraformaldehyde for 12 h at 4°C. The brain was removed of overlying membranes and embedded in 5% (w/v) agarose (ISC Bioexpress, Kaysville, UT) in saline and sliced coronally by vibratome (The Vibratome Company) at a thickness of 50 µm. Sections were placed on gelatin-subbed glass slides and allowed to dry at room temperature (R/T).

Sections were treated for immunohistochemical analysis for BrdU alone, or double label immunohistochemistry for BrdU in combination with GFAP, TOAD-64 or GAP-43. For all sections in which BrdU was to be localized, DNA strands were denatured with room temperature (RT) 2 N hydrochloric acid (HCl; Fisher Scientific, Pittsburgh, PA) for 2-5 minutes. Sections were incubated in murine monoclonal anti-BrdU (1:1000; Sigma B2531), or rat monoclonal anti-BrdU (1:1000; ab6326 AbCam), and if processed for double label immunohistochemistry, were also incubated with glial cell marker, glial fibrillary acidic protein (GFAP; 1:100; Sigma G9269), the early neural marker, Turned-On-After-Division (TOAD-64; 1:5000; BD PharMingen, San Diego, CA), or Growth-Associated Protein, 43kDa (GAP-43; 1:5000: Sigma; G9264). Sections were incubated in blocking buffer (1X PBS supplemented with 10% horse serum, 1.0% BSA, and 0.1% Triton X-100) for 3 days (4 °C, shaking) followed by wash in fresh blocking buffer and incubation for 12 hours in blocking buffer supplemented with the appropriate corresponding fluorescent secondary antibodies (goat anti-mouse Alexa Fluor

594; 1:750; A11005; goat anti-rabbit Alexa Fluor 488; 1:750; A11008, or donkey anti-rat Alexa Fluor 488; 1:750; A21208; all from Molecular Probes, Eugene, OR).

Elucidating New Cell Phenotype: Confocal Microscopy

Slides were viewed through an Olympus BX-60 fluorescence microscope attached to a MagnaFire digital camera (Optronics, Goleta, CA). Images were captured as described previously (Chapman et al., 2006; Simmons et al 2006). BrdU-positive cells fluoresced either red or green, GAP-43-positive label fluoresced red, and GFAP- or TOAD-64-positive cells fluoresced green, all against a yellow-orange background.

A sample of sections processed for lipophilic tracer, BrdU/GAP-43, BrdU/GFAP and BrdU/TOAD-64 were mounted in AntiFade (Molecular Probes) and imaged using a Leica TCS SP2 confocal microscope system (sequential scan mode; Leica Microsystems, Bannockburn, IL). Low or high power z stack images were taken through each section of interest and viewed in orthogonal planes using Leica confocal software (Leica Microsystems).

CHAPTER 4: RESULTS

Western Blot Analysis of TOAD64, GFAP and GAP43:

Glial Fibrillary Acidic Protein, GFAP

Figure 4.1 shows western blot analysis of a polyclonal antibody directed against GFAP antigen. Fig.4.1 (Left) Numbers, ranging from 30-100, correspond to the relative locations of the prestained known-mass proteins in the ColorBurst molecular weight marker which was run alongside the three samples during SDS PAGE. Molecular masses are represented in kilodaltons (kDa). Lane 1 contains no tissue sample to which the antibody may bind and serves as a negative control. No DAB signal is shown in Lane 1, indicating nonspecific binding did not occur. Lane 2, a positive control lane, contains rodent brain homogenate which is known to bind the GFAP antibody. Presence of the intense and discrete DAB signal following incubation with the antibody for GFAP, in the positive control lane indicates the protocol is valid, and reagents are fresh. Lane 3, contains *Xenopus laevis* brain homogenate, and although DAB signal is lighter than in the control lane, black arrows indicate the positive signal as a thin upper band (one black arrow, top), and a second, thick, lower band. This indicates that the GFAP antibody recognizes two isoforms of GFAP protein in *Xenopus laevis*

*****INSERT FIGURE 4.1 ABOUT HERE*****

Turned On After Division, 64 kDa, TOAD-64 kDa

Figure (Fig 4.2) shows the results of western blot analysis to determine the relative specificity and quality of antibody binding of the polyclonal antibody specific for the early neural marker TOAD-64. Figure 4.2 shows western blot results of TOAD-64 antibody specificity when probing protein from rodent and *Xenopus* tissues. Lane 1: Contains no protein sample and is a control for nonspecific binding of antibody. There is no DAB signal in this lane. Lane 2: Contains concentrated rodent brain homogenate, to which TOAD-64 is expected to bind. A positive DAB reaction product is seen as one band [Fig. 4.2; Lane 2: white arrow]. Lane 3: Contains the *Xenopus laevis* brain homogenate, and shows a positive DAB reaction product shown as one band [Fig. 4.2; Lane 3; black arrow]. Bands between Lanes 2 and 3 appear similar in pattern and molecular weight.

*****INSERT FIGURE 4.2 ABOUT HERE*****

Growth-Associated Protein, 43 kDa , GAP-43 kDa

Figure 4.3 shows the results of western blot analysis to determine the specificity of monoclonal-GAP-43-specific antibody between mammalian (rodent) and *Xenopus laevis* tissue. Western blotting procedures were performed as described previously and nitrocellulose membrane is reprobed from a previous experiment in which a polyclonal antibody generated in rabbit was used as the initial probe. Procedures are performed as

described previously, except following incubation of the blot with the antibody directed against GAP-43, to reduce cross-reactivity from the previous experiment the secondary detection antibody used previously is replaced with one that is specific for the murine antibody followed by a pink chromogenic detection method (Vector VIP; Vector Laboratories) which is easily discriminated from the blue-black DAB signal.

The nitrocellulose has been probed previously using non-GAP-43 antibody (purple-black positive reaction using DAB in Lanes 2,3). Positive label for GAP-43 is indicated in pink only. [Fig. 4.3; Lane 1]: Negative Control. The absence of chromogenic development in Lane 1 indicates there are no nonspecific binding issues for either of the antibodies, nor is there false positive development of the chromagen. Lane 2: Positive Control (Rodent Brain Homogenate). Lane 2 exhibits a large pink band (Fig. 4.3; Lane 2; white arrow) which is localized according to the expected approximate molecular mass for GAP-43 protein, at 43kDa. Lane 3: *Xenopus laevis* adult brain tissue. One pink band is seen in tissue from *Xenopus laevis*, [Fig. 4.3; Lane 3; black arrow], although the molecular mass is less than the band seen in mammalian tissue, and appears to approximate a mass of 35kDa. A high degree of specificity was noted for each of the reprobe antibodies and chromagenic substrate as no ectopic banding patterns were seen outside of Lanes and molecular mass ranges expected for GAP-43.

*****INSERT FIGURE 4.3 ABOUT HERE*****

Verification of n.VIII Lesion: Lipophilic Dyes

Figure 4.4 shows the n.VIII and its medullary projection sites in nonsurgical, sham, and post n.VIII lesion conditions after tracer is deposited in the nerve branch proximal to the saccule and distal to the crush site (for nonsurgical and sham controls the tracer is deposited along the same relative position along the nerve as in crush conditions). A schematic showing the approximate level and region photographed in Fig 4.4A-C is indicated at left. Figure 4.4 shows the n.VIII in nonsurgical (Fig 4.4A) and sham surgical (Fig 4.4B) controls projects to target sites in the medulla, as indicated by the red-orange fluorescent dye in both the n.VIII and medulla. In contrast, in n.VIII lesioned animals, the n.VIII and medullary target tissues ipsilateral to n.VIII crush (7 days post-operative, Fig 4.4C) show little red-orange fluorescence due to relative absence of the lipophilic dye in both the n.VIII (proximal to the crush site) and medullary targets. The yellow-orange fluorescence seen in figure 4.4C is background auto fluorescence from the tissue and no red-orange fluorescence from tracer can be seen in the ipsilesional medulla after seven days post-crush.

*****INSERT FIGURE 4.4 ABOUT HERE*****

Figure 4.5 shows a confocal microscopy image of the same DiI-Ph-labeled nonsurgical control n.VIII shown in figure 4.4(A). Confocal microscopy allows higher resolution and more specific wavelength excitation/emission spectra to visualize fluorescent lipophilic tracers placed into the n.VIII. Nonsurgical control animals that had n.VIII placement of DiI-Ph show the parallel fibers in the peripheral n.VIII [lateral to n.VIII- medullary junction [see Fig 4.4(A, B)] become highly branched, individual fibers

upon entry into the CNS [see Fig. 4.5 (A,B,E)]and are intimately associated with cell bodies [Fig. 4.5 (C,E); blue DAPI-labeled cells, solid white arrowheads]. The proximity of fibers to cell bodies is further demonstrated by rotation of the confocal Z-stack in orthogonal planes [Fig. 4.5(E)].

In the medulla, n.VIII fibers are also seen to form terminal- like endings [Fig 4.5 (B, E); hollow white arrowheads]. These terminal-like structures are prevalent in the medulla and many do not appear to contact fibers or cells [Fig. 4.6 (A and A'); DAPI labeled cells in blue (hollow arrowheads); DiI-Ph-labeled terminal-like projections (A and A' solid arrowheads)]. Confocal Z - stack images of a terminal-like structure rotated in orthogonal planes show it does not make contact with other brain structures [Fig 4.6 (B; terminal-like structure, orange crosshairs, solid arrowheads; DAPI-labeled cells, open arrowheads)]. Some of these terminal-like structures however, may make contact with cell bodies [Fig. 4.6(B') DAPI labeled cell (open white arrowhead); DiI-Ph labeled terminal-like structure (solid white arrowhead)]. Scale bar = 25μm.

Fluorescent lipophilic tracer in n.VIII lesioned and sham tissues was semi-quantitatively analyzed according to the relative amount of red-fluorescence in the medullary target sites ipsi and contra-lateral to the lesion. Figure 4.7 shows tracer travels to the medulla in the sham-operated nerve indicated by red-orange fluorescence (Fig 4.7: 1 Day, Left Panel). Minimal tracer is seen in the medulla after one day post n.VIII lesion (Fig 4.7: 1 Day, Right Panel) and is limited to slight punctate fluorescence. An increased amount of fluorescence is seen in the medulla after one week post operative n.VIII-lesion (Fig 4.7: 1 Week, Right Panel), although the amount of fluorescence seen in the medulla is less than that seen in the sham operated side (Fig 4.7: 1 Week, Left Panel). After two

months post-n.VIII lesion (Fig 4.7: 2 Months, Right Panel), red-orange fluorescence approximates that seen in sham operated tissue (Fig 4.7: 2 Months, Left Panel). Figure 4.7 Chart (Bottom): Tracer was placed bilaterally in n.VIII and the amount of tracer traveling to the medulla was analyzed using Corel PhotoPaint Software (v.13) to quantify the relative amount of red fluorescence between sides ipsilateral and contralateral to the lesioned n.VIII.

In control animals not injected with tracer (Days Post-Op = 0; Blue Circles), the proportion of red-fluorescent contribution was similar in the medulla for each side and data points overlap on the chart. After post operative survival of one day [Days Post-Op = 1; Contralateral to n.VIII Lesion (Sham) Medulla = Gray Square; Ipsilateral to n.VIII Lesion (Lesion) Medulla = Red Triangle] and seven days after n.VIII lesion [Days Post-Op = 7; Contralateral to n.VIII Lesion (Sham) Medulla = Gray Square; Ipsilateral to n.VIII Lesion (Lesion) Medulla = Red Triangle], the contribution of red fluorescence is higher in medullary target tissue contralateral to the n.VIII lesion. Only after two months post operatively [Days Post-Op = 60; Contralateral to n.VIII Lesion (Sham) Medulla = Gray Square; Ipsilateral to n.VIII Lesion (Lesion) Medulla = Red Triangle], do the ipsilateral and contralateral to n.VIII lesion medulla have a similar proportion of red fluorescence for the error bars to overlap. N=4 (1 Animal per recovery point).

*****INSERT FIGURE 4.7 ABOUT HERE*****

Lesioned n.VIII Appears Thickened Compared to Sham n.VIII

Within twenty-four hours of n.VIII crush surgery, the lesioned n.VIII in *Xenopus laevis* appears thicker than in the contralateral (sham operated) n.VIII (shown in Fig 4.8) or nonsurgical controls.

*****INSERT FIGURE 4.8 ABOUT HERE*****

Quantification of Cell Count in Central Auditory Medulla

In order to determine the effect of n.VIII lesion on the number of mitotic cells in the adult *Xenopus laevis* we counted the total number of cells present in n.VIII medullary target nuclei. Total cell counts (T) were counted from 50µm thick horizontal brain tissue stained with 4' 6-diamidino-2-phenylindole (DAPI; Sigma) to allow localization of DAPI positive cell nuclei upon excitation of the fluorophore with fluorescence (λ=~350nm) microscopy. DAPI positive cell counts are expressed as the total number of cells (T; within the auditory/vestibular nuclei of interest) to determine a baseline cell count in normal animals and to determine any effects of n.VIII injury on the overall increase or decrease in the total number of cells and numbers of mitotic cells as determined by incorporation of BrdU.

Figure 4.9 shows mean DAPI positive cell counts (T; +/- SEM) in n.VIII medullary target nuclei (brainstem vestibular and auditory nuclei were counted in 50µm horizontal tissue section). Cells were counted in medullary tissue in six different experimental conditions. Figure 4.9 shows a bar chart summarizing T in animals treated with BrdU compared with T in non BrdU treated animals and T in n.VIII deafferented

nuclei (by crush lesion), sham surgery, and in nonsurgical controls. Naive animals which are not subjected to surgery or BrdU injection have approximately 3,060 (+/-78.8) cells in n.VIII medulla targets which is similar to counts seen in the contralateral medulla of 1-Day post n.VIII-lesion animals not treated with BrdU [T=3257 +/- (4.6)]. Nonsurgical and double sham surgical animals injected twice with BrdU over two days and allowed to recover for one month have T of 3657 +/-(156.7) and 2521 +/- (8.6), respectively. An animal injected with BrdU twice over two days plus receiving n.VIII crush (and contralateral sham) surgery followed by one month post-operative recovery had T= 4341 +/- (123.4) in medullary tissue ipsilateral to the lesion and T= 3454 +/- (134.4) in the contralateral medulla. Pair wise statistical analysis indicates T is not affected by BrdU injection [T- Test; two tailed; P(T<=t), 0.45] or n.VIII lesion [T-Test; two tailed; P(T<=t), 0.27].

*****INSERT FIGURE 4.9 ABOUT HERE*****

Quantification of BrdU Positive Cell Count in Central Auditory Medulla

BrdU Positive Cell Counts

BrdU positive cells were counted in the *Xenopus laevis* medulla after two days, one week, or one month following BrdU injections. Counts were performed as described

for DAPI labeled cells except the appropriate fluorescence excitation wavelength and filters were used for the chosen antibody.

Example confocal Z-Stack images show BrdU positive cells are present in one week survival medulla following n.VIII lesion (Fig. 4.10A; BrdU positive cell is blue, white arrowheads) and after bilateral n.VIII surgical sham (Fig 4.10B; BrdU positive cell is blue, white arrowheads).

*****INSERT FIGURE 4.10 ABOUT HERE*****

No Effect of Sham Surgery on BrdU Positive Cell Counts

Counts of BrdU positive cells in n.VIII medullary targets (mean counts are normalized by section thickness) indicate there is no effect of sham surgery on numbers of mitotic cells. Pair wise statistical analysis of BrdU positive cell counts over all recovery periods investigated indicate nonsurgical or sham surgical animals exhibit no significant difference between the two groups (Fig. 4.11; [T- Test; P(T<=t); 0.33, two tailed].

*****INSERT FIGURE 4.11 ABOUT HERE*****

Effect of Recovery Period on BrdU Positive Cell Counts in Controls

Pair wise comparisons of nonsurgical and sham surgical control animals at two days survival and those at one week and one month indicate there is a significant effect of survival period on BrdU positive cell counts. There is a reduction in counts of BrdU positive cells in control surgical animals between two days and one week or one month recovery period [T- Test; P(T<=t); 0.001, two tailed]. Figure 4.12 shows significantly more cells are counted in central nuclei at two days after BrdU injection [mean, (+/- SEM); 60.1, (+/- 2.7)], than after one week [mean, (+/- SEM); 17.8, (+/- 5.8)] and one month [mean, (+/- SEM); 12.6, (+/- 1.2)].

*****INSERT FIGURE 4.12 ABOUT HERE*****

Effect of Lesion on BrdU Positive Cell Counts in Long Recovery Period

Statistical analysis of BrdU positive cell counts in one month survival animals show a significant effect of n.VIII lesion on increasing cell counts in both the n.VIII deafferented medulla (ipsilateral to the lesion), as well as in tissue contralateral to n.VIII lesion [Fig 4.13; mean (+/-SEM); 94.1, (+/- 15.9); T- Test; P(T<=t)= 0.014; two tailed] versus long recovery period nonsurgical and sham surgical animals [Fig. 4.13; mean (+/- SEM); 12.6, (+/- 1.2)]. Significant effect is shown by asterisk (Fig 4.13).

*****INSERT FIGURE 4.13 ABOUT HERE*****

BrdU positive cell counts are greater in n.VIII medullary targets in n.VIII-lesioned animals after one-month post-operative time point versus nonsurgical and sham as surgical control animals. (see Fig.4.14)

*****INSERT FIGURE 4.14 ABOUT HERE*****

*****INSERT FIGURE 4.15 ABOUT HERE*****

BrdU-Positive Cells Express Neural Markers at Long Survival Time

Although BrdU positive cells were occasionally seen in the ventricular zone in *Xenopus laevis,* TOAD-64 was not expressed periventricularly in any animal for which the TOAD-64-antigen was localized. Cells located in parenchyma were occasionally double labeled with BrdU and TOAD-64 but were only observed but only after long survival times of [one month; Fig.4.15B, C; BrdU/TOAD-64]. BrdU/TOAD-64 double label is regularly seen following post n.VIII-lesion both ipsilateral and contralateral to the lesion [one month; Fig.4.15B, C; BrdU/TOAD-64]. and less frequently in sham operated animals.[one month; Fig.4.15A; BrdU/TOAD-64].

In medullary sections of *Xenopus laevis* one month post n.VIII lesion, newly mitotic BrdU/TOAD-64 double labeled cells can be seen in the 50µm horizontal sections through the medulla both, contralateral [see Fig 4.16A] ipsilateral [see Fig 4.16B,C]. to the lesion site [(see Fig 4.16, BrdU (Red) and TOAD-64 (Green); 30 days after n.VIII crush lesion indicating the addition of new neurons ipsi- and contra-lateral to n.VIII

crush. There is presumptive co-localization of BrdU/TOAD-64 in the same cell after lesion [(Fig 4.16 B,C]; presumptive co-localization of BrdU and TOAD-64 is shown by the white arrowhead.

*****INSERT FIGURE 4.16 ABOUT HERE*****

Immunohistochemical localization of GAP-43 in adult *Xenopus laevis* are found at qualitatively low levels in the DLN of bilateral sham or nonsurgical animals [nonsurgical animal DLN shown in [Fig 4.17 (A), GAP-43 (Red)], and is similar to animals subjected to sham surgery (data not shown), and is largely restricted to cell bodies [Fig 4.17 (A), nonsurgical condition]. In contrast, higher levels of GAP-43 are detected in the 30-day post-sham medulla [Fig 4.17 (B)] with contralateral n.VIII crush lesion. Figure 4.17 (B) shows an increase in red fluorescent label over bilateral sham conditions and multiple red fluorescent cell bodies can be seen [Fig 4.17 (B) white arrows, 2 example cells are shown]. In addition, there is limited GAP-43 localization in neurites [Fig 4.17 (B), white arrowheads]. In medullary tissue ipsilateral to n.VIII lesion, one month post-operatively [Fig. 4.17 (C and C')], there are high levels of GAP-43 positive cell bodies and neurites [Fig 4.17 (C and C')]. Large concentrations of GAP-43 positive neurites are often found in clusters in the medulla ipsilateral to n.VIII lesion [Fig 4.17 (C and C'; Fig 4.17 C' shows the same 10x image shown in C, except open arrowheads indicate a cluster of GAP-43 positive neurites). Auto fluorescent vascular cells are frequently found in the CNS of animals subjected to lesion and are distinguished

from cells labeled with red-fluorescent antibodies (example artifact RBC is shown by solid white arrowhead, Fig 4.17 C').

*****INSERT FIGURE 4.17 ABOUT HERE*****

CHAPTER 4: DISCUSSION

Fiber Analysis

These studies have shown n.VIII surgical crush lesion effectively reduces n.VIII fibers projecting to target sites in the medulla immediately following lesion indicated by reduction in fluorescent lipophilic tracer in the DLN ipsilateral to crush (Figure 4.4). Western blot analyses established the validity of use of antibodies against Glial Fibrillary Acidic Protein (GFAP), Turned On After Division 64 kDa (TOAD-64), and Growth-Associated Protein, 43 kDa (GAP-43) for use in anuran tissue. Figures 4.1, 4.2, and 4.3 established the specificity and selectivity of each antibody was comparable to mammalian controls. The discrepancy in staining intensity between Lanes 2 and 3 may be the result of reduced specificity of the GFAP antibody for the *Xenopus laevis* isoform, although is likely a function of the difference in protein concentration between lanes, rodent brain homogenate protein which was loaded in Lane 2 is highly concentrated and marketed to researchers as a positive control, in contrast *Xenopus laevis* brain tissue is low density, containing many lipids, nonprotein volume which may compete for valuable acrylamide gel well space.

In medullary sections of *Xenopus laevis* one month post n.VIII lesion, newly mitotic BrdU/TOAD-64 double labeled cells can be seen in the 50µm horizontal sections through the medulla both, ipsilateral and contralateral to the lesion site [(see Fig 4.15, BrdU (Red) and TOAD-64 (Green); 30 days after n.VIII crush lesion (shown in C and B) and less are seen 30 days post operative sham surgery (shown in A)], indicating the addition of new neurons primarily ipsi- and contra-lateral to n.VIII crush. Of greater

interest than the addition of new neurons, is the retention of new neurons 30 days after lesion [(Fig 4.16 C; presumptive co-localization of BrdU and TOAD-64 in the same cell (white arrowhead)].

GAP-43

These studies additionally indicate extension of neurites are up regulated 30 days after n.VIII in comparison with tissue from a sham and nonsurgical control animals as indicated by GAP-43 localization (nonsurgical adult *Xenopus laevis* medulla is shown in Fig 4.17A; sham surgical contralateral to n.VIII crush shown in Fig 4.17C and C' is shown in Fig 4.17B). Medullary tissue from a 30-day post unilateral n.VIII crush lesioned animal shows an up regulation in immunohistochemical localization of GAP-43 (shown in Fig 4.17C and C'), with sham surgery on the contralateral side (shown in Fig 4.17B). Very low levels of GAP-43 are detected in nonsurgical animals, and is similar to animals subjected to bilateral sham surgery (data not shown), and are largely restricted to cell bodies (Fig 4.17A, nonsurgical condition; white arrows, 3 cells are shown). In contrast, higher levels of GAP-43 are detected in the 30 day post-sham medulla (Fig 4.17B) if the contralateral n.VIII is lesioned by crush. Fig 4.17B shows an increase in red fluorescent label over bilateral sham conditions and multiple red fluorescent cell bodies can be seen (Fig 4.17B white arrows, 2 example cells are shown). In addition there is limited GAP-43 localization in neurites (Fig 4.17B, white arrowheads). In medullary tissue ipsilateral to n.VIII lesion (Fig4.17C and C'), there are many GAP-43 positive cell bodies and neurites (Fig4.17C and C'). Further, large concentrations of GAP-43 positive

neurites are often found in clusters ipsilateral to n.VIII lesion (Fig 4.17C and C'; Fig 4.17C' shows the same 10x magnification image shown in C, except open arrowheads indicate a cluster of GAP-43 positive neurites).

These findings of newly mitotic neurons and up regulation of neurite extension in medullary sites one month post-n.VIII crush, indicate two possible mechanisms for anuran regenerative ability, neuron replacement, and fiber extension post injury.

CHAPTER 5: GENE EXPRESSION IN THE ADULT VERTEBRATE CNS POST N.VIII CRUSH: RANA CATESBEIANA AND XENOPUS LAEVIS

CHAPTER 5: INTRODUCTION

This study examines the gene expression in the regenerating adult *Rana catesbeiana* and *Xenopus laevis* n.VIII. The hypothesis of these experiments is that specific mRNAs will be expressed and identified at different time points after injury and during the recovery process; some of these gene products are expected to have homologs to those previously described in other vertebrates, while others are predicted to be novel.

In order to determine what mRNA transcripts are implicated in n.VIII regeneration, this study will utilize the technique of differential display (DD-PCR) to discover known and/or novel genes (DNA) involved in such aspects of post-injury regeneration as neural survival, outgrowth, path finding, and reformation of functional synapses. The DD-PCR technique was chosen over other methods (microassays) because it requires very little RNA and splice variants and rare mRNAs can be detected, and can be applied to any species for simultaneous discovery of known and novel genes. Although DD-PCR has limitations in that it can lead to false positives, it is the established technique of these studies (e.g., Greeve et al., 2000). To minimize false positive results, all PCR experiments will be performed in duplicate and data compared between animals. Differentially expressed genes (cDNAs) will be cloned into TOPO4 vectors and sequenced for comparison to those in Genbank to determine if these genes exist in humans. Original sequence or novel expression conditions will be submitted to Genbank to forward neural regeneration research.

The results of this study can have implications for treatment of VIII nerve disease or trauma which contribute to certain auditory and vestibular disorders in humans. Some

progress has recently been made in identifying genes expressed during hair cell regeneration and supporting cell proliferation in chicks and in knockout mice (Lowenheim et al., 1999; Stone & Rubel, 1999). It is likely that different mRNAs are expressed during regeneration of the n.VIII itself. Identification of mRNA expression in the damaged and regenerating n.VIII of frogs may elucidate homologs present in mammals that may be induced pharmacologically to restore such capabilities to humans suffering from auditory and vestibular deficits based on cranial nerve pathology or trauma.

CHAPTER 5: MATERIALS AND METHODS

Tissue Procurement

Following survival times at previously described time points, frogs were terminally anesthetized by immersion in MS-222, the roof of the mouth exposed, and n.VIII, associated ganglia, and the medullary region (demarcated by the insertion regions of cranial nerves VII and IX) extracted (bilaterally) (*Rana catesbeiana* n=20 or *Xenopus laevis*, n=4),. Animals given bilateral sham surgery were used as a negative control, as genes expressed upon exposure to anesthetic and surgery prior to nerve trauma are not the focus of this experiment. The medulla was processed in addition to n.VIII in order to obtain larger quantities of RNA and to find genes which may be expressed in the deafferented medulla and act to target the n.VIII during regeneration. Medullary tissues were partitioned along the sagittal midline, separating lesioned from the unlesioned (control) sides, and placed in RNAse/DNAse/pyrogen-free microcentrifuge tubes containing 1.0ml RNAzol (Tel-Test) and 0.2ml chloroform:isoamyl alcohol (24:1; Fisher) and placed at -80°C until processed. Care was taken during harvesting to make symmetrical cuts through the medulla. It is recognized that this procedure involves severing of efferent fibers, which may be important in regulating regeneration.

RNA Extraction:

Total RNA was extracted from n.VIII and medulla using molecular biology grade, RNAse-/DNAse-/pyrogen-free reagents and consumables. RNA was extracted using the RNAzol (Tel-Test) method of total RNA extraction. The RNAzol mixture containing

tissue was thawed on ice for 15 minutes while vortexing occasionally. Microcentrifuge tubes were centrifuged at 12,000 rpm for 20 minutes at 4° C; the clear supernatant was removed and placed into a fresh 1.5 ml microcentrifuge tube. An equal volume of isopropanol was added to the supernatant. Tubes were mixed by gentle inversion and placed at -80°C for 20 minutes to aid in precipitation of the RNA. Samples were then thawed, and centrifuged at 12,000 rpm (20 minutes, 4°C). Supernatant was poured off and the RNA pellet was resuspended in 1ml of 75% ethanol (v/v). Samples were again centrifuged at 12,000 rpm (20 minutes, 4°C), and the supernatant decanted. The pellet was resuspended in 1ml of 75% ethanol (v/v) and centrifuged as previously described. Again, the ethanol supernatant was removed and the RNA pellet was resuspended in 50 µl of nuclease-free water (Sigma). Content and purity of RNA was determined by UV spectroscopy (OD260/280). Subsequent to quantification, contaminating DNA was removed by a DNAse I digestion using RNAse free DNAse I (Pharmacia Biotech). The reaction conditions were as follows: RNA in nuclease-free water (0.5 mg/ml), Tris-HCl, pH 7.5 (50mM), $MgCl_2$ (10mM) and RNAse free DNAse I (0.08 U/µl). The reaction was incubated for 30 minutes at 37°C. In order to stop the digestion, 200 µl of phenol: chloroform (1:1 v/v) was added to the reaction mixture and vortexed for 10 seconds and then placed on ice. The reaction mixture was then centrifuged at 12,500 rpm for 15 minutes at 4°C. The upper phase was removed and to it was added 23 µl of lithium chloride (9M $LiCl_2$; Sigma) and 200 µl of absolute ethanol. The solution was mixed by gentle inversion and placed at -80°C for 10 minutes. Subsequently, the mixture was centrifuged for 12,000 rpm for 20 minutes at 4°C. The supernatant was poured off and to

the pellet was added 75% ethanol (v/v), which was removed by centrifugation at 12,000 rpm, for 20 minutes at 4°C. This step was then repeated one additional time. Ethanol was poured off and pellets were air-dried. Pellets were resuspended in nuclease-free water and quantified by UV spectroscopy.

One microgram of RNA was run on a 1.2% (w/v) agarose gel using RNAse free 1X TBE (Tris Borate EDTA; Sigma) running buffer at 75 volts for 1.5 hours. To the loading buffer (Sigma) was added 1 µl of ethidium bromide (1mg/ml). RNA integrity was determined by the presence of 28S and 18S ribosomal RNAs, which migrate at 4.7kb and 1.9kb respectively.

RNA extractions were typically performed in batches of three animals at a time (two samples per animal) as it is necessary to minimize the time RNA is above -20°C to avoid degradation. Twenty-nine differential display gels were run and placed against Biomax film for 7-10 days. Only bands that were different between experimental conditions (lesion vs. sham or different recovery periods) but showed the same banding pattern between duplicate reactions were excised due to the high rate of false positives using this technique.

cDNA Synthesis

RNA was diluted to 0.1 µg /µl in nuclease free water. RNA was then reverse transcribed using the SuperscriptII® (Gibco BRL) kit for cDNA synthesis. HeLa RNA (0.1µg/µl) was used as a positive control. RNA minus RT (reverse transcriptase) enzyme

was used as negative control. The first strand cDNAs was obtained using one of twelve oligo (dT) anchored primers (Genomyx) to preferentially select for mRNA populations. Reverse transcription was performed in a Genomyx CycleLR thermal cycler GX102 using 0.2 ml thin walled MicroAmp PCR tubes (Perkin-Elmer). Each reaction consisted of 7.8 µl nuclease free water, 4.0µl SuperScript II 5X RT buffer, 2.0µl of 250µM each dNTPs (1:1:1:1), 2.0µl DTT (100mM), 0.2µl SuperScript II RT enzyme (200U/µl), 2.0µl RNA (0.1µg/µl), and 2.0µl (2µM) T7(dT_{12}) anchored primer. Reverse transcriptase reactions were cycled at 42°C for 5 minutes, 50°C for 50 minutes, 70°C for 15 minutes, and held at 4°C. These first strand cDNAs were stored at -20°C, and used in PCR reactions within one week.

Differential Display:

Each cDNA was PCR amplified with the original anchor primer used in the reverse transcription reaction, and one of four arbitrary primers:

ARP1: 5' ACAATTTCACACAGGACGACTCCAAG 3';

ARP2: 5' ACAATTTCACACAGGAGCTAGCATGG3' ;

ARP3: 5' ACAATTTCACACAGGAGACCATTGCA3';

ARP4: 5' ACAATTTCACACAGGAGCTAGCAGAC3'.

Each PCR reaction contained 9.95µl sterile, nuclease free water, 2.0 µl of PCR Buffer I (Perkin-Elmer), 1.6µl 250µM dNTP mix (1:1:1:1), 2.0µl of 2µM 5' arbitrary primer, 2.0µl of 2µM 3' anchor primer, 2.0µl reverse transcriptase reaction, 0.2µl of

5U/µl AmpliTaq® enzyme (Perkin-Elmer), and 0.25µl of 10µCi/µl [α-^{33}P]dATP (New England Nuclear, MA). PCR reaction conditions were as follows: Step I: 95°C for 2 minutes; StepII: (4 cycles) 92°C for 15 seconds, 50°C for 30 seconds, 72°C for 2 minutes; StepIII: (25 cycles) 92°C for 15 seconds, 60°C for 30 seconds, 72°C for 2 minutes; StepIV: 72°C for 7 minutes; StepV: hold at 4°C. To each 20µl reaction was added 10µl Sample Loading Dye (Sigma) and heat denatured at 95°C for 2 minutes. Four µl of each sample was run on 4.5% denaturing HR-1000 polyacrylamide gel (Beckman, CA) poured 340µm thick. Gels were run at 940V, 100W, at 50°C for 16 hours in a Genomyx LR Sequencer (Genomyx). Subsequent to separation of bands, the gel was dried, and urea removed. Gels were placed against Kodak Biomax HR film (Beckman, CA) for seven to ten days. Each differentially expressed cDNA was located on the polyacrylamide gel using the overlying autoradiograph as a template. Holes were punched in the autoradiograph on either side of the band, through which, the location of the band in the gel was marked using pencil. The band was then excised using a #15 scalpel and placed in 50µl sterile Tris-EDTA buffer (pH 7.4) and vortexed for 15 minutes. Twenty-three micro liters of eluent from each of the three bands was then amplified by PCR using EasyStart® tubes containing 0.65µl each of 2µM AP4 and 2µM ARP2 primers and 0.25µl AmpliTaq® (5U/µl) DNA Polymerase. PCR amplification and cloning was performed as described above.

Reamplification of Differentially Expressed cDNAs:

Differentially expressed bands were excised from the gel, and reamplified using EasyStart™ PCR tubes (Molecular BioProducts). The reaction conditions were: 2µl (50mM) MgCl2, 2µl (10X) PCR Buffer, 4µl (2.5mM of 1:1:1:1)dNTP, 14µl H2O, 0.65µl (25M) Anchor Primer, 0.65µl (25M) Arbitrary Primer, 23.45µl excised cDNA band (in 100µl H2O), 0.25µl AmpliTaq DNA polymerase (Perkin Elmer). Reamplification conditions were: 95°C for 5 minutes, 50°C for 50 minutes, and 72°C for 15 minutes. Five µl of loading buffer (containing EtBr) was added to EasyStart® tubes which were heat denatured at 95°C. Reamplified DNA was purified by electrophoresis on 2% (w/v) agarose gel at 75V for 1.5 hours. The DNA bands were cut from the gel and purified using QiaQuick gel extraction kit (Qiagen). UV spectroscopy determined quantity of DNA subsequent to purification. Each differentially expressed cDNA was located on the polyacrylamide gel using the overlying autoradiograph as a template. Holes were punched in the autoradiograph on either side of the band, through which, the location of the band in the gel was marked using pencil. The band was then excised using a #15 scalpel and placed in 50µl sterile Tris-EDTA buffer (pH 7.4) and vortexed for 15 minutes. Twenty-three micro liters of eluent from each of the three bands was then amplified by PCR using EasyStart® tubes containing 0.65µl each of 2µM AP4 and 2µM ARP2 primers and 0.25µl AmpliTaq® (5U/µl) DNA Polymerase.

Transformation of Bacteria:

Purified DNA was ligated into TOPO4 TA vectors (Invitrogen, CA). The procedure was as follows. 20ng of the fresh PCR product was added to 1μl of pCR®TOPO4®vector in a final volume of 5μl. The mixture was incubated at 25°C for 5 minutes. One μl of TOPO® 6X Cloning Stop Solution was added after this incubation period and placed on ice. Two μl of the TOPO4® Cloning reaction was placed into a vial of OneShot™ DH5α (DH5α-T1R bacteria genotype: F- f80lacZ.M15 .(lacZYA-argF)U169 deoR recA1 endA1 hsdR17(rk-, mk+) phoA supE44 thi-1 gyrA96 relA1 tonA) competent cells and was incubated on ice for 30 minutes. The cells were then heat shocked at 42°C for 30 seconds, and placed on ice. Two hundred fifty microliters of SOC medium was added to the heat shocked cells and shaken at 200rpm at 37°C for one hour. Cells were then cultured on LB media plates containing 50 μg/ml kanamycin. Plates were incubated overnight at 37°C. Three to six colonies were removed and placed separately in 250 ml of LB broth containing 50 μg/ml kanamycin. Broth cultures were incubated for 18 hours at 37°C and 200rpm in a rotating incubator.

Each PCR product was immediately purified and cloned as the pCR®4-TOPO® vector makes use of the 3' A-overhang generated by DNA polymerase I in the PCR reaction. DH5α-T1R bacteria were transformed with vectors and plated on kanamycin containing LB plates. Positive recombinants were isolated using a sterile inoculating needle after three days and placed in sterile LB broth containing kanamycin. Bacteria were grown to log phase (approximately 18 hours) at 37ºC while shaking (200rpm). Plasmids were purified using the QiaQuick Plasmid Isolation Kit. Inserts were restriction digested using Ecor1 and sequenced at the Brown University Core Facility.

Plasmid Isolation:

Plasmids were isolated according to the QiaQuick Plasmid Isolation Kit protocol (Qiagen). Broth cultures were centrifuged in microfuge tubes at 7000rpm for 10 minutes and supernatant was poured off. The pellet was resuspended with 250 μl Resuspension buffer. The cells were lysed with 250μl of Lysis Buffer and mixed by gentle inversion for 5 minutes. Three hundred fifty microliters of Neutralization Buffer was added to the solution and mixed by gentle inversion. Microcentrifuge tubes were centrifuged at 13,000 rpm for 10 minutes. Supernatant was placed into a Qiagen column and centrifuged for 1 minute at 13,000 rpm. Seven hundred micro liters of Buffer PE was added to the column and centrifuged for 1 minute at 13,000rpm. The column was re-centrifuged for 1 minute at 13,000rpm in order to remove excess Buffer PE. Fifty micro liters of Elution Buffer was added to the column and a fresh microcentrifuge was placed under the column. The column was centrifuged at 14,000rpm for 1 minute. The eluent was quantified by UV spectrometry.

Sequencing of Insert:

Purified plasmid DNA was sequenced at Brown University's Core Laboratory (Providence, Rhode Island). In a 200μl PCR tube was placed 4.8 picomoles of arbitrary primer used in the reamplification reaction and 0.75μg of purified plasmid DNA.

Genbank Database Search:

The NIH website, http://www.ncbi.nlm.nih.gov/BLAST/, was consulted for a Genbank search.

Confirmation of Transcript:

In order to confirm the presence of transcripts found by DD-PCR, primers were specifically designed to amplify the cDNA of interest (later termed BR1).

CHAPTER 5: RESULTS

Sequence Data:

Three genes (cDNAs) of interest were identified on the differential display of *Rana* tissue in this study. These genes of interest expressed 24 hours after lesion of the nerve VIII. Two were expressed on the ipsilateral side of the lesion but not on the contralateral side. The third was expressed on the contralateral side but not the ipsilateral side

Gene BR1

BR1 appears at the top arrow in lanes 3 and 4 of Figure 5.1B. This gene expressed on the ipsilateral side but not the contralateral side to the lesion at 24 hours.This non-vector DNA has 681 nucleotides (Fig 5.3). BLAST searches of Genbank revealed that BR1 with its 681 nucleotides had an ORF Finder sequence of 195 nucleotides that

matched Genbank data This segment correlated with CGI-38 which is a brain specific protein. The 64aa translation had 67% identity (91% positive).

Gene BR2

BR2 (Fig 5.1B bottom) like BR1was expressed on the ipsilateral side but not the contralerteral side of the lesion. BR2 was 667 nucleotides in length (Fig 5.4). BLAST searches revealed that BR2 was not similar to any known Genbank data indicating no ORF matches.

Gene BL2

Gene BL2 (Fig 5.1A) in contrast to BR1 and BR2 expressed on the contralateral side but not on the ipsilateral side to the lesion. This gene contained 843 nucleotides (Fig 5.5). A 675 ORF sequence was possibly identified. PSI-BLAST of 188aa of the translated ORF shares 26% identity (40% positive) with a murine cell-adhesion protein.

These differences in the expression of these genes at 24 hours is in contrast to the findings at one hour and 41 days. These genes were not expressed at 1 hour post-op. At 41 days post-op these genes were present in tissue on both sides of the lesion.

Confirmation of BR1:

In order to confirm the presence of BR1 in tissue ipsilateral to n.VIII lesioned tissue and absence of transcript in contralateral tissue, the primers:

5’CGGGGCTGTGGAACGTCTTACAGA3’ and

5’CTATTTCTTTACCTTGGACTCATAA3’

Primers were used to select for the BR1 sequence by PCR. Tissue from three *Rana catesbeiana* was used for the confirmation experiment. The left and right tissue from each animal was treated separately. The three animals included a nonsurgical control, a left n.VIII lesion (right n.VIII sham) after 41 days of recovery, and a left n.VIII lesion (right n.VIII sham) processed 1 hour post surgically. Figure 5.6 shows the ethidium bromide stained gel results of the BR1 confirmation experiment. 20µl of DirectLoad™ Step Ladder (Sigma) was run alongside the samples (Ladder). Lane 1 was left blank. The nonsurgical control left (Lane 2) and right (Lane 3) n.VIII samples did not result in a band on this gel. The tissue from the 41 day recovery animal subjected to leftVIII nerve lesion resulted in a band amplified by these primers in tissue from both the ipsilateral (Lane 4) and contralateral (Lane 5) side. However, the lesioned animal processed at 1 hour did not exhibit a band in tissue ipsilateral (Lane 6) or contralateral (Lane 7) to the lesion.

*****INSERT FIGURE 5.1 ABOUT HERE*****

DISCUSSION

DD-PCR suggested there were changes in gene expression patterns between lesion- and sham-operated n.VIII and target tissues of the medulla. As these were wild-caught animals (in the case of *Rana catesbeiana*), or laboratory bred (*Xenopus laevis*), the sham- and lesion-operated sides were processed separately so that the animal could serve as its own control. However, it would be an error not to consider gene expression in the contralateral tissue would not vary in response to the lesion. As a result, sham operated animals were utilized to control for gene expression following surgery with consideration that variation between lesion- and sham-operated animals may not be due to n.VIII recovery, but genetic variation within the sample population. As a second control, all DD-PCR reactions were performed in duplicate to minimize error due to PCR amplification of products not specific frog's mRNA (i.e. dust). Third, gels containing differences between samples were run multiple times for consistency of pattern. A related control was used to ensure "housekeeping genes" (genes that do not vary in response to the lesion) (in *Rana catesbeiana* tissue, Fig. 5.1C, and *Xenopus laevis* tissue, Fig 5.., Bottom), were present on the gel. These "housekeeping" genes are expected to vary in comparison to the targeted genes. The lack in variation of these genes shows the reproducibility of this technique within and between tissue samples.

The finding that two of the genes, BR1 and BR2, were expressed on the ipsilateral side raises the question as to whether these genes are upregulated on that side or whether the lack of these genes being expressed on the contralatal is the result of down regulation. Since the DD-PCR data could not parse whether BR1 or BR2 expression was up

regulated in response to the lesion, or if they were normally expressed in n.VIII and/or targets of the medulla, primers were generated to selectively amplify the cDNA of interest, BR1. The use of the primers would confirm the banding pattern found by DD-PCR. A nonsurgical control animal showed that BR1 is not expressed in unoperated n.VIII or medulla (Fig 5.6; Lanes 2 and 3). Further, BR1 expression was up regulated sometime between 1 hour and 24 hours post lesion, as BR1 was not found in tissue ipsilateral (Fig 5.6; Lane 6) or contralateral (Fig 5.6; Lane 7) to n.VIII lesion after 1 hour of recovery. Surprisingly however, BR1 was confirmed in tissue 41 days post surgically in both ipsilateral (Fig5.6; Lane 4) and contralateral (Fig5.6; Lane 5) tissue.

These data may not contrast the data from the DD-PCR experiments as BR1 was found unilaterally in DD-PCR samples from tissue 24 hours post lesion and the PCR confirmation utilized tissue after 41 days of recovery. n.VIII regeneration is a global process, and during the latter stages, these genes may be more widely expressed, even contralateral to the injury.

CHAPTER 6: GENERAL DISCUSSION

CHAPTER 6: GENERAL DISCUSSION

Summary of findings

In this thesis, I examined plasticity in the anuran auditory system over development and in the adult after injury. My data show, as predicted, that the anuran central nervous system (CNS) is capable of extensive plasticity and regeneration from larval development through adult. In Section I, Chapter 2, I quantified mitotic cells in three auditory nuclei [dorsolateral (DLN), superior olivary (SON), and torus (TS)] over metamorphic development. Mitotic trends do not simply parallel changes in overall brain growth but, appear to correlate with developmental hurdles. In Section II, Chapters 3, 4, and 5, I investigated plasticity in n.VIII-lesioned adult ranids. Immediately following unilateral n.VIII crush, Rana catesbeiana and Xenopus laevis display stereotyped postural vestibular deficits that gradually decrease in magnitude with post-lesion recovery time (Chapter 3). Surgical n.VIII crush causes n.VIII and medullary target tissues to disconnect, and not reinnervate before 1 week recovery. After 2 months post-n.VIII crush, the n.VIII has reinnervated medullary target tissues and neurite densities resemble controls (Chapter 4). After one month post-n.VIII lesion, the deafferented medulla tissue contains many more newly mitotic cells than in nonlesioned tissue. Some of these cells co-localize with neural- or glial- specific phenotypic markers (Chapter 4). Growth associated protein, 43 kDa (GAP-43), implicated in neurite outgrowth and plasticity, is expressed at higher levels following n.VIII lesion than in controls (Chapter 4). Finally, I found mRNA populations that were selectively expressed between n.VIII lesioned and n.VIII non-lesioned tissue (n.VIII and medullary targets) using differential display

polymerase chain reaction (DD-PCR) that have a high similarity to genetic sequences from mammals (Chapter 5).

What are the observed effects following n.VIII lesion?

A unilateral n.VIII lesion affecting both, the auditory [n.VIII(a.)] and vestibular [n.VIII(v.)] branches, causes deafness in the deafferented ear, and balance deficits, respectively. n.VIII(v.) lesioned animals display a number of stereotyped vestibular behaviors that are broadly categorized as "static" or "postural" (if the animal is stationary) or "dynamic" effects (if the animal is in motion).

Static effects can include spontaneous nystagmus, head tilt ("yaw" or "roll"), limb sprawl, and ocular counter roll. Dynamic effects include reduced gain and abnormal timing of vestibulo-ocular and vestibulo-spinal reflexes (Straka H., et al., 2005).

Static Effects

The postural effects seen following unilateral n.VIII deafferentation are generally most pronounced immediately following lesion (or labyrinthectomy), and causes a pronounced asymmetry in neural activity between bilateral vestibular nuclei. Following deafferentation of the ipsilesional vestibular nuclei (iVN), resting activity in the iVN is substantially reduced. iVN activity dependent inhibition of the contralesional vestibular nuclei (cVN) via comissural fibers is consequently reduced and effectively disinhibits the cVN. The cVN becomes "over"responsive because it is continually activated by peripheral endorgans, the iVN commisural projections are no longer

inhibitory, and cVN inhibits the iVN via commisural projections (Smith & Curthoys, 1989; Curthoys & Halmagyi, 1995; Dieringer, 1995; Vibert et al., 1997; Darlington et al., 2002).

The overresponsive cVN causes the animal to incorrectly perceive that his head is rotating towards the nonlesioned (cVN) side. The observed postural effect is due to the animal's attempt to posturally correct for the perceived head rotation, displaying a head tilt toward the lesioned side, as discussed in Chapter 3 (*Rana catesbeiana*, n.VIII lesion; *Xenopus laevis*, n.VIII lesion).

Vestibular compensation

The postural effects following unilateral VN deafferentation either by n.VIII lesion or labrynthectomy is highly variable between species and differs on the type and magnitude of deficit in addition to the timeline and extent of recovery. The partial normalization of static vestibular behavior in the acute post-operative period is described by the process of "vestibular compensation." A vestibular compensatory response occurs to some extent in most species, even in animals that are not capable of n.VIII regeneration following lesion (e.g.. adult mammals) and in animals subjected to hemilabyrinthectomy from which regeneration does not occur.

Vestibular compensation following n. VIII injury occurs due to the plasticity within the central nuclei and is not due to regeneration. Compensation in the absence of regeneration has been evidenced by its fast onset of marked behavioral recovery and can occur on the order of hours to days (much faster than the timeline for regeneration).

Hypotheses on vestibular behavior

I hypothesized that my findings would be similar to previous reports in ranids. I expected that the magnitude of head tilt in both, *Rana catesbeiana* and *Xenopus laevis* would be most pronounced at early post-operative time points, followed by a decrease in head tilt magnitude with post-operative recovery, finally approaching normal after the longest post-operative recovery periods. Furthermore, although this is the first study investigating head tilt after unilateral n.VIII in adult *Xenopus*, I expected that head tilts from *Xenopus* would approximate those of *Rana*. However, I also expected thaat the smaller *Xenopus* would regenerate lesioned n.VIII more quickly than *Rana*, due to the shorter distance necessary to extend neurites , thus expediting *Xenopus'* behavioral normalization.

As discussed in Chapter 3, unilateral n.VIII lesion was performed in two species of adult male anurans, the American bullfrog (*Rana catesbeiana*), and the African clawed frog (*Xenopus laevis*). Both species exhibited the stereotyped posture which included a head tilt toward the lesioned side.

I also analyzed limb sprawl in *Xenopus.* Animals exhibited a postural limb sprawl in which ipsilesional limbs were flexed and contralesional limbs were extended. The magnitude of limb sprawl decreased (similar to the tilt data) with post-operative recovery.

Behavioral recovery is delayed in Xenopus

My hypothesis that the magnitude of head tilt following n.VIII lesion in both *Rana* and *Xenopus* would exhibit a general decrease with post-lesion time point was confirmed. However, I incorrectly theorized that *Xenopus* would recover more quickly due to their smaller size. Not only was the magnitude of tilt greater in *Xenopus* after n.VIII lesion than in *Rana* (Chapter 3), but the general trend of head tilt angle deccreased more quickly in *Rana.* Both head tilt and limb sprawl slowly approach patterns seen in nonsurgical and sham animals, although full normalization was not seen in our longest survival groups, and may require longer post-operative survival times after n.VIII lesion to see full behavioral recovery.

BrdU injection does not affect head tilt

A subset of *Xenopus* were injected with the thymidine analog, 5-bromo -2'-deoxyuridine (BrdU) at the time of surgery (n.VIII lesion or sham) for "pulse/chase" labeling of mitotic cells (Chapter 4). I was concerned whether BrdU treatment affected the behavioral head tilt recovery in *Xenopus* as there are conflicting reportes regarding BrdU's toxicity.

I theorized that BrdU treatment would not have a significant effect on head tilt behavior. Most toxic effects are attributed to high concentrations of BrdU, and for rapidly dividing cell populations (e.g. fetal tissue). *Xenopus* were injected with a medium-high dose either once, or twice (24 hours apart). I chose to inject BrdU as a bolus, intraperitoneally (i.p.), instead of using a chronic BrdU exposure protocol (e.g. soaking, or BrdU in drinking water). The i.p. injection method offers dosage control,

especially in comparison to studies in which BrdU is added to drinking water. Furthermore, BrdU is only transiently available for DNA incorporation following injection, and is likely to be even more transient in frogs, due to the small size of the BrdU molecule, and the ability of frogs to excrete many substances through their skin. Finally, since BrdU is only incorporated into the DNA of actively cycling cells (not RNA or protein), and since the majority of adult cell populations quiescent, I do not expect to see an effect of BrdU on head tilts.

Statistical analysis was performed on mean tilts versus recovery time point (bins) between BrdU treated versus untreated animals indicated there was no significant effect of BrdU treatment on head tilt. These findings confirmed my theory that BrdU injection does not affect *Xenopus* head tilts. However, the longest post-operative recovery for a BrdU-treated animal was one month. As a result, statistical comparisons were restricted to data between one day through one month recovery. It is possible that BrdU treatment could show a statistically significant effect at later post-operative recovery times than I investigated here since there is more variability in measured tilt angles (n.VIII lesion condition) at early time points than after longer survival. It would be interesting to further investigate head tilt trends between BrdU treated and untreated groups at longer post-operative recovery times in a future experiment.

Immediately following n.VIII lesion, *Xenopus* consistently tilt toward the lesioned side and generally exhibit a decreasing trend in tilt magnitude with post-operative survival. There is more variability in measured tilts at shorter post-operative recovery time points than those taken at later recovery periods. This variance may be a factor in the nonsignificant statistical result. It would be of extreme interest to investigate the

effect of BrdU treatment on head tilt recovery in animals allowed to recover for longer post-operative times than I investigated here.

Comparisons between frog species

Comparisons were difficult to make between *Rana catesbeiana* and *Xenopus laevis.* *Xenopus* remain aquatic post-metamorphosis, unlike *Rana* that are amphibious as adults. It was necessary to photograph each species in seperate environments because *Xenopus* exhbited no measurable head tilt when photographed terrestrially, even at early post-n.VIII lesion survival times (when the greatest head tilt magnitudes should be seen).

Contribution of buoyancy to behavioral tilt

Xenopus laevis are air breathing frogs that remain aquatic post-metamorphosis, unlike *Rana catesbeiana* that are amphibious as adults. Each frog was photographed in its respective environment (e.g. *Xenopus*, in water; *Rana,* terrestrially). It was difficult to make comparisons between *Rana* and *Xenopus* under these conditions since the frogs are so different.

The head tilt angle measured for *Rana* includes the rotation of the head-neck joint with minimal contribution of body roll. *Xenopus*, however, when photographed underwater display head tilt angles which include the head-neck joint plus a major contribution of the body roll. Underwater, the neutrally buoyant frog is required to exert less force to overcome gravity (pushing downward) than *Rana*. The end result is that less

effort is required underwater to compensate for the perceived vestibular effect of n.VIII lesion and rotate the body axis. As a result, *Xenopus* generally exhibited greater magnitude head tilts over *Rana.*

Contribution of anatomy to behavioral tilt

The effect of body roll in *Xenopus* may be the primary contributor to the measured head tilt angle, while in *Rana*, rotation of the head-neck joint is likely the major contribuutor to measured head tilt. During pilot studies both species were photographed terrestrially. *Rana* exhibited head tilts similar to data reported here, but *Xenopus* displayed no measureable head tilt. There are two likely contributing factors for this discrepancy. First, *Xenopus* have extremely limited mobility in their head-neck joint compared to *Rana*. Second, the ventral postural musculature in *Xenopus* is so weak, that the animal lies flat and cannot rise up off its breastplate. The postural musculature in *Rana* is so highly developed, not only does the animal regularly sit with the breastplate up off the ground- but will use ventral musculature to absorb the body's impact after jumping.

Recovery following n.VIII lesion: Vestibular compensation

Vestibular compensation referrs to the improvement or recovery of vestibular deficits from unilateral VN deafferentation or labyrinthectomy. Vestibular compensation

not due to regeneration. Instead, recovery is due to plasticity within central nuclei and often occurs much faster than regeneration.

Propioceptive inputs

Although Xenopus were photographed in their native (aquatic) habitat for all post-operative timepoints, for the first 7-15 days following surgery, they were housed in a terrestrial environment to limit the probability of drowning. Vestibular compensation is affected by substitution from other sensory systems (Black, 2001). The change from a terrestrial housing type of environment to an aquatic one immediately changes visual, auditory, vestibular, and propioceptive inputs. Furthermore, not only is there a significant change in housing condidtions, but introducing the animal to an aquatic environment effectively abates postural propioceptive input. Vestibular compensation is thought to be more heavily affected by changes within the brachial propio-spinal inputs and less affected by changes within the brainstem nuclei (Straka et al., 1993; Kunkel & Dieringer, 1994; Straka & Dieringer, 1995; Straka 2005). The change from a terrestrial to aquatic environment may at least partially explain the slower behavioral recovery trend in *Xenopus* versus *Rana* who have consistent propioceptive inputs throughout the experiment.

Molecular factors affecting recovery

I investigated gene expression patterns in the attempt to discover gene products expressed during regeneration and behavioral recovery of the lesioned n.VIII. The experimental approach employed the use of technique of differential display (DD-PCR) to discover the mRNA expression with the aim of identifying genes in n.VIII after various recovery periods (Chapter 5).

Though the function of cDNAs discovered by this study remains unknown, this research has allowed us to examine genetic factors which are expressed during CNS regeneration in an adult model in the absence of pharmacological intervention. Further, the high degree of homology seen in the protein coding region between BR1.

Various molecular factors have been implicated in the vestibular compensatory response and/or regeneration. For example, cFos, BDNF, NT-3 and NOS are activated immediately following n.VIII lesion or labyrinthectomy (Paterson et al., 2000; Smith et al., 2001; Zheng et al., 2001; Liu et al., 2003; Kitahara et al., 1999a ; Smith et al.,1998; Li et al., 2001; Bolger et al.,1999; Maingay et al., 2000). Many of the immediate early genes that are activated post-lesion (e.g. cFOS) are transiently expressed (hours) and serve to activate downstream transcription and second messenger-pathways. Neurotrophic factors, such as NT-3 and BDNF have been implicated in the vestibular compensatory response (Khetarpal, 1998 Gacek 1998; Maingay 2000) and may increase numbers of neurons in deafferented tissues.

Lesion-induced cell proliferation

In Chapter 4, I have shown that new cells are present in n.VIII medullary targets in all surgical groups (controls and n.VIII-lesion) for recovery periods ranging between two days and one month. These findings are consistent with other studies investigating mitotic events in nonsurgical adult brain (in *Rana*, Simmons, et al., 2008). In control animals (nonsurgical and sham) there are significantly more new cells after two days post BrdU injection, than after one week and one month. The decreased numbers of cells at later recovery times could be due to labeled cells migrating away from the medullary regions of interest, they may undergo apoptotic or necrotic cell death, be phagocytized by immune response cells, or may be rapidly proliferating cells. Since BrdU treatment was given in a bolus rather than chronically, mitotic events which occur subsequently to BrdU clearance will dilute the BrdU label with each division.

Gliogenesis

Rapid proliferation of labeled cells is not likely the major factor contributing to the decreased numbers of labeled cells seen at later recovery times in the control animals. If cells were rapidly proliferating, I would expect to see an increase cell numbers between two days and one week post injection, and that these cells would be less strongly labeled. Instead, there is a significant decrease in numbers of cells after one week and one month (Chapter 4). Cells found in the brain parenchyma at the two day time point were likely born *in situ.* These cells are likely glia.

Neurogenesis

One month after n.VIII lesion, there are significantly more newly born cells in medullary targets (ipsilateral and contralateral to the lesion) than in control tissue. However, at one week post injection, there are significantly fewer cells in lesioned animals and counts are indistinguishable from controls (Chapter 4). The increased cell counts in one month medulla versus one week could be due to rapid proliferation of BrdU labeled cells. However the increased numbers of cells would require cells to divide on average three times. If this did occur, the BrdU label intensity would be significantly reduced and I would expect to observe cells undergoing division within tissue sections (Chapman et al.., 2006). The intensity of BrdU label did appear slightly lighter in some animals than in others but did not correlate with recovery time. Also, since these studies employed general immunohistochemical techniques using fluorescent-conjugated secondary antibodies for a qualitative determination of cell labeling (positive or negative), a discussion on fluorescence intensity as it relates to BrdU concentration within cellular DNA is not appropriate here.

I did not regularly observe mitotic cells in adult *Xenopus* n.VIII medulla for either, n.VIII lesioned or control tissue at any time point investigated. BrdU positive mitotic cells, if present, are easily discerned in tissue sections. As shown in Chapter 2, the DLN and SON in developing *Rana catesbeiana* regularly exhibited mitotic cells during metamorphic climax.

The BrdU labeled cells present in the *Xenopus* medulla one month post-operatively, underwent at least one mitotic event within the relatively short time period free BrdU was available, one month prior (the first BrdU injection was given

immediately following n.VIII crush lesion; the second BrdU pulse was given 24 hours later). Since there is a significant increase in the number of BrdU labeled cells in the medulla after one month post-n.VIII lesion over one week post-operatively, mitotic cells are not readily seen in situ for either time point, and BrdU treatment is "pulsed" rather than chronic, it is reasonable to theorize three things. First, these cells underwent mitosis during the relatively short period that free BrdU was available for incorporation into DNA. Second, mitosis occurred at a distant site and then cells migrated to the auditory and vestibular medulla. Finally, these cells may be new neurons.

In Chapter 4, I show a cell within the vestibular nuclei one month post-deafferentation is double labeled with BrdU/TOAD-64. Also, brain derived neurotrophic factor (BDNF) has been implicated in vestibular compensation and is known to recruit new neurons.

Developmental plasticity in the metamorphosing bullfrog

This set of experiments uses techniques of BrdU immunohistochemistry to test the hypothesis that cell proliferation in three central auditory nuclei persists over the entire course of larval development. Results show that the bullfrog's brain exhibits dramatic growth in overall size and volume from hatchling through postmetamorphic developmental stages. In particular, the DLN, SON, and TS all show an increase in the total number of cells across larval stages, as expected. Within each nucleus, however, the total number of cells per tissue section (total cell count, T) varied across developmental stages. This is likely due to variability in cell packing densities between stage groups.

Mitotic indices, the ratio of newly proliferated cells to T, do not simply parallel changes in T, as has been reported in species of fish that continuously add new cells through life as brain size increases (Raymond and Easter, 1983; Nguyen et al., 1999; Zupanc, 2001).

Cell Proliferation Peaks in Metamorphic Climax

During larval development, numbers of mitotic cells in all three auditory nuclei peak during metamorphic climax. The major effector of metamorphic change, thyroid hormone, is likely to drive the increase in numbers of mitotic cells.

Cell Proliferation is reduced in the deaf period

and in the medullary DLN and SON, MI were lowest in the deaf and postmetamorphic froglet stage groups. The MI in the DLN increased slightly between hatchling through immediately before the deaf period, whereas in the SON, although there was a similar increase in MI between hatchlings and early larval periods, MI decreased in late larval animals. The lowest MI in the TS was seen in hatchlings but remained at low levels until the deaf period where MI increased dramatically, peaking in climax, decreasing slightly in postmetamorphic froglets approximating MI in deaf animals. These differences in the pattern of proliferation in the TS on the one hand and in the DMN and SON on the other suggest that the mechanisms underlying cell proliferation differ in these different nuclei in the auditory pathway.

Plasticity in adulthood: Regeneration

This study investigated behavioral effects following unilateral nVIII lesion, and quantified trends in head tilt angles over post operative survival in two anurans, the semi-terrestrial American bullfrog, *Rana catesbeiana* and the aquatic African clawed frog, *Xenopus laevis*. I hypothesized that the vestibular effects would offer a behavioral measure of recovery to correlate with our anatomical data that would not require invasive measures such as electrophysiology or surgery to visualize the original lesion site.

The behavioral deficits seen immediately following unilateral n.VIII would allow a behavioral measurement of n.VIII functional regeneration. In both species, I quantified behavioral trends in head tilt angles over post operative survival and postural deficits, using limb sprawl angles, were quantified in *Xenopus laevis.*

Regeneration of lesioned n.VIII ?

In order to investigate the time course of n.VIII regeneration after lesion I used fluorescent lipophilic tracers to determine whether connectivity was reestablished between n.VIII and medullary targets for each of the post-operative time points studied here.

I have shown that n.VIII crush-lesion effectively disrupts n.VIII-medulla connectivity in *Xenopus laevis* adults until one week post-operatively, but is once again restored after two months (Chapter 4). These anatomical data are discordant with the behavioral findings showing normal posture is not reestablished in n.VIII lesioned

Xenopus after two months and head tilt angle measures between 15-20 degrees. This was an unexpected finding. I chose my post-n.VIII lesion recovery time points based on previous literature in *Rana*. Although there were no studies which investigated n.VIII regeneration in adult *Xenopus laevis*, studies in *Rana* indicated n.VIII was functionally regenerated post- crush lesion during this time (Zakon 2001). Since the distance the n.VIII must regenerate is substantially greater in *Rana sp.* than in *Xenopus,* due to the frog's larger size, I felt that it would be appropriate to use similar post-operative recovery times that were used in the *Rana sp*. studies. Furthermore, studies investigating regeneration following n.II (optic cranial nerve) crush lesion (at the orbit) in juvenile *Xenopus laevis* noted regenerating fibers reach the optic tectum (OT) in as early as 15 days (Gervasi 2003), much earlier than my recovery time.

The slope of the line indicating behavioral recovery (reduction in head tilt angle) following n.VIII lesion was substantially steeper in *Rana* than in *Xenopus* (Chapter 3). The delayed behavioral recovery in *Xenopus* may be due to a generalized delay in healing following neural injury in *Xenopus* and may not be limited to the n.VIII. Or, this finding may be due to one of the many dissimilarities between these anuran species requiring different experimental treatments.

Formation of vestibulo-topic maps

The discrepancy between findings of anatomical n.VIII regeneration (Chapter 4) and lack of behavioral recovery (Chapter 3) parallels other studies investigating neural regeneration. In frogs, lesion to the n.VIII (in *Rana catesbeiana*) leads to recovery of

SON auditory function after 2 months post-operatively, although electrophysiological studies indicate that many tuning curves are broad or W shaped and do not become narrowly tuned until 2 weeks later. However, some W shaped tuning curves can still be found even at this time point but are never found in nonlesioned animals. It is possible that the *Xenopus laevis* in my studies did regenerate the crush lesioned n.VIII into medullary targets but that appropriate branch pruning and fine-tuning of vestibulo-topic maps had not yet occurred, leading to the partial, but delayed behavioral recovery.

Conclusions

This study has demonstrated plasticity in anurans from larval development to adulthood. In larval Rana, I have quantified mitotic cells over metamorphic development in central auditory nuclei. I have also shown that a subset of these cell become neurons. I have also shown that new neurons are generated in adults (after n.VIII lesion) and preferentially reside in lesioned tissue (control animals have few cells). Also, GAP-43 is expressed at higher levels following n.VIII and levels stay high even after one month. These studies have also shown n.VIII surgical crush lesion interrupts n.VIII fiber projection to target sites in the medulla immediately following lesion, and restoration of fiber connectivity is not seen until post-operative survival time points of 2 months.

In contrast to the fiber connectivity results, I did not see full behavioral recovery following n.VIII-lesion, especially in *Xenopus*. It is possible that the aquatic environment did not allow enough propioceptive input for tilt to appropriately compensate. Taken together, these findings indicate anurans are highly plastic in

development and as adults demonstrate regenerative ability, including, neuron replacement, fiber extension post injury, and BR1 found in this study, homologous in humans, argues for anurans as a model for investigation of CNS regeneration.

FIGURES

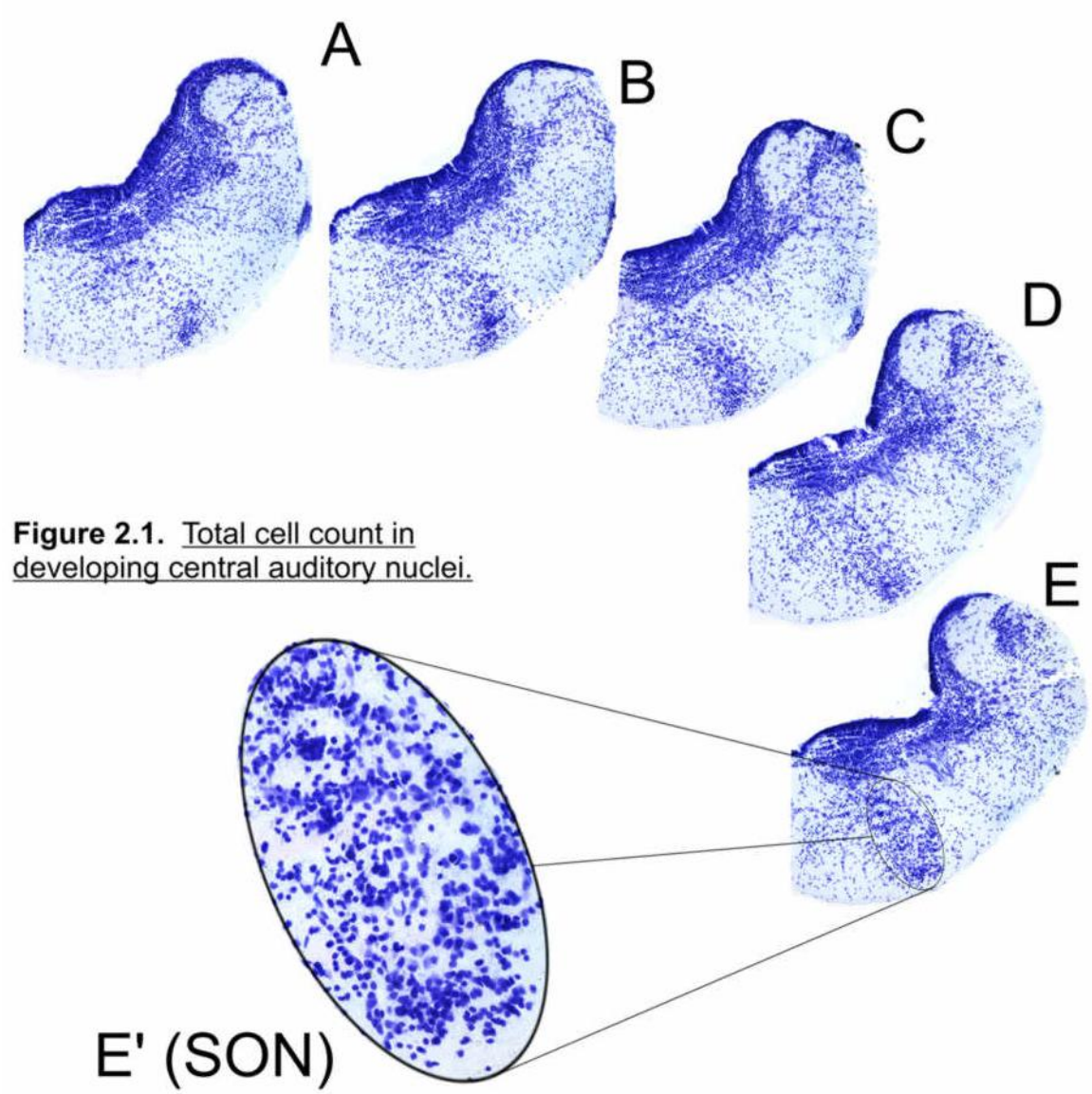

Figure 2.1. Total cell count in developing central auditory nuclei.

Figure 2.1 Shows every second 50µm thick coronal brain slice (rostral to caudal) through a stage 36/37 Rana catesbeiana medulla. Brain slices have been stained using cresyl violet acetate showing cell nuclei (in blue) at 10x (A-L) and 40x (E', F') magnification. The relative volume and cell number in the DLN and SON vary from minimum to maximum to minimum with advancement through the brain slices. Cell number and volume occupied by the DLN is at a minimum in Fig 2.1B, reaches a maximum in Fig 2.1(F) [DLN in Fig 2.1(F) is shown under high power magnification in Fig 2.1(F ')] and decreases to minimum volume and cell number in Fig 2.1(L). Cell number and volume occupied by the SON are at a minimum in Fig 2.1(A), and gradually increase in volume and cell count until reaching a maximum in Fig 2.1(E) [(SON in Fig 2.1(E) is shown under high power magnification in Fig 2.1(E')], and decreases to a minimum volume and cell number in Fig 2.1(H), and disappears in Fig 2.1(L).

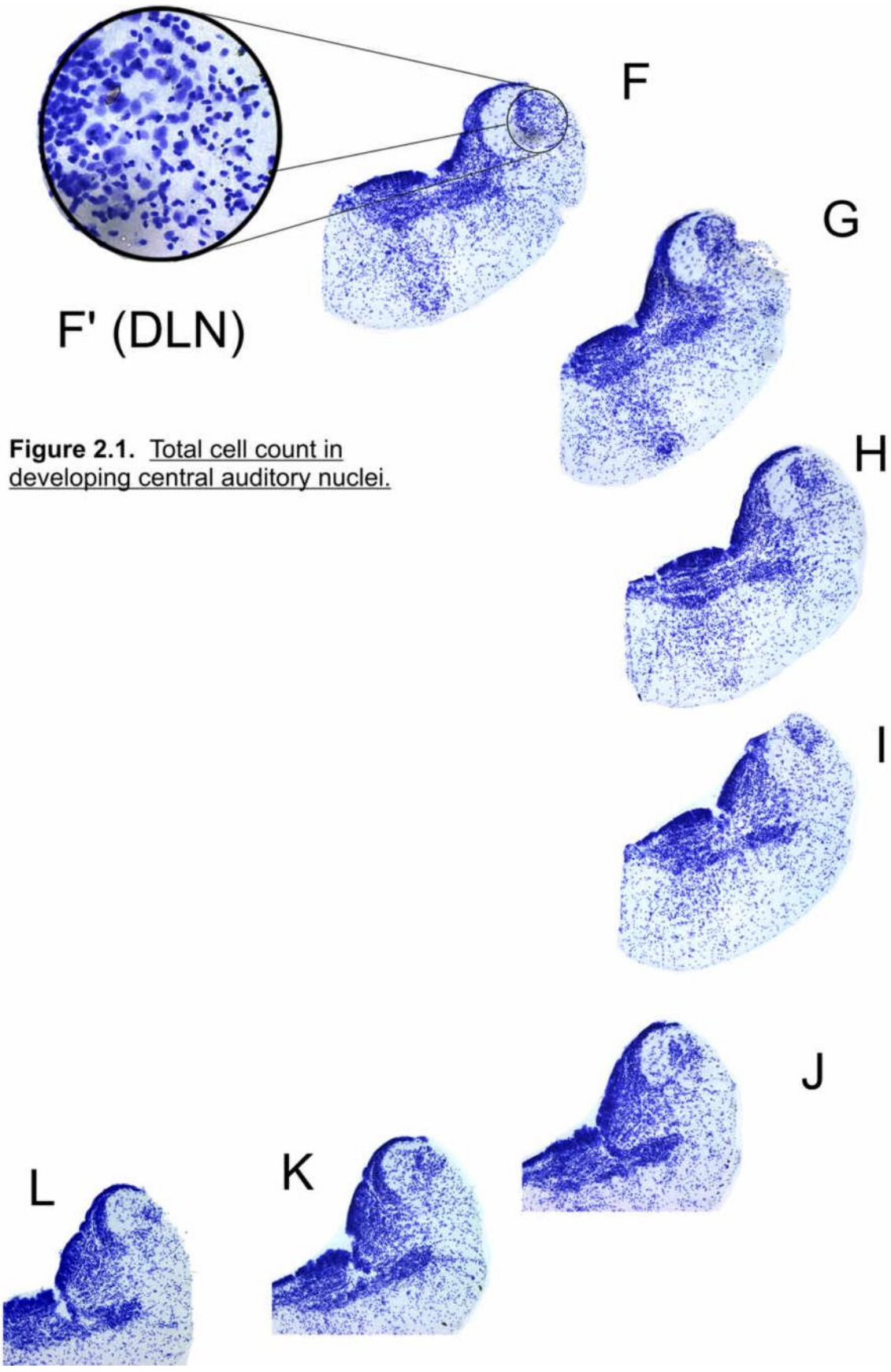

Figure 2.1. Total cell count in developing central auditory nuclei.

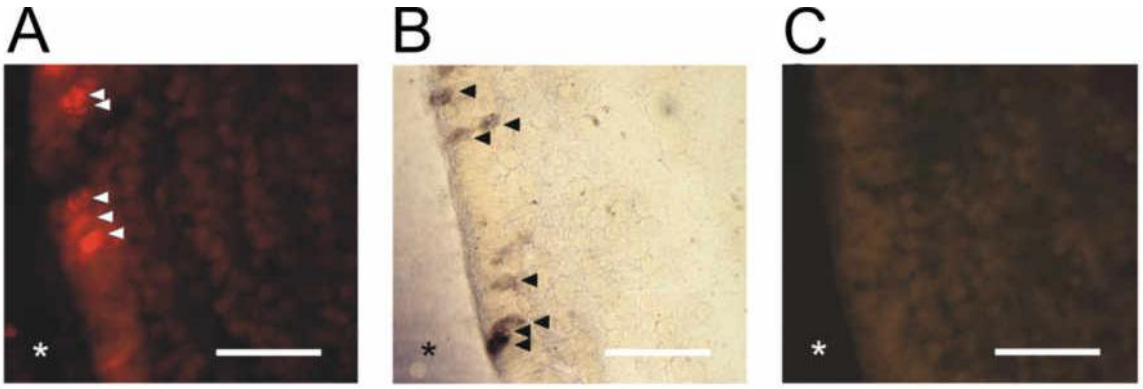

Figure 2.2. Immunohistochemical positive label and negative control.

Figure 2.2. Positive and negative controls: Images taken from three adjacent 50 µm coronal sections (same XY plane) through the tegmental midbrain of a late larval tadpole (stage 31). BrdU-positive cells are located immediately adjacent to the ventricle (asterisk). Positive BrdU-labeled cells are seen as red-orange when the fluorescent-labeled secondary antibody is used [white arrowheads (A)], and as purple-black [black arrowheads (B)] when biotinylated secondary antibodies are used. Panel (C) shows no labeled cells in a fluorescent image of the third section in the series treated exactly as in (A) except the primary antibody was omitted. Scale bar = 50 µm.

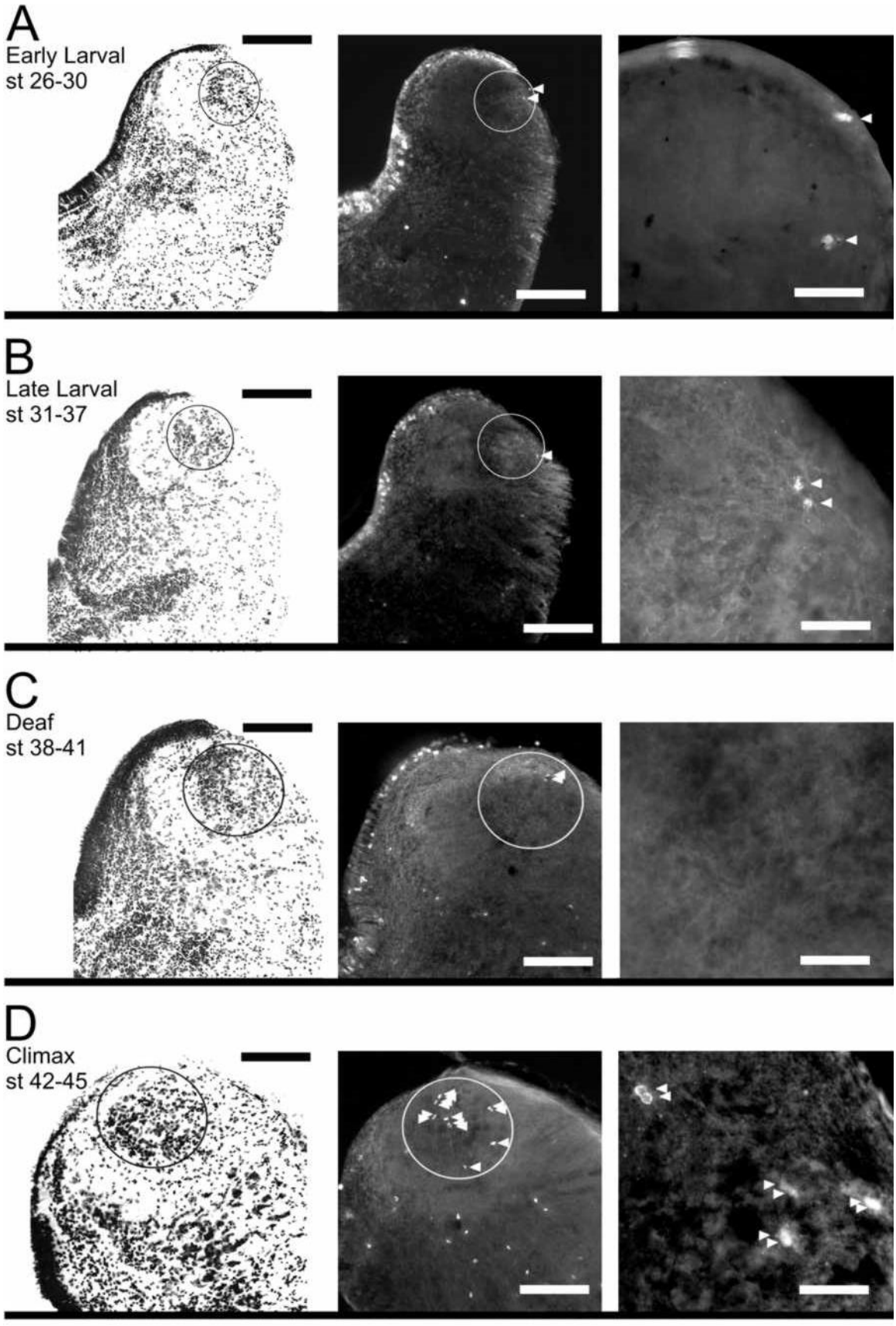
A
Early Larval
st 26-30
B
Late Larval
st 31-37
C
Deaf
st 38-41
D
Climax
st 42-45

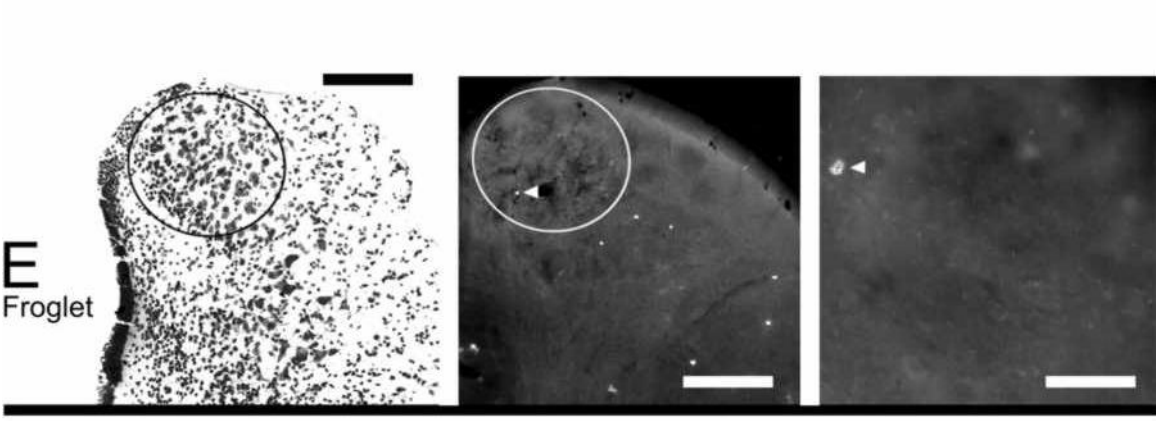

Figure 2.3. BrdU positive cells in the DLN 48 hours after injection.
The left panel shows cresyl violet stained 50 µm representative sections of the dorsal medulla from each stage group to locate the changing DLN boundaries (circled). The center (low power, 10x images) and right panels (high power, 40x images) show grayscale example images of fluorescently labeled BrdU positive cells (shown as white cells, positive cells are indicated by white arrowheads).

(A): Early larval (stages 26-30). The DLN is located dorsal and lateral in the medulla (stage 26, left). Two BrdU positive cells are shown in a stage 28 DLN (center). A high power image from a stage 26 DLN also shows 2 BrdU positive cells (right).

(B): Late larval (stages 31-37). The position of the DLN is slightly more dorsal and medial (stage 37, left). One BrdU positive cell is shown in a stage 31 DLN (center) and 2 BrdU positive cells are shown in a high power image of a stage 35 DLN (right).

(C): Deaf period (stages 38-41). The DLN is located similarly as in late larval animals (stage 40, left). A low power image of a stage 41 DLN shows 2 BrdU positive cells (center), and a high power image of a separate DLN section shows 0 cells positively labeled (right).

(D): Metamorphic climax (stages 42-46). The DLN is located more dorsally and medially (stage 43, left). Thirteen BrdU positive cells are shown in a stage 43 DLN (center). A high power image shows 8 BrdU positive cells (stage 43, right).

(E): Froglets. The DLN is in a more dorsal position typical of adult frogs (left panel). A low (center) and high power (right) shot of a froglet DLN show one BrdU positive cell in each case (arrowheads). Scale bars left, center panels = 200 µm; right panel = 50 µm.

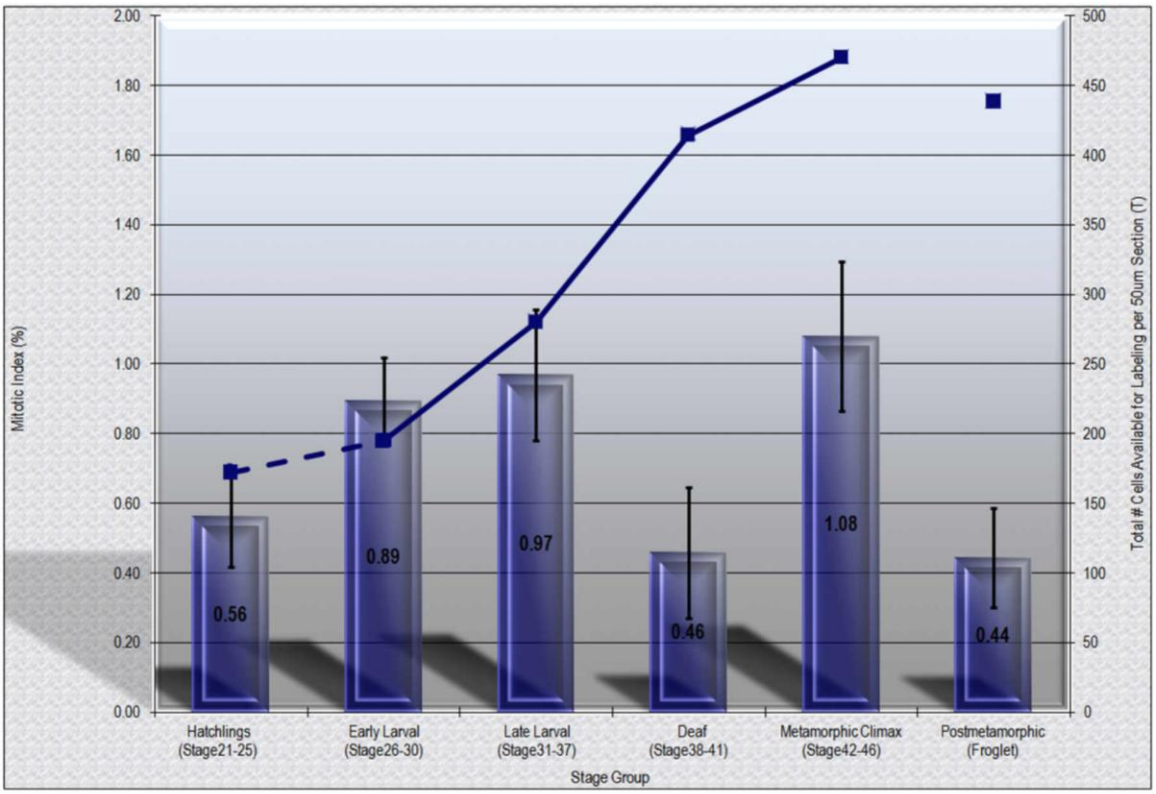

Figure 2.4. Summary of the mean mitotic indices for the DLN across developmental groups 48 hours post-BrdU injection.

Mean M.I. (Y axis, left) and mean cell count (T; Y axis, right) per 50 µm section for the DLN over different stage categories (X axis). Error bars are +/- s.e.m. Data are based on mean counts of BrdU-positive cells from 47, 38, 50, 52, 33, and 22 (total n = 242) sections, consecutively, from hatchlings through froglets. For each DLN section in which BrdU positive cells were counted, T is calculated using the trend line equation (larval animals, n = 7) or is the mean of actual counts (froglets, n = 2).

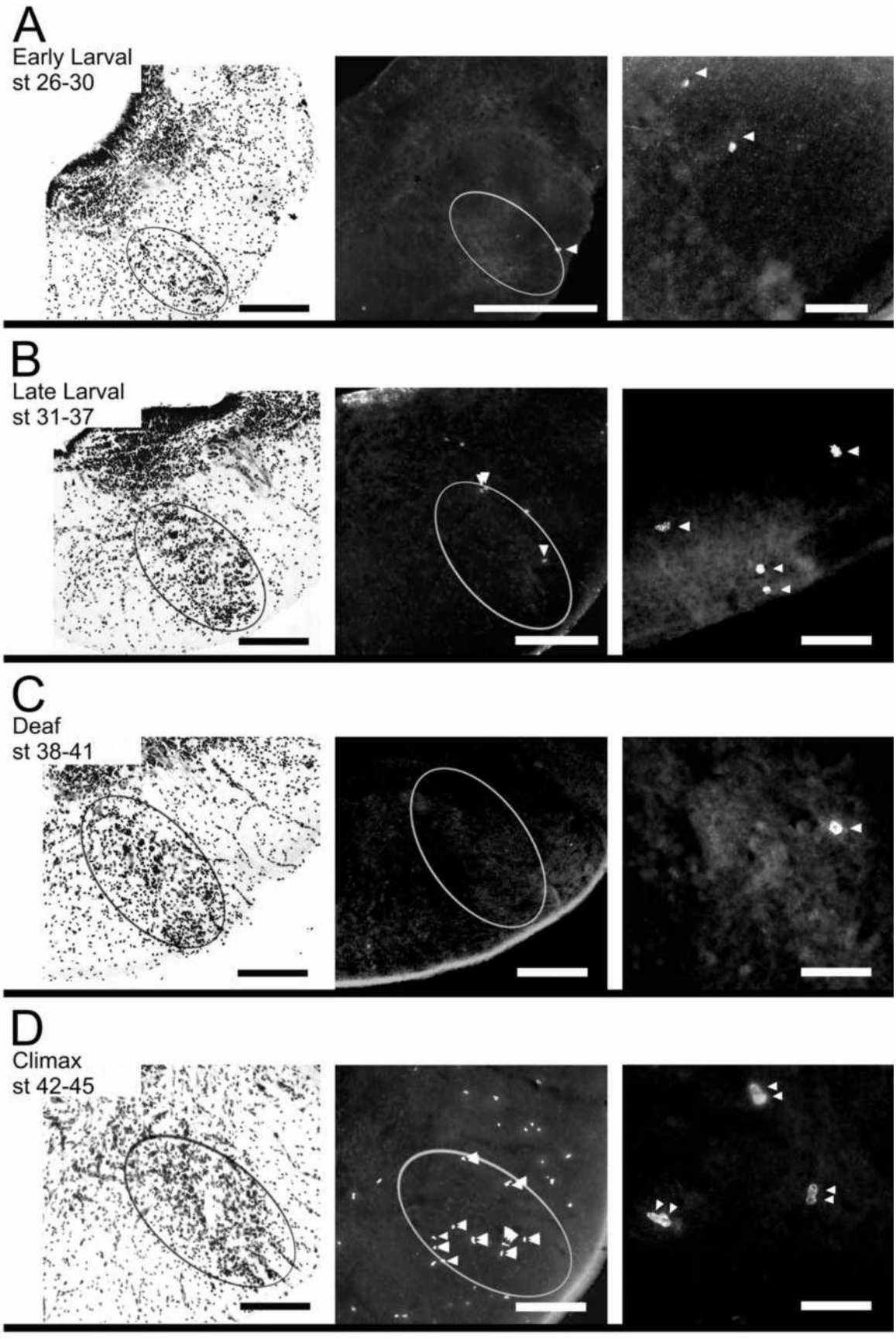
A
Early Larval
st 26-30
B
Late Larval
st 31-37
C
Deaf
st 38-41
D
Climax
st 42-45

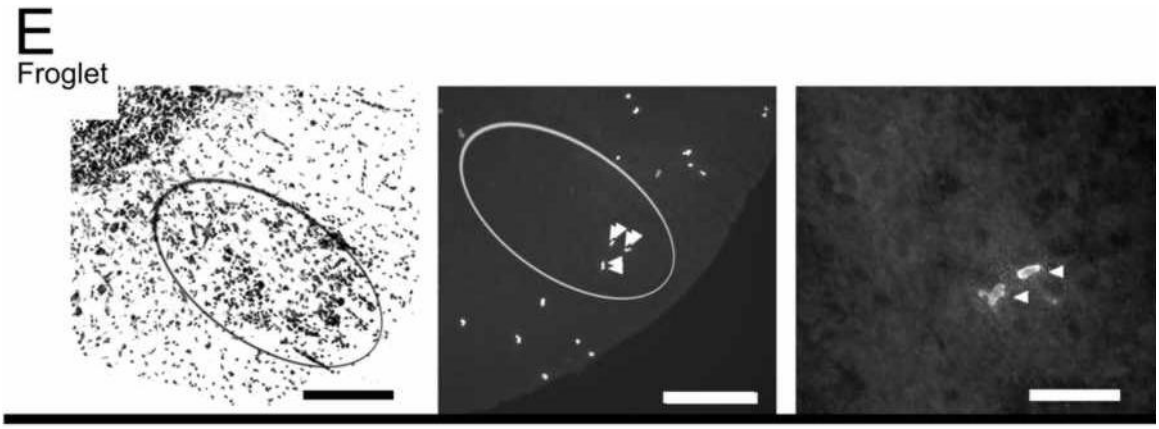

Figure 2.5. BrdU positive cells in the SON 48 hours after injection.
The left panel shows sample images of the cresyl violet stained ventral medulla from each stage group to indicate relative boundaries of the SON (circled). The SON varies little in its position in the ventral medulla over development. The center (low power, 10x images) and right panels (high power, 40x images) show grayscale example images of fluorescently labeled BrdU positive cells (shown in white, positive cells are indicated by arrowheads) from each stage group.

(A) Early larval (stages 26-30). Number of BrdU positive cells is low (1 cell, stage 26, center) and appear on the SON border (stage 26, center) or centrally (2 cells, stage 26, right).

(B): Late larval (stage 31-37). Some labeled cells appear on the border of the SON early in this group (3 cells, stage 31, center) and more ventrally at later stages (4 cells, stage 36, right).

(C): Deaf period (stages 38-41). Representative images showing 0 (stage 41, center) and 1 labeled cell (stage 41, right).

(D): Metamorphic climax (stages 42-46). Numbers of BrdU positive cells increase (19 cells, stage 43, center) and appear mainly as doublets (6 cells, stage 43, right).

(E): Froglets. The number of positive cells declines, while areas adjacent to the SON continue high rates of cell proliferation (center).
Scale bars left, center = 200 μm; right = 50 μm.

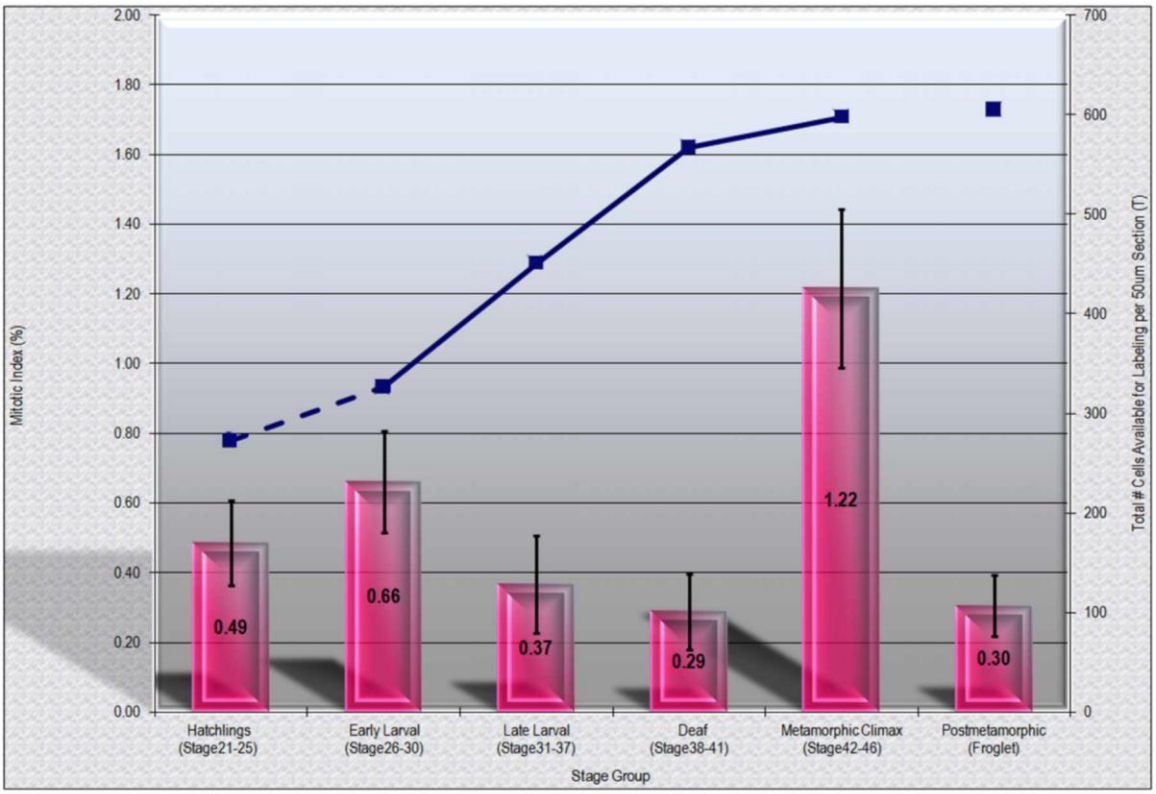

Figure 2.6. Summary of the mean mitotic indices for the SON across developmental groups 48 hours post-BrdU injection.

Mean M.I. (Y axis, left) and mean cell count (T; Y axis, right) per 50 µm section for the SON over different stage categories (X axis). Data are based on mean (+/-s.e.m.) counts of BrdU-positive cells from 53, 16, 26, 40, 23, and 16 sections, consecutively, from hatchlings through froglets (n = 174). Error bars are +/- s.e.m. For each SON section in which BrdU positive cells were counted, T is calculated using the trend line equation (larval animals, n = 8) or is the mean of actual counts (froglets, n = 2).

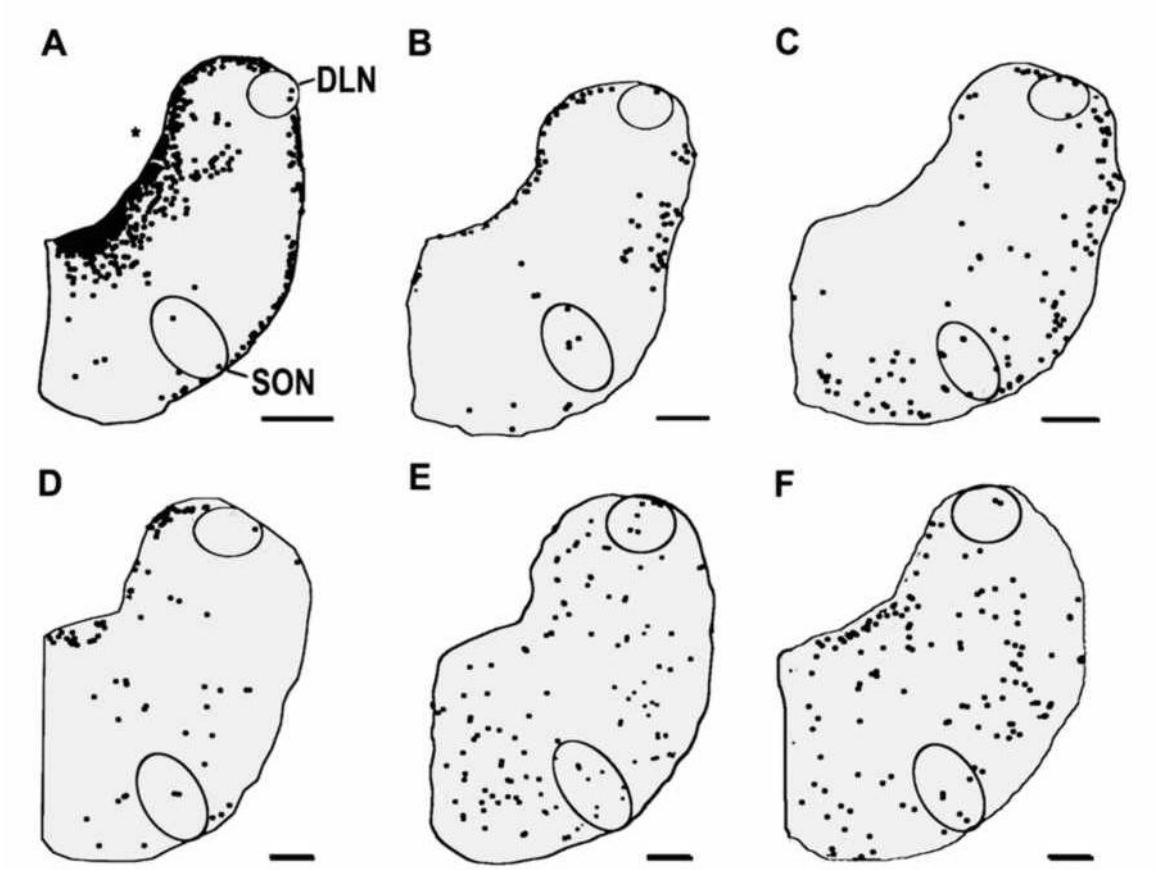

Figure 2.7. Distribution of BrdU positive cells (black dots) in representative sections 48 hours post-injection.
Schematic is based on images of fluorescent label. (A): Early larval (stages 26-30). A stage 26 tadpole shows BrdU positive cells heavily clustered around the ventricle. Two BrdU labeled cells are seen in both the DLN and SON. (B): Late larval (stage 31-37). This sample image from a stage 31 tadpole shows a slight decrease in number of labeled cells in the DLN (1 cell is shown) and increased cell label in the SON (4 cells are shown). (C): Late larval (stage 31-37). A stage 36 tadpole section shows an increase in the number of proliferating cells in the DLN (3 cells are shown) but little change in the SON (4 cells are shown). (D): Deaf period (stages 38-41). Cell proliferation in both the DLN and SON decrease (1 cell in the DLN, 2 cells in the SON) in this stage 41 tadpole example image. (E): Metamorphic climax (stages 42-46). Example stage 43 section shows numbers of BrdU labeled cells are high in both the DLN (6 cells) and SON (9 cells). (F): Froglets. Cell proliferation decreases in both the DLN (2 cells) and SON (5 cells). Scale bar = 200 μm.

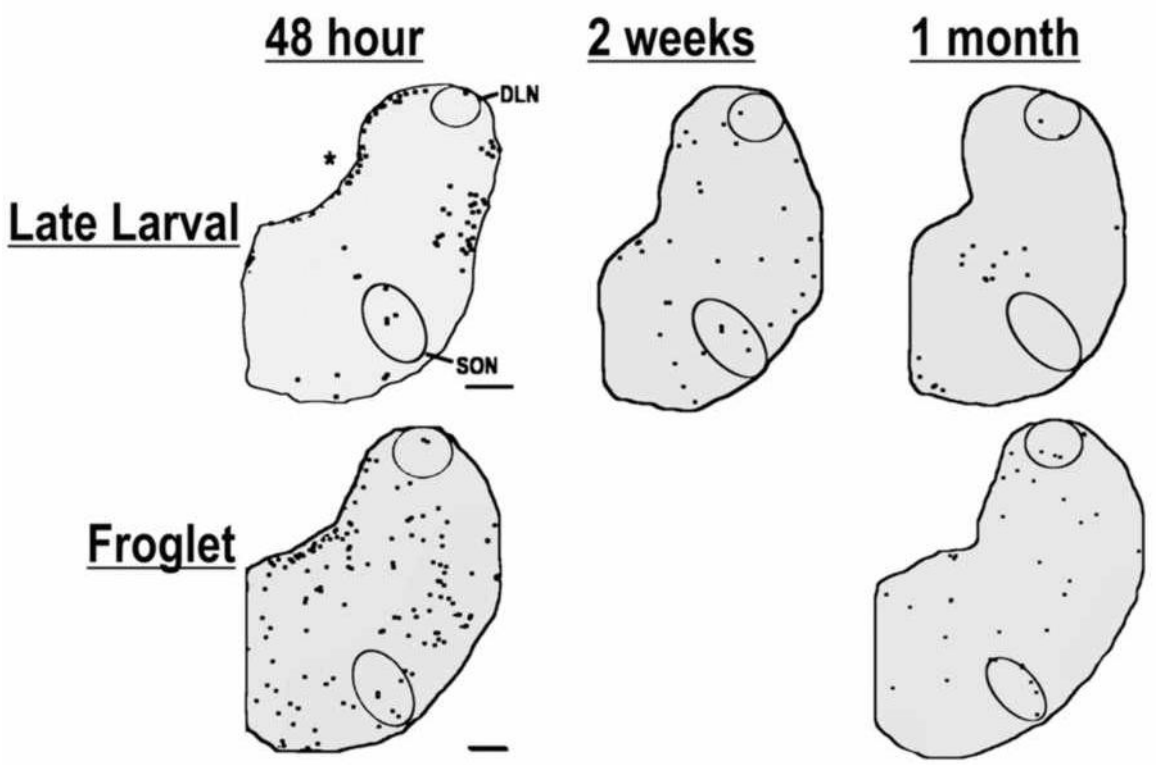

Figure 2.8. Distribution of proliferating cells in late larval and froglet medulla after variable survival points post-BrdU injection.
In representative sections for late larval (top) and froglet (bottom) animals, proliferating cells were found around the ventricle (asterisk). Late Larval (stage 31-37): At stage 31 (top, left), there are labeled cells throughout the medulla including the ventricle, DLN, and SON. After 2 weeks survival, the numbers of labeled cells in the DLN and SON are similar to that seen after 48 hours, but the number of labeled cells around the ventricles decreases (stage 34; top, center). After 1 month of survival (stage 34; top, right), there is an overall decrease in the number of labeled cells including loss of labeled cells in the ventricle and SON. Froglets: At 48 hours post-injection (bottom, left), there are many labeled cells throughout the medulla including the ventricle, DLN, and SON. After 1 month post-injection (bottom, right), the number of labeled cells in the ventricular areas decreases while the numbers in the DLN and SON are similar. Scale bar = 200 μm.

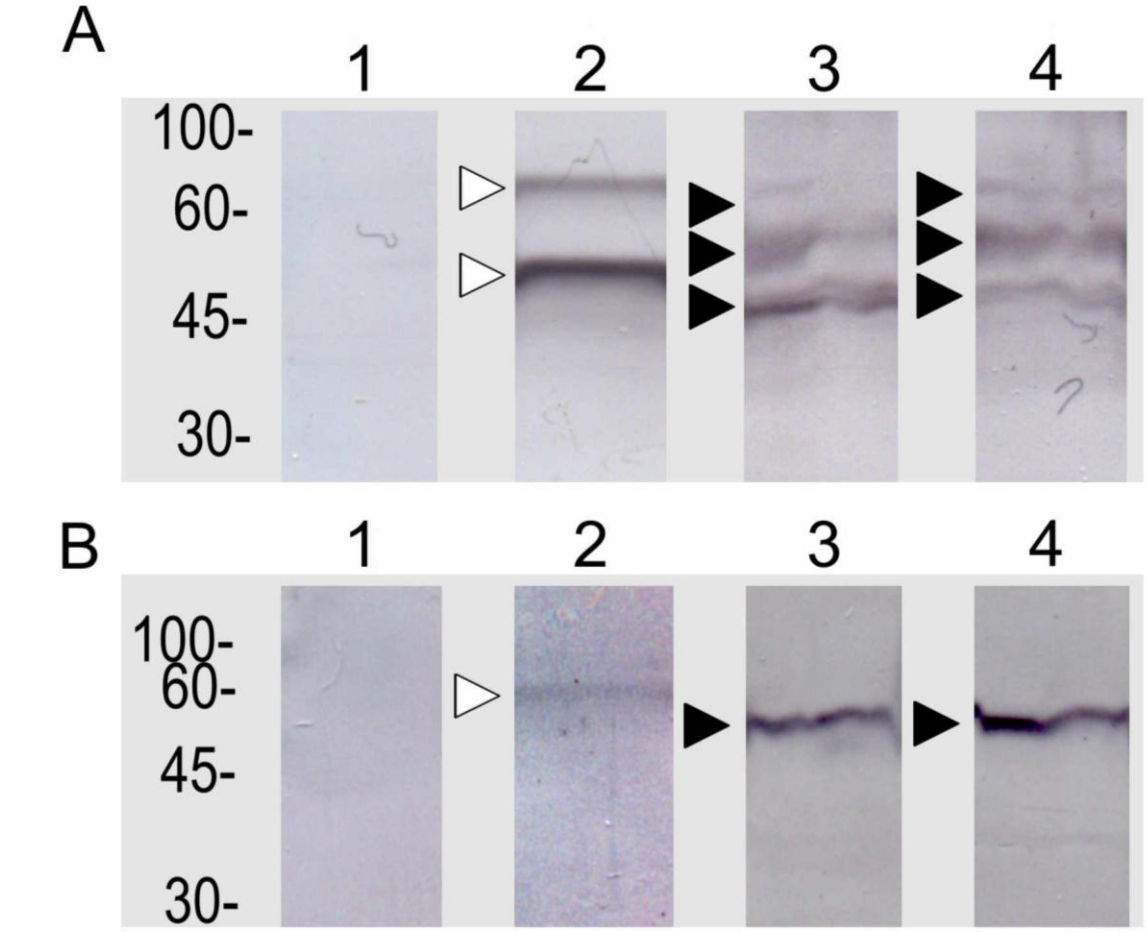

Figure 2.9. Specificity of Monoclonal Antibodies for the Two Proteins, Glial Fibrillary Acidic Protein (GFAP) and Turned On After Division 64kDa (TOAD-64) in larval *Rana catesbeiana*.

Figure 2.9A shows western blot results of GFAP antibody specificity when probing protein from rodent and *Rana catesbeiana* tissues. Lane 1: Contains no protein sample and is a control for nonspecific binding of antibody. There is no DAB signal in this lane, indicating no nonspecific binding. Lane 2: Contains concentrated rodent brain homogenate, to which GFAP is expected to bind. A positive DAB reaction product is seen as two bands (Lane 2: white arrows). Lanes 3 and 4: Contain the *Rana catesbeiana* brain homogenate, and show a positive DAB reaction product shown as two, or three bands (Lanes 3, 4; black arrows). Bands in Lane 2 and the bottom two bands between Lanes 3 and 4 appear similar in pattern, although bands in Lanes 3 and 4 appear slightly lower in molecular weight. Figure 2.9B shows western blot results of TOAD-64 antibody specificity when probing protein from rodent and *Rana catesbeiana* tissues. Lane 1: Contains no protein sample and is a control for nonspecific binding of antibody. There is no DAB signal in this lane, indicating no n onspecific binding. Lane 2: Contains concentrated rodent brain homogenate, to which TOAD-64 is expected to bind. A positive DAB reaction product is seen as one band (Lane 2: white arrow). Lanes 3 and 4: Contains the *Rana catesbeiana* brain homogenate, and shows a positive DAB reaction product shown as one band (Lanes 3, 4; black arrow). Bands in Lane 2 and between Lanes 3 and 4 appear similar in pattern, although bands in Lanes 3 and 4 appear slightly less in molecular weight.

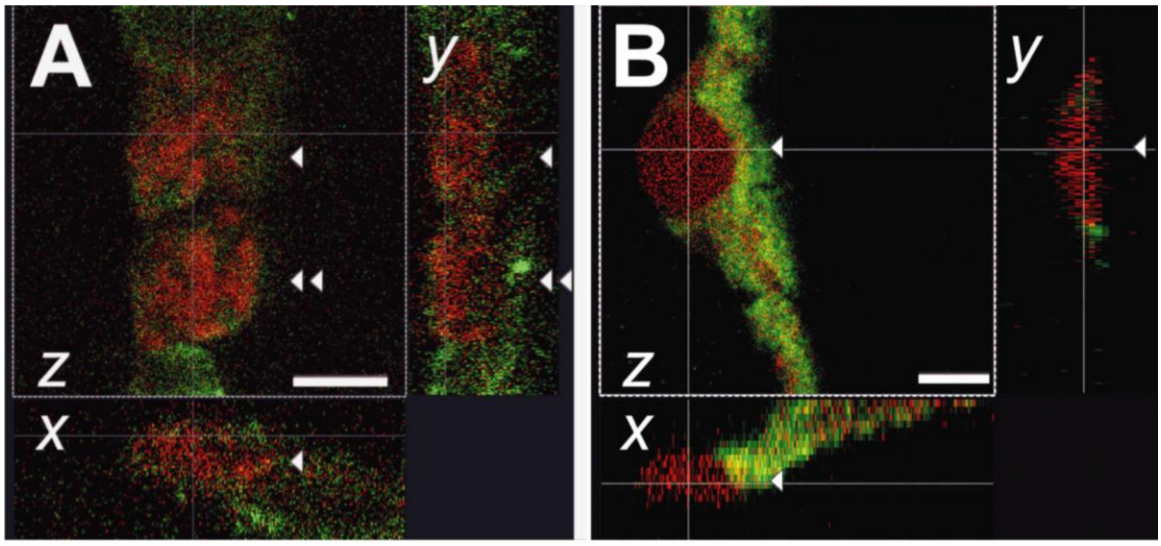

Figure 2.10. BrdU positive cells express glial and neural markers.
(A): BrdU positive cells express glial phenotypic marker, GFAP. An example confocal laser micrograph z stack of the froglet DLN one month post-BrdU injection rotated in orthogonal planes (x, y, z) shows the presence of BrdU/GFAP double labeled cells (BrdU, red; GFAP, green; 2 cells are shown, arrowheads).

(B): BrdU positive cells express neural phenotypic marker, TOAD-64. An example confocal laser micrograph z stack of a stage 36 DLN one month post-BrdU injection rotated in orthogonal planes (x, y, z) shows the presence of a BrdU/TOAD-64 double labeled cell (BrdU, red; TOAD-64, green; 1 cell is shown, arrowhead). Scale bar = 5 μm

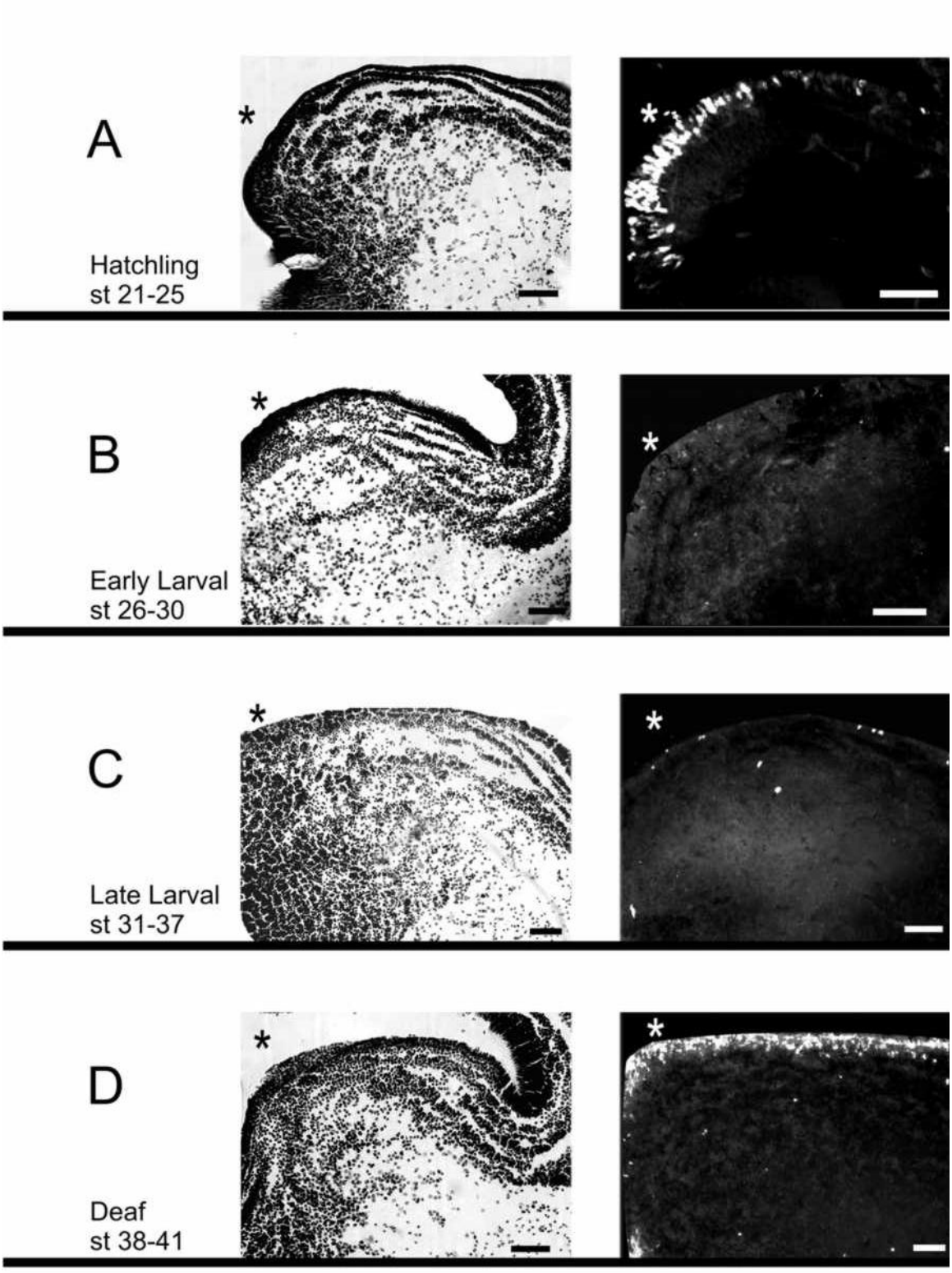
A
Hatchling
st 21-25
B
Early Larval
st 26-30
C
Late Larval
st 31-37
D
Deaf
st 38-41

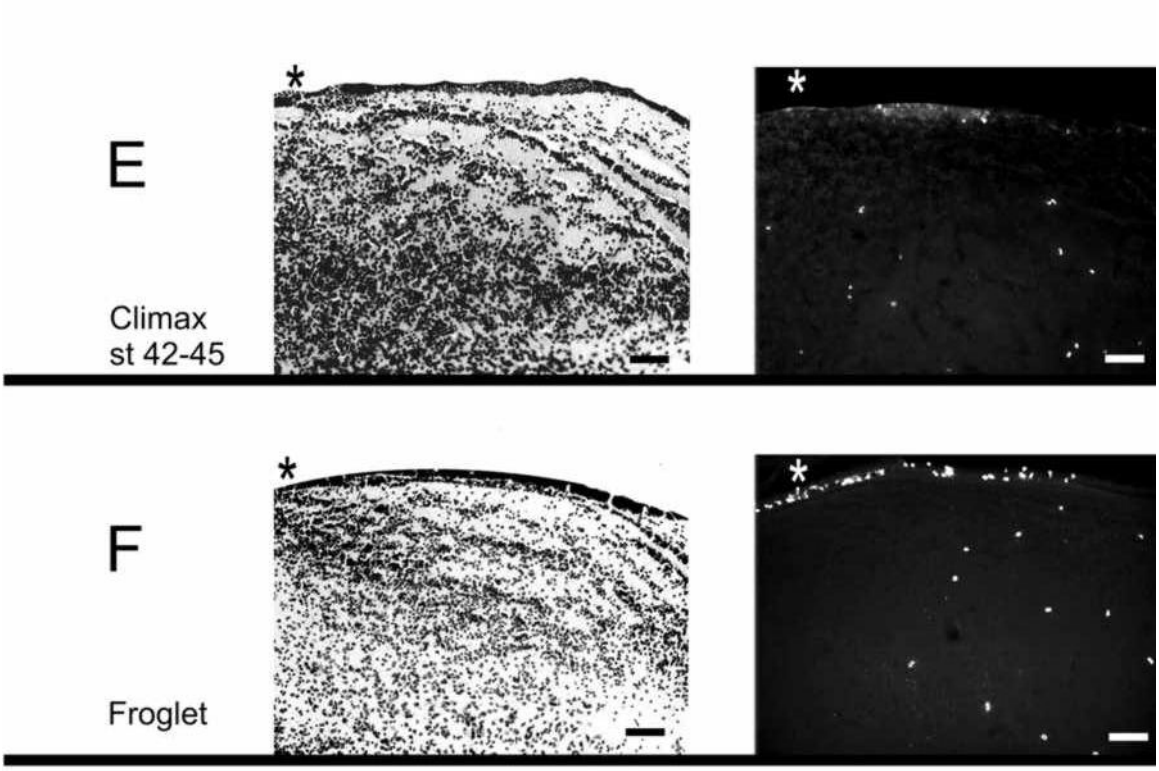

Figure 2.11. BrdU labeled cells in the TS 48 hours post injection.
The middle column shows representative examples of cresyl violet- stained sections (4 and 10X magnification) through the rostral-caudal midpoint of the TS for each of the six developmental groups (labeled in the first column). The top of each section shows the optic ventricle (*). The right panel shows black and white images of fluorescently labeled BrdU-positive cells (white). Cells in the ventricular zone are labeled at all developmental stages, but are relatively more numerous in hatchling, deaf period, and froglet animals. More BrdU-labeled cells are seen in the TS itself of deaf period, metamorphic climax, and froglet animals than in earlier stages. In all images, medial is to the left and dorsal is to the top. Scale bars = 100 μm.

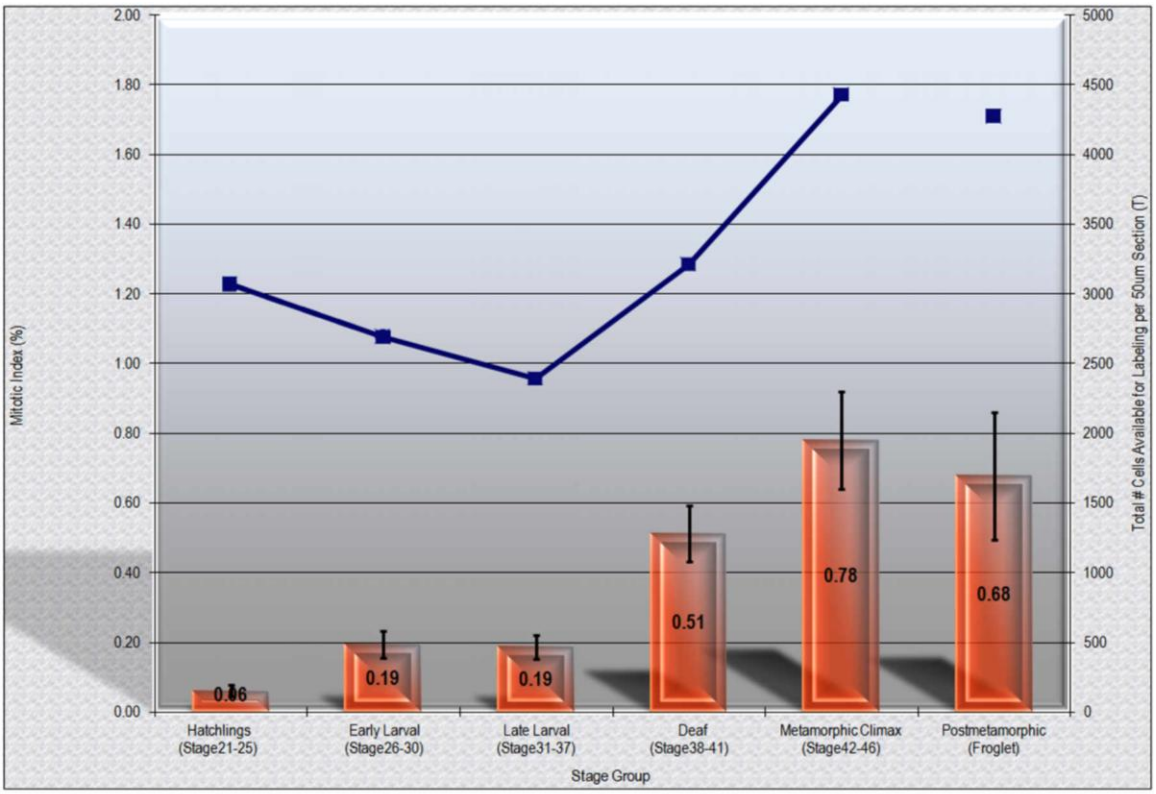

Figure 2.12. Summary of changes in mitotic indices in TS across larval development in *Rana*.

Mean mitotic index (solid bars, y axis, left), normalized over number of BrdU injections, for all animals in each developmental stage group (x axis). Standard deviations of the means are represented by the vertical error bars. Cresyl count per 50 µm section (T, filled circles, y axis, right) for each developmental group as calculated from the regression analysis (see text for details). Mean mitotic index varies significantly across developmental stage groups.

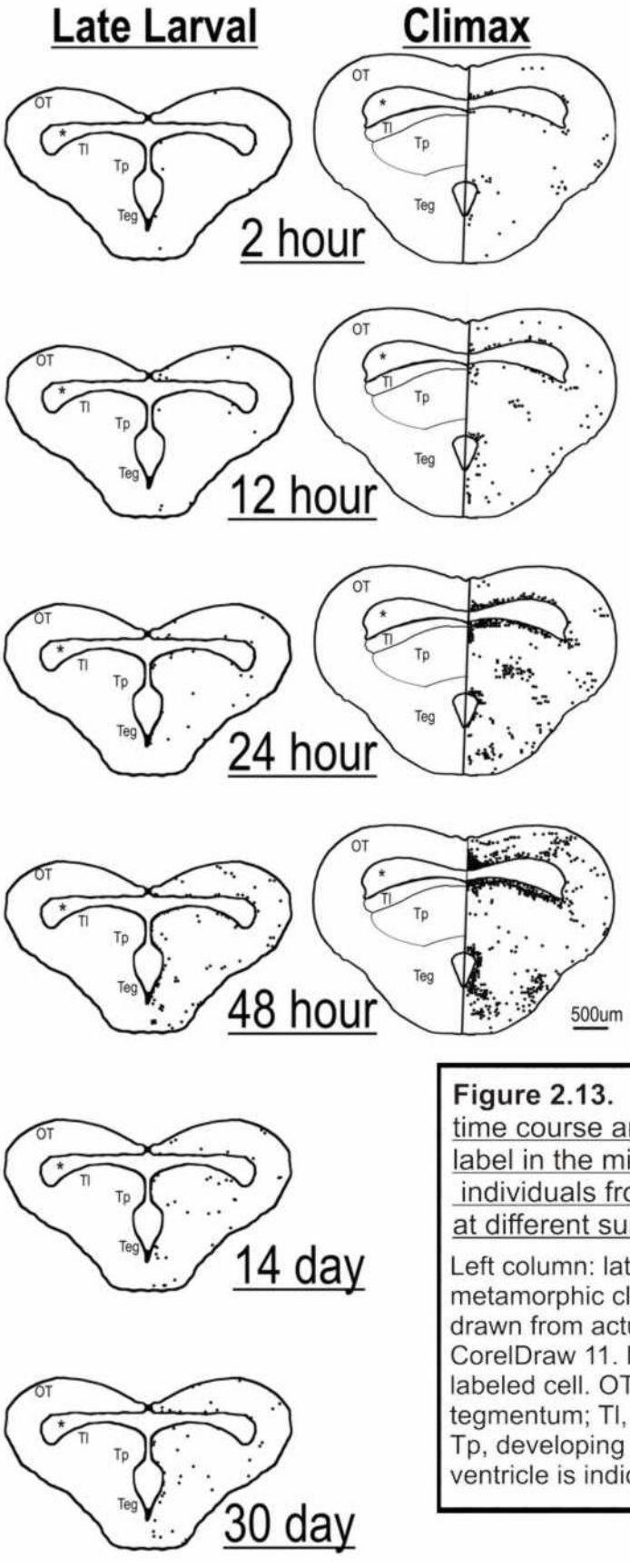

Figure 2.13. Schematics showing the time course and distribution of BrdU label in the midbrain for representative individuals from two groups of animals at different survival times.

Left column: late larval animals; right column: metamorphic climax animals. Schematics are drawn from actual tissue sections using CorelDraw 11. Each dot represents one BrdU labeled cell. OT, optic tectum; Teg, tegmentum; Tl, developing laminar nucleus; Tp, developing principal nucleus. The third ventricle is indicated by the asterisk (*).

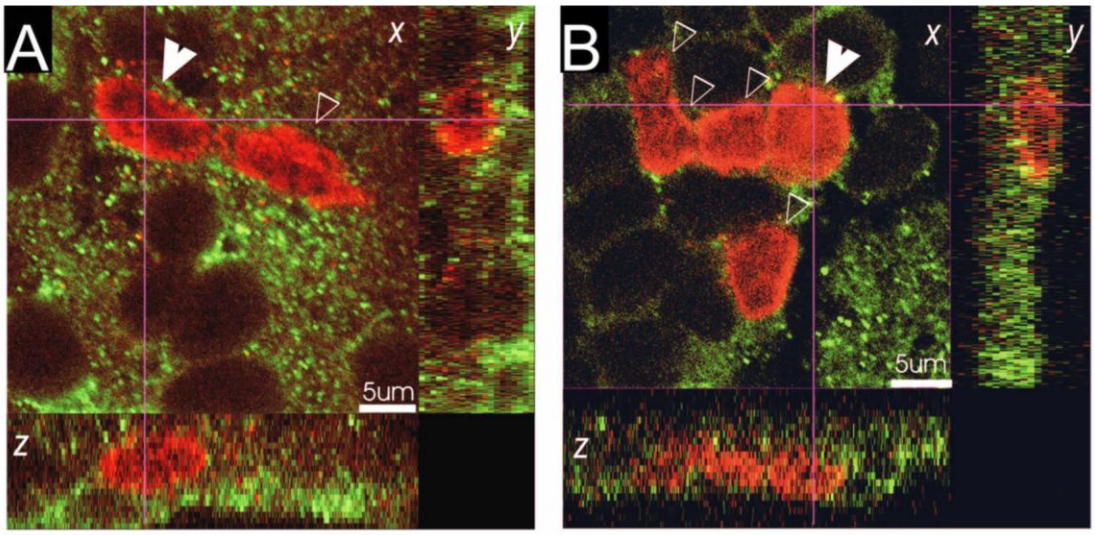

Figure 2.14. Confocal images (100X) of labeled cells in the developing TI of a froglet surviving 30 days after BrdU injection.

(A) Z-stack image of double-labeled BrdU/GFAP cells. BrdU fluoresces red, GFAP fluoresces green. Two cells are shown. Solid arrowhead shows one BrdU/GFAP double-labeled cell (crosshairs) rotated in orthogonal planes (x,y,z). Hollow arrowhead shows a second cell, also double-labeled, but not visible in the y and z planes.

(B) Z-stack image of double labeled BrdU/TOAD cells. BrdU fluoresces red, TOAD-64 fluoresces green. Five cells are shown. One BrdU-positive cell (crosshairs) double-labeled with TOAD-64 (solid arrowhead) is shown rotated in orthogonal planes (x,y,z). Four cells (hollow arrowheads) are also double-labeled but are not shown rotated in all three planes, and the TOAD-64 label is not obvious in this particular plane of focus. Scale bars = 5 μm.

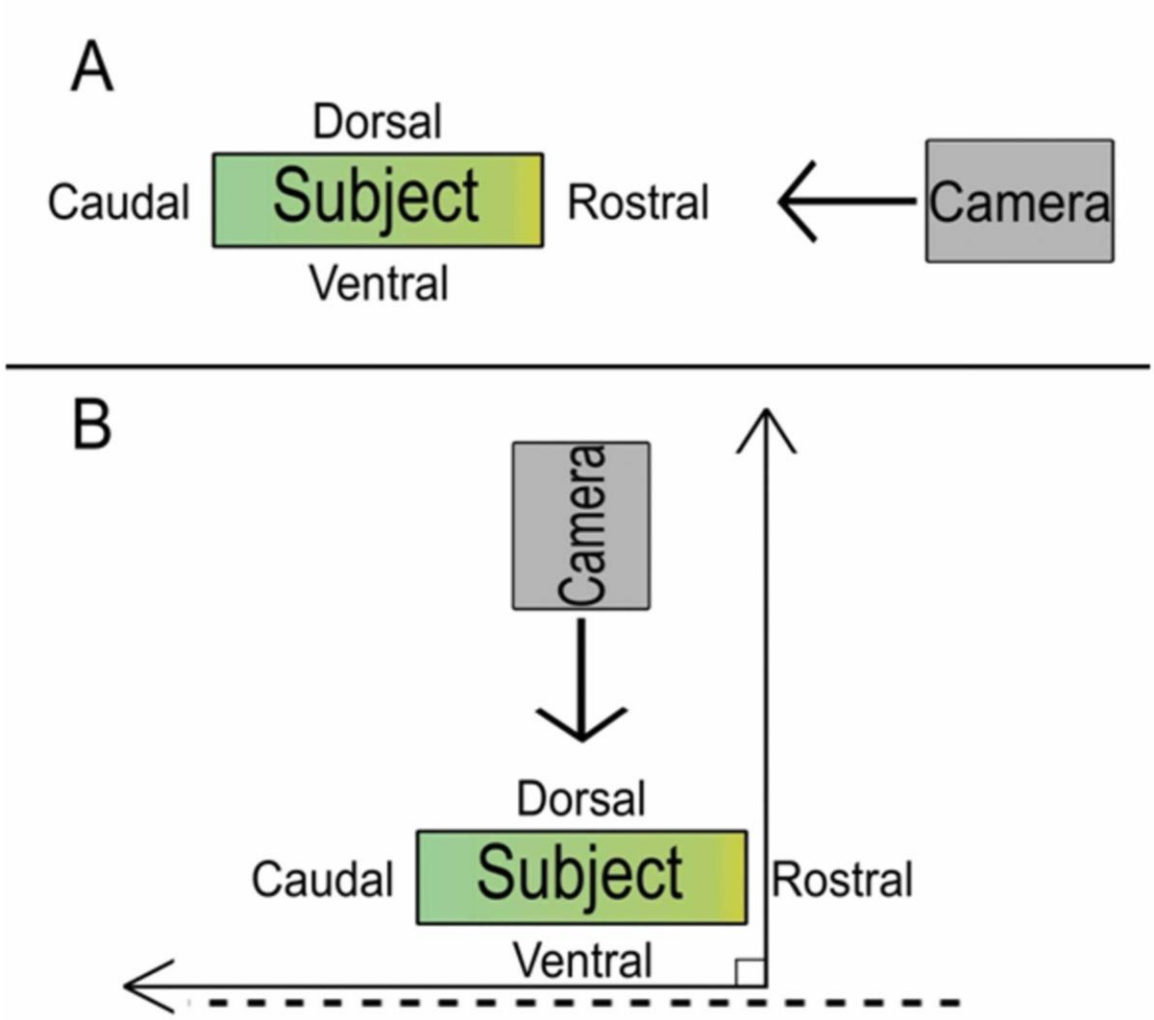

Figure 3.1. Quantification of behavioral recovery: Photography of tilt and sprawl schematic.

Figure 3.1 shows a schematic of how animals are photographed in order to measure the angle of head tilt (A) or limb sprawl (B) and how each behavior recovers over time. Figure 3.1A shows the relative position of the camera during the photography for head tilt. The photograph is taken with the camera held at the level of the animal's head vertically and facing, but in parallel with the direction of the animal's gaze. Figure 3.1B shows the angle of the camera with respect to the subject to photogaph limb sprawl. The dotted line indicates the floor. Photographs to be measured for limb sprawl are taken directly over the animal's dorsal surface with every attempt to make the camera placement at a 90° angle to the floor.

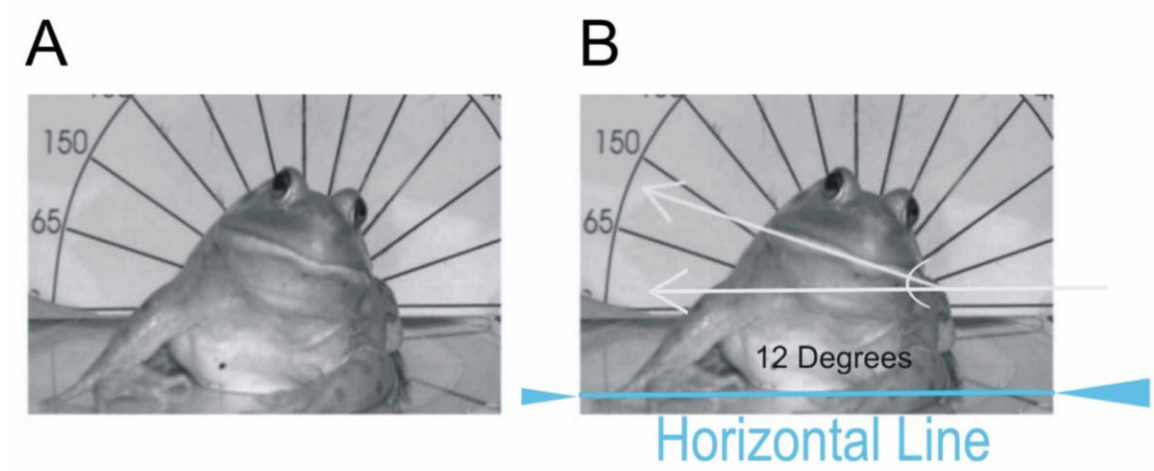

Figure 3.2. Behavioral procedures: Measurement of head tilt in *Rana catesbeiana.*

Figure 3.2A shows a representative photograph of a post operative *Rana catesbeiana* subjected to left n.VIII crush surgery. The same image shown in Fig3.2A is measured using CorelDraw software to determine the head tilt angle in degrees. A horizontal line is generated from the tabletop edge (shown in blue) and represents 0 degrees tilt. The angular dimension tool shown in white and one ray is generated through the line of the frog's mouth. The second ray is generated in parallel with the horizontal line shown in blue. Corel Draw reports the head tilt angle for this animal as 12 degrees.

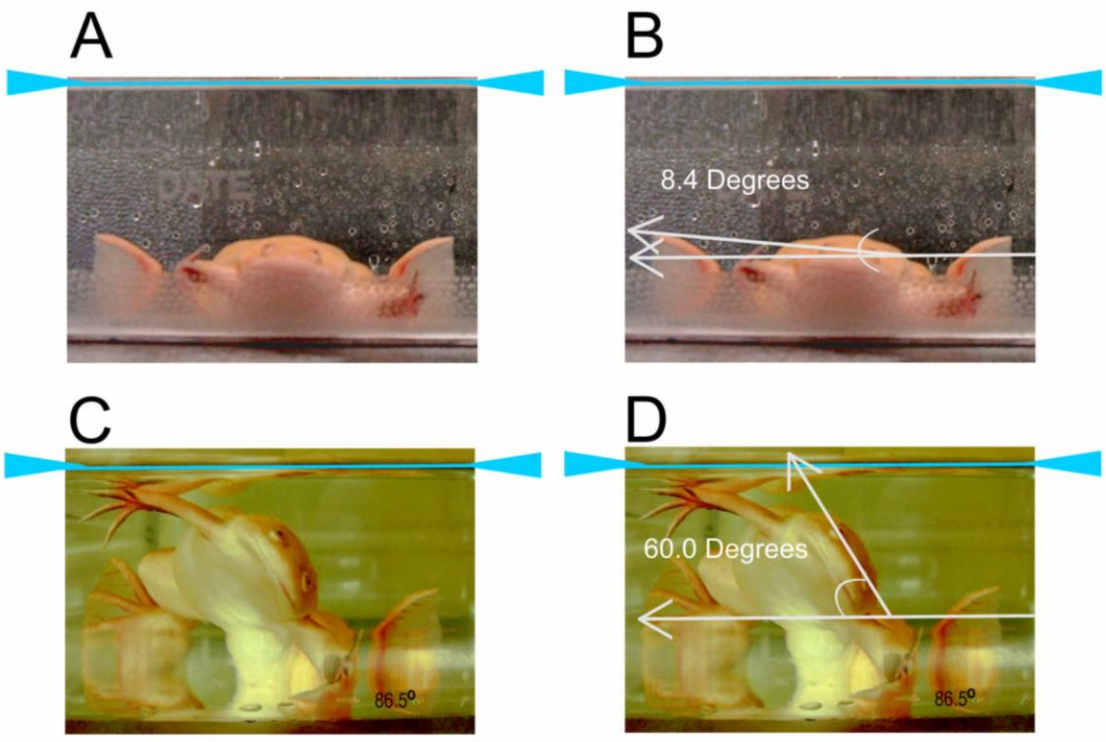

Figure 3.3. Quantification of behavioral recovery: Measurement of tilt in *Xenopus*.

Figure 3.3. Measurement of Tilt: Measurement of head tilt in head on photographs of nonsurgical *Xenopus laevis* results in tilts of less than 10 degrees (Fig 3.3A, and measured in Fig 3.3B). Fig 3.3C, (measured in Fig 3.3D) shows the same animal in Fig 3.3(A) and Fig 3.3(B) 72 hours post left-nVIII crush exhibits a head tilt of 60 degrees toward the side of the lesion.

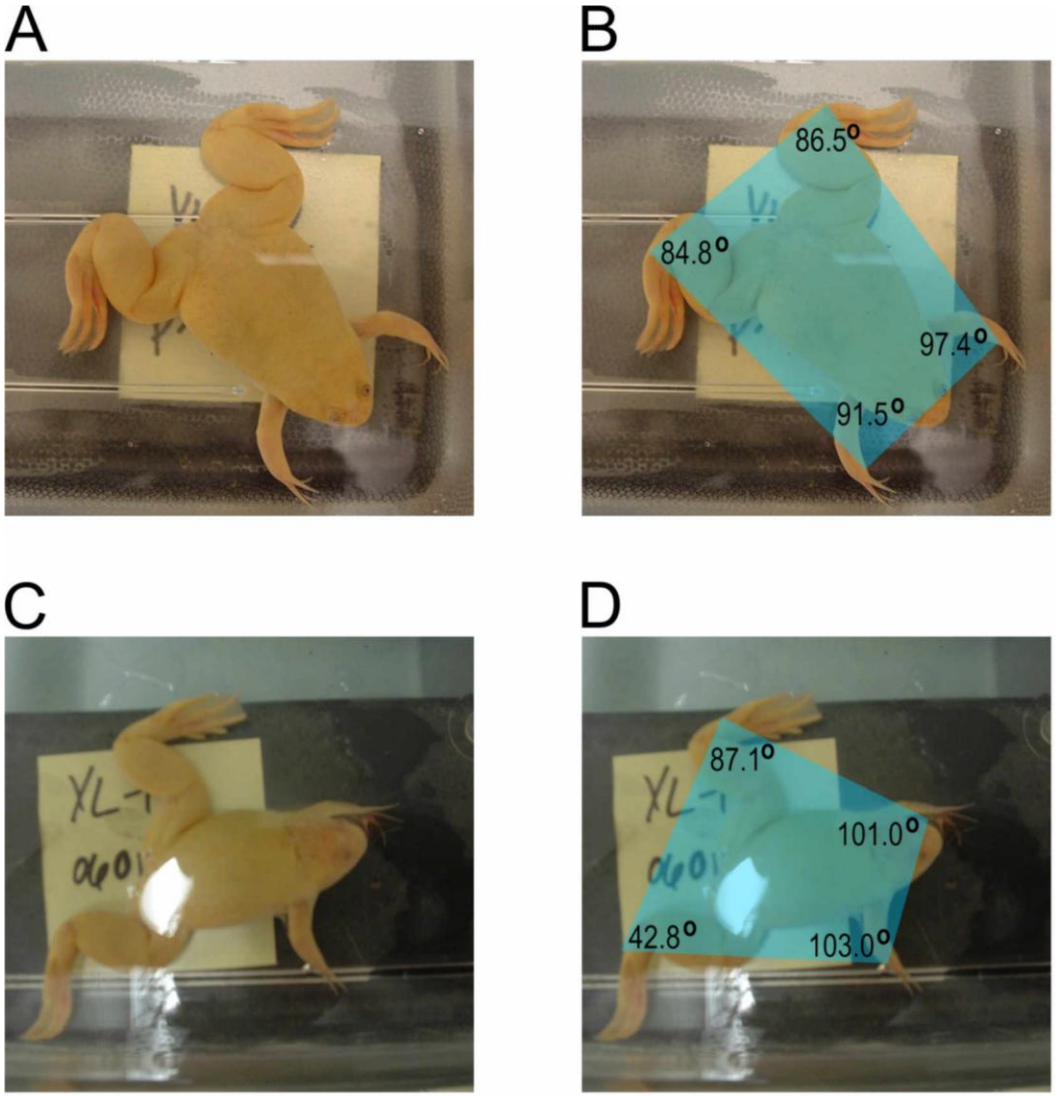

Figure 3.4. Quantification of behavioral recovery: Measurement of sprawl in *Xenopus.*

Figure 3.4. Measurement of Sprawl: Measurement of sprawl in overhead photographs of nonsurgical *Xenopus laevis* (shown in Fig 3.4A, and measured in Fig 3.4B) results in roughly symmetric angle measurements between the left and right arm (Fig 3.4B Left Arm, 97.4◦, Right Arm, 91.5◦) and the left and right leg (Left Leg, 86.5◦, Right Leg, 84.8◦). Twenty four hours post left- nVIII crush lesion, the same animal shown in Fig 3.4A and B exhibits an asymmetric sprawl (shown in Fig 3.4C and measured in Fig 3.4D; Left Arm, 101.0◦, Right Arm, 103.0◦ ,Left Leg, 87.1◦, Right Leg, 42.8◦).

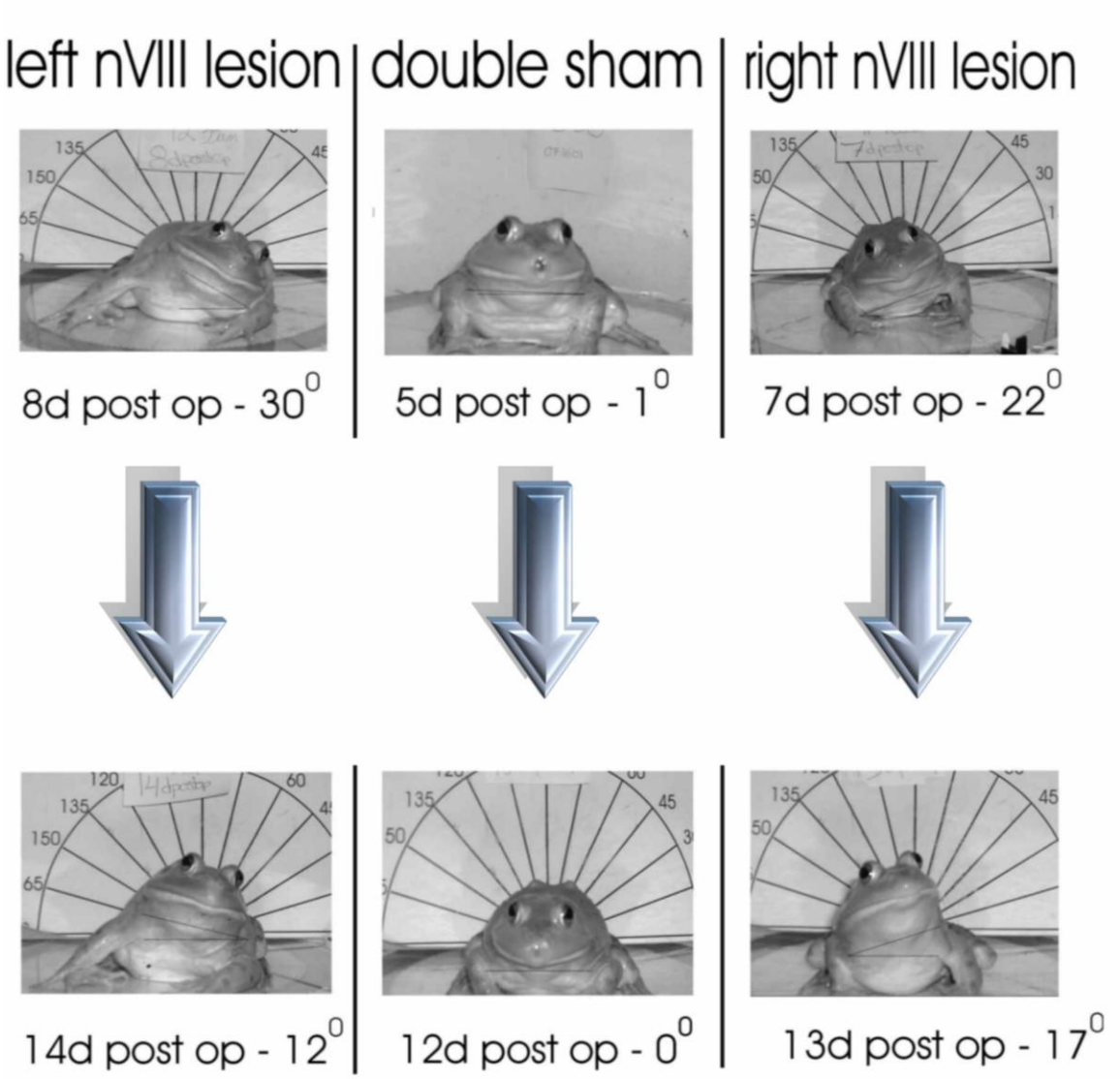

Figure 3.5. Head tilt angles following unilateral n.VIII lesion show directionality toward the lesioned side. Tilt magnitude decreases with post- operative survival.

Figure 3.5 shows representative *Rana catesbeiana* from each of the three surgical conditions: Left: Left n.VIII Lesion. Center: Double Sham, Right:Right nVIII Lesion. Animals subjected to Left and Right nVIII lesion exhibit head tilt directionality towards the left and right, respectively. The bilateral sham surgical animal exhibits no significant head tilt. The bottom pictures are images of the same animals in the photos shown above, except the photo is shot with advanced post operative survival time and shows a reduction in head tilt magnitude in each of the unilateral lesion conditions.

Figure 3.6

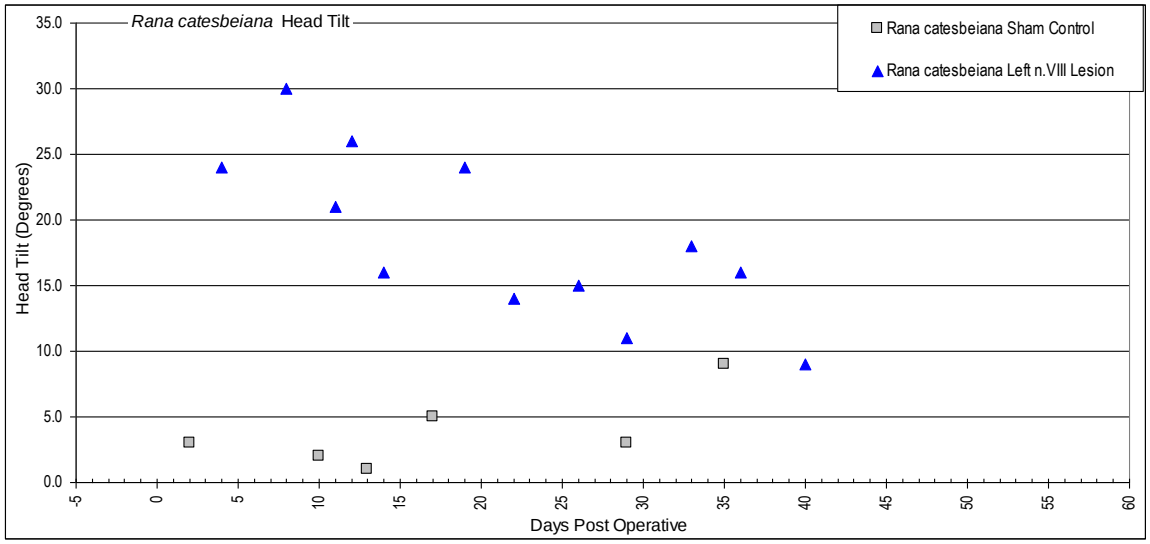

Figure 3.6. Unilateral n.VIII lesion results in increased post-operative head tilt compared to that seen in sham surgical controls. Representative adult *Rana catesbeiana* show an increase in head tilt post-n.VIII lesion followed by gradual decrease in magnitude of tilt over post-operative survival period.

Figure 3.6 shows head-tilt data versus post operative timepoint for two *Rana catesbeiana* adults representing typical trends for sham surgical controls (gray squares) and animals subjected to unilateral left n.VIII crush surgery (blue triangles). Two representative head tilt datasets are plotted as degrees head tilt on the abscissa versus postoperative survival timepoint. Head tilt angles at or below the 8 degree threshold in these studies are categorized as non-tilted. The sham surgical control animal exhibits head tilt angles below the 8 degree threshold for post operative days 10, 13 ,17, and 29 with tilt angles measuring 2, 1, 5 and 3 degrees respectively. Only for the last post-operative head tilt measurement at 35 days does the head tilt measurement break the set threshold at 9 degrees tilt (Fig. 3.6, sham, Gray Square; Post-Operative Days =10, 13, 17, 29, 35, Respective Head Tilt Angles = 2, 1, 5, 3, 9 Degrees). Figure 3.6 shows representative head tilt data in a left n.VIII crush-lesioned animal that follows this general trend (Fig 3.6, unilateral n.VIII lesion, Solid Blue Triangles plot head tilt angle in degrees per post operative recovery timepoint, Post Operative Days Range = 4 – 40, Head Tilt Angle Range (in Degrees) = 30 - 9).

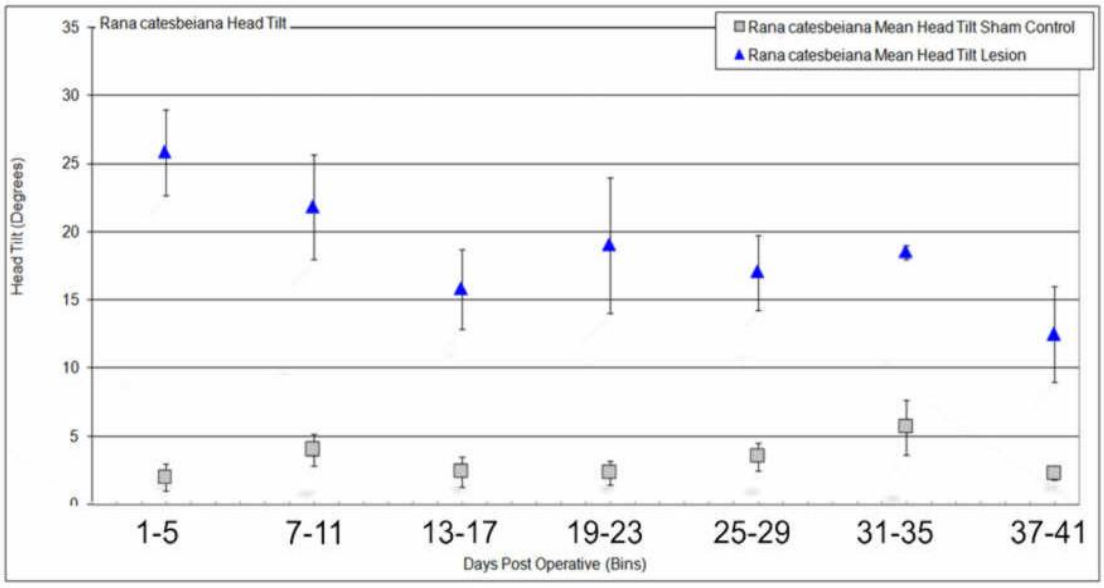

Figure 3.7. Head tilt angles are increased following unilateral n.VIII lesion in pooled datasets of *Rana catesbeiana* adults followed by a decrease in head tilt over post-operative survival.

Figure 3.7 shows mean head-tilt data versus post operative timepoint pooled across seven *Rana catesbeiana* adults subjected to unilateral n.VIII lesion (Blue Triangles) compared to pooled mean head tilts from six sham surgical animals (Gray Squares). Mean head tilt angles from each group (measured in degrees, Abcissa) is plotted against post-operative recovery period (in bins, measured in days, Ordinate). Animals subjected to unilateral n.VIII crush (Blue Triangles) exhibit a mean head tilt angle of 25.8 degrees in the earliest post operative period (1-5 Days). Mean head tilt angles in unilateral n.VIII-lesioned animals gradually decrease in magnitude with post-operative recovery. However, mean head tilt angles are still greater than mean head tilts seen in sham surgical animals (Gray Squares) even at 37-41 post-operative days.

Mean head tilt angles in sham surgical groups show no significant head tilt, even in the earliest post-operative periods (Gray Squares). Sham surgical animals are categorized as "non-tilted" as measurements are equal to or less than the 8 degree threshold determined by head tilt measurements of nonsurgical animals and precision of our tilt measurement protocols. Error Bars = S.E.M.

	Rana catesbeiana Mean Head Tilt (Degrees) Lesion					*Rana catesbeiana* Mean Head Tilt (Degrees) Sham			
Bins Lesion Days		**n**	**SEM**	**# Animals**			**n**	**SEM**	**# Animals**
1-5	25.8	6	3.16	4		2.0	2	1.00	2
7-11	21.8	5	3.85	3		4.0	6	1.15	4
13-17	15.8	5	2.94	3		2.4	5	1.08	3
19-23	19.0	2	5.00	1		2.3	3	0.88	2
25-29	17.0	4	2.74	2		3.5	4	1.04	3
31-35	18.5	2	0.50	2		5.7	3	2.03	3
37-41	12.5	2	3.50	1		2.3	4	0.48	2

Figure 3.7. (*chart*) Mean head tilt angles versus post operative recovery period in adult unilateral n.VIII crush lesioned or surgical sham treated adult *Rana catesbeiana.*

Figure 3.7 (*chart*) shows head-tilt angle means versus post operative recovery period for adult *Rana catesbeiana* subjected to unilateral n.VIII crush lesion or sham surgery. Data are are reported as binned post operative days and are reported graphically in Figure 3.7.

Data are separated according to post operative recovery and type of surgery [either n.VIII Lesion (Left Chart) or Sham surgical (Right Chart) conditions]. Head tilt angles are measured in degrees for each surgical group and for each binned post operative recovery period. Tilt means are averaged across all animals that were measured and across all photographs (from which tilts are measured) for all days within the binned post-operative period. The number of photographs measured for each group is reported in the "n" column. The Standard Error of the Mean (SEM) is reported in the "SEM" column and the number of animals is reported in the "# Animals" column. SEM is calculated using "n" data in the denominator..

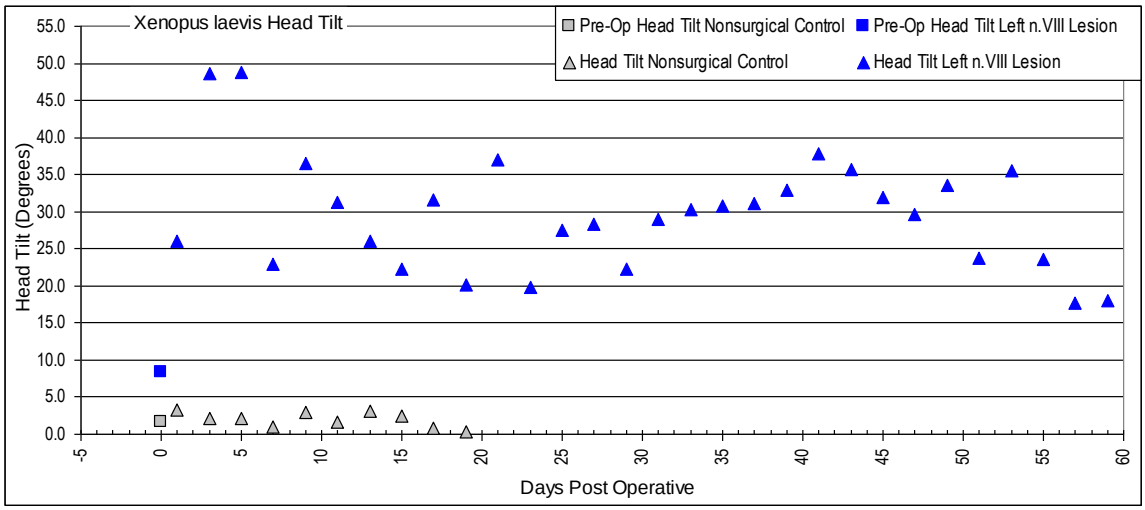

Figure 3.8 Unilateral n.VIII Lesion Results in Increased Post-Operative Head Tilt Versus Nonsurgical Controls. Representative Adult *Xenopus laevis* Show an Increase in Head Tilt Post-n.VIII Lesion, Followed by Gradual Decrease in Magnitude of Tilt Over Post-Operative Survival Period.

Figure 3.8 shows example head-tilt measurement datasets plotted from two *Xenopus laevis* adults representing typical head tilt trends for control and unilateral n.VIII-lesioned animals. Head tilts are recorded and analyzed in degrees (the air-water interface represents 0.0 degrees as indicated above, see Materials and Methods). Preoperatively, mean head tilt angles for both, the nonsurgical control and n.VIII-lesioned animals are 1.6 and 8.3 degrees, respectively (Fig 3.8, Control; Gray Square, 1.6 Degrees, Ordinate = 0; Pre-Operative Measurement, Left n.VIII Lesion and Right n.VIII Sham; Blue Square, 8.3 degrees, Ordinate = 0).

Figure 3.9

Figure 3.9A

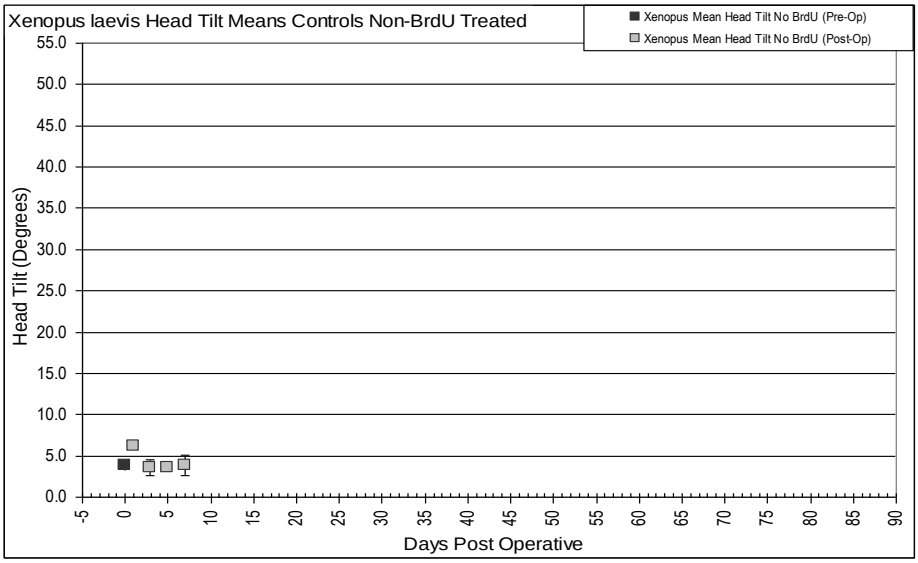

Figure 3.9B

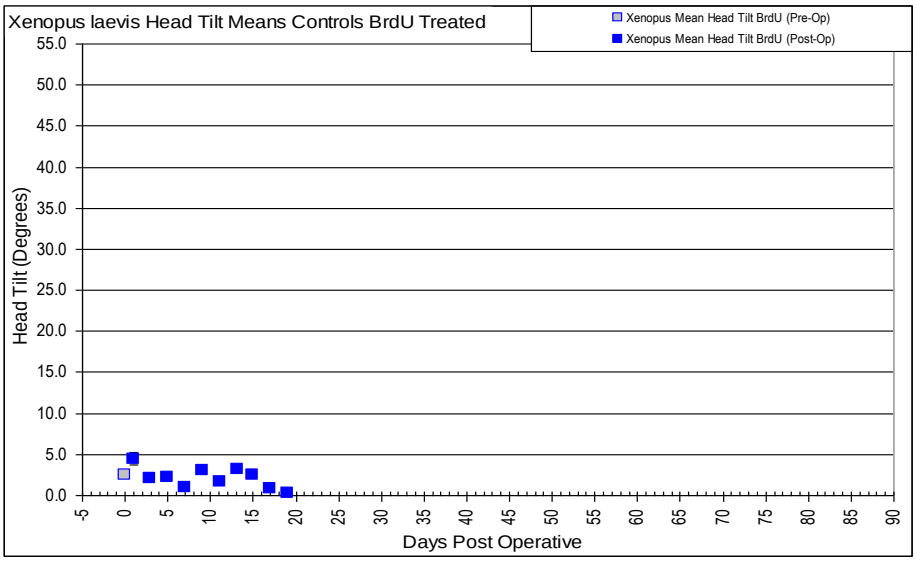

Figure 3.9. Effect of BrdU Injection on Head Tilt in Controls.

Figure 3.9 shows mean head-tilt measurement data plotted from *Xenopus laevis* unlesioned animals either, uninjected (Fig 3.9A) or injected with BrdU (Fig3.9B). At timepoint=0 (Fig 3.9A, Black Square; Fig 3.9B, Gray Square), the mean head tilt angle for both, animal means is below 8 degrees indicating no tilt. From timepoint=1 Day forward, mean angle measurements are below 8 degrees for the non injected (Fig 3.9A) and BrdU injected (Fig 3.9B) conditions. (Bars = +/- S.E.M).

Figure 3.10

Figure 3.10A

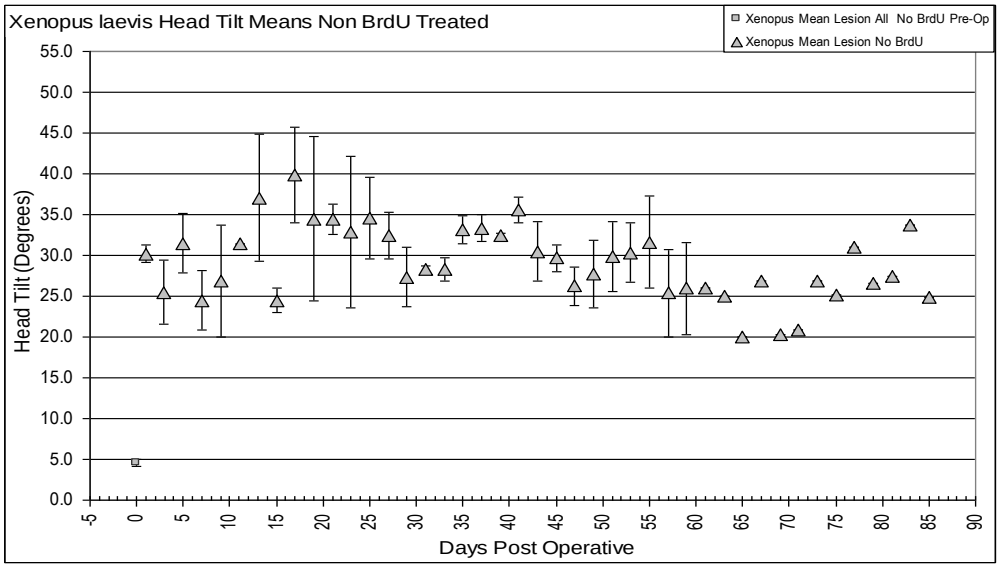

Figure 3.10B

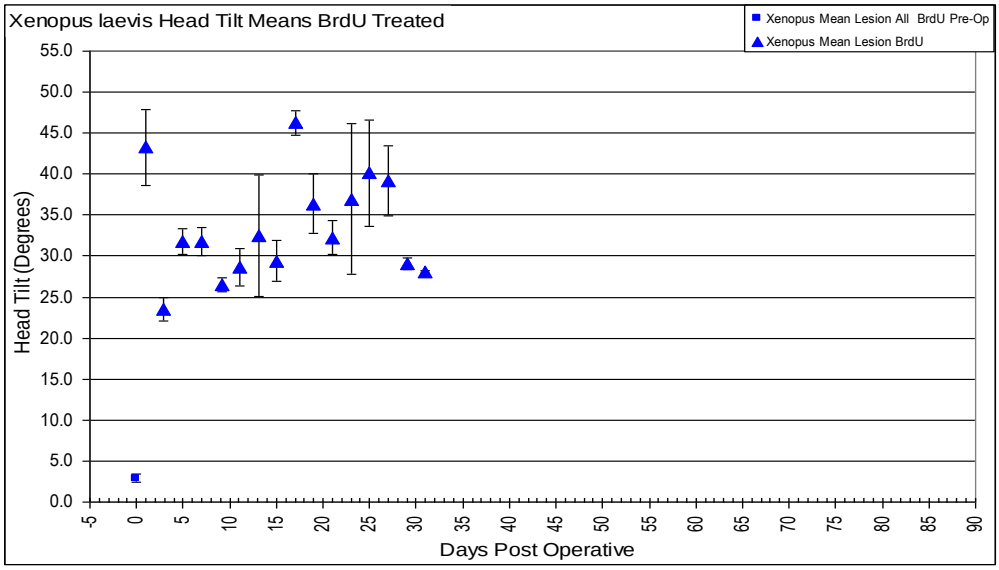

Figure 3.10. Effect of BrdU Injection on Head Tilt in n.VIII Lesioned Animals

Figure 3.10 shows mean head-tilts from *Xenopus laevis* n.VIII lesioned animals either, uninjected (Fig 3.10A) or injected with BrdU (Fig3.10B). At time = 0 (Fig 3.10A, Gray Square; Fig 3.10B, Blue Square), the mean tilt angle for both animal means is below 8 degrees indicating no tilt. From time =1 day forward, mean angle measurements for noninjected (Gray Triangles) and BrdU injected (Blue Triangles) animals are very tilted. The magnitude gradually decreases with recovery period in the noninjected animals (animals still exhibit significant tilt). The BrdU injected animals do not exhibit a similar tilt reduction but they have a shorter post operative

recovery and trends are similar in the noninjected animals during post-operative timepoints through 30 days. (Bars = +/- S.E.M).

Figure 3.11

Figure 3.11: Limb Sprawl Versus Post Operative Recovery in *Xenopus laevis*.

Figure 3.11A:: Limb Sprawl Versus Post Operative Recovery in Representative Control *Xenopus laevis*.

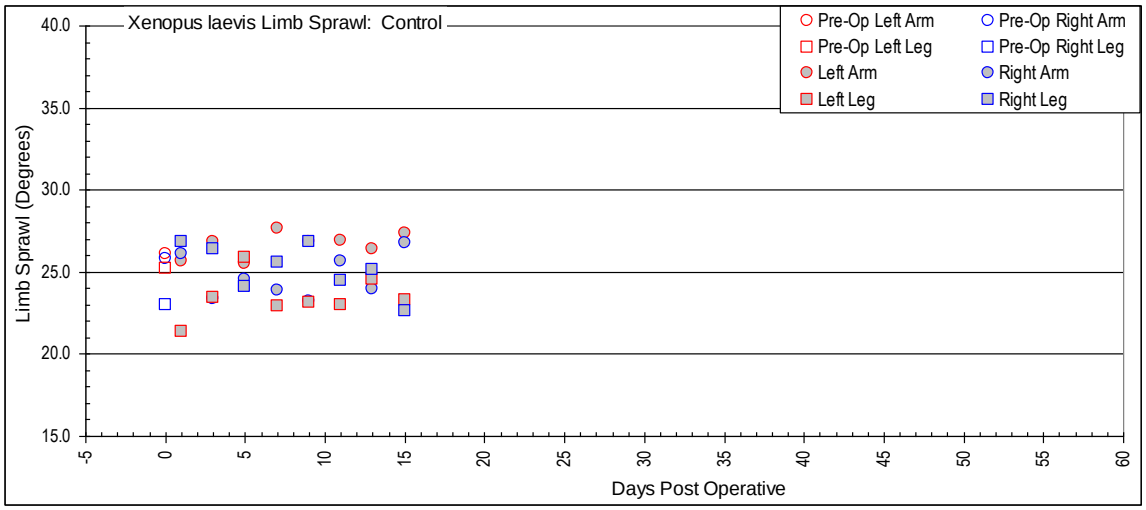

Figure 3.11B:: Limb Sprawl Versus Post Operative Recovery in Representative n.VIII-Lesioned *Xenopus laevis*.

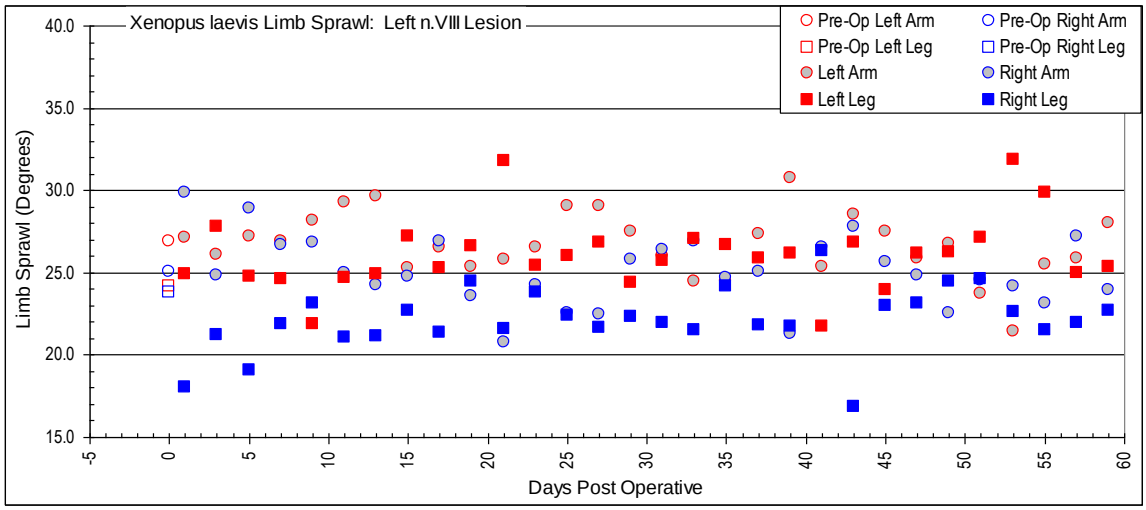

Figure 3.11. Limb Sprawl Data in Representative n.VIII *Xenopus laevis* Shows Limb Angle Discrepancy Over Survival Period when Compared with Control Surgical Animals.

Figure 3.11 shows limb sprawl data from two adult *Xenopus laevis* representative of typical limb sprawl magnitude and trends over survival period for nonsurgical control subjects (Fig 3.11A, top) and animals subjected to unilateral n.VIII lesion (Fig 3.11B, bottom).
Figure 3.11A (top) shows normalized limb angle data (Fig 3.11A, Abcissa, in degrees, significance 0.0) from a representative nonsurgical control adult *Xenopus laevis* over multiple survival points (Fig 3.11A, Ordinate, Days Post Operative). Limb angles are normalized according to the proportion each limb angle represents of all four angles per survival point. For each survival point, all four limb angles are summed to generate the total angle. Each limb angle is then normalized as a proportion of the total measured angle and multiplied by 100.
The preoperative angle measurements for the right and left arms are nearly identical (Fig 3.11A, Ordinate = 0; Pre-Op Left Arm, Open Red Circle, Angle= 26.1; Pre-Op Right Arm, Open Blue Circle, Angle= 25.8). The preoperative left leg angle measurement is similar to the arm measurements and data points overlap (Fig 3.11A, Ordinate = 0; Pre-Op Left Leg, Open Red Square, Angle = 25.2). The preoperative right leg angle (Fig 3.11A, Ordinate = 0; Pre-Op Right Leg, Open Blue Square, Angle = 23.0).
Figure 3.11B (bottom) shows normalized limb angle data (Fig 3.11B, Abcissa, in degrees, significance 0.0) from a representative adult *Xenopus laevis* subjected to unilateral n.VIII lesion over multiple preoperative and post operative survival points (Fig 3.11B, Ordinate, Days Post Operative).
The preoperative angle data for each of this animal's limbs are similar to angle data shown in the nonsurgical control condition (Fig 3.11A), and leg angle datapoints are overlapping (Fig 3.11B, Ordinate = 0; Pre-Op Left Leg, Open Red Square Angle= 24.2; Pre-Op Right Leg, Open Blue Square, Angle= 23.8). The post operative limb sprawl beginning 24 hours post left n.VIII crush lesion (with contralateral n.VIII sham surgery) indicates a discrepancy between limb angles.

Figure 3.11B (bottom) shows normalized limb angle data (Fig 3.11B, Abscissa, in degrees, significance 0.0) from a representative adult *Xenopus laevis* subjected to unilateral n.VIII lesion over multiple preoperative and post operative survival points (Fig 3.11B, Ordinate, Days Post Operative).

The preoperative angle data for each of this animal's limbs are similar to angle data shown in the nonsurgical control condition (Fig 3.11A), and leg angle data points are overlapping (Fig 3.11B, Ordinate = 0; Pre-Op Left Leg, Open Red Square Angle= 24.2; Pre-Op Right Leg, Open Blue Square, Angle= 23.8). The post operative limb sprawl beginning 24 hours post left n.VIII crush lesion (with contralateral n.VIII sham surgery) indicates a discrepancy between limb angles.

Figure 3.12

Figure 3.12: Mean Head Tilt Versus Post Operative Recovery in *Xenopus laevis* and *Rana catesbeiana* After Unilateral n.VIII Lesion.

Figure 3.12A: Mean Head Tilt Versus Post Operative Recovery in Unilateral n.VIII-Lesioned *Rana catesbeiana* and *Xenopus laevis*.

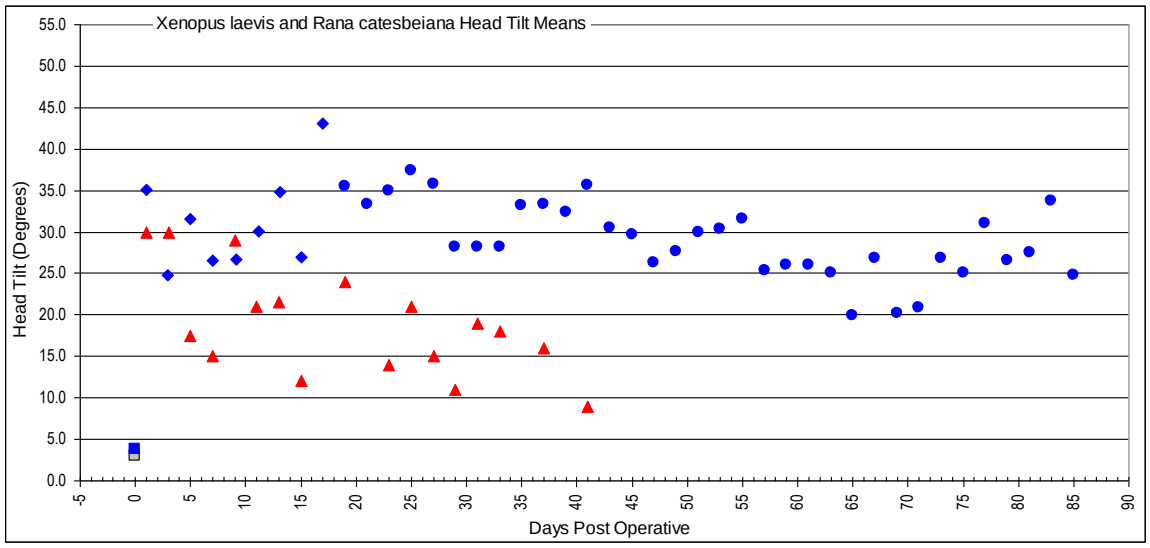

Figure 3.12B: Mean Head Tilt Versus Post Operative Recovery in Unilateral n.VIII-Lesioned *Rana catesbeiana*.

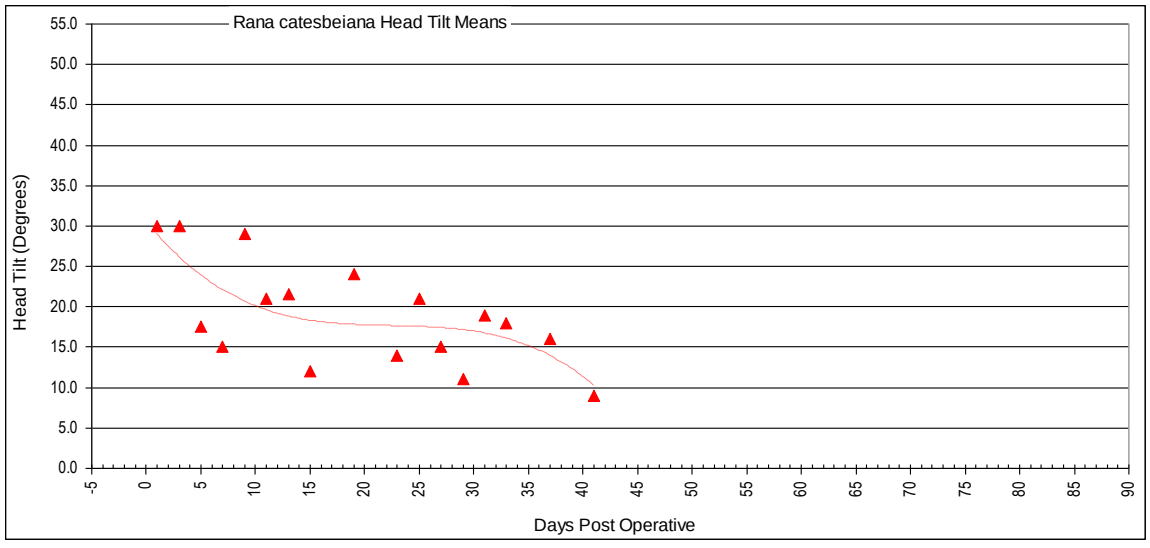

Figure 3.12C: Mean Head Tilt Versus Post Operative Recovery in Unilateral n.VIII-Lesioned *Xenopus laevis*, Post Operative Recovery 1 – 18 Days.

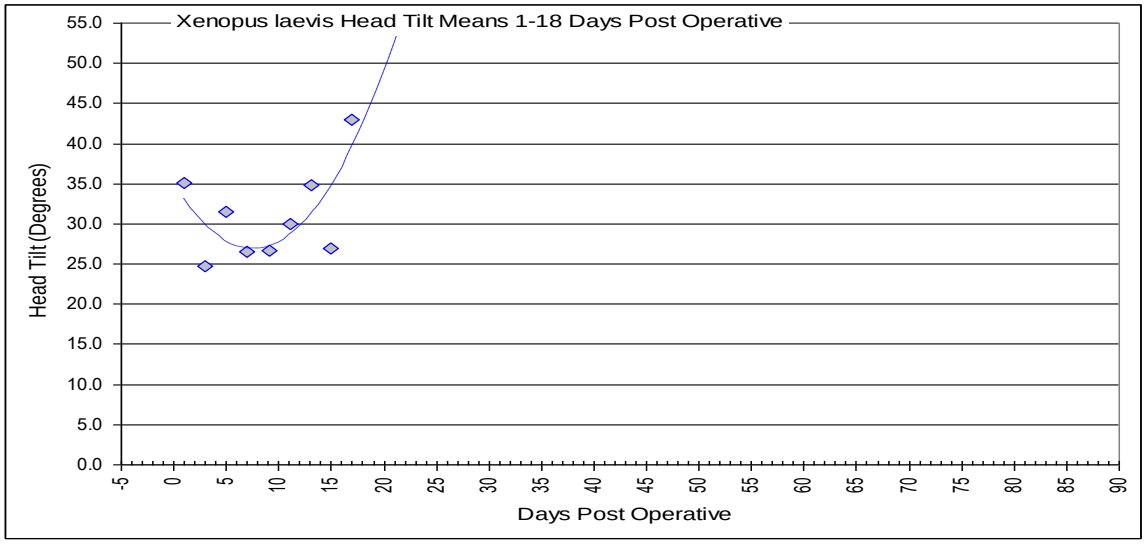

Figure 3.12D: Mean Head Tilt Versus Post Operative Recovery in Unilateral n.VIII-Lesioned *Xenopus laevis*, Post Operative Recovery 18 – 85 Days.

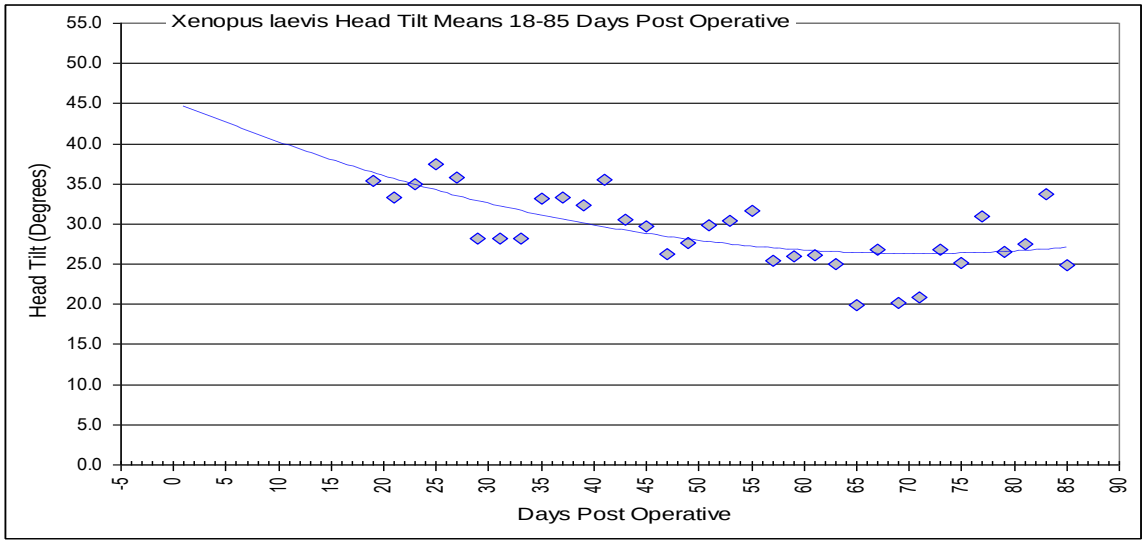

Figure 3.12. Trend in Head Tilt Recovery Subsequent to Unilateral n.VIII Lesion in Rana catesbeiana and Xenopus laevis Varies Over Post-Operative Time Point.

Figure 3.12 shows mean head-tilt measurement data plotted from *Xenopus laevis* and *Rana catesbeiana* adults representing typical head tilt trends for control and unilateral n.VIII-lesioned animals.

Figure 3.12A shows the mean degree head tilt for *Rana catesbeiana* (Fig 3.12A; red triangles) and *Xenopus laevis* (Fig 3.12A; blue circles) subjected to unilateral n.VIII lesion between post operative day 1 through day 85.

Figure 3.12B shows mean head tilt data shown in 3.12A for *Rana catesbeiana* over post operative recovery period without data from *Xenopus laevis* for clarity. Head tilt shows an overall decrease with post-operative recovery, although fluctuating slightly, after post-operative day 41 is reduced to 9°. These data are best described as following a cubic trend (Fig 3.12B; shown as red dotted line, $y = -0.0011x^3 + 0.0728x^2 - 1.6689x + 30.579$; $R^2 = 0.48$).

Figure 3.12C shows mean head tilt data shown in Figure 3.12A for *Xenopus laevis* for post operative recovery days 1 – 18. Beginning 1 day post n.VIII lesion, *Xenopus* tilt toward the lesioned side, which then decreases until approximately 7-9 days post operatively, followed by an increase in head tilt, reaching a peak at approximately 17 days post-op The mean head tilt data for days 1-18 are best described as following a cubic trend [see Fig 3.12C; blue trend line, $y = 0.0029x^3 + 0.0633x^2 - 1.5911x + 34.227$ ($R^2 = 0.52$)].

Figure 3.12D shows the mean degree head tilt for *Xenopus laevis* from Figure 3.12A post operative day 18 through day 85. After 18 days post n.VIII lesion, the animal continues to tilt towards the side of the lesion similarly to the head tilt exhibited during post operative day 1 (see Fig 3.12A, and 3.12C) however is significantly less than the magnitude of head tilt at post operative day 17. Subsequent to post operative day 18, mean head tilt will vary, but decreasing slowly with increasing post operative survival period. The mean head tilt data for days 18-85 are best described as following a quadratic trend [(see Fig 3.12D; blue trend line, $y = 0.0038x^2 - 0.5345x + 45.182$ ($R^2 = 0.48$)].

Figure 4.1

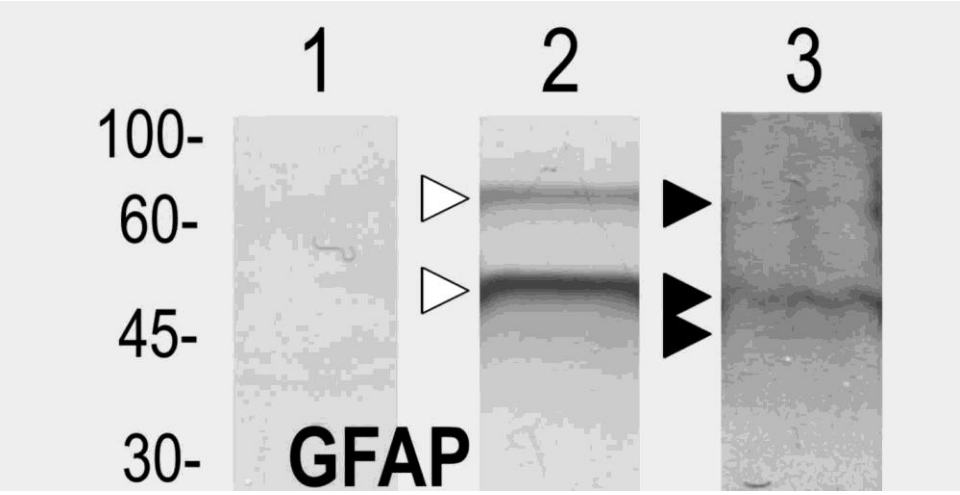

Figure 4.1. Glial Fibrillary Acidic Protein, GFAP antibody recognizes antigen in Xenopus laevis.

Figure 4.1 shows the results of western blot analysis to determine specificity and selectivity of the polyclonal antibody raised against glial fibrillary acidic protein (GFAP) as the antigen. Western blot results for each of 3 lanes each representing different conditions: Left. Numbers, ranging from 30-100, correspond to the relative locations of the prestained known-mass proteins in the ColorBurst molecular weight marker which was run alongside the three samples during SDS PAGE. Molecular masses are represented in kilodaltons (kDa). Lane 1: Negative Control (Denaturizing Sample Buffer Only, 0.9% sterile saline replaces the volume of Protein); Lane 2: Positive Control (Rodent Brain Homogenate); and Lane 3: *Xenopus laevis* adult brain tissue.

Figure 4.2

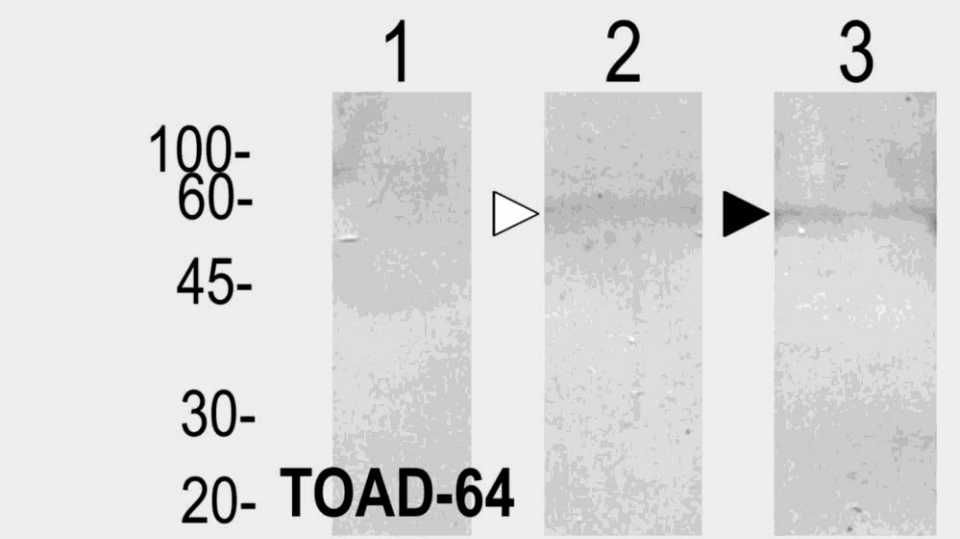

Figure 4.2. Turned On After Division, 64 kDa, TOAD-64 kDa antibody recognizes antigen in *Xenopus laevis*.

Figure 4.2 shows the results of western blot analysis to indicate specificity of the polyclonal antibody raised against Turned On After Division, 64 kDa, TOAD-64 kDa antigen. Fig.4.2 shows western blot results for each of 3 lanes each representing different conditions: Lane 1: Negative Control (Denaturizing Sample Buffer Only, 0.9% sterile saline replaces the volume of Protein),; Lane 2: Positive Control (Rodent Brain Homogenate); and Lane 3: *Xenopus laevis* adult brain tissue.

Figure 4.3

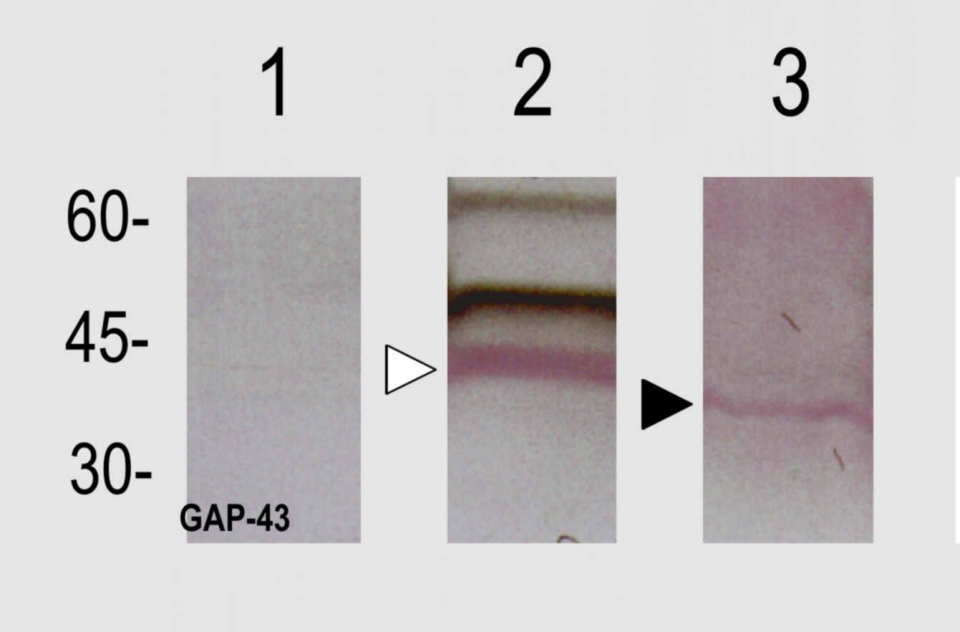

Figure 4.3. Growth-Associated Protein, 43 kDa , GAP-43 kDa antibody recognizes antigen in *Xenopus laevis*.

Figure 4.3 shows the results of western blot analysis to indicate specificity of the polyclonal antibody raised against Growth-Associated Protein, 43 kDa , GAP-43 kDa antigen. Fig.4.3 shows western blot results for each of 3 lanes each representing different conditions: Lane 1: Negative Control (Denaturizing Sample Buffer Only, 0.9% sterile saline replaces the volume of Protein),; Lane 2: Positive Control (Rodent Brain Homogenate); and Lane 3: *Xenopus laevis* adult brain tissue.

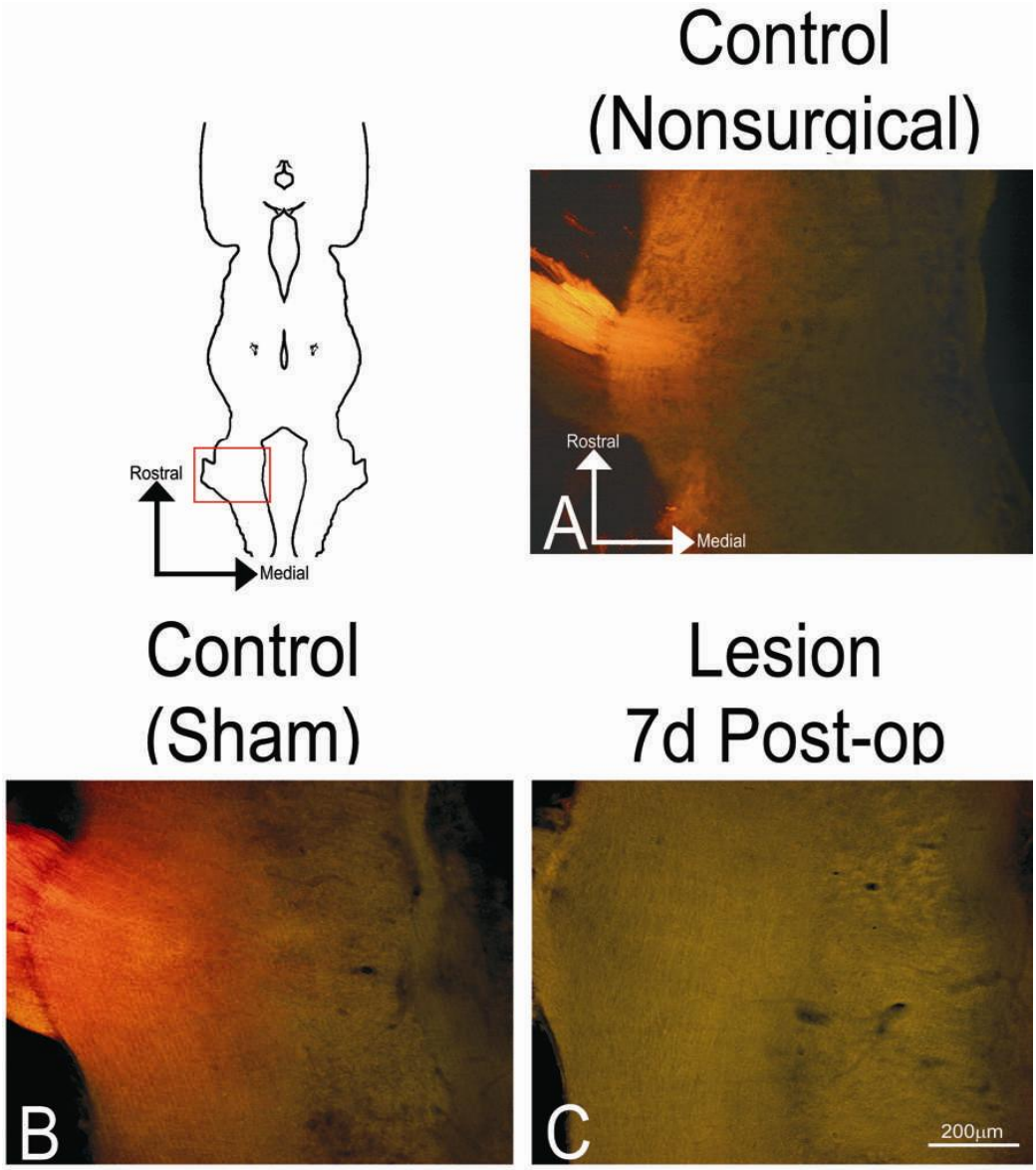

Figure 4.4. Fluorescent lipophilic dyes placed in n.VIII travel to medullary targets in controls but not after post-n.VIII crush.

The leftmost panel is a representative schematic indicating the approximate location of photos of the 50µm horizontal sections in panels A-C. All photos in Fig 4.4A-C are imaged under 10x magnification. (A) A nonsurgical control animal shown. The n.VIII exhibits the red-orange fluorescence resulting from DiI-Ph deposition and bidirectional travel along the intact nerve path including entry into the target tissue of the medulla. (B) Deposition of DiI-Ph tracer in an animal subjected to n.VIII sham surgery shows a similar pattern of red-orange fluorescence along the intact nerve fibers and medullary target tissue. (C) Crush lesion of the contralateral n.VIII from the same animal shown in (B) does not exhibit red-orange fluorescence in medullary targets following DiI deposition distal to n.VIII crush site. All tracer deposition for A-C follows euthanasia and aldehyde fixation. The animal shown in B,C was allowed to recover from n.VIII sham/lesion surgery for 7 days prior to euthanasia.

Figure 4.5

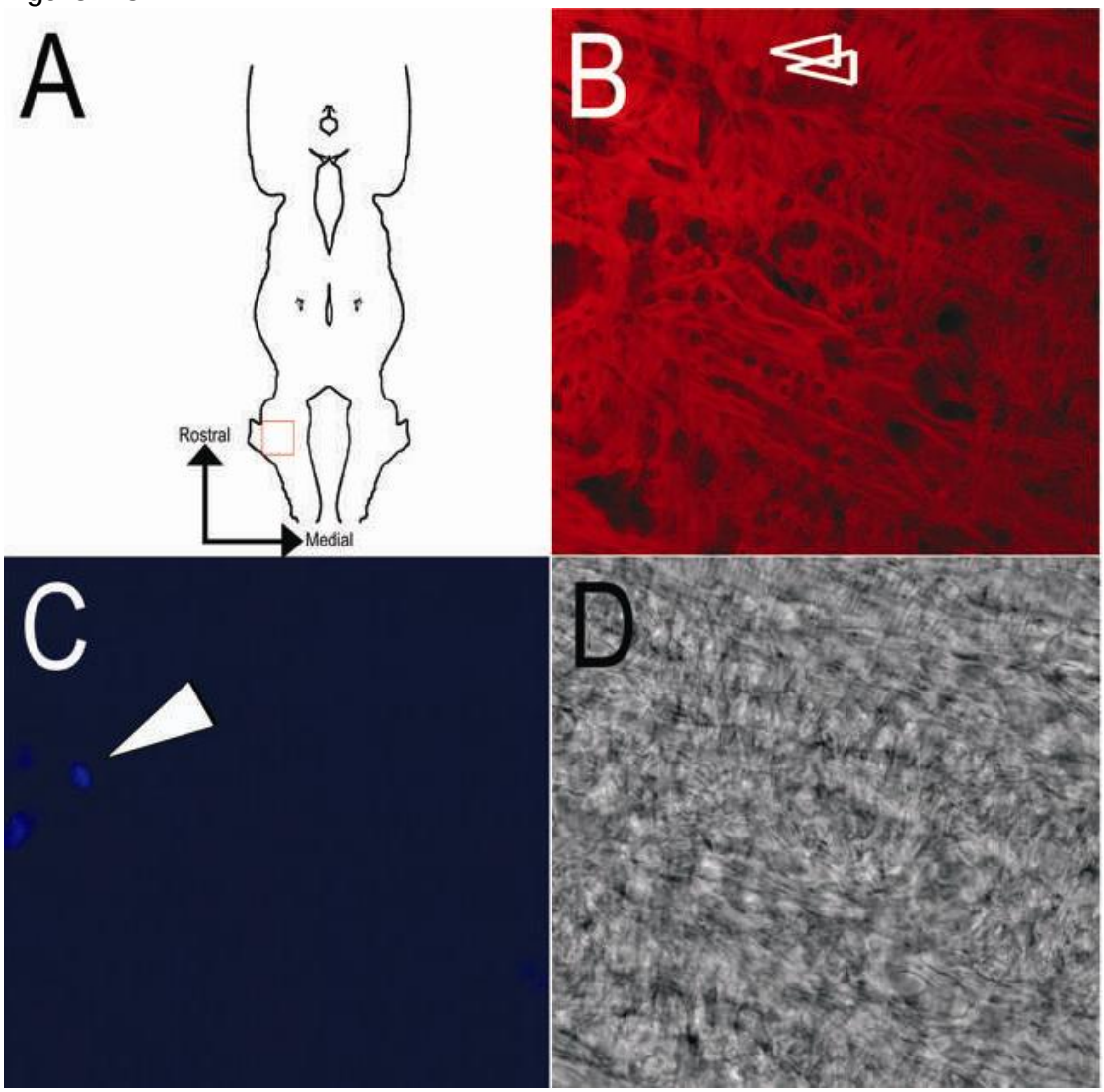

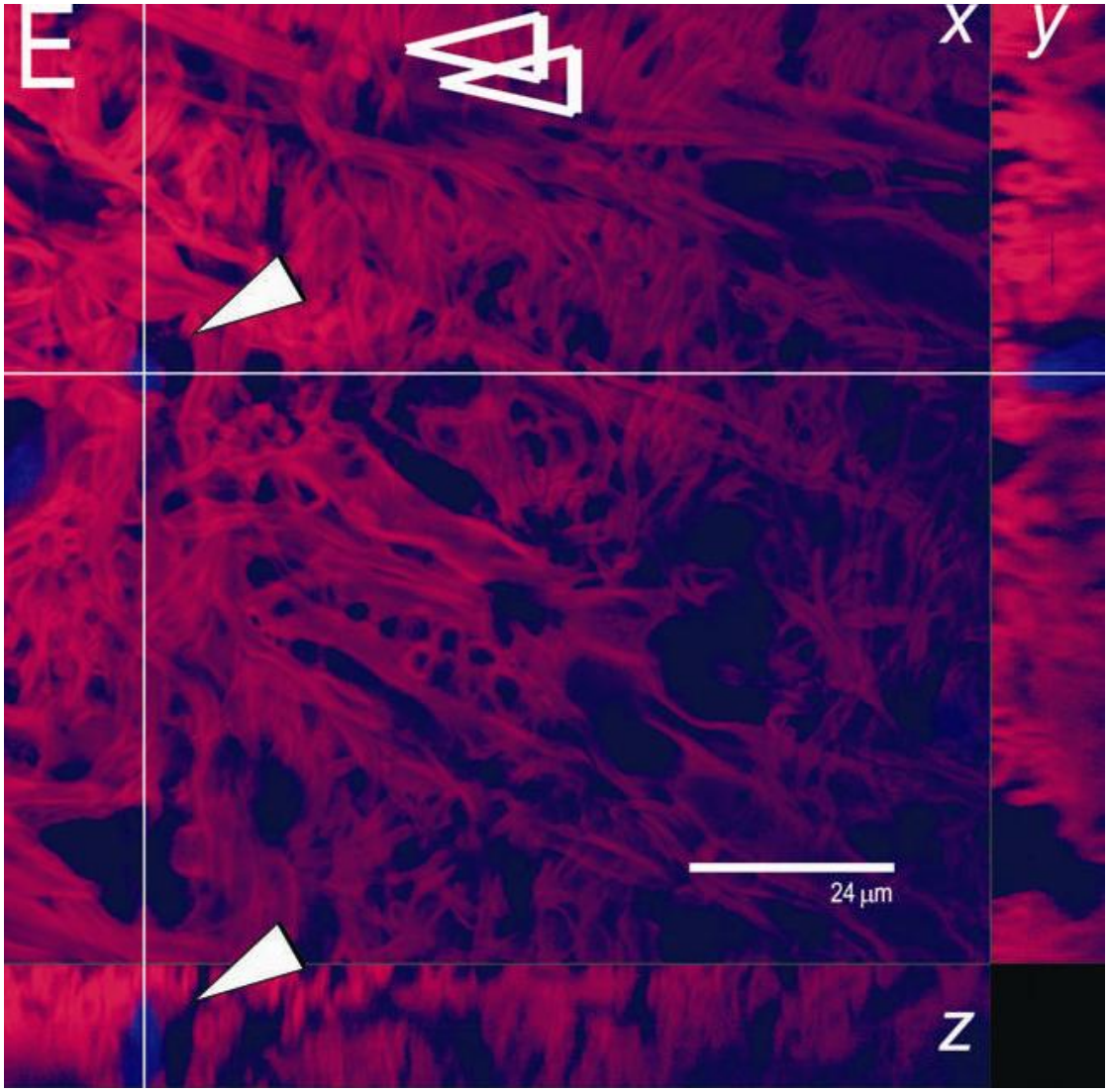

Figure 4.5. Confocal microscopy of DiI-Ph -labeled n.VIII projections and DAPI-labeled cell nuclei in control medulla.

The Z stack in Fig 4.5 (B-D) is generated from the nonsurgical control animal shown in Fig 4.4A using a Leica confocal microscope under 63x magnification (zoom = 2). (A) A schematic indicating the approximate XY location along the 50µm horizontal brain slice from which the Z stack snapshot is comprised. (B-D) (B) One snapshot image of the DiI-Ph channel shows fibers ending in terminal-like fibers (white hollow arrowheads) and (C) DAPI channel shows a DAPI labeled cell (white arrowhead). The transmitted light channel is shown in (D). Z stack images of DiI-Ph and DAPI channels are rotated in orthogonal planes in (E) showing terminal-like processes (white hollow arrowheads) and the DAPI-labeled cells (in blue; one cell is shown, white crosshairs, white arrow). Scale bar = 24µm.
Figure 4.6

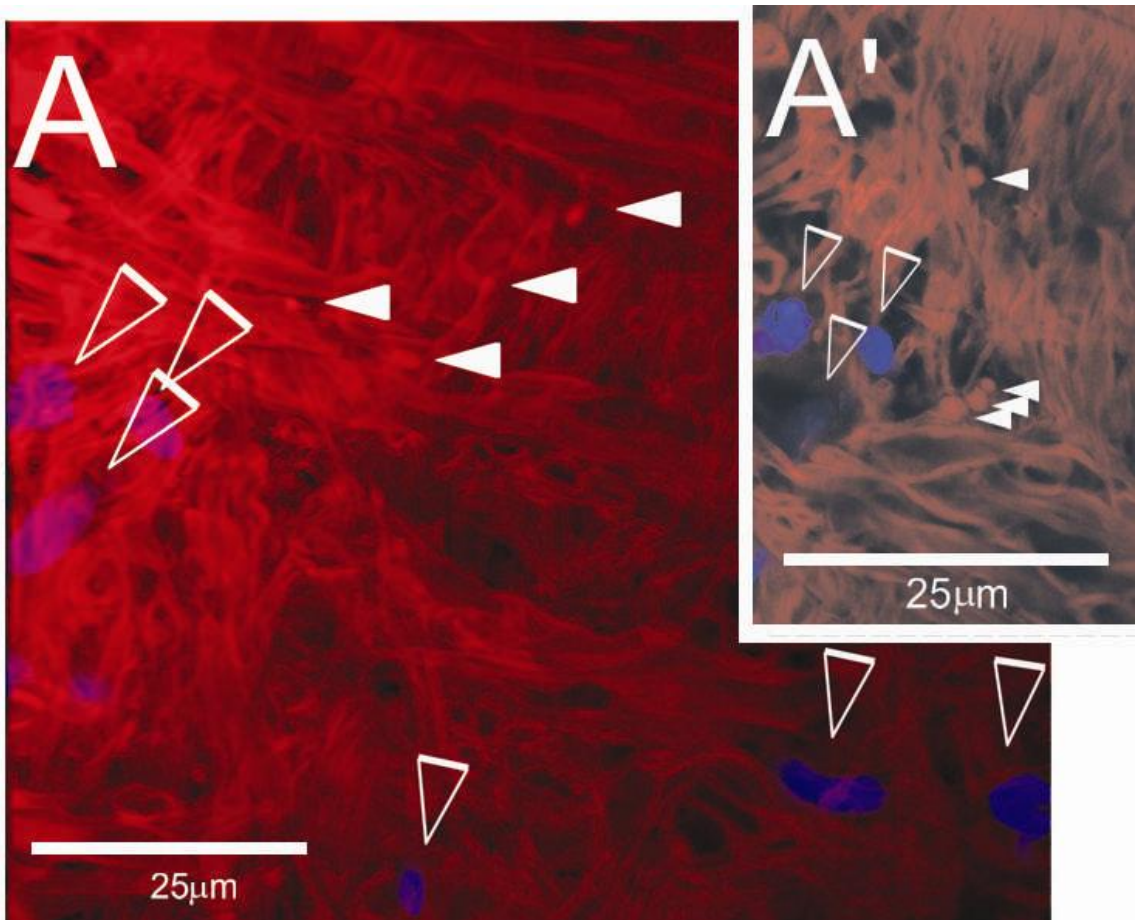
A
A'
25μm
25μm

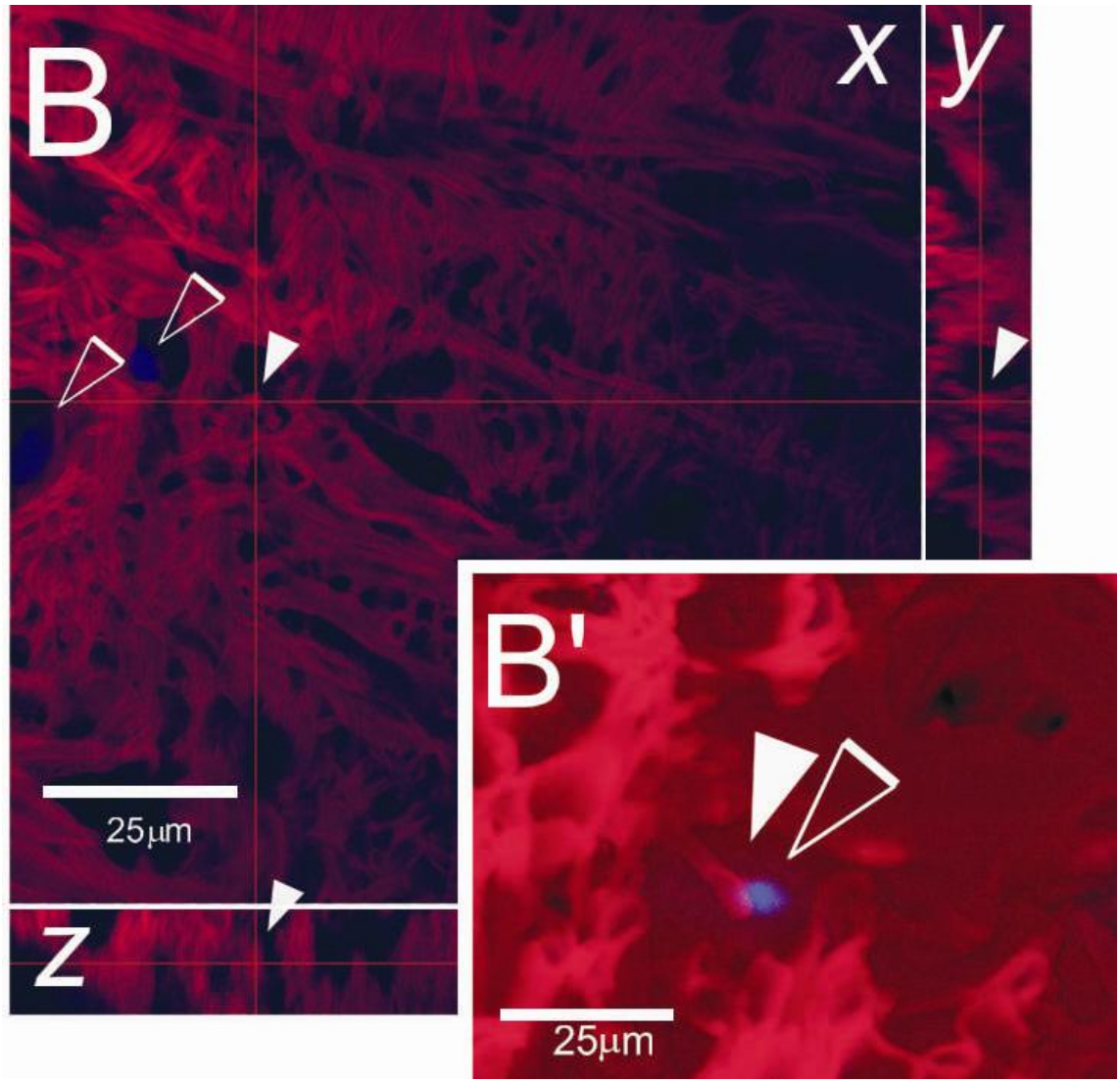

Figure 4.6. Confocal microscopy of n.VIII terminal-like projections in control medulla.

Figure 4.6 A and A' show DAPI labeled cells in blue (hollow arrowheads) and DiI-Ph-labeled terminal-like projections (A and A' solid arrowheads). In Figure 4.6B a fiber terminal-like structure is rotated in orthogonal planes (orange crosshairs and solid arrowheads). DAPI-labeled cells are shown with open white arrowheads (Fig 4.6B). Figure 4.6B' shows a DAPI labeled cell (open white arrowhead) appears to be contacted by a DiI-Ph labeled fiber terminal-like structure (solid white arrowhead). Scale bar = 25µm.

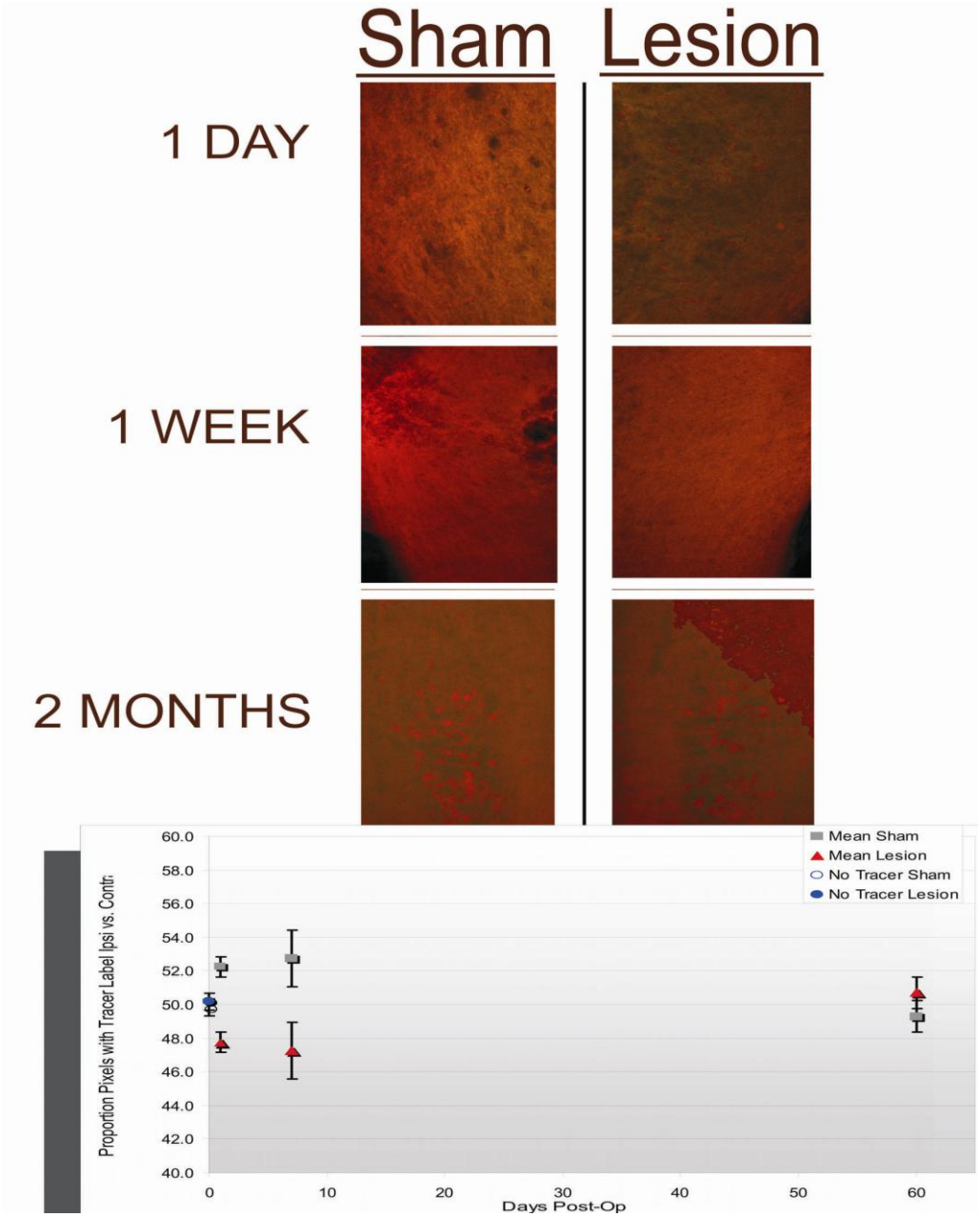

Figure 4.7. Tracer Placed in Lesioned n.VIII Travels to Medulla After Two Months.

Figure 4.7 shows the medulla ipsilateral (Lesion: Right Panel) and contralateral (Sham: Left Panel) to nVIII lesion in post-operative recovery animals of 1 Day, 1 Week and 2 Months in which fluorescent lipophilic tracer (red-orange fluorescence) had been placed bilaterally into the nVIII. Intact nVIII-medulla connectivity is indicated by red-orange fluorescence in the medulla. Figure 4.7 Chart (Bottom) shows the proportion of red fluorescence measured between ipsi- and contralesional medulla for each animal. Control medulla [no injected tracer (Days Post-Op = 0; Blue Circles; Contralesional (Sham) Medulla = Gray Square, Days Post-Op = 1, 7, 60; Ipsilesional (Lesion) Medulla = Red Triangle, Days Post-Op = 1, 7, 60]. Error bars indicate variance within three measured sections.

Figure 4.8

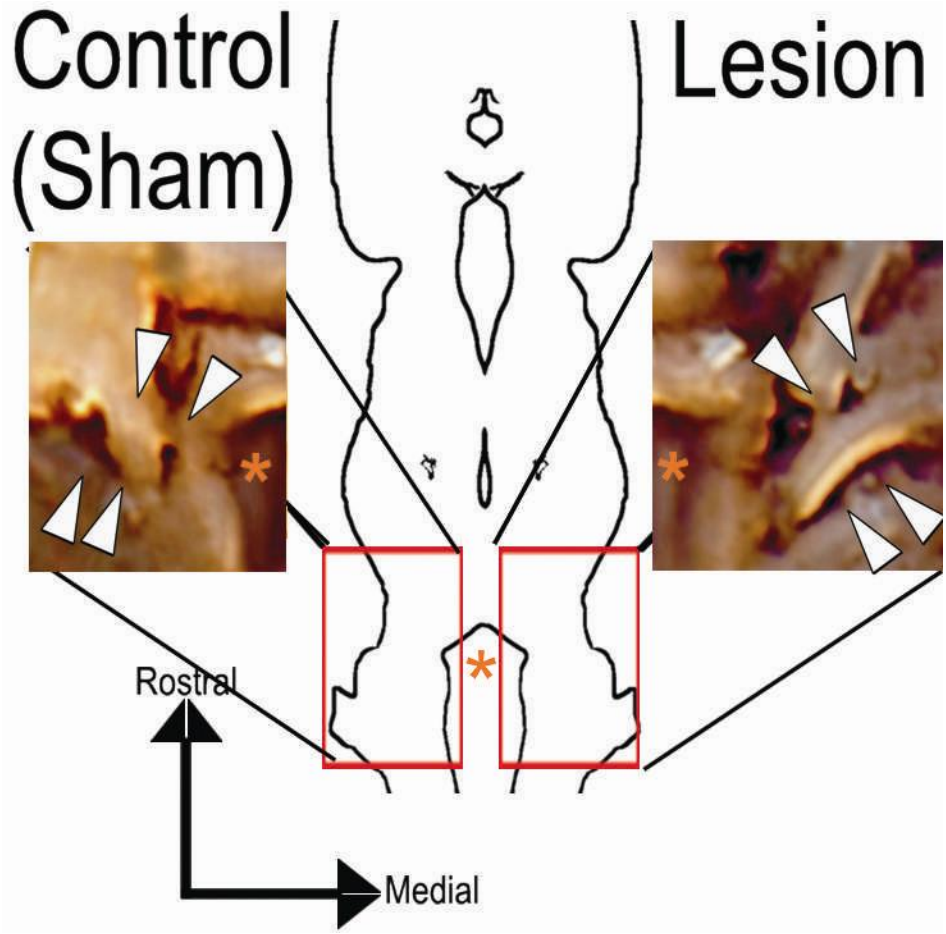

Figure 4.8. Lesioned n.VIII in *Xenopus laevis* appears thicker than sham operated nVIII 24 hours post-lesion.

Figure 4.8 shows a whole mount dorsal view of a sham operated n.VIII (4 arrowheads; Left) and a crush lesioned n.VIII (4 arrowheads; Right) after 24 hours post lesion. The approximate region photographed for each nerve is indicated by the orange boundary (schematic, center). The lesioned n.VIII (Right) appears to have a greater diameter than the sham-operated side in the same animal (Left). a whole mount dorsal view of a sham operated n.VIII (4 arrowheads; Left) and a crush lesioned n.VIII (4 arrowheads; Right) after 24 hours post lesion.

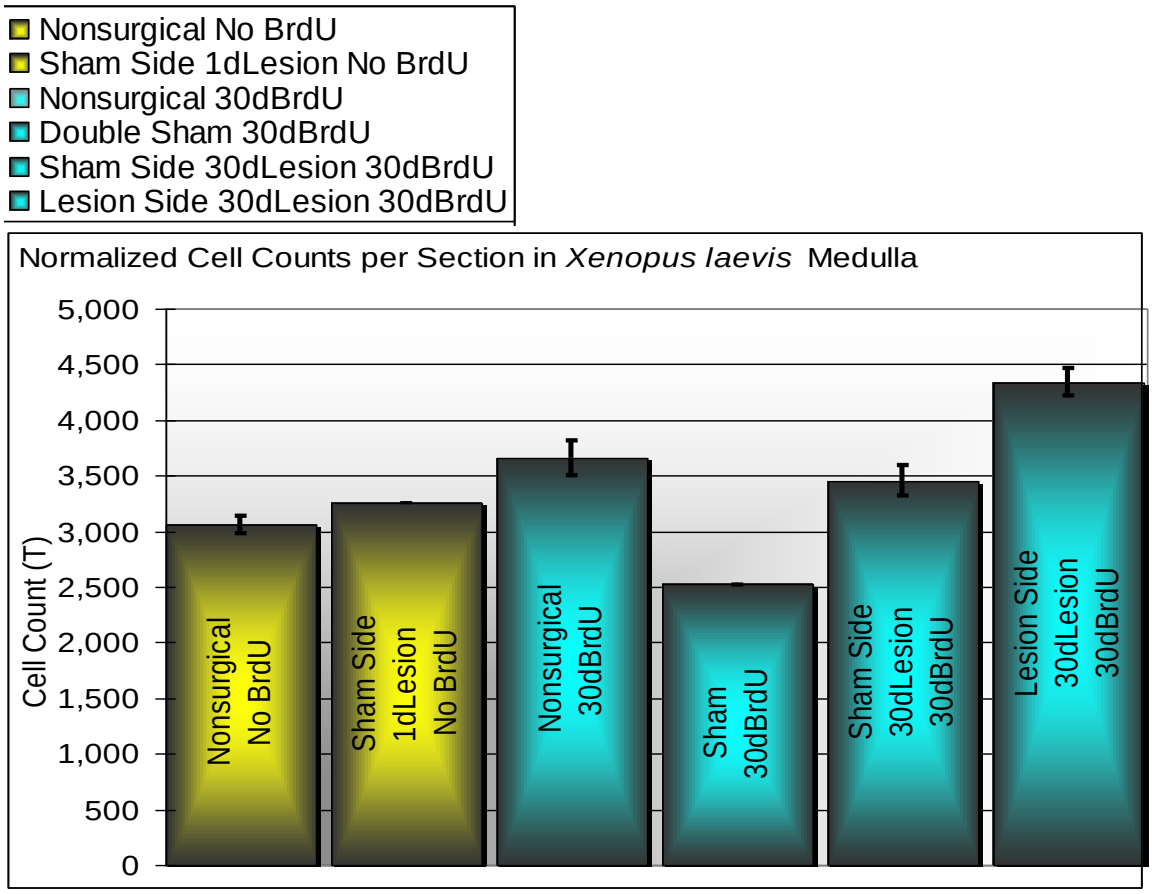

	DAPI					
	Normalized					
	Means					
	Z=30um					
Experimental Group						
	Nonsurgical	1 Day Lesion	Nonsurgical	Double Sham	30 Day Lesion	30 Day Lesion
	No BrdU	No BrdU	30dBrdU	30dBrdU	30dBrdU	30dBrdU
		Contra			Contra	Ipsi
T	3060	3257	3657	2521	3454	4341
SEM	+/- (78.8)	+/- (4.6)	+/- (156.7)	+/- (8.6)	+/- (134.4)	+/- (123.4)

Figure 4.9. DAPI-labeled cell counts (T) in nVIII medullary targets.

Figure 4.9 shows mean DAPI positive cell counts (T; +/- SEM) in nVIII medullary target nuclei of adult *Xenopus laevis*. T is reported as number of cells per 50µm horizontal tissue section for six different experimental conditions. Data are summarized in a bar chart [Non BrdU treated animals (Gold Bars); BrdU treated animals (Blue Bars)] and summary table [(Bottom)]. T (and SEM) are reported for nVIII deafferented nuclei (by crush lesion), sham surgery, and in nonsurgical controls.

Figure 4.10

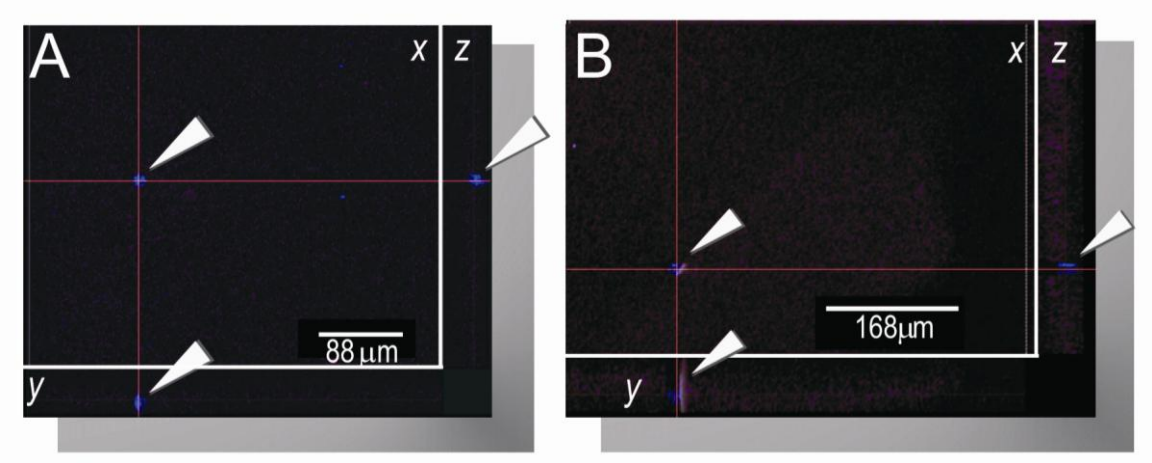

Figure 4.10. BrdU-positive cells are found in nVIII deafferented and sham operated medullary target tissue after one week post operatively.

Figure 4.10 shows example confocal images of BrdU positive cells (in blue) located in nVIII target tissue of the medulla seven days after nVIII lesion (Fig 4.10 A) or bilateral sham (Fig 4.10 B). White arrows and crosshairs in Fig 4.10 A(x) and B(x) show the BrdU positive cell (in blue) rotated in orthogonal planes in Fig 4.10 A(y,z) and B(y,z). Although it is possible to see additional BrdU positive cells, only the cell indicated by the white arrowhead in each image can be viewed in all three orthogonal planes. Scale bar in Fig. 4.10A = 88µm; Fig. 4.10B = 168 µm.

Figure 4.11

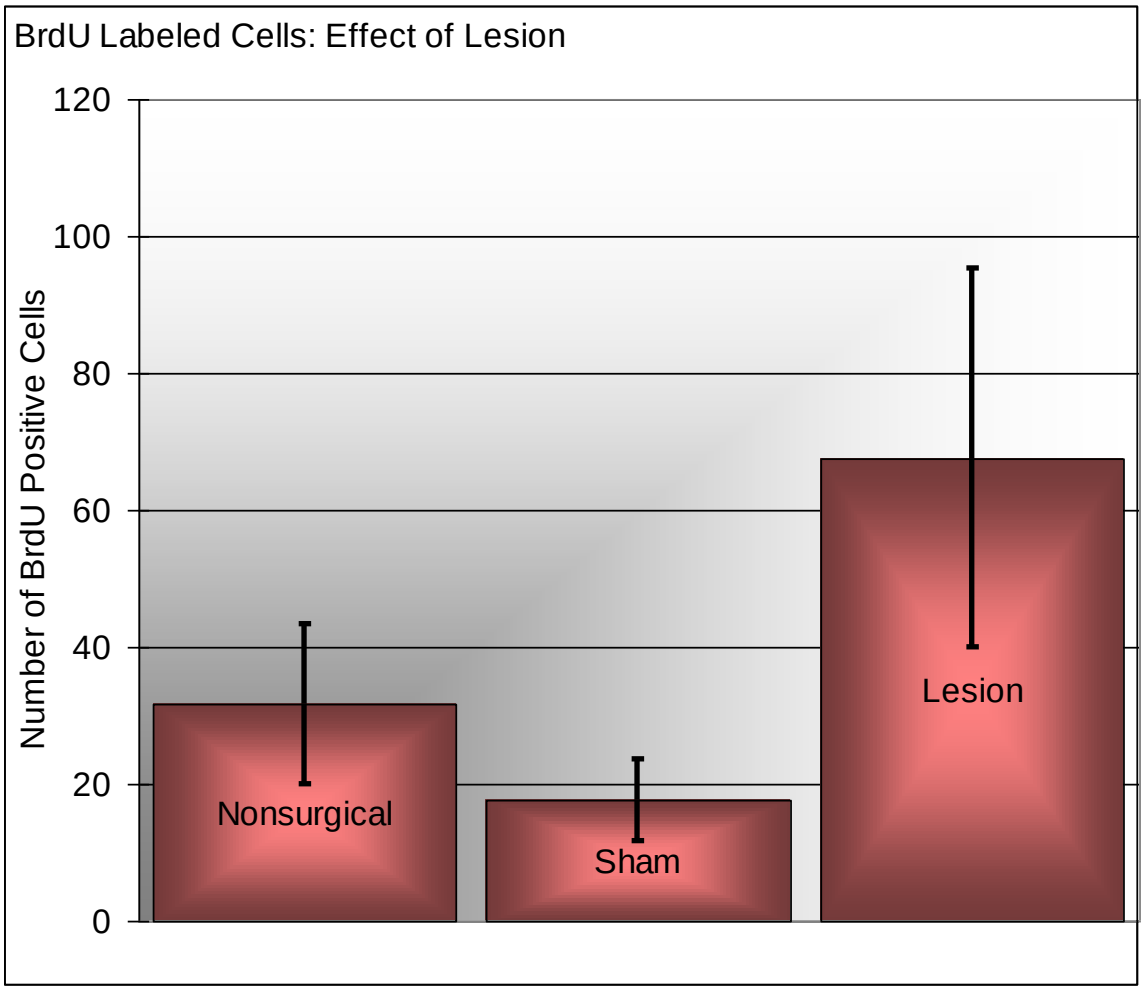

Figure 4.11. BrdU positive cell counts are similar in nonsurgical and sham surgical animals.

Counts of BrdU positive cells in nVIII medullary targets indicate similar findings in nonsurgical (“Nonsurgical”) or sham surgical animals (“Sham”). Statistical analysis of nonsurgical and sham counts indicate no significant difference between the two groups [T- Test; P(T<=t); 0.33, two tailed]. Error Bars = SEM.

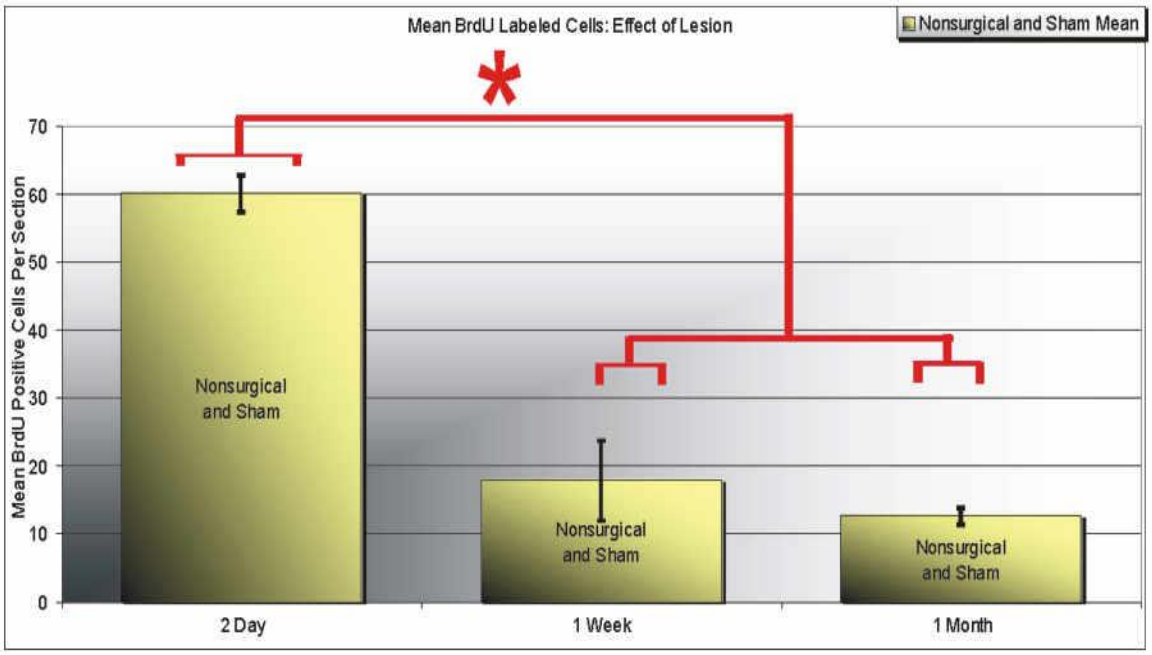

	Nonsurgical and Sham Mean	Nonsurgical and Sham SEM
2 Day	60.1	+/- (2.7)
1 Week	17.8	+/- (5.8)
1 Month	12.6	+/- (1.2)

t-Test: Two-Sample Assuming Unequal Variances		
	2 Day Nonsurgical	7,31 Day Nonsurgical
Mean	60.06	14.70
Variance	14.45	27.47
Observations	2	5
Hypothesized Mean Difference	0	
df	3	
t Stat	12.721	
P(T<=t) two-tail	0.0010	
t Critical two-tail	3.1824	

Figure 4.12. BrdU Positive Cell Counts in Nonsurgical and Sham Surgical Animals are Affected by Recovery Period.

Counts of BrdU positive cells in nVIII medullary targets show higher counts in two day recovery animals "2 Day") than one week "1 Week") or one month survival animals ("1 Month"). Statistical analysis of nonsurgical and sham counts indicate a significant difference between two day survival groups and one week/one month survival animals [T- Test; P(T<=t) = 0.001, two tailed]. Error Bars = SEM.

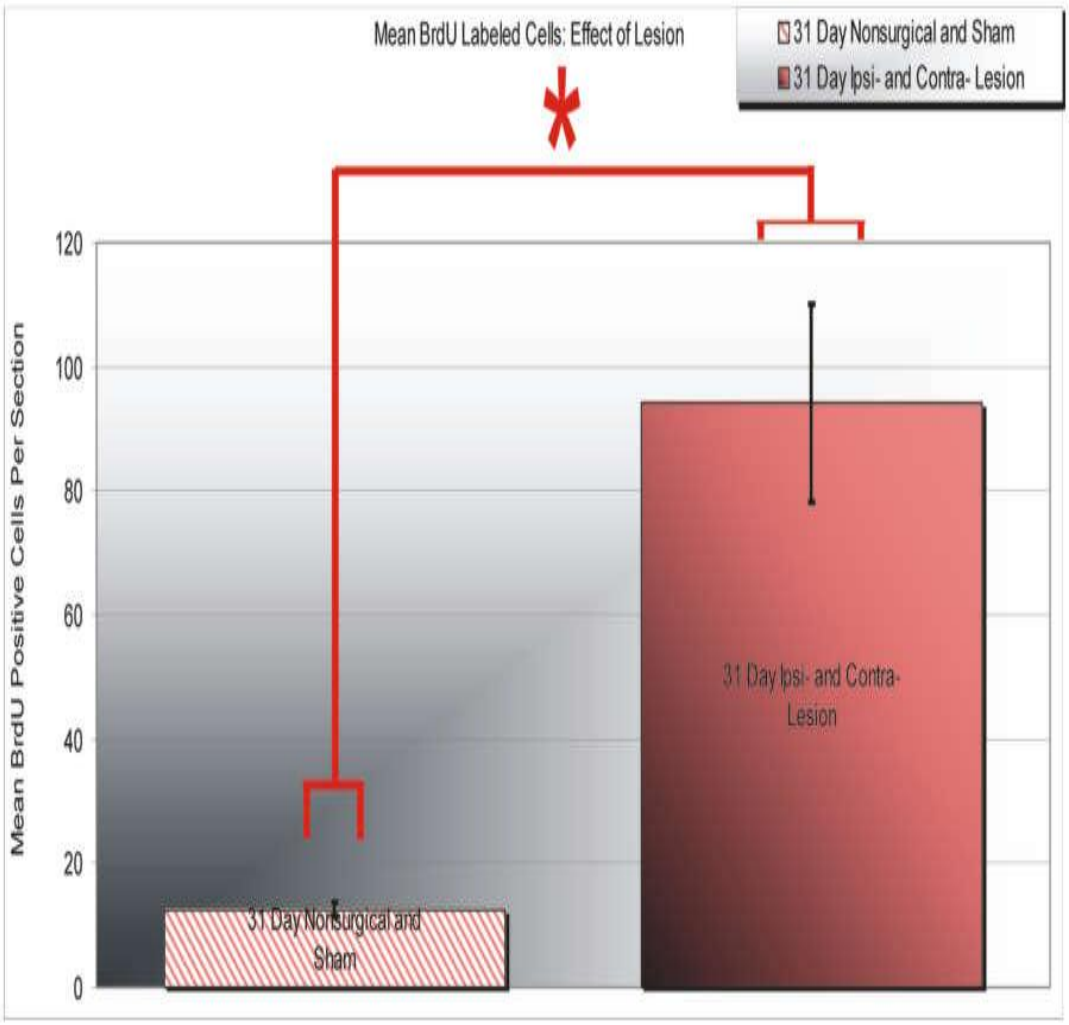

Survival	31 Day Nonsurgical and Sham	31 Day Ipsi- and Contra- Lesion
31 Day	11.2	131.3
	15.0	88.9
	11.6	101.8
		54.5
Mean	12.6	94.1
SEM	+/- (1.2)	+/- (15.9)

t-Test: Two-Sample Assuming Unequal Variances		
	31 Day Nonsurgical	*31 Day Lesion and Contralateral Sham*
Mean	**12.60610717**	**94.12215702**
Variance	**4.516451972**	**1011.471639**
Observations	**3**	**4**
Hypothesized Mean Difference	**0**	
df	**3**	
t Stat	**-5.111016513**	
P(T<=t) one-tail	**0.007245791**	
t Critical one-tail	**2.353363435**	
P(T<=t) two-tail	**0.014491582**	
t Critical two-tail	**3.182446305**	

Figure 4.13. BrdU positive cell counts are increased in long recovery period after n.VIII lesion.

Counts of BrdU positive cells in nVIII medullary targets indicate a significant difference in one month recovery animals between control (1 Month Nonsurgical and Sham surgical") and nVIII lesioned groups (1 Month Ipsi and Contra Lesion"). on increasing cell counts in both the nVIII deafferented medulla (ipsilateral to the lesion), as well as in tissue contralateral to nVIII lesion [mean (+/-SEM); 94.1, (+/- 15.9); T- Test; P(T<=t)= 0.014; two tailed] versus long recovery period nonsurgical and sham surgical animals [; mean (+/-SEM); 12.6, (+/- 1.2)]. Significant effect is shown by asterisk.

Figure 4.14

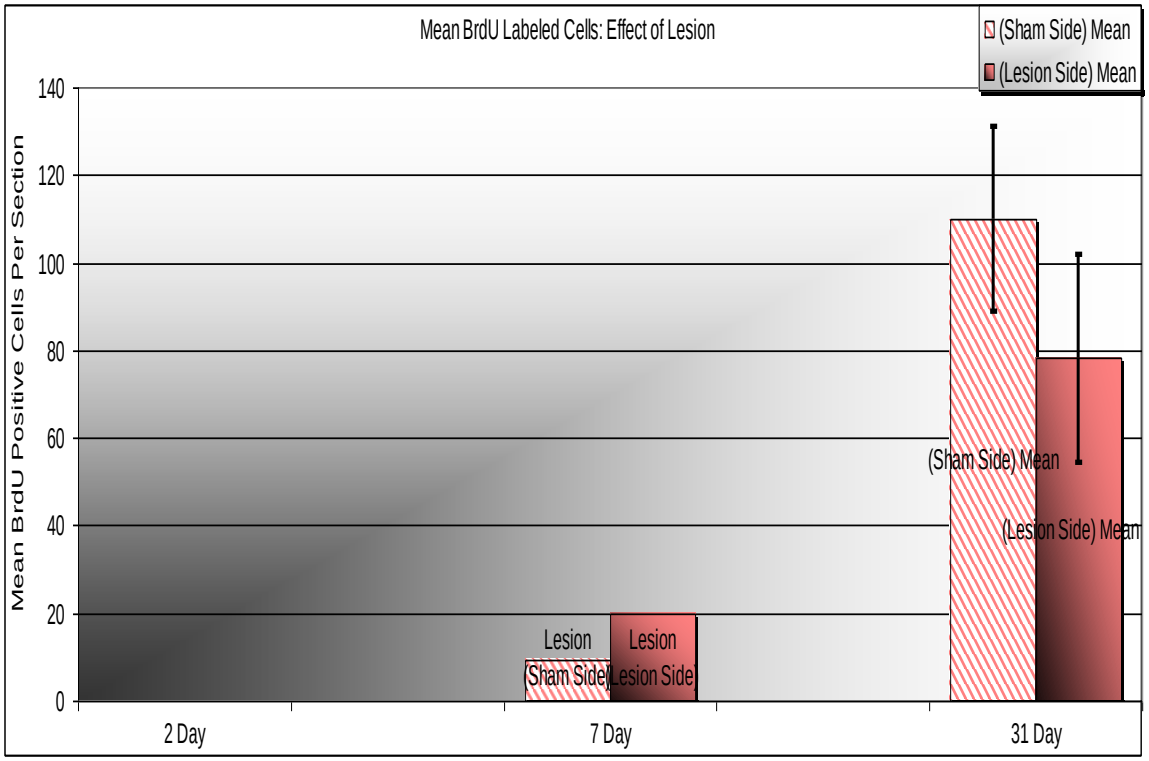

Fig. 4.14: BrdU in Individual Animals Chart

Survival	Nonsurgical and Sham	Lesion (Sham Side)	Lesion (Lesion Side)
2 Day	62.8		
2 Day	57.4		
7 Day	12.0	9.5	19.8
7 Day	23.7		
31 Day	11.2	131.3	101.8
31 Day	15.0	88.9	54.5
31 Day	11.6		

Figure 4.14. BrdU Positive Cell Counts Decrease in Control Animals and Increase in Lesioned Animals At Long Recovery Timepoints.

Counts of BrdU positive cells in nVIII medullary targets indicate a significant difference in long timepoint recovery animals in control animals (Top Chart; "Nonsurgical and Sham surgical") but increase in the sham operated side of lesioned animals and nVIII lesion groups (Fig. 4.14; Bottom Chart; "Sham Side: Lesion" and "Lesion Side: Lesion"). BrdU cell counts from individual animals are shown in the bottom chart for control and lesion condition animals for recovery periods ranging between 2 days and one month.

Figure 4.15

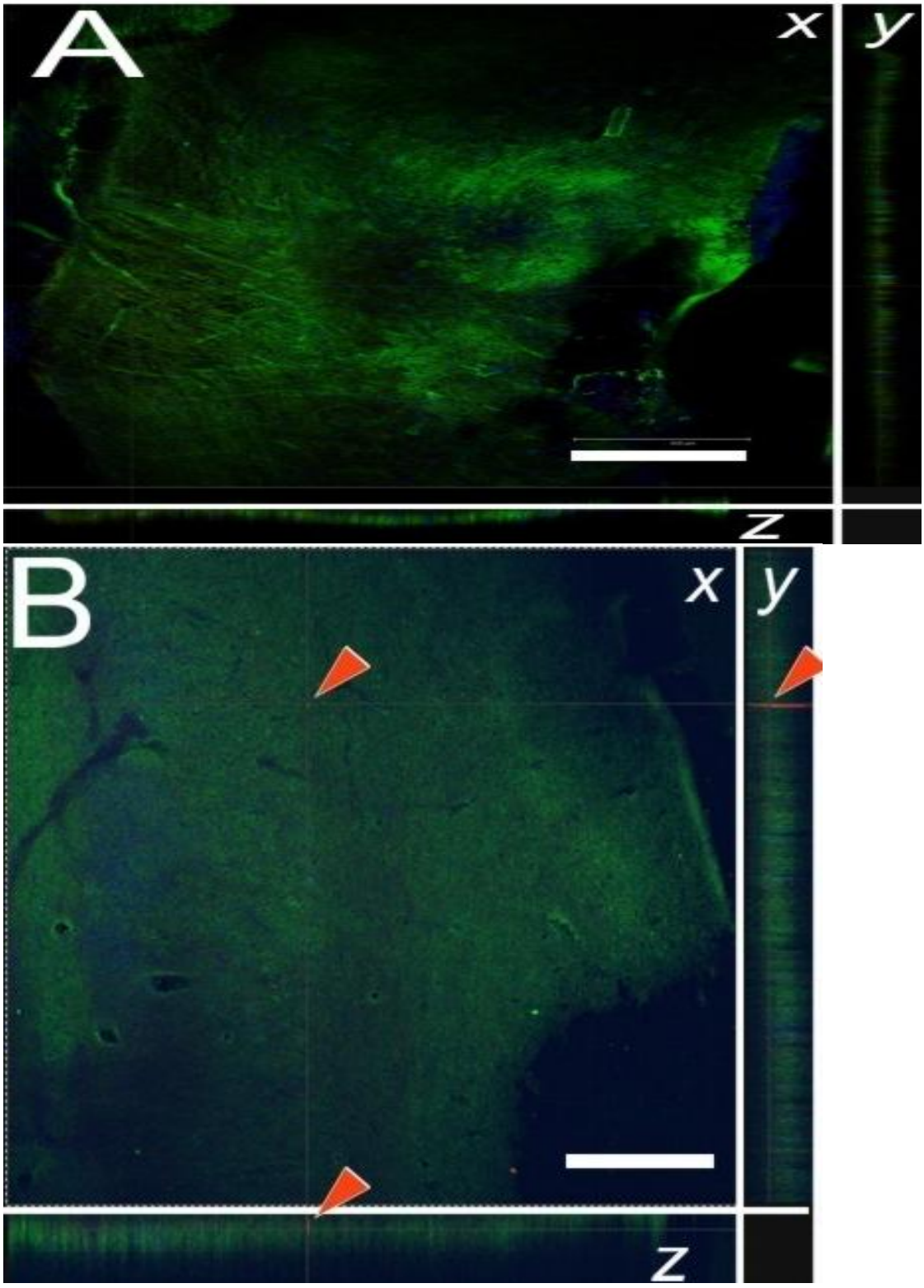

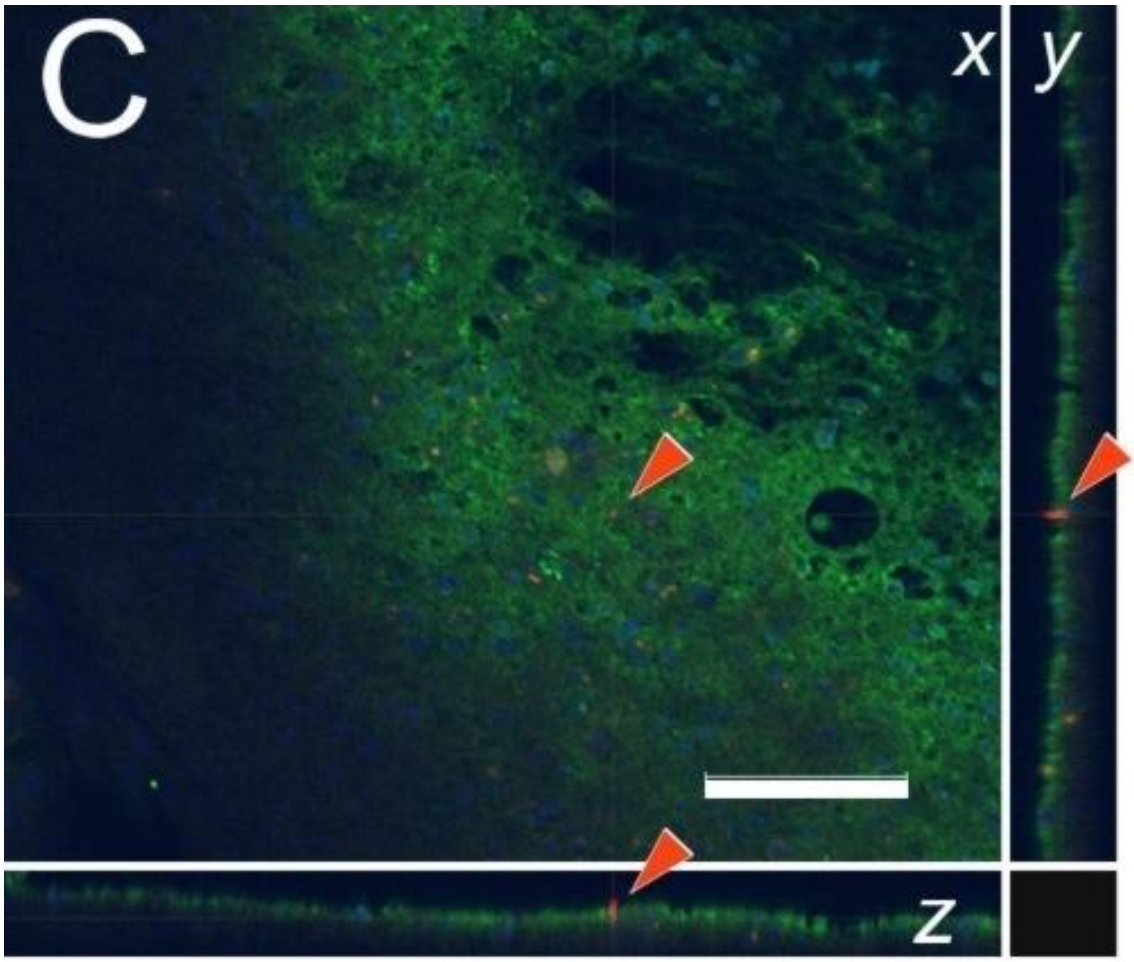

Figure 4.15. BrdU and TOAD-64 are co-localized in *Xenopus laevis* medulla ipsilateral to n.VIII lesion 1 month post-operatively.

Figure 4.15 shows confocal Z stack images rotated in orthogonal planes from results of immunohistochemical localization of BrdU (Red) and TOAD-64 (Green), and DAPI (in blue) in adult *Xenopus laevis* 50µm horizontal sections through the medulla 30 days after sham surgery (shown in A), contralateral n.VIII lesion surgery (B), and in the brain parenchyma after ipsilateral (C) n.VIII crush lesion. Arrows in B and C show BrdU-positive cells in x,y, and z planes.

Figure 4.16

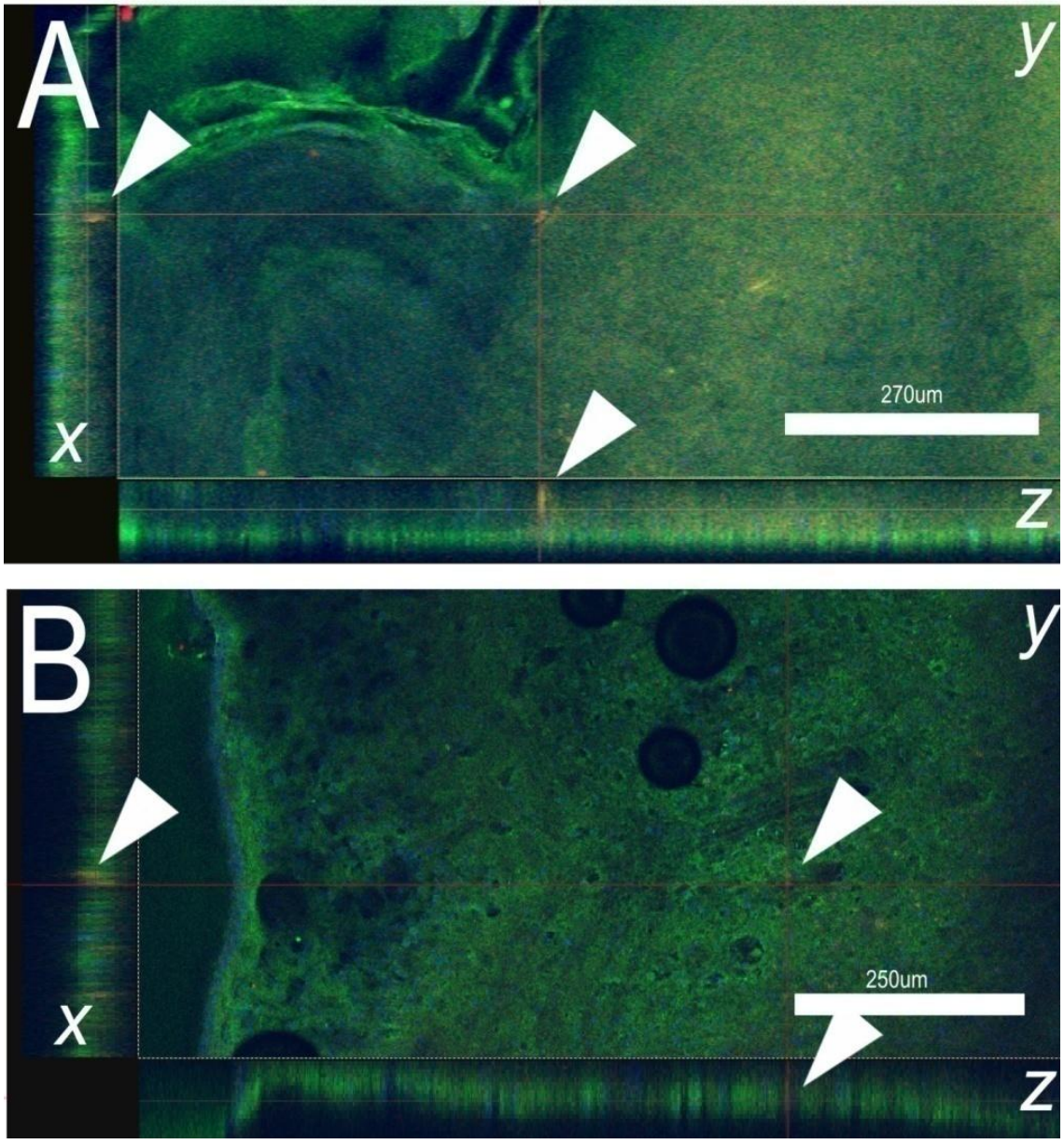

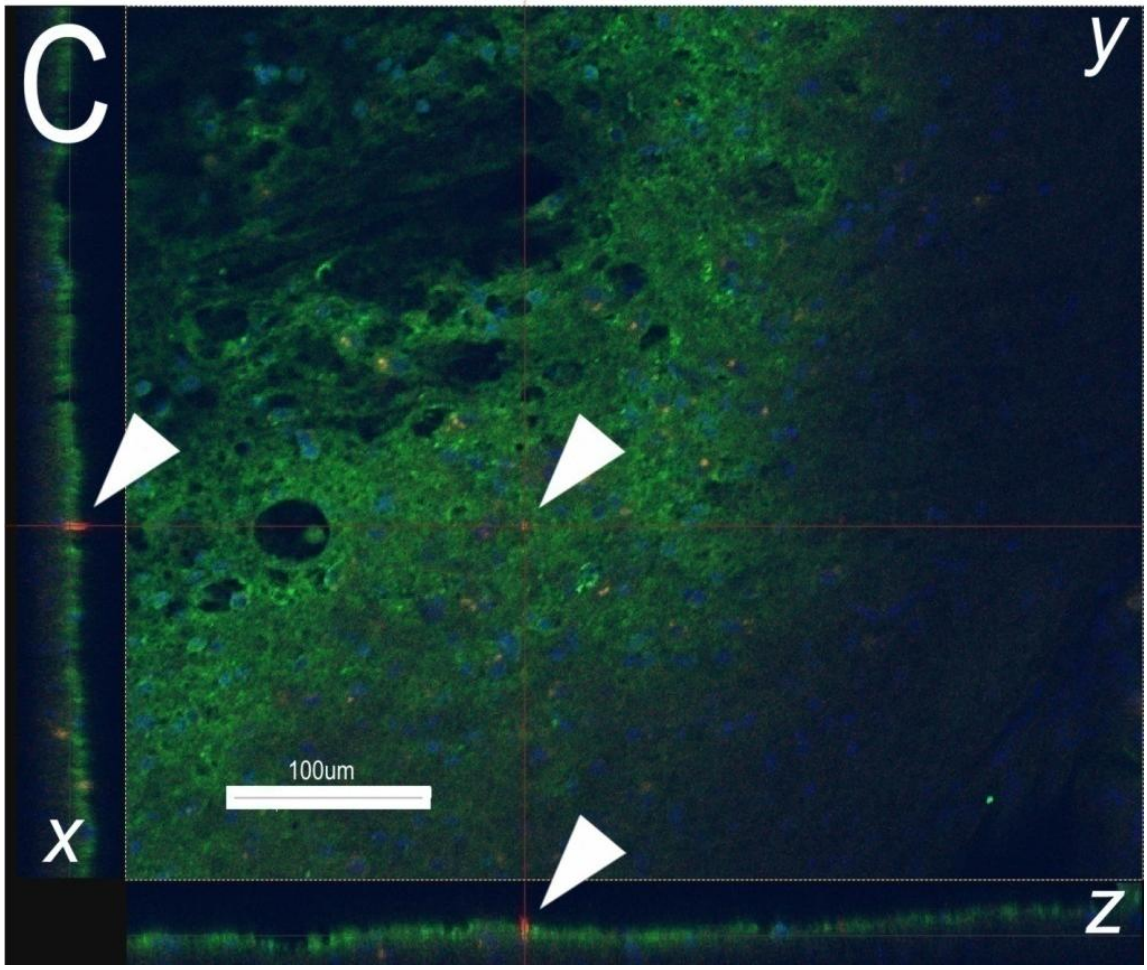

Figure 4.16. BrdU and TOAD-64 are co-localized in *Xenopus laevis* medulla ipsilateral to n.VIII lesion 30 days post-operatively.

Figure 4.16 shows confocal Z stack images rotated in orthogonal planes from results of immunohistochemical localization of BrdU (Red) and TOAD-64 (Green), and DAPI (in blue) in adult *Xenopus laevis* 50µm horizontal sections through the medulla 30 days after contralateral n.VIII lesion surgery a BrdU positive cell is present at the nVIII medulla interface (shown in A),and in the brain parenchyma after ipsilateral (B and C) n.VIII crush lesion. Arrows in A, B and C show BrdU-positive cells in x,y, and z planes.

Figure 4.17

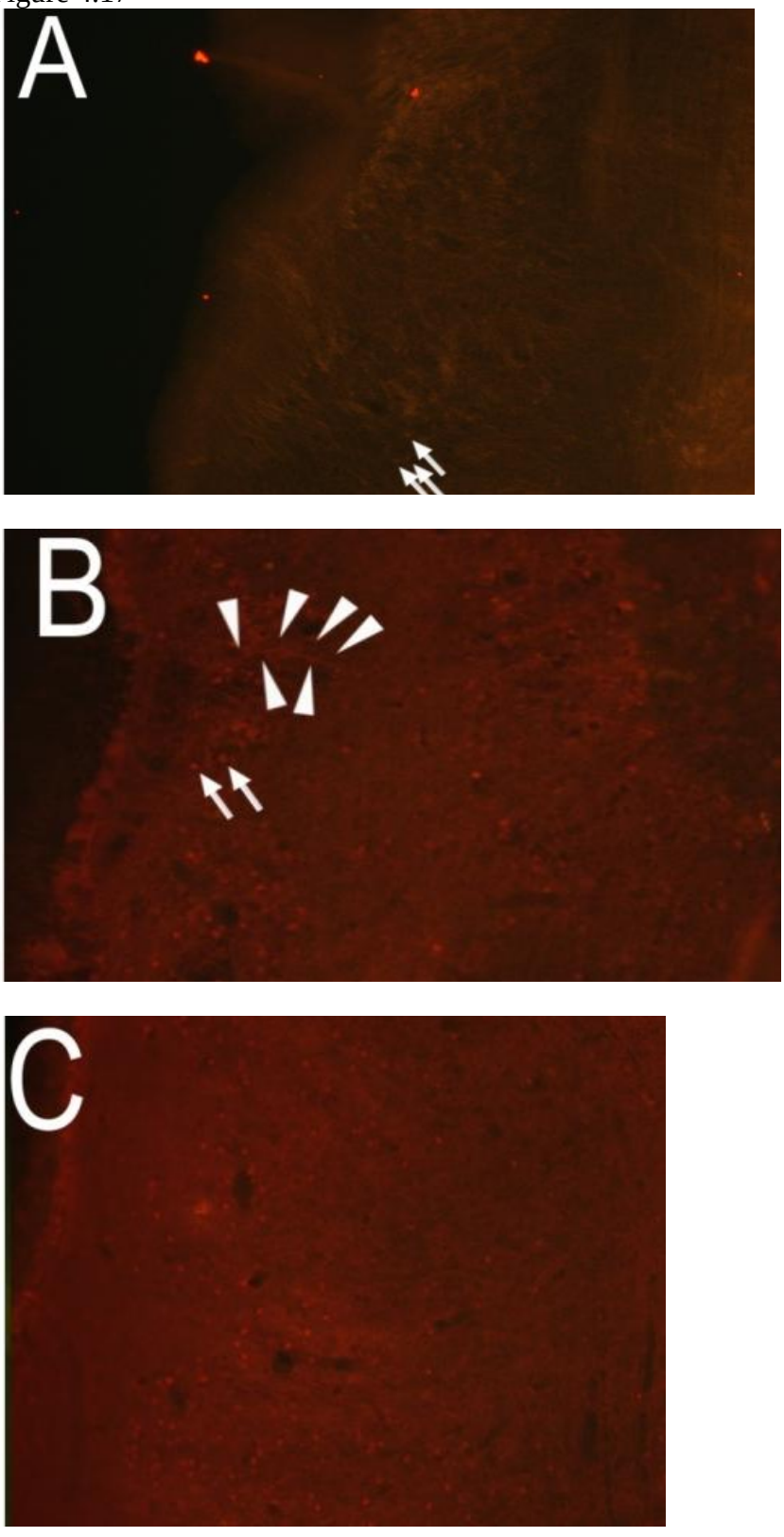

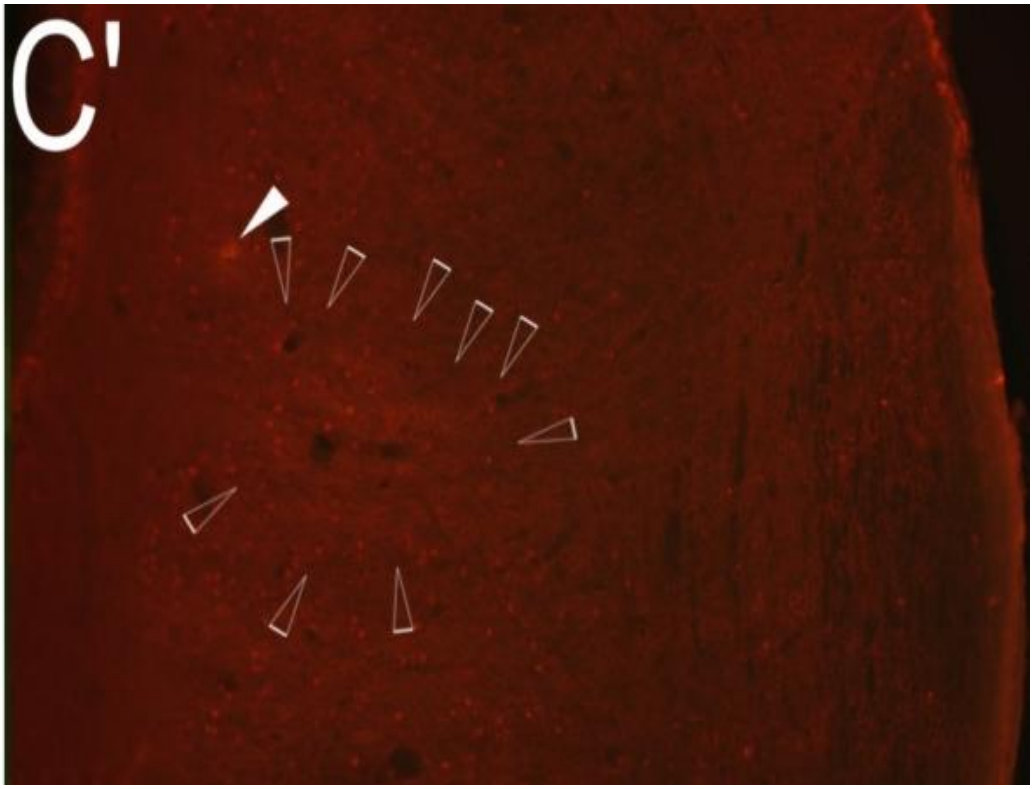

Figure 4.17. GAP-43 is expressed at higher levels in Xenopus laevis neurites ipsilateral to n.VIII lesion 30 days post-operatively.

Figure 4.17 shows 10x magnification fluorescent images taken from *Xenopus laevis* brain tissue subjected to immunohistochemical localization of GAP-43 (Red). Adult *Xenopus laevis* were nonsurgical (shown in Fig4.17), or unilateral n.VIII crush lesion (shown in Fig 4.17C and C'), with contralateral sham (shown in Fig 4.17B). Animals were allowed to recover for 30 days prior to euthanasia and immunohistochemical analysis of the 50µm horizontal sections through the medullary tissue. Fig 4.17A showsThere is qualitatively little to no red fluorescence in nonsurgical animals, and is similar to animals subjected to sham surgery (data not shown), and is largely restricted to cell bodies (Fig 4.17A, nonsurgical condition). In contrast, qualitatively more red fluorescence is detected in the 30 day post-sham medulla (Fig 4.17B) if the contralateral n.VIII is lesioned by crush. Fig 4.17B shows an increase in red fluorescent label over bilateral sham conditions and multiple red fluorescent cell bodies can be seen (Fig 4.17B). In addition there is limited GAP-43 localization in neurites (Fig 4.17B). In medullary tissue ipsilateral to n.VIII lesion (Fig 4.17C and C'), there are many GAP-43 positive cell bodies and neurites (Fig 4.17C and C'). Large concentrations of GAP-43 positive neurites are often found in clusters in the medulla ipsilateral to n.VIII lesion (Fig 4.17C and C'; Fig 4.17 C' shows the same 10x magnification image shown in C, except white dotted boundary indicates a cluster of GAP-43 positive neurites). Auto fluorescent vascular cells are frequently found in the CNS of animals subjected to lesion and must be distinguished from cells labeled with red-fluorescent antibodies (artifact RBC is shown by solid white arrowhead, Fig 4.17C'). Rostral is up and lateral is to the right for all images.

Fig 5.1A: BL1 (arrow) expressed in sham operated n.VIII and medulla (lanes 1,2) 24 hours after n.VIII lesion.

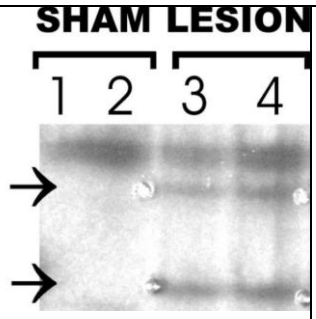

Fig 5.1B: cDNAs, BR1 (top arrow) and BR2 (bottom arrow), ipsilateral (lanes 3,4) but not contralateral (lanes 1,2) to n.VIII lesion in n.VIII and medulla 24 hours post-op.

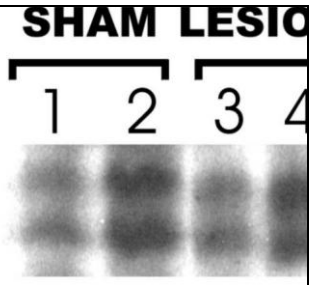

Fig 5.1C: Conservation of gene expression between sham (lanes 1,2) and lesioned (lanes 3,4) tissue, show reproducibility of differential display techniques.

Figure 5.1. Differential display of cDNAs expressed in Rana catesbeiana adult CNS twenty-four hours post unilateral n.VIII lesion.

Figure 5.1 shows an example of differentially expressed cDNAs 24 hours post unilateral n.VIII lesion between the lesioned side (right n.VIII) and sham (left n.VIII) sides of pooled n.VIII and medullary tissue. The DD-PCR reactions and differential display gel was repeated as a control with the same resulting pattern.

Figure 5.1A shows a cDNA, (arrow) expressed in the sham operated tissue (Fig5.1A, lanes 1, 2) not present in the control (lanes 3, 4). Two cDNAs are additionally expressed ipsilateral to the lesion (Fig5.1B, lanes 1, 2), not found contralaterally (Fig5.1B, lanes 3, 4). Most cDNAs did not vary in response to the lesion (Fig5.1C), which was expected, and used as a further control.

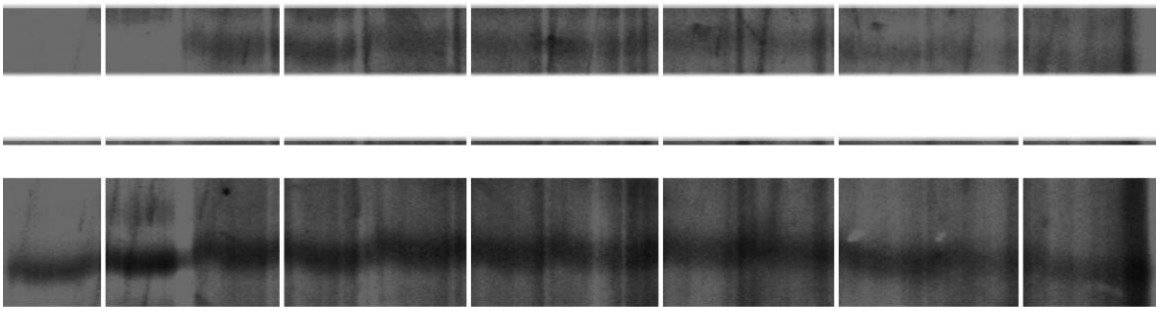

Figure 5.2. Differential display of cDNAs expressed in Xenopus laevis adult CNS 7 days post unilateral n.VIII lesion.

Figure 5.2 shows an example of differentially expressed cDNAs 7 days post unilateral n.VIII lesion between the lesioned side (right n.VIII) and sham (left n.VIII) sides of pooled n.VIII and medullary tissue of Xenopus laevis. Lanes 1 and 2 are tissue samples from a Xenopus laevis subjected to left n.VIII sham (Fig 5.2, Lane 1) and right n.VIII lesion (Fig 5.2, Lane 2), and Lanes 3 and 4 are tissue samples from a Xenopus laevis subjected to left n.VIII lesion (Fig 5.2, Lane 3) and right n.VIII sham (Fig 5.2, Lane 4), both animals are 7 days post operative. Figure 5.2 top shows a cDNA, (Lanes 2,3, Top, arrowhead) expressed in the lesion-operated tissue, not present in the sham operated sides (Fig 5.2, Top; lanes 1, 4, arrowhead) from two separate animals. One cDNA is found in all lanes (Fig 5.2, Bottom, Arrow Lanes 1-4), and is shown as a positive control for all lanes.

Figure 5.3. Nucleotide sequence of BR1 expressed in *Rana catesbeiana* twenty-four hours post n.VIII lesion.

681 bp
DEFINITION BR1

SOURCE n.VIII and medulla
ORGANISM Rana catesbeiana

1..681
BASE COUNT 207 a 125 c 154 g 193 t 2 others
ORIGIN

```
      1 gagttaccaa agctcatcag ccggggctgt ggaacgtctt acagacacaa ccaaatacac
     61 gggatcccac aaggaacgct tcgatgagag tgggaaagga aagggtaaag gtggccggga
    121 gaaccttgtg gaaaacactg gctatgtagg tgcatacaaa catgctggca cttatgagtc
    181 caaggtaaag aaataggaat tcctcaagag gagacagcct accttaactc ctgcatagac
    241 atatttgacc tctttgttcc cagtggtgaa gagcagtcca cagcagtagt gaaggtgatc
    301 atggttctat tctggcccct tctagcacca aagcaagtga atgatttgtg aagnacaaat
    361 attcctaccc ttttatgttg ctaattccaa aaacaagatt ttgttttgat gacatcatgc
    421 acgtctctac aatggttaat tgggtttgag gtatatgcat tgctgttttt gtgtagcagc
    481 tgattatatt gactgctcag ttatcactta tttatgtctg aaaattgaat tacagtttat
    541 tatctgttat aactaacttg ttccgtgatg catgcacatg ctcttcaagt tttcaaagta
    601 aggactacat tttgtgaaaa ctgtaaaggc ctaaagtgaa tgtgtggata caaaaaaaaa
    661 aagcccttag tgggggtcgn a
//
```

Figure 5.4. Nucleotide sequence of BR2 expressed in Rana catesbeiana twenty-four hours post n.VIII lesion.

667 bp
DEFINITION BR2
SOURCE n.VIII and medulla
ORGANISM Rana catesbeiana

1..667
BASE COUNT 228 a 108 c 120 g 207 t 4 others
ORIGIN

```
      1 ataatgttct ggctcacgtt gccccaagca ttcccaaagt ccattgagac catctattgc
     61 atttggtaac cattgggagg gtgacctcna gcattgccat gtgaactctg gtcacgatat
    121 aagtcagaat atgaccagga taacaacgta tctctgatca tatcatgtac tgaactacct
    181 aaaacacacc aggattctag aattctggaa ggctgtgnaa aaaaatctga aaatggaatt
    241 aggacctggc tgctttatgg actanaggca gcttaaatga gtgatcgcag gttctcttta
    301 aatgtcaggc gttccaggtc attgtctttt caattagctt ttgaaatgtg aaccatattc
    361 aagtttgtac cgctatagtg ttaaatctgt tttcttatta cctgaattgc attgtgttct
    421 taaatattat attttatgtt attngagcaa ccgctaatga aaataatata taaaggaaat
    481 gtgaaaatgt acctaagctt atattattct gcacagtaac atatttaaaa catgttgtac
    541 agaaatgttt gtcaatgtaa ataacattat gttaatgcat ctataagaag aataattgaa
    601 agtaagcaaa ataataaaaa gctctatttg aactacaaaa aaaaaaaagc cctatagtgg
    661 ggtcgga
//
```

Figure 5.5. Nucleotide sequence of BL2 expressed in Rana catesbeiana twenty-four hours post n.VIII lesion.

833 bp
DEFINITION BL2
SOURCE n.VIII and medulla
ORGANISM Rana catesbeiana
1..833
BASE COUNT 304 a 147 c 190 g 181 t 11 others
ORIGIN

```
      1 agagagcata ctggtagagg gccaaggana aaagcttaga ggaagtgcaa atagaacaaa
     61 gtgagattat tgtttcgaaa gctatctctg aaattgttga tattgacagg catgagttag
    121 tcacatacgt tcttacagca caggtgagag aagaagcaga gcttatgcat ttggactctt
    181 caattgaatt accctcaact gaaacaacca aatctgagac aatggaatta gttgtggaga
    241 aggaatacac tanngggaa aagtctgagg attctgaaca gttgccaata cttnaagaga
    301 ctgacacaga tgagaaacta aaagttgaag tggatgaaac cttaacagag gatgttgatg
    361 ttgataagga atcacctaca gacagcatga aagtaaaggg caaatccaaa aagcacagga
    421 aagagattgc aaaggttgan aaaacantca gaactgtaaa gactactggt gtagaagcta
    481 tttctcctac gcttgagctt cacctagcca cccctgaaat aaagactgta gcggaagagg
    541 gtgaagtaaa ggaagcttct ccacaatccc aagtcactgt gtcagcttat gaagagcaag
    601 aacaagtcag cacaccaaca actgaaacca ccatcattca agtatcagtt aaacctgaag
    661 aaggtgttga aaaagcagca actgtanaag atgtctctac tgagacaata acagcagaag
    721 aggaggaaga gaagtctttc ggatggaagt tgcccacatt caaaattcca ctctttagng
    781 ctacagacgt tactgganaa tcttctgngg atgagtccag tgtaatanct cca
//
```

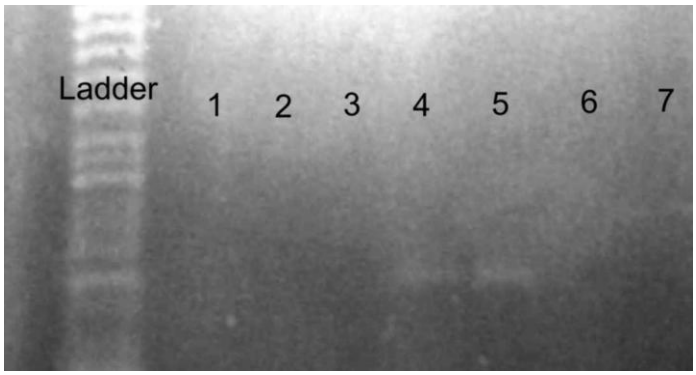

Figure 5.6. <u>BR1 Specific Primers Amplify a Band in *Rana catesbeiana* 41 Days Post-Lesion.</u>
Primers specific for the DD-PCR-generated band, BR1 (see Fig 5.1) were generated to specifically reamplify the BR1 band using PCR with new *Rana catesbeiana* tissue to investigate whether BR1 expression was upregulated in response to the lesion and if it were upregulated after 24 hours post lesion. A molecular mass ladder was run in Lane 1. In lanes 2 and 3, are results from a nonsurgical control animal indicating that BR1 is not expressed in unoperated n.VIII or medulla (Fig5.6; Lanes 2 and 3). Further, BR1 expression is upregulated sometime between 1 hour and 24 hours pot lesion, as BR1 was not found in tissue ipsilateral (Fig5.6; Lane 6) or contralateral (Fig5.6; Lane 7) to n.VIII lesion after 1 hour of recovery. Surprisingly however, BR1 was confirmed in tissue 41 days post surgically both ipsilateral (Fig5.6; Lane 4) and contralateral (Fig5.6; Lane 5) to the n.VIII lesion.

REFERENCES

Aberg, MA., Aberg, ND., Hedbäcker, H., Oscarsson, J., Eriksson ,PS. (2000) Peripheral infusion of IGF-I selectively induces neurogenesis in the adult rat hippocampus. J Neurosci. 20(8):2896-903.

Absil P, Pinxten R, Balthazart J, Eens M. 2003. Effect of age and testosterone on autumnal neurogenesis in male European starlings (Sturnus vulgaris). Behav Brain Res 143: 15-30.

Agata, K., Saito, Y., Nakajima, E. (2007). Unifying principles of regeneration I: Epimorphous versus morphallaxis. Develop Growth Differ (49): 73-78.

Altman, J. (1962). Are new neurons formed in the brains of adult mammals? Science. 135: 1127–1128.

Altman JS., Dawes EA.1983. A cobalt study of medullary sensory projections from lateral line nerves, associated cutaneous nerves, and the VIIIth nerve in adult Xenopus. J Comp Neurol 213(3): 310-326.

Alvarez-Buylla A, Lim DA. 2004. For the long run: maintaining germinal niches in the adult brain. Neuron. 41(5):683-6.

Alvarez-Buylla A, Theelen M, Nottebohm F. 1988. Birth of projection neurons in the higher vocal center of the canary forebrain before, during, and after song learning. Proc Natl Acad Sci USA 85:8722-8726.

Ausubel FM, Brent R, Kingsteon RE, Moore DD, eds. (1997) Short Protocols in Molecular Biology, third edition. New York: Wiley.

Becker T, Becker CG, Niemann U, Naujoks-Manteuffel C, Bartsch U, Schachner M, Roth G (1995) Immunohistological localization of tenascin-C in the developing and regenerating retinotectal system of two amphibian species. The Journal of Comparative Neurology 360(4): 643-57.

Bendotti C, Baldessari S, Samanin R, De Biasi S. 1994.Ultrastructural immunolocalization of GAP-43 in the sprouted mossy fibres of kainic acid lesioned rats. Neuroreport. 5(18):2645-8.

Bendotti C, Servadio A, Samanin R. 1991. Distribution of GAP-43 mRNA in the brain stem of adult rats as evidenced by in situ hybridization: localization within monoaminergic neurons. J Neurosci. 11(3):600-7.

Benowitz LI, Perrone-Bizzozero NI, Neve RL, Rodriguez W. 1990. GAP-43 as a marker for structural plasticity in the mature CNS. Prog Brain Res 86: 309–320.

Benowitz LI, Routtenberg A, 1997. GAP-43: an intrinsic determinant of neuronal development and plasticity. Trends Neurosci 20: 84–91.

Benraiss A, Chmielnicki E, Lerner K, Roh D, Goldman SA.(2001) Adenoviral brain-derived neurotrophic factor induces both neostriatal and olfactory neuronal recruitment from endogenous progenitor cells in the adult forebrain. J Neurosci. 21(17):6718-31.

Berkelaar M, Clarke DB, Wang YC, Bray GM, Aguayo AJ. (1994) Axotomy results in delayed death and apoptosis of retinal ganglion cells in adult rats. J Neurosci. 14(7):4368-74.

Black, FO. 2001. What can posturography tell us about vestibular function? Annals NY Acad Sci 446-464.

Blaschke AJ, Weiner JA, Chun J (1998). Programmed cell death is a universal feature of embryonic and postnatal neuroproliferative regions throughout the central nervous system. J Comp Neurol.396(1):39-50..

Billinton N, Knight AW.(2001) Seeing the wood through the trees: a review of techniques for distinguishing green fluorescent protein from endogenous autofluorescence.Department of Biomolecular Sciences, University Anal Biochem.291(2):175-97.

Boatright-Horowitz S, Simmons AM. 1995. Post metamorphic changes in auditory sensitivity of the bullfrog midbrain. J Comp Physiol A 177: 577-590.

Boatright-Horowitz SS, Garabedian CE, Odabashian KH, Simmons AM. 1999. Coding of amplitude modulation in the auditory midbrain of the bullfrog (Rana catesbeiana) across metamorphosis. J Comp Physiol A 184: 219-231.

Boatright-Horowitz SS, Simmons AM. 1997. Transient “deafness” accompanies auditory development during metamorphosis from tadpole to frog. Proc Natl Acad Sci USA 94: 14877-14882.

Bradford M. 1976. A rapid and sensitive method for the quantitation of microgram quantities of protein utilizing the principle of protein-dye binding. Anal. Biochem. 72: 248-254.

Brunk UT, Terman A .(2002) Lipofuscin: mechanisms of age-related accumulation and influence on cell function. Free Radic Biol Med.33(5):611-9.

Buffo A, Zagrebelsky M, Huber AB, Skerra A, Schwab ME, Strata P, Rossi F. (2000) Application of neutralizing antibodies against NI-35/250 myelin-associated neurite growth inhibitory proteins to the adult rat cerebellum induces sprouting of uninjured purkinje cell axons. J Neurosci.20(6):2275-86.

Burggren WW, Infantino RL. 1994 The respiratory transition from water to air breathing during amphibian metamorphosis. Amer Zool 34: 238-246.

Cant NB. 1998. Structural development of the mammalian central auditory pathways. In: Rubel EW, Popper AN, Fay RR, editors. Development of the auditory system. New York: Springer-Verlag, p 315-413.

Carbonetto S (1991) Facilitatory and inhibitory effects of glial cells and extracellular matrix in axonal regeneration. Curr Opin Neurobiol 1: 407-413.

Caston J (1995) Vestibular compensatin in the European green frog (Rana esculenta L.) and effect of training on compensation. Brain, behavior and evolution 45: 266-271.

Cayre M, Malaterre J, Scotto-Lomassese S, Strambi C, Strambi A. 2002. The common properties of neurogenesis in the adult brain: from invertebrates to vertebrates. Comp Biochem Physiol B Biochem Mol Biol 132: 1-15. 7

Clorfene JB, Pollack ED. 1994. Late-generated cells in the lateral motor columns of developing frog spinal cord. Brain Res Dev Brain Res 79: 93-100.

Coe CL, Kramer M, Czeh B, Gould E, Reeves AJ, Kirschbaum C, Fuchs E. 2003. Prenatal stress diminishes neurogenesis in the dentate gyrus of juvenile rhesus monkeys. Biol Psychiatry 54: 1025-1034.

Craig AM, Huttner WB.(2007) Neuronal and glial cell biology. Curr Opin Neurobiol.17(5):505-6.

Cooper-Kuhn CM, Kuhn HG. 2002. Is it all DNA repair? Methodological considerations for detecting neurogenesis in the adult brain. Brain Res Dev Brain Res 134: 13-21.

Cotanche DA, Lee KH (1994) Regeneration of hair cells in the vestibulocochlear system of birds and mammals. Curr Biol 4:509-514.

Curthoys IS, Halmagyi GM, Dai MJ. (1991) The acute effects of unilateral vestibular neurectomy on sensory and motor tests of human otolithic function. Acta Otolaryngol Suppl. 481:5-10.

Curthoys & Halmagyi, 1995. Vestibular compensation: a review of the oculomotor, neural, and clinical consequences of unilateral vestibular loss. J Vestib Res. 5(2):67-107.

Darlington CL, Smith PF (2000) Molecular mechanisms of recovery from vestibular damage in mammals: recent advances. Prog Neurobiol 62: 313-325.

Darsalia V, Heldmann U, Lindvall O, Kokaia Z. (2005) Stroke-induced neurogenesis in aged brain. Stroke 36(8):1790-5.

Denver RJ. 1998. The molecular basis of thyroid hormone-dependent central nervous system remodeling during amphibian metamorphosis. Comp Biochem Physiol C Pharmacol Toxicol Endocrinol 119: 219-228.

DeWulf and Bottjer 2002. Age and sex difference in mitotic activity within the zebrafinch telencephalon. J. Neurosci 22(10): 4080-4094.

Dewulf V, Bottjer SW. 2005. Neurogenesis within the juvenile zebra finch telencephalic mventricular zone: a map of proliferative activity. J Comp Neurol 481: 70-83.

Diaz ME, Varela-Ramirez A, Serrano EE. 1995. Quantity, bundle types, and distribution of hair cells in the sacculus of Xenopus laevis during development. Hear Res 91: 33-42.

Dieringer N (1995) Vestibular compensation: Neural plasticity and its relations to functional recovery after labyrinthine lesions in frogs and other vertebrates. Prog. Neurobiol. 46: 97-129

Dieringer N, Precht W (1982). Compensatory head and eye movements in the frog and their contribution to stabilization of gaze. Exp Brain Res 47: 394-406

Doetsch, F. and Scharff, C. (2001) Challenges for Brain Repair: Insights from Adult Neurogenesis in Birds and Mammals. Brain Behavior and Evolution. 58: 306–322.

Doster et al.,1991

Dawson, A., King,V.M., Bentley, G.E., and Ball, G.F. (2001) Photoperiodic control of seasonality in birds. Journal of Biological Rhythms 16(4): 365-380.

Dunlop 2003

Eriksson PS, Perfilieva E, Björk-Eriksson T, Alborn AM, Nordborg C, Peterson DA, Gage FH. (1998) Neurogenesis in the adult human hippocampus. Nat Med. 4(11):1313-7.

Fallon J, Reid S, Kinyamu R, Opole I, Opole R, Baratta J, Korc M, Endo TL, Duong A, Nguyen G, Karkehabadhi M, Twardzik D, Patel S, Loughlin S. (2001) In vivo induction of massive proliferation, directed migration, and differentiation of neural cells in the adult mammalian brain. Proc Natl Acad Sci U S A. b97(26):14686-91. Erratum in: Proc Natl Acad Sci U S A 98(14):8157.

Fawcett and Asher 1999Fawcett JW, Asher RA. 1999. The glial scar and central nervous system repair. Brain Res Bull. 49(6):377-91.

Fawcett JW (1992) Intrinsic neuronal determinants of regeneration. Trends Neurosci 15: 5-8.

Fernandez A, Radmilovich M, Trujillo-Cenoz O. 2002. Neurogenesis and gliogenesis in the spinal cord of turtles. J Comp Neurol 453: 131-144.

Font E, Desfilis E, Pérez-Cañellas M, Alcántara S, García-Verdugo JM.(1991) 3 Acetylpyridine-induced degeneration and regeneration in the adult lizard brain: a qualitative and quantitative analysis. Brain Res. 754(1-2):245-59.

Font C, Casals C, Kaifi T, Coll E, Cid J, Villalta J, Grau JM. (1997) Constitutional syndrome and lumbar pain. Postgrad Med J.73(863):599-601.

Font E, Desfilis E, Pérez-Cañellas MM, García-Verdugo JM (2001) Neurogenesis and neuronal regeneration in the adult reptilian brain. Brain Behav Evol.58(5):276-95.

Fournier AE, Strittmatter SM (2001) Repulsive factors and axon regeneration in the CNS. Current Opin Neurobiol 11: 89-94.

Frank E, Sah DW (1986) Reformation of specific synaptic connections by regenerating sensory axons in the spinal cord of the bullfrog. Neurochem Pathol 5: 165-185.

Fritz A, Gorlick DL, Burd GD. 1996. Neurogenesis in the olfactory bulb of the frog Xenopus laevis shows unique patterns during embryonic development and metamorphosis. Int J Dev Neurosci 14: 931-943.

Fritzsch B, Nikundiwe AM, Will U. 1984. Projection patterns of lateral line afferents in anurans: a comparative HRP study. J Comp Neurol 229: 451-469.

Fuchs and Gould 2000

Gage, 2000

Garcia-Verdugo, J.M., Ferron, S., Flames, N., Collado, L. Desfilis, E., and Font, E. (2002) The proliferative ventricular zone in adult vertebrates: A comparative study using reptiles, birds, and mammals. Brain Research Bulletin 57(6): 765-775.

Gaze RM (1959) Regeneration of the optic nerve in Xenopus laevis. Q J Exp Physiol 44: 290-308.

Gaze RM, Jacobson M (1963) A study of the retinotectal projection during regeneration of the optic nerve in the frog. Proc R Soc London Ser B 17: 420-448.

Gervasi C, Thyagarajan A, Szaro BG. (2003) Increased expression of multiple neurofilament mRNAs during regeneration of vertebrate central nervous system axons. J Comp Neurol 461(2):262-75.

Gilbert SF. 2000. Developmental Biology (sixth edition). Massachusetts: Sinauer Associates.

Goergen EM, Bagay LA, Rehm K, Benton JL, Beltz BS. 2002. Circadian control of neurogenesis. J Neurobiol 53: 90-95.

Goldberg, JL and Barres, BA (2000) The relationship between neuronal survival and regeneration Annu.Rev. Neurosci.2000;23:579-612. Review.

Golding JP, Tonge DA. 1993. Expression of GAP-43 in normal and regenerating nerves in the frog. Neurosci 52: 415–426.

Goldman and Nottebohm 1983, 1998

Goridis C, Brunet JF. 1999. Transcriptional control of neurotransmitter phenotype. Curr Opin Neurobiol 9: 47-53.

Gorlick DL, Kelley DB. 1987. Neurogenesis in vocalization pathway of Xenopus laevis. J Comp Neurol 257: 614-627.

Gosner KL. 1960. A simplified table for staging anuran embryos and larvae with notes on identification. Herpetologica 16: 183-190.

Goto, F. Straka, H., Dieringer, N. 2001. Postlesional Vestibular Reorganization in Frogs: Evidence for a Basic Reaction Pattern After Nerve Injury. J Neurophysiol 85:2643-2646.

Goto, F. Straka, H., Dieringer, N. (2002) Gradual and reversible central vestibular reorganization in frog after selective labyrinthine nerve branch lesions. Exp Brain Res 147:374–386

Goldman, S.A. (1998) Adult Neurogenesis: From Canaries to the Clinic. Journal of Neurobiology 36: 267–286.

Goldman, S.A. and Nottebohm, F. (1983) Neuronal production, migration and differentiation in a vocal control nucleus of the adult female canary brain. Proc Natl. Acad. Sci. USA 80: 2390-2394.

Gould, E. and Tanapat, P. (1999) Stress and hippocampal neurogenesis. Biol Psychiatry. 46:1472–9.

Gould, E., Beylin, A., Tanapat, P., Reeves, A., and Shors, T.J. (1999) Learning enhances adult neurogenesis in the hippocampal formation. Nature Neuroscience. 2: 260–5.

Gould E, Gross CG. 2002. Neurogenesis in adult mammals: some progress and problems. J Neurosci 22: 619-623.

Gould E, Tanapat P, Cameron HA. (1997) Adrenal steroids suppress granule cell death in the developing dentate gyrus through an NMDA receptor-dependent mechanism. Brain Research. Developmental Brain Research. 103: 91–3.

Gould, E., Tanapat, P., McEwen, BS., Flugge, G., and Fuchs, E. (1998). Proliferation of granule cell precursors in the dentate gyrus of adult monkeys is diminished by stress. mProceedings of the National Academy of Sciences USA. 95: 3168-3171.

Gould, E., Tanapat, P., Hastings, N.B., and Shors, T.J. (1999). Neurogenesis in adulthood: a possible role in learning. Trends in Cognitive Sciences. 3(5): 186-192.

Greeve I, Hermans-Borgmeyer I, Brellinger C, Kasper D, Gomez-Isla T, Behl C, Levkau B, Nitsch RM (2000) The Human DIMINUTO/DWARF1 homolog Seladin-1 confers resistance to Alzheimer's disease-associated neurodegeneration and oxidative stress. J. Neurosci. 20:7345-7352.

Grill RJ, Tuszynski MH (1999) Axonal responses to injury. In CNS Regeneration, MH Tuszynski, J Kordower, eds. New York: Academic Press, pp. 27-53.

Hafidi A, Lanjun G, Sanes DH (1999). Age-dependent failure of axon regeneration in organotypic cultures of gerbil auditory midbrain. J. Neurobiol. 41: 267-280.

Hamalgyi GM, Curthoys IS, Cremer PD, Henderson CJ, Todd MJ, Staples MJ, D'Cruz DM (1990) The human horizontal vestibule-ocular reflex in response to highm accereration before and after unilateral vestibular neurectomy. Exp Brain Res 81: 479 490.

Hatten ME. 1999. Central nervous system neuronal migration. Ann Rev Neurosci 22: 511-539.

Hernandez , JD., Hoffman LF., Honrubia, V. 1998. Vestibular nerve regeneration in the bullfrog, Rana catesbeiana: Peripheral dendrites. Otolaryngology- Head and Neck Surgery. 119: 244-254.

Hertwig I. 1987. Morphogenesis of the inner ear of Rana temporaria (Amphibia, Anura). Zoomorph 107: 103-114.

Hetherington TE. 1987. Timing of development of the middle ear of Anura (Amphibia). Zoomorph 106: 289-300.

Higgs DM, Burd GD. 2001. Neuronal turnover in the Xenopus laevis olfactory epithelium during metamorphosis. J Comp Neurol 433: 124-130.

Holzenberger, M., Jarvis, E/D/, Chong, C.. Grossan M. Nottebohm, F., and Sharff, C. (1997) Selective expression of insulin-like growth factor Ii in the songbird brain, Journal of Neuroscience 17(18): 6974-6987.

Hoopfer ED, Huang L, Denver RJ. 2002. Basic transcription element binding protein is a thyroid hormone-regulated transcription factor expressed during metamorphosis in Xenopus laevis. Dev Growth Differ 44: 365-381.

Horowitz SS, Chapman JA, Kaya U, Simmons AM. 2001. Metamorphic development of the bronchial columella of the larval bullfrog (Rana catesbeiana). Hear Res 154: 12-25.

Horowitz SS, Chapman JA, Simmons AM (2007) Plasticity of auditory medullary midbrain connectivity across metamorphic development. Brain, behavior and evolution 69:1–19.

Horowitz SS, Tanyu LH, Simmons AM. 2007b. Multiple mechanosensory modalities

Horowitz SS, Simmons AM. 2007. Dynamic visualization of the developing nervous system of the bullfrog, Rana catesbeiana. Brain Res. 1157:23-31.

Horowitz SS, Tanyu LH, Simmons AM. 2007. Multiple mechanosensory modalities influence development of auditory function. J Neurosci. 27(4):782-90.

Horowitz SS, Chapman JA, Simmons AM. 2007. Plasticity of auditory medullary midbrain connectivity across metamorphic development in the bullfrog, Rana catesbeiana. Brain Behav Evol. 69(1):1-19.

Huang L, DeVries GJ, Bittman EL. 1998. Photoperiod regulates neuronal bromodeoxyuridine labeling in the brain of a seasonally breeding mammal. J Neurobiol. 36(3):410-420.

Illing RB, Cao QL, Forster CR, Laszig R. 1999. Auditory brainstem: development and plasticity of GAP-43 mRNA expression in the rat. J Comp Neurol 412: 353–372.

Ishizuya-Oka A, Ueda S. 1996. Apoptosis and cell proliferation in the Xenopus small intestine during metamorphosis. Cell Tissue Res 286: 467-476.

Jacoby J, Rubinson K. 1983. The acoustic and lateral line nuclei are distinct in the premetamorphic frog, Rana catesbeiana. J Comp Neurol 216: 152-161.

Jiang et al., 1998;

Katbamna B, Jelaso AM, Ide CF. 2004. Connexin 43 expression in glial cells ofm developing rhombomeres of Xenopus laevis. Int J Dev Neurosci 22: 47-55.
Kaufman GD, Shinder ME, Perachio AA (1999) Correlation of Fos expression and circling asymmetry during gerbil vestibular compensation. Brain Res 817: 246-255.

Kirn, J., O'Loughlin, B., Kasparian, S., Nottebohm, F. (1994) Cell Death and Neuronal Recruitment in the High Vocal Center of Adult Male Canaries are Temporally Related to Changes in Song. Proceedings of the National Academy of Sciences of the United States of America. 91(17): 7844-7848.

Kolb B, Pedersen B, Ballermann M, Gibb R, Whishaw IQ. 1999. Embryonic and postnatal injections of bromodeoxyuridine produce age-dependent morphological and behavioral abnormalities. J Neurosci 19: 2337-2346.

Kornack DR, Rakic P. 2001. The generation, migration, and differentiation of olfactory neurons in the adult primate brain. Proc Natl Acad Sci USA 98: 4752-4757.

Kubke MF, Carr CE. 2005. Development of the auditory centers responsible for sound

;

Kumaresan V, Kang C, Simmons AM. 1998. Development and differentiation of the anuran auditory brainstem across metamorphosis: An acetylcholinesterase histochemical study. Brain Behav Evol 52: 111-125.

Kunkel AW, Dieringer N (1994) Morphological and electrophysiological consequences of unilateral pre-versus postganglionic vestibular lesions in the frog. J Comp Physiol A 174: 621-632.

Laemmli UK. 1970. Cleavage of structural proteins during the assembly of the head of bacteriophage T4. Nature 227: 680-685.

Li CW, Lewis ER, 1974. Morphogenesis of auditory receptor epithelia in the bullfrog. In: Johari, O., Corvin, I. (Eds.), Scanning Electron Microscopy. IIT Res. Inst., Chicago, IL, pp. 791-798.

Liuzzi FJ, Lasek RJ (1986) Regeneration of montoneuron axons into the adult frog spinal cord

Lohmann C, Ehrlich I, Friauf E (1999) Axon regeneration in organotypic slice cultures from the mammalian auditory system is topographic and functional. J. Neurobiol. 41: 596 611.

Lopez-Anaya VL, Lopez-Maldonado D, Serrano EE. 1997. Development of the Xenopus laevis VIIIth cranial nerve: increase in number and area of axons of saccular and papillar branches. J Morph 234: 263-276.

Lowenheim H, Furness DN, Kil J, Zinn C, Gultig K, Fero ML, Frost D, Gummer AW, Roberts JM, Rubel EW, Hackney CM, Zenner HP (1999) Gene disruption of p27 Kipl allows cell proliferation in the postnatal and adult organ of Corti. Proc Natl Acad Sci USA 96: 4084-4088.

Ludemann W, Stan AC, Tatagiba M, Samil M (2000) Sporadic unilateral vestibular schwannoma with islets of meningioma: case report. Neurosurgery 47: 452-452.

Malloch GD, Clark JB, Burnet FR. 1987. Glial fibrillary acidic protein in the cytoskeletal mammalian auditory system is topographic and functional. J. Neurobiol. 41: 596-611.

Marsh-Armstrong N, Cai L, Brown DD. 2004. Thyroid hormone controls the development of connections between the spinal cord and limbs during Xenopus laevis metamorphosis. Proc Natl Acad Sci USA 101: 165-170.

Marsh-Armstrong N, Huang H, Remo BF, Liu TT, Brown DD. 1999. Asymmetric growth and development of the Xenopus laevis retina during metamorphosis is controlled by type III deiodinase. Neuron 24: 871-878.

Matties C, Carvalho G, Tatagiba M, Lima M, Samil M (1996) Meningiomas of the cerebellopontine angle. Acta Neurochir Suppl (Wien) 65: 86-91.

McDiarmid RW, Altig R. 1999. Research: materials and techniques. In: McDiarmid, R.W., Altig, R. (Eds), Tadpoles: The Biology of Anuran Larvae. University of Chicago Press, Chicago, IL, pp. 7–23.

McGill T (2000) Carcinomatous encephalomyelitis with auditory and vestibular manifestations. Ann Otol Rhinol Laryngol 85: 120-126.

Mears SC, Frank E (1994) Specific regeneration of cutaneous sensory afferent fibers in the amphibian spinal cord. Exp. Neurol. 130: 115-119.

Mearow et al., 1994

Miller MW, Nowakowski RS. 1988. Use of bromodeoxyuridine immunohistochemistry

Minturn J, Geschwind D, Fryer H, Hockfield S. 1995a. Early postmitotic neurons transiently express TOAD-64, a neural specific protein. J Comp Neurol 355: 369–379.

Minturn JE, Geschwind DH, Fryer HJ, Hockfield S. 1995. TOAD-64, a gene expressed early in neuronal differentiation in the rat, is related to unc-33, a C. elegans gene involved in axon outgrowth. J Neurosci 15: 6757-6766.

Newman A, Honrubia V (1992) Regeneration of the eighth cranial nerve in the bullfrog, Rana catesbeiana. Exp. Neurol. 115: 115-120.

Nikundiwe and Nieuwenhuys, 1983)

Nguyen V, Deschet K, Henrich T, Godet E, Joly JS, Wittbrodt J, Chourrout D, Bourrat F. 1999. Morphogenesis of the optic tectum in the medaka (Oryzias latipes): a morphological and molecular study, with special emphasis on cell proliferation. J Comp Neurol 413: 385-404.

Nottebohm, F. (2002) Neuronal replacement in the adult brain. Brain Research Bulletin 57(6) 737-749.

Oppenheimer JH, Schwartz HL. 1997. Molecular basis of thyroid hormone-dependent brain development. Endocr Rev 18: 462-475.

Patel SN, Clayton NS, Krebs JR. 1997. Spatial learning induces neurogenesis in the avian brain. Behav Brain Res 89: 115-128.

Peunova N, Scheinker V, Cline H, Enikolopov G. 2001. Nitric oxide is an essential negative regulator of cell proliferation in *Xenopus* brain. J Neurosci 21: 8809-8818.

Pencea et al., 2001

Peng YY, Frank E (1988) Anatomical specificity of regenerated muscle sensory afferents in the spinal cord of the bullfrog. J. Neurobiol. 19: 727-742.

Peterson EH. (1998) Are There Parallel Channels in the Vestibular Nerve? News Physiol Sci. 13:194-201.

Peterson B, Knotts T, Cummings BS. (2007) Involvement of Ca2+-independent phospholipase A2 isoforms in oxidant-induced neural cell death. Neurotoxicology.28(1):150-60.

Peunova N, Scheinker V, Cline H, Enikolopov G. 2001. Nitric oxide is an essential negative regulator of cell proliferation in Xenopus brain. J Neurosci 21: 8809-8818.

Pizarro IV, Swain GP, Selzer ME. 2004. Cell proliferation in the lamprey central nervous system. J Comp Neurol 469: 298-310.

Pollack ED. 1976. Presumptive relationships between ventricular proliferation and development of the lateral motor columns in the spinal cord of Rana pipiens larvae. Am J Anat 147: 183-192.

Pulec JL, Patterson MJ (1997) Vestibular nerve pathology in cases of intractable vertigio: an electronmicroscopic study. Am J Otol 18: 475-483.

Quick QA, Serrano EE. 2005. Inner ear formation during the early larval period in Xenopus laevis. Devel Dyn 234: 791-801.

Radmilovich M, Fernandez A, Trujillo-Cenoz O. 2003. Environment temperature affects cell proliferation in the spinal cord and brain of juvenile turtles. J Exp Biol 206: 3085 3093.

Rakic, P. (1985). Limits of neurogenesis in primates. Science 227:154–156.

Rao MS, Mayer-Proschel M. 2000. Precursor cells for transplantation. Prog Brain Res 128: 273-292.

Rasika S, Alvarez-Buylla A, Nottebohm F. (1999) BDNF mediates the effects of testosterone on the survival of new neurons in an adult brain. Neuron. 22: 53–62.

Rasika, S., Nottebohm, F., Alvarez-Buylla, A. (1994) Testosterone increases the recruitment and/or survival of new high vocal center neurons in adult female canaries. Proceedings of the National Academy of Sciences of the United States of America 91: 7854–7858.

Raymond PA, Easter SS Jr. 1983. Postembryonic growth of the optic tectum in goldfish I: Location of germinal cells and numbers of neurons produced. J Neurosci 3: 1077-1091.

Reh and Kliavin 1989

Ris L, de Waele C, and Serafin M, 1995. Neuronal activity in the ipsilateral vestibular nucleus following unilateral labyrinthectomy in the alert guinea-pig. J Neurophysiol. 74:2087-99.

Rodger J, Bartlett CA, Harman AM, Thomas C, Beazley LD, Dunlop SA. 2001. Evidence that regenerating optic axons maintain long-term growth in the lizard Ctenophorus ornatus: growth-associated protein-43 and gefiltin expression. Neurosci 102: 647–654.

Russell FA, Moore DR (1995) Afferent reorganization within the superior olivary complex of the gerbil: development and inducation by neonatal, unilateral cochlear removal. J. Comp. Neurol. 352: 607-625.

Sah DWY, Frank E (1984) Regeneration of sensory-motor synapse in the spinal cord of the bullfrog. J. Neurosci. 4: 2784-2791.
Schaden et al., 1994;

Scharff, C., J.M. Garcý´a-Verdugo, F. Doetsch, M. Grossman, A. Mateo, F. Nottebohm, and A. Alvarez-Buylla (1998) Large network of tangential pathways for chain migration in adult songbirds. Soc. Neurosci. Abstr., *24:* 1189.

Scharff, C., J.R Kirn, M.R. Grossmann, J.D. Macklis, and F. Nottebohm (2000) Targeted neuronal death affects neuronal replacement and vocal behavior in adult songbirds. Neuron, *25:* 481–492.

Schrama et al., 1997

Schlosser G, Koyano-Nakagawa N, Kintner C. 2002. Thyroid hormone promotes neurogenesis in the Xenopus spinal cord. Dev Dyn 225: 485-498.

Schreiber AM, Das B, Huang H, Marsh-Armstrong N, Brown DD. 2001. Diverse developmental programs of Xenopus laevis metamorphosis are inhibited by a dominant negative thyroid hormone receptor. Proc Natl Acad Sci USA 98: 10739-10744.

Schreyer and Skene 1991

Schuknecht HF, Woellner WC (1955) An experimental and clinical study of deafness from lesions of the cochlear nerve. J Laryng 69: 75-97.

Schwab ME, Bartholdi D (1996) Degeneration and regeneration of axons in the lesioned spinal cord. Physiol. Rev. 76: 319-370.

Shi Y-B. 2000. Amphibian Metamorphosis: From Morphology to Molecular Biology. New York: Wiley-Liss.

Simmons AM, and Chapman JA. 2002. Metamorphic changes in GABA immunoreactivity in the brainstem of the bullfrog, Rana catesbeiana. Brain Behav Evol 60: 189-206.

Simmons AM, Horowitz SS (2006) Plasticity in the auditory system across metamorphosis. In: Hearing and sound communication in amphibians

Simmons AM, Horowitz SS, Brown RA (2008a) Cell proliferation in the midbrain and forebrain of the adult frog, Rana catesbeiana . Brain Behav Evol 71: 41–53.

Simmons AM, Tanyu LH, Horowitz SS, Chapman JA, Brown RA. 2008. Developmental and Regional Patterns of GAP-43 Immunoreactivity in a Metamorphosing Brain

Brain Behav Evol. 71(4):247-262.

Skene JH, Jacobson RD, Snipes GJ, McGuire CB, Norden JJ, Freeman JA (1986) A protein induced during nerve growth (GAP-43) is a major component of growth-cone membranes. Science 233: 783–786.

Skene JH, Willard M. 1981a. Axonally transported proteins associated with axon growth in rabbit central and peripheral nervous systems. J Cell Biol 89: 96–103.

Skene JH, Willard M. 1981b. Changes in axonally transported proteins during axon regeneration in toad retinal ganglion cells. J Cell Biol 89: 86–95.

Skene JH. 1989. Axonal growth–associated proteins. Annu Rev Neurosci 12: 127–156.

Smirnov S. 1993. The anuran amphibian papilla development, with comments on its timing, rate, and infuence on adult papilla morphology. Zoo Jb Anat 123: 273-289.

Smith PF, Curthoys IS (1989) Mechanisms of recovery following unilateral labyrinthectomy: a review. Brain Res Rev 14:155–180.

Smith DS, Skene, JHP (1997) A transcription-dependent switch controls competence of adult neurons for distinct modes of axon growth. J. Neurosci. 17: 646-658.

Soto I, Marie B, Baro DJ, Blanco RE. 2003. FGF-2 modulates expression and distribution of GAP-43 in frog retinal ganglion cells after optic nerve injury. J Neurosci Res 73: 507–517.

Spaeti U. 1978. Development of the sensory systems in the larval and metamorphosing European grass frog (Rana temporaria L). J Hirnforsch 19: 543-575

Sperry RW (1944) Optic nerve regeneration with return of vision of anurans. J Neurophysiol 7: 57-70.

Sperry RW (1945) Centripetal regeneration of the 8th cranial nerve root with systematic restoration of vestibular reflexes. Am J Physiol 144: 735-741.

Spoendlin H (1971) Degeneration behavior of the cochlear nerve. Arch Klin Exp Ohr-Nas-u Kelk Heilk 200: 275-291.

Spoendlin H (1975) Retrograde degeneration of the cochlear nerve. Acta Otolaryngol 79: 266-275.

Stockdale F, Okazaki K, Nameroff M, Holtzer H. 1964.

Stone JS, Oesterle EC, Rubel EW (1998). Recent insights into regeneration of auditory and vestibular hair cells. Curr Opin Neurobiol 11: 17-24.

Stone JS, Rubel EW (1999) Deltal expression during avian hair cell regeneration. Development 126: 961-973.

Straka H, Dieringer N (1995) Spinal plasticity after hemilabyrinthectomy and its relation to postural recovery in the frog. J Neurophysiol 73:1617–1631

Straka H, Vibert N, Vidal PP, Moore LE, Dutia MB. 2005. Intrinsic membrane properties of vertebrate vestibular neurons: function, development and plasticity.Prog Neurobiol. 76(6):349-92.

Swingle WW. 1926. The germ cells of anurans. II. An embryological study of sex differentiation in Rana catesbeiana. J Morphol 41: 441–547.

Takahashi T, Nowakowski RS, Caviness VS Jr. 1992. BUdR as an S-phase marker for quantitative studies of cytokinetic behaviour in the murine cerebral ventricular zone. J Neurocytol. 21(3):185-97.

Taupin P, Gage FH. 2002. Adult neurogenesis and neural stem cells of the central nervous system in mammals. J Neurosci Res. 69(6):745-9.

Templin T, Simmons AM. 2005. Cellular and spatial changes in the anuran superior olive across metamorphosis. Hearing Research. 207 :87–98.

Terman, A. and Brunk, UT. (2004). Molecules in focus: Lipofuscin. The International Journal of Biochemistry & Cell Biology. 36: 1400–1404.

Thored P, Arvidsson A, Cacci E, Ahlenius H, Kallur T, Darsalia V, Ekdahl CT, Kokaia Z, Lindvall O.(2006) Persistent production of neurons from adult brain stem cells during recovery after stroke. Stem Cells. 24(3):739-47.

Tropepe et al., 1997; Uray NJ, Gona AG, Hauser KF. 1987. Autoradiographic studies of cerebellar histogenesis in the premetamorphic bullfrog tadpole: I. Generation of the external granular layer. J Comp Neurol 266:234-246.

Van der Zee CE, Nielander HB, Vos JP, Lopes da Silva S, Verhaagen J, Oestreicher AB, Schrama LH, Schotman P, Gispen WH. 1989. Expression of growth-associated protein B-50 (GAP43) in dorsal root ganglia and sciatic nerve during regenerative sprouting. J Neurosci 9: 3505–3512.

Vibert, N., deWaele, C., Serafin, M., Baba;oam. A,. Muhlethaler, M., Vidal, P-P. 1997. The vestibular system as a model of sensorimotor trnsformations. A com bined in vivo and in vitro approach to study the cellular mechanisms of gae and posture stabilization in mammals. Progressin Neurobiology 51:243 -286.

Vidal , P-P., deWaele, C., Vibe4rt, N., Muhlethaler, M.1998. Vestibular compensation revisited. Otolaryngol Head Neck Surg 119: 34-42.

Vitkovic L. 1992. GAP-43 expression in macroglial cells: potential functional significance. Perspect Dev Neurobiol 1: 39–43.

Wever EG, Neff WD (1947) A further study of the effects of partial section of the auditory nerve. J Comp Physiol Psych 40: 217-226.

Witschi E. 1949. The larval ear of the frog and its transformation during metamorphosis. Z Naturforsch 4b: 230-242.

Woellner, RC., Schuknecht, HF. 1955. Hearing loss from lesions of the cochlear nerve: an experimental and clinical study. Trans Am Acad Ophthalmol Otolaryngol. 59(2):147 9.

Wullimann MF, Rink E, Verneir P, Schlosser G. 2005. Secondary neurogenesis in the brain of the African clawed frog, Xenopus laevis, as revealed by PCNA, Delta-1, Neurogenin-related-1, and NeuroD expression. J Comp Neurol 489: 387-402.

Yeo W, Gautier J. 2003. A role for programmed cell death during early neurogenesis in Xenopus. Dev Biol. 260: 31-45.

Yip HK, So KF. 2000. Axonal regeneration of retinal ganglion cells: effect of trophic factors. Prog Retin Eye Res. 19(5):559-75.

Zakon HH (1983) Reorganization of connevtivity in amphibian central auditory system following VIIIth nerve regeneration: Time course. J. Neurophysiol. 49: 1410-1427.

Zakon HH, Capranica RR (1981). An anatomical and physiological study of regeneration of the eighth nerve in the leopard frog. Brain Res. 209: 325-338.

Zupanc GK. 2001. Adult neurogenesis and neuronal regeneration in the central nervous system of teleost fish. Brain Behav Evol 58: 250-275.

Zupanc GK, Horschke I.1995. Proliferation zones in the brain of adult gymnotiform fish: a quantitative mapping study. J Comp Neurol. 353(2):213-33.